NOISE FEATURE ANALYSIS, SYSTEM IDENTIFICATION AND MODELING FOR SELECTION OF PULSE TEMPERATURE FREQUENCY OF MOS GAS SENSORS

A THESIS SUBMITTED IN PARTIAL FULFILLMENT OF THE
REQUIREMENTS FOR THE DEGREE OF
DOCTOR OF PHILOSOPHY

NIMISHA DUTTA
Registration Number 007 of 2009

SCHOOL OF ENGINEERING
DEPARTMENT OF ELECTRONICS AND COMMUNICATION ENGINEERING
TEZPUR UNIVERSITY
DECEMBER, 2012

I dedicate this thesis to my parents Late Tulshi Nath Dutta, Aruna Dutta and my most beloved brother Rituraj Dutta whose love inspired me to complete this work successfully.

ABSTRACT

There has been an increasing demand for accurate, reliable and inexpensive gas sensors that can discriminate between various types of gases such as CO, NO, NO_2, NH_4, SO_2, CO_2, CH_4 and other hydrocarbons. Historically, gas sensors were primarily used in coal mines in the accurate monitoring of hazardous gases however gas sensors began to appear in other applications such as in chemical industry, environmental pollution monitoring, the health sector, food industry etc. During the last decade the electronic nose (E-Nose), based on array of gas sensors for food flavour, environmental monitoring and medical diagnosis etc. are the more recent embodiments of gas sensing owing to its enhanced analytical power.

The odour recognition process in E-nose begins in the senor system which is responsible for the measurement of the odourant stimulus through the sensitivity of its sensors. Some of the commonly used gas sensors include, metal oxide semiconductor (MOS), conducting polymer sensors, surface acoustic wave (SAW) sensors, field-effect gas sensors, pellistors, and fibre-optic sensors. MOS sensors are one of the most widely used devices for E-nose applications due to their low cost, acceptable response, low recovery times and robustness.

Noise in gas sensors is considered to be any unwanted effect that obscures the detection of the desired gas. It can arise at various stages of the measurement process - the sensors, the analog processing system, the data acquisition stage and the digital signal processing system out of which the noise in the sensors is most harmful as it propagates and can be amplified through the subsequent stages.

Although the most convectional way of operating the MOS gas sensor is to apply a fixed voltage to the inbuilt sensor heater, recently, the performance of the MOS gas sensors has been enhanced by applying modulated temperature to the sensor instead of applying a fixed temperature. Several approaches have been explored for deriving higher numbers and better features for enhancing gas classification. Application of periodic heating voltage to MOS sensors has several advantages:

i) Different rates of reaction of various gases at different temperatures, providing a unique signature for each gas.
ii) Sensitivity and selectivity may be enhanced.

Many authors have indicated that modulation of the sensor temperature[1-3] provides more information from a sensor than in isothermal operation, allowing improved research works in gas detection such as - carbon mono-oxide[4-6] and hydrogen sulphide[7, 8]. To discriminate between different gases, modulating waveforms such as sawtooth, triangular and square pulse were also applied to the sensors[9]. The sinusoidal variation in the temperature also enhanced the identification of different gases. A number of works on the cyclic variations of the sensor heater have been reported by many authors [10, 11] where feature extraction is done using various heater voltage functions with different frequencies. The temperature profile of the sensor surface greatly influence the response behavior due to rapid thermal fluctuations in respect of its noise and stability. Researchers have tried to improve selectivity by modulating the heater voltage however analysis of noise and stability of the sensor responses under modulated heater voltage has not been explored so far. Therefore the aim of this research is to analyse the baseline noise behavior and stability of MOS gas sensors by applying pulse voltages to the heater with different frequencies and duty cycles.

Objectives of this research work:

The objectives of this research are cited below:

1. The statistical and frequency analysis of MOS gas sensor noise under pulsed modulated heater voltage for selection of best pulse frequencies and thereby improvement of discrimination of different gases.
2. Filtering of noise using Amplitude Demodulation (AD) technique and its comparison with Wavelet Transform (WT) based technique.
3. Sensor system identification and stability analysis under pulsed temperature modulation, selection of best pulse frequency and improvement of classification of gases.
4. Modeling of MOS sensor based on theoritical analysis and system identification and their comparison.

Chapter 1 gives a brief introduction on the research work and comprehensive literature.

Baseline noise analysis of the MOS sensors under different pulse temperature modulating frequency and duty cycle was conducted on three MOS gas sensors- TGS-822, TGS-842 and TGS-2611 from Figaro, INC, Japan used in an array. Data acquisition and online logging of the responses from the gas sensors is achieved by PC based data acquisition systems. All data processing work is done in MATLAB 7.4 environment. The discrimination of the data for ten different gas samples was done using ANN classifiers – Multilayered Perceptron (MLP) and Radial Basis Function (RBF) for comparison. The sensor data correlation was tested by Principal Component Analysis (PCA) before applying to ANN.

With the above listed objectives, the work was carried out as discussed below -

Noise Feature Analysis of MOS gas sensors:

In chapter 2, the statistical and frequency analysis of noise in MOS gas sensors is described and best frequency and duty cycle is selected from the set of experimental data for further analysis.

a) **Experimental:** The experimentation was aimed at noise feature analysis of MOS gas sensor responses with pulsed modulated heater voltage of frequencies - 10mHz, 40mhz, 80mHz and 120mHz and at two different duty cycles - 50% and 75% without the application of any gas. The MOS gas sensor noise analysis under signal inactive period i.e. without application of gas, is important to determine a suitable time duration of the pulsed heater voltage at four different heater pulse frequencies. Therefore the frequency and duty cycle of the heater pulse voltage is required to be correlated to severity of noise. For noise analysis the statistical and frequency spectrum of the MOS gas sensors that have been performed are - the Probability Distribution Function (PDF), signal to noise ratio (SNR), histogram and Fast Fourier Transform (FFT). Two new noise characteristics- NSF (Noise Spread Figure) and NPF (Noise Population Figure) have been developed for analyzing

noise in a signal which is one of the significant contributions of this part of the research.

b) **Results:** In this research both statistical and frequency analysis of the noise has been performed for the three sensors with pulsed heater voltages of the above mentioned frequencies and duty cycles. The statistical analysis reveals that - the noise floor level decreases as the duty cycle of the pulsed modulated heater voltage is increased and pulse frequency is decreased. The same observation is evident for the FFT of the sensor responses that produces higher noise-bandwidth at higher heater pulse frequency however at lower duty cycle. The sensor noise is found to be $1/f$ or pink and it increases with the increase in pulsed heater voltage frequency and vice-versa. The PDF for the sensor noise signals satisfies the requirement for the noise to be coloured i.e. with non-zero mean. The newly introduced characteristics - NSF and NPF ratios also conforms to our previous statistical and FFT results i.e. decrease at lower frequency and higher duty cycle. Hence we are able to conclude that the heater pulse frequency and duty cycle considerably influences the noise behavior of the sensor. This analysis facilitates that for improving the classification efficiency of the sensor array, sensor responses can be generated by using a suitable pulse frequency and duty cycle. The method for improvement of classification efficiency by using the best frequency and duty cycle is discussed in the next section.

Gas classification with the best heater pulse frequency using dynamic features:

Extraction of dynamic features of the MOS gas sensors is conducted for different heater pulse modulating temperature in the presence of ten different gases namely ethylacetate, acetonitrile, ethanol, kerosene, petroleum ether, chloroform, methanol, isopropyl alcohol, acetone and n-hexane using time constant as the feature for classification. In[12] the sensor response curves were determined using six features which represented the differences of dynamic behaviour of sensors to different sample gases, in phase space. The degree of difference was used to evaluate how much information was extracted from the response curves by the proposed method. Although response voltage is used by many researchers as

feature, the time constant (τ) may be different for the same response voltage. We have extracted the time-constant of all the response cycles of the sensor modulated by the heater pulse voltage. Two sets of feature data were generated – one with an arbitrary temperature pulse frequency of 120mHz and 50% duty cycle, another with the selected pulse frequency of 10mHz and 75% duty cycle that gives the least noise as already discussed.

We have found that the PCA accounted for upto 98.0004% of the variance for the arbitrary heater pulse frequency and duty cycle while 99.2687% of the variance with the selected best frequency and duty cycle. Similarly, an accuracy of 85.62% was achieved in the classification using RBF network compared to 58.21% using an MLP. The time required for training with MLP was higher than that required for training the network with RBF.

This part of the research focuses on the development of a heater pulse frequency and duty cycle selection technique that relies on the fact that frequency and duty cycle of the heater influences the noise behavior of the sensor response and thereby the classification efficiency also.

Noise Filtering:

Inspite of having certain advantages of MOS gas sensors such as robust, low-cost etc., noise is one of the most important issues to be addressed for MOS gas sensor based gas detectors and E-noses. Operating the sensor at a suitable heater pulse frequency and duty cycle to get the least noise, has been explained in the previous section, however at fixed heater pulse operation the noise persists. Chapter-3 is dedicated to the development of noise filtering techniques based on Amplitude Demodulation (AD) and Wavelet Transform (WT). Different methods have been employed by researchers to eliminate noise in signals[13-22]. In one work[23] an amplitude modulation / demodulation system is proposed to modulate the $1/f$ noise in capacitive sensors, where the signal is modulated to a higher frequency and then the signal is low-pass filtered. In another work, an AD based noise filtering technique was proposed for an instrumentation amplifier[24]. Also, the adverse effects of the amplifier offset and flicker ($1/f$) noise of a differential low-noise high-resolution switched-capacitor readout circuit is minimized using amplitude modulation/demodulation in another work[25].

An AD-based noise reduction algorithm has been applied in multichannel audio processing[26, 27, 28] which is capable of increasing the SNR in the overall signal. This algorithm reduces noise interference by reducing the noise-dominant channels to the overall signal. Since AD based techniques for noise filtering has been used in a number of multichannel sensor environment, it shows potential application in multisensor MOS gas array based E-nose.

Although a number of works have been performed on signals for filtering using Finite Impulse Response (FIR), Infinite Impulse Response (IIR) or High Frequency Response (HFR) techniques, these methods may not be suitable in a rapidly changing temperature condition of MOS gas sensor (due to pulse heater voltage) because these techniques involve filter parameters, namely center frequency and bandwidth which are situation dependent and their selection is knowledge demanding. Hence, the objective of this chapter 3 is to explain two parameter free techniques developed - AD and WT technique to recover the original signal from the noisy sensor signal as discussed below-

a) **Experimental:** For filtering we have chosen a very low sensitivity MOS gas sensor (TGS-2611) so that we get a high noise bandwidth before filtering for justifying the performance of our developed technique. The sensor signal was at first filtered in LabVIEW by a smoothing filter and then it was modulated by adding -14dB white noise and a low frequency sine signal so that we obtain a completely noise buried sensor signal for applying the AD technique. In wavelet filtering method, the sensor signal was decomposed by Daubechies' WT and a level was selected as the filtered signal based on two analyses - Cross-correlation (CC) with the original sensor signal and FFT. CC shows which level is highly correlated to the original sensor signal in time-domain while FFT determines the noise bandwidth.

b) **Results:** We have found from FFT that the noise bandwidth of the signal before AD based filtering is 0.0371Hz whereas after AD filtering the noise was filtered out giving a reduced bandwidth of *0.0086Hz*. In the WT filtering, approximation/reconstructed levels (a_5) was selected as the highest correlated level with cross-correlation co-efficient as 0.9986. The bandwidth at level 5 was found to

be 0.0369Hz which clearly shows that the performance of AD filter is better than the WT filtering.

Hence chapter 3 enumerate a novel technique of filtering MOS gas sensor responses using AD based algorithm which shows potential application in E-nose signal processing.

Heater pulse frequency selection by System Identification:

Dynamic response of MOS gas sensors plays an important role in gas detection and gas classification. Among other factors like noise behavior, obtaining a quasi-isothermal condition of the sensor surface and sensor stability are also important criterions when the sensor is operated by pulse modulated heater voltage. A quasi-isothermal state provides a slow change in sensor adsorption kinetics which on the other hand, determines the stability of the response. Since attainment of a proper isothermal sensor state is determined by the heater pulse fluctuation, a study on stability of the sensor will lead to a method of selection of suitable heater pulse frequency and duty cycle. The frequency of modulation is selected on trial and error method in many of the works based on temperature modulation[2, 29, 30]. One method of selecting optimized frequency was based on system identification through multilevel pseudorandom sequences[31] and pseudorandom binary sequences[32]. In these methods pseudorandom sequences (PRSs) and pseudorandom binary sequences (PRBSs) of maximum-length sequences (MLSs) was used to identify systems and how these method could be extended to systematically study temperature-modulated gas sensors, however the identification of systems using pulsed heater voltage for sensor stability analysis by system identification technique has not been explored so far. In this research we have determined the transfer functions of the MOS gas sensors baseline model by system identification technique. The prediction error minimization (PEM) algorithm was used to derive the sensor Linear Time Invariant (LTI) model transfer function from measured input-output data without the application of any gas. The objective of this part of the research was to analyse the sensors' stability behavior when its temperature is pulsed by a heater pulse voltage. Therefore, the transfer function derived should relate heater pulse voltage as input and sensor response voltage as output. The stability of the derived model transfer functions was tested by determining the overshoot percentage of the step response and from the pole-zero plots. Based on these two parameters the most stable transfer function was determined

followed by the model validation. For the most stable transfer function, the frequency and duty cycle of the heater pulse voltage is considered as the best operating values.

a) **Experimental:** For performing system identification using PEM algorithm, we have applied a large input-output pair of data set for two sensors (TGS-2611 and TGS-842) each operated by heater pulse of frequencies 10mHz, 40mHz, 80mHz and 120mHz and duty cycles of 50% and 75%. Moreover we have performed the same analysis for lower frequency range of frequencies 1mHz, 2mHz, 3mHz, 4mHz and 5mHz and duty cycles of 50% and 75% for two sensors (TGS-2611 and TGS-822). Lower frequency is preferred because of the following reasons-
    i) To attain a quasi-isothermal state a slow change in sensor heater voltage is desirable such that the sensor dynamics is preserved[33].
    ii) At lower frequencies, since the time-period is already high, smaller duty cycle may lead to attain the stable sensor dynamics.
    iii) As the frequency is increased, the duty cycle has to be increased such that sufficient amount of heating takes place at the sensor surface in order to preserve the sensor dynamics.

b) **Results:** The system identification results higher order transfer functions (order 2 or more) however we have reduced the order by model order reduction technique to 1. The overshoot percentage was determined from the step response of the transfer function while stability was ascertained from the pole-zero plots. From these two tests, the most stable transfer function was obtained with the following heater pulse voltage frequency and duty cycle-
    Lower frequency range: TGS-822: 1mHz, 50%; TGS-2611: 2mHz, 50%
    Higher frequency range: TGS-842: 120mHz, 75%; TGS-2611: 40mHz, 75%
    The transfer functions obtained were further simulated for best fit analysis and it was found that the most stable transfer functions yielded the best fit percentage namely-
    Lower frequency range: TGS-822: 78.81%; TGS-2611: 68.31%
    Higher frequency range: TGS-842: 63.43%; TGS-2611: 67.24%

Once the most stable transfer functions and their corresponding best values of pulse frequency and duty cycle are obtained, the PCA was worked out with two pairs of sensors: TGS-822/TGS-2611 and TGS-842/TGS-2611 for ten different gas samples. The PCA accounted for higher percentage when sensors are operated by the best heater pulse frequency compared to arbitrary chosen frequency and duty cycle. Further, using these best suited frequencies and duty cycle for both the ranges of frequencies, the classification of different gases is performed using two ANN classifiers – MLP and RBF. The ANN classifier also better classification efficiency when the best frequency is used.

The objectives for developing a technique for selection of heater pulse frequency and duty cycle based on stability criterion and system identification is achieved in this research. As stated earlier for chapter 2 we have found that the best pulse frequency and duty cycle for the three sensors are 10mHz, 75% duty cycle, which is based on noise analysis however, the stability analysis shows that this value is 40mHz, 75% duty cycle (TGS-2611) and 120mHz, 75% duty cycle (TGS-842) for upper frequency range and for lower frequency range the stability was found at 1mHz, 50% duty cycle (TGS-822) and 2mHz, 50% duty cycle (TGS-2611). Therefore selection of best operating frequency of heater pulse voltage is a trade-off between requirement of noise behavior and stability of the MOS gas sensor responses.

Modeling of MOS Gas sensors:

Sensor modeling and simulation is an important issue for study, development and analysis of sensor systems. The modeling of MOS gas sensors helps to describe its dynamic behavior in the presence of various gases. A thick film MOS gas sensor operates on the principle of change in conductance due to the chemisorption of gas molecules on the sensor surface. Several experimental and theoretical analysis describing the electric responses of the MOS gas sensors have been proposed[34-45]. In[40] SPICE model for the static and transient response of resistive gas sensor has been reported. These analysis aims at relating sensitivity and gas concentration[41], a diffusion reaction model[42], electron theory of chemisorption mechanism[43, 44], absorption desorption noise[45] and thermal modulation[36-39], however transfer function derivation under thermal modulation has not been addressed.

The objective of this research is modeling of the sensor dynamics based on the system measured input-output data by modulating the heater voltage. We have derived the theoritical model equation from a simple, reversible, binding Freundlich isotherm equation. Model parameters have been determined from.the experimental data and the baseline model equation has been established. The established model has been validated with the model derived by system identification (as discussed in chapter 4).

a) **Experimental results:** Two MOS gas sensors (TGS-2611 and TGS-842) were used to analyze the sensor resistance variation with varying applied hater voltage and temperature. The temperature of the sensor was indirectly measured by using the heater filament as the temperature sensor by measuring the heater current. The heater voltage versus temperature variation characteristics gives the heater model by a 1^{st} order model transfer function. Further the time constant (τ) of the heater model was determined as 6 seconds (TGS-2611) and 1.3 seconds (TGS-842) to derive the baseline model of the sensors. Since the theoritical model of the Freundlich equation is based on the activation energy (E_{Ao}) of the sensor material, we have determined the activation energy from Arrhenius plot of the sensor. The activation energy of TGS-2611 and TGS-842 sensors is calculated as 0.05eV and 0.058eV respectively. Using the activation energy and time-constant, the theoretical model equation was simulated. The simulated model responses obtained from system identification were compared with that of the theoritical model and it was found that the fit percentage for the two sensors TGS-2611 and TGS-842 are 67.24% and 63.43% respectively.

This part of the research fulfills the objective of modeling of MOS gas sensors based on theoritical analysis and system identification.

Scope of future work:

Noise analysis and filtering under pulsed modulation temperature is explored with selection of best frequencies and duty cycles. The system identification also proved to be a potential study area for the selection of suitable frequencies and duty cycles and sensor system modeling. The optimal thermal modulation of the working temperature of the MOS gas

sensor based E-nose can significantly increase the selectivity of metal oxide sensors. Therefore, the systematic optimization process to employ the selection of modulating frequencies, permits to ensure a remarkable increase in performance for metal oxide based multisensor systems.

This research can be extended for further study on the following directions-

i) Systematic optimization technique can be employed for selection of pulse heater voltage frequency and duty cycle.
ii) The study on modeling can be extended for a condition of application of gas.
iii) Wavelet based filtering can be improved and explored.

Thesis Outline:

Chapter 1 gives the introduction to an inclusive literature as basic knowledge for the research work. Chapter 2 presents the experimental set-up of the MOS gas sensor based E-nose of the entire work and the noise analysis (statistical and frequency based) of the sensor response and selection of best heater pulse frequency and duty cycle. Chapter 3 describes the techniques of noise reduction in the MOS gas sensors using two different filtering methods. The AD and WT techniques were analyzed and used in this research to extract the original signal from the responses of noise modulated low sensitivity sensor signal. Chapter 4 presents the method of system identification in the area of gas sensors. The method consists of studying the sensor baseline model stability when their operating temperature is modulated. Chapter 5 gives an analysis on the theoretical modeling of the sensor dynamics and compared with the measured input output data obtained.

Contribution of this thesis:

1. Dutta, N., & Bhuyan, M. Chapter 3, Measurement of Odour by Sensor Arrays, *Odour Impact Assessment Handbook*, Wiley Publisher. (In Press).
2. Dutta, N., & Bhuyan, M. Noise Feature Analysis in Pulse Temperature Modulated MOS Gas Sensors, *Sensors and Transducers* **120** (9), 107--118, 2010.
3. Dutta, N., & Bhuyan, M. Statistical Analysis of Noise in MOS Gas Sensor Based Electronic Nose with Pulsed Temperature Modulation, in Computational Vision and Robotics (ICCVR'2010), Bhubaneswar, India, 23-27.

4. Dutta, N., & Bhuyan, M. Amplitude Demodulation and Spectrum Analysis of Noise in MOS Gas Sensor Based Electronic Nose, in Advances in Communication, Network, and Computing (CNC'2010), Calicut. Kerala, India, 160-162.
5. Dutta, N., & Bhuyan, M. Dynamic Response Based Odour Classification Using MOS Gas Sensors, in Emerging Applications of Information Technology (EAIT'2011), Kolkata, India, 231-234.
6. Dutta, N., & Bhuyan, M. Optimal Temperature Modulation of MOS Gas Sensors by System Identification, *Journal of Signal Processing, Image Processing and Pattern Recognition* **5** (2), 17-27, 2012.
7. Dutta, N., Dewan, S.K., & Bhuyan, M. System Identification of MOS Gas Sensors and Stability Analysis, *Sensors and Transducers* **143** (8), 127--135, 2012.
8. Dutta, N., & Bhuyan, M. System Identification of MOS Gas Sensors and Classification Enhancement through Optimal Temperature Modulation, in International Multi-conference on Intelligent Systems, Sustainable, New and Renewable Energy Technology and Nanotechnology'2012, Klawad, Haryana, India, 149-153.
9. Dutta, N., & Bhuyan, M. Classification Enhancement of MOS Gas Sensors by Optimized Temperature Modulation Using System Identification, *Journal of Signal Processing and Pattern Recognition,* Association for the Advancement of Modelling and Simulation Techniques in Enterprises. (In Press)

Contribution under review:

1. Dutta, N., & Bhuyan, M. Modeling of MOS Gas Sensor Based Electronic Nose Using System Identification, *International Journal of Engineering Systems Modelling and Simulation.* (Under Communication)

References:

1. Lee, P.A., & Reedy, B.J. Temperature modulation in semiconductor gas sensing, *Sensors and Actuators B* **60** (1) 35--42, 1999.
2. Heiling, A., et al. Gas Identification by Modulating Temperatures of SnO_2-Based Thick Film Sensors, *Sensors and Actuators B* **43** (1-3) 45--51, 1997.

3. Huang, X., et al. Gas sensing behaviour of a single tin dioxide sensor under dynamic temperature modulation, *Sensors and Actuators B* **99** (2-3) 444–450, 2004.
4. Vine, H. D. Le. *Method and apparatus for operating a gas sensor*, **U.S. Patent No. 3906473**, September 16, 1975.
5. Eicker, H. *Method and apparatus for determining the concentration of one gaseous component in a mixture of gases*, **U.S. Patent No. 4012692**, March 15, 1977.
6. Owen, L.J. *Gas monitors*, **U.S. Patent No. 4185491**, January 29, 1980.
7. Advani, G. N., Beard, R. and Nanis, L. *Gas measurement method*, **U.S. Patent No. 4399684**, August 23, 1983.
8. Lantto, V., & Romppainen, P. Response of some SnO_2 gas sensors to H_2S after quick cooling, *J. Electrochem. Soc.* **135 (10)**, 2550--2556, 1988.
9. Bulkowiecki, S., Pfister, G., Reis, A., Troup, A.P. and Ulli, H.P. *Gas or vapor alarm system including scanning gas sensors*, **U.S. Patent No. 4567475**, January 28, 1986.
10. Sears, W.M., et al. General characteristics of thermally cycled tin oxide gas sensors, *Semicond. Sci. Technol.* **4**, 351--359, 1989.
11. Sears, W.M., et al. Algorithms to improve the selectivity of thermally cycled in oxide gas sensors, *Sens. Actuators B* **19** (4), 333--349, 1989.
12. Zhang, S., et al. An entire feature extraction method of metal oxide gas sensors, *Sens. and Actuators B* **132** (1), 81-89, 2008.
13. Hosur, S., & Tewfik, A. H. Wavelet transform domain adaptive FIR filtering, *IEEE Trans. Signal Processing* **45** (3), 617–630, 1997.
14. Erdol, N., & Basbug, F. Wavelet transform based adaptive filters: analysis and new results, *IEEE Trans. Signal Processing* **44** (9), 2163–2171, 1996.
15. Donoho, D. L., & Johnstone, I. M. Adaptating to unknown smoothness via wavelet shrinkage, *J. Amer. Statist. Assoc.* **90** (432), 1200–1224, 1995.
16. Donoho, D. L., Johnstone, I. M., Kerkyacharian, G., & Picard, D. Wavelet shrinkage: Asymptopia?, *J. Roy. Statist. Soc. B.* **57** (2), 301–337, 1995.
17. Donoho, D. L. De-noising by soft-thresholding, *IEEE Trans. Inform. Theory* **41** (3), 613–627, 1995.
18. Nason, G. P. Wavelet shrinkage by cross-validation, *J. Roy. Statist. Soc. B* **58**, 463–479, 1996.

19. Bruce, A., & Gao, H.Y. UnderstandingWaveShrink: Variance and bias estimation," *Biometrika* **83** (4), 727-745, 1996.
20. Lang, M., et al. Noise reduction using an undecimated discrete wavelet transform, *IEEE Signal Processing Lett.* **3** (1), 10–12, 1996.
21. Johnstone, I. M., & Silverman, B.W. Wavelet threshold estimators for data with correlated noise, *J. Roy. Statist. Soc. B* **59** (2), 319–351, 1997.
22. Abramovich, F., Sapatinas, T., & Silverman, B. W. Wavelet thresholding via a Bayesian approach, *J. Roy. Statist. Soc. B* **60** (4), 725-749, 1998.
23. Chou, W.C., Hsu, Y.C., & Liao, L. P. Modulation/ Demodulation System for Capacitive Sensors, in IEEE International conference on Microsystems, Packaging, Assembly Conference Taiwan (IMPACT'2006), Taipei, Taiwan, 1 – 4.
24. Lita, I., Sofron, E., Serban, G., & Visan, D. A Method of Noise Reduction in Data Acquisition Systems from Sensors, in 24th International Spring Seminar on Electronics Technology: Concurrent Engineering in Electronic Packaging' 2001, Calimanesti-Caciulata, Romania, 253 – 257.
25. Chung, K., et al. Effects of directional microphone and adaptive multi-channel noise reduction algorithm on cochlear implant performance, *Journal of Acoustical Society of America* **120** (4), 2216–2227, 2006.
26. Boymans, M., & Dreschler, W.A. Field trials using a digital hearing and with active noise reduction and dualmicrophone directionality, *Audiology* **39** (5), 260–268, 2000.
27. Walden, B., et al. Comparison of benefits provided by different hearing aid technologies, *Journal American Academy of Audiology* **11** (10), 540–560, 2000.
28. Chung, K., et al. Effects of directional microphone and adaptive multi-channel noise reduction algorithm on cochlear implant performance, *Journal of Acoustical Society of America* **120** (4), 2216–2227, 2006.
29. Cavicchi, R.E., et al. Fast temperature programmed sensing for micro-hotplate gas sensors, *IEEE Electron Device Lett.* **16** (6), 286–288, 1995.
30. Cavicchi, R.E., et al. Optimized temperature-pulse sequences for the enhancement of chemically specific response patterns from micro-hotplates gas sensors, *Sensors and Actuators B* **33**, 142–146, 1996.

31. Vergara, A., et al. Optimised temperature modulation of metal oxide micro-hotplate gas sensors through multilevel pseudo random sequences, *Sensors and Actuators B* **111–112** (11), 271–280, 2005.

32. Vergara, A., et al. Optimized Temperature Modulation of Micro-Hotplate Gas Sensors Through Pseudorandom Binary Sequences, *IEEE Sensors Journal* **5** (6), 1369 -1378, 2005.

33. Gutierrez, O. R., Korah, S., & Perera, A. Multi-frequency temperature modulation for metal-oxide gas sensors, in 8th Intl. Symp. On Olfaction and Electronic Nose'2001, Washington DC, 1-7.

34. Clifford, P. K. Homogenous semiconducting gas sensors: A comprehensive model, in Int. Meet. Chemical Sensors'1983, Fukuoka, Japan, Kodansha, Tokyo/Elsevier, Amsterdam, 135-146.

35. Morrison, S. R. Semiconductor Gas Sensors, *Sensors and Actuators* **2**, 329-341, 1982.

36. Fort, A., et al. CO sensing with SnO_2-based thick film sensors: surface state model for conductance responses during thermal-modulation, *Sensors and Actuators B Chem.* **116**(1-2), 43–48, 2006.

37. Fort, A., et al. Simplified models for SnO2 sensors during chemical and thermal transients in mixtures of inert, oxidizing and reducing gases, *Sensors and Actuators B Chem.* **124** (1), 245–259, 2007.

38. Fort, A., et al. Surface state model for conductance responses during thermal-modulation of SnO2-based thick film sensors: Part I—Model derivation, *IEEE Trans. Instrum. Meas.* **55** (6), 2102–2106, 2006.

39. Fort, A., et al. Surface state model for conductance responses during thermal-modulation of SnO2-based thick film sensors: Part II—Experimental verification, *IEEE Trans. Instrum. Meas.* **55** (6), 2107–2117, 2006.

40. Gardner, J. W., Llobet, E., & Hines, E.L. PSpice model for resistive gas and odour sensors, *Circuits, Devices and Systems* **146** (3), 101-104, 1999.

41. Morrison, S. R. Mechanism of semiconducting gas sensor operation, *Sensors and Actuators* **11** (3), 283-287, 1987.

42. Gardner, J.W. Electrical conduction in solid state gas sensors, *Sensors and Actuators* **18** (3-4), 373-387, 1989.

43. Geinstlinger, H. Electron theory of thin film gas sensors, *Sensors and Actuators B* **17** (1), 47-60, 1993.

44. Geinstlinger, H. Device modeling of semiconductor gas sensors, *Sensors and Actuators B* **13**, 685-686, 1993.

45. Gomri, S., et al. Modelling on oxygen chemisorption induced noise in metallic oxide gas sensors, *Sensors and Actuators B* **107** (2), 722–729, 2005.

DECLARATION

I do hereby declare that the thesis entitled **"Noise Feature Analysis, System Identification and Modeling for Selection of Pulse Temperature Frequency of MOS Gas Sensors"**, being submitted to the Department of Electronics and Communication Engineering, Tezpur University, is a record of original research work carried out by me. All sources of assistance have been assigned due acknowledgment. I also declare that neither this work as a whole nor a part of it has been submitted to any other University or Institute for any other degree, diploma or award.

Nimisha Dutta

Place: Tezpur (Nimisha Dutta)

Date: 3-6-13

Manabendra Bhuyan, B.E., M.Tech, Ph.D
Professor

TEZPUR UNIVERSITY
Department of Electronics & Communication Engineering
Napaam-784028

CERTIFICATE BY THE SUPERVISOR

This is to certify that the matter embodied in the thesis entitled **"Noise Feature Analysis, System Identification and Modeling for Selection of Pulse Temperature Frequency of MOS Gas Sensors"** submitted by Nimisha Dutta for the award of degree of Doctor of Philosophy of Tezpur University is a record of bona-fide research work carried out by her under my supervision and guidance. The results embodied in this thesis have not been submitted to any other University or Institute for the award of any degree or diploma.

Date: 03-06-13

(M.Bhuyan)

TEZPUR UNIVERSITY
(A Central University established by an Act of Parliament)
NAPAAM, TEZPUR-784028, INDIA
Ph: 03712-267004, 267005 Fax: 03712-267005, 267006

CERTIFICATE

This is to certify that the thesis entitled ***"Noise Feature Analysis, System Identification and Modeling for Selection of Pulse Temperature Frequency of MOS Gas Sensors"*** submitted to the Tezpur University in the Department of Electronics and Communication Engineering under the School of Engineering; in partial fulfillment for the award of the Degree of Doctor of Philosophy, has been examined by us on 17.6.2013 and found to be satisfactory.

The committee recommends for the award of the degree of Doctor of Philosophy.

Supervisor

Date: 17-06-13

External Examiner

Date: 17-6-2013

ACKNOWLEDGEMENT

In the endeavor of the journey towards my Ph.D., this thesis has been kept on track and seen through to completion with the support and encouragement of numerous people including my mentors, well-wishers, friends, colleagues and various laboratories. It is a pleasant opportunity to express my heartfelt thanks to all those people who made this thesis possible and contributed in different ways.

First and foremost, I would like to take the opportunity to thank my mentor, Prof. Manabendra Bhuyan for his motivation, guidance, support and encouragement. His profound knowledge and understanding in Instrumentation inspired me to pursue my doctoral research in the field of Instrumentation. I convey my deep gratitude for his insightful guidance, valuable advice, periodic constructive suggestions and extensive discussions during my work. His understanding attitude, constant support, encouragement and personal attention provided good and smooth basis for my research work. I am thankful for his devoted contribution in reviewing my progress, writing, making correction to improve and finalize the research papers as well as the thesis. I developed the attitude of independent thinking in his association, and build the confidence to pursue independent research. I have him as a systematic and broadly skilled professor, who helped me polish my grasp on the principles of both experimental and analytical procedures as well as critical analysis during the tenure of the work. I convey my heartfelt thanks to him for sharing this with me.

I convey my gratefulness to Prof. P.P. Sahu, Prof. J.C. Dutta, Prof. S. Bhattacharyya, Dr. S. Sarmah, Dr. S. Roy, Dr. B. Deka, Mr. Riku Chutia, Mrs. D. Hazarika, Dr. V.K. Nath, Mr. N.M. Kakati , Mr. B. Mondol, Mr. R. K. Bora, Mr. D. Sonowal, Ms. Priyanka Kakoty and Ms. Ananya Bonjyotsna for their constant support, encouragement and valuable advice. I convey my special gratitude to Mr. A. Baishya for his immense help and valuable advices during my research period.

Most of the results described in this thesis would not have been obtained without the help of Mr. Prakash Kurmi and Mr. Naba Kumar Gogoi who helped me to build the set-up for the experiment. I would also like to convey my gratitude to Mr. Kulendra Sharma, Mr. Jiten C. Boro, Mr. Satya Prasad Saikia, Mr. Mantu Mali, Mr. Rupak Sharma and Mr. Jibon Das for their helping hand whenever I needed.

I convey my sincere expression of thanks to my Doctoral committee members Prof. P. P Sahu and Prof. J.C. Dutta for their valuable advice, helpful suggestions, comments and encouragement.

I am thankful to Mr. Dwipendra Chandra Das, Mr. Bubul Das and Mr. Mahanta for their help.

I am indebted to many of my friends and student colleagues for providing a stimulating and fun filled environment. I wish to thank Aradhana Dutta, Nilima Gogoi, , Shashikala Kalita, Bidyut Deka, Awadhesh Pachauri, Madhurjya Pratim Das, Dr. Mousumi Borthakur, Anup Kr. Bordoloi , Pranjal Bora, Hemanga Kr. Das, Champak Talukdar and Lachit Dutta for their love, care and moral support. Maumita Chakraborty and Sumi Kankana Dewan deserves special mention here for constant support and motivation during the tenure of my research. I would also like to devote my sincere thanks to Jeena Jyoti Baruah, and Rashmi Rekha Devi of Department of Chemical Sciences and Lipika Aideo and Krishna Gogoi of Department of Molecular Biology and Biotechnology for providing me with some chemicals required during the experiments. Also, Pranaya Mallick (M.Tech ELDT, project student) deserves my special thanks for his help during my thesis writing period.

I would also like to pay best regards and gratefulness to my Parents, Brother, Uncle, Aunty and cousins, for their sincere encouragement, inspiration, love, care, and support. I owe all my accomplishment to them who stood by me all the time throughout my research work and all throughout my difficult times.

I am thankful to the Tezpur University Library for the wealth of the books and journals, which I referred for invaluable support of literature review. I take this opportunity to sincerely acknowledge Tezpur University for its initial financial support in form of Institutional Fellowship which supported me to pursue my research conveniently. My sincerest thanks to all those who helped and guided me directly or indirectly.

Last but not the least, I thank my beloved father whose blessings helped me to complete my research despite of all the odds of life.

(Nimisha Dutta)

TABLE OF CONTENT

LIST OF TABLES

LIST OF FIGURES

LIST OF ABBREVIATIONS

AD	Amplitude Demodulation
AM	Amplitude Modulation
ANN	Artificial Neural Network
ARMAX	Autoregressive moving average exogenous
ART	Adaptive Resonance Theory
ARX	Autoregressive exogenous
AWGN	Additive White Gaussian Noise
CA	Cluster Analysis
DAQ	Data Acquisition
DFA	Discrete Fourier Transform
DFT	Discriminate Function Analysis
ECG	Electrocardiogram
EEG	Electro Encephalography
EMG	Electromyogram
FET	Field-effect transistor
FFT	Fast Fourier Transform
FIR	Finite Impulse Response
FIS	Fast Ion Sensor
FM	Frequency Modulation
GA	Genetic Algorithm
HFR	High Frequency Resonance
HMM	Hidden Markov Models
IIR	Infinite Impulse Response
LDA	Linear Discriminant Analysis
LMS	Least Mean Square
LSE	Least Square Error
LTI	Linear Time Invariant
LVQ	Linear Vector Quantization
MEG	Magneto Encephalography
MICS	Magnetospheric Ion Composition Sensor
MLP	Multi-Layered Perceptron

MLR	Multiple Linear Regression
MOS	Metal Oxide Semiconductor
MSE	Mean Square Error
NFS	Neuro Fuzzy System
NPF	Noise Population Figure
NSF	Noise Spread Figure
PARC	Pattern Recognition
PCA	Principal Component Analysis
PCR	Principal Component Regression
PDF	Probability Distribution Function
PEM	Prediction Error Minimization
PLS	Partial Least Square
PM	Phase Modulation
PSD	Power Spectral Density
PTC	Positive Temperature Co-efficient
QCM	Quartz Crystal Microbalance
RBF	Radial Basis Function
RLS	Recursive Least Square
RST	Rough Set Theory
RTS	Random Telegraph Signal
SAW	Surface Acoustic Wave
SNR	Signal-to-Noise Ratio
SOM	Self Organizing Map
SS	State-Space model
SSE	Sum-of-Squares Error
SVM	Support Vector Machine
SVR	Support Vector Regression
UST	Underground Storage Tank

CHAPTER 1

CHAPTER 1

INTRODUCTION

Over the past five decades, there has been an increasing demand for accurate, portable, reliable and inexpensive gas sensors that can discriminate between various types of gases such as CO, NO, NO_2, NH_4, SO_2, CO_2, CH_4 and other hydrocarbons. Historically, gas sensors were first primarily used in coal mines in the accurate monitoring of hazardous gases. Soon gas sensors began to appear in the chemical industry, environmental pollution monitoring units and in the human health sector. Some other important applications of gas sensors include the analysis of organic vapours, such as toluene, methanol and benzene, for laboratory and industrial safety[1] and, breathe analysis for traffic safety[2] and disease diagnosis. An electronic nose (E-Nose), based on an array of gas sensors for testing the smell of food, perfumes and artificial fragrances etc., is one of the more recent embodiments of gas sensing that has received much attention owing to its enhanced analytical power. In an optimized gas sensor design, the power consumption should be as low as possible and the heat losses owing to convection, conduction or radiation by the sensor heater should thus be minimized. In order to minimize the power consumption, the mass of both the heater and the sensor element must be reduced and optimization of the design must be done for uniformity of heating. With the advancement of micro- and nanofabrication techniques, sensors evolved from small catalytic bead platinum wire detectors and Taguchi gas sensors to micro- and nano- solid-state gas-sensing devices.

1.1 Gas measurement

Gases can be measured using objective, quantitative and standardized scientific methods in odour testing laboratories, however commercial gas detectors uses automatic sensing, calibrating and readout devices.

Odour can be measured basically by two methods:

i) Instrumental Analysis

ii) Chemical Sensor

For gas measurement, there have been instrumental methods which use instruments such as gas chromatograph to determine the gas concentration in ppm and gaseous molecules. But instrumental methods of measuring gas samples, such as gas chromatography/mass spectrometry (GC/MS), are expensive, time consuming and require trained personnel. As a result, for rapid and inexpensive analysis of gases, chemical sensors have become popular. Employing chemical sensors in an array form with pattern recognition capability provides a higher degree of selectivity leading to an extensive range of applications. When such systems are used for odour analysis they are termed as 'Electronic Nose' (E-Nose) which mimics the human or animal nose. The concept of biological processes implemented as artificial devices have made the human interpretation and understanding much easier. E-Nose offers an efficient way to analyze, compare and classify different odours. It is an instrument that consists of an array of electronic chemical receptors which detect volatile chemicals or categories of chemicals then uses the information to predict sensory-like properties. However, analysis and classification of gases using E-Nose is quite complex and require more computational effort.

Research is being carried on the development of E-Nose that automatically evaluate odour category, evaluate the intensity of odour regardless of its category and classify odours for the identification of odour sources by using unsupervised learning algorithms. Many research areas are focused on the sensor technology and better classification algorithm development. But the selection of sensors has often been ignored in most cases. It is seen that in most cases, a subset of sensors provides better recognition rate than the whole set of sensors. Hence, the number of sensors can be minimized for a certain application since the fewer number of sensors offers lesser cost and less computational time.

1.2 Gas Sensors

The phenomena occurring at the interface between solid and gas are used for operation of semiconductor sensors for the detection and quantitative determination of the composition of the gases. These sensors incorporate sensor element that reacts to

different gases. The odour recognition process in E-Nose begins in the senor system which is responsible for the measurement of the odourant stimulus through the sensitivity of its sensors. The area of gas sensors comprises of several different types of sensing materials that contribute to the gas sensor. Some of the commonly used gas sensors include, metal oxide semiconductor (MOS), conducting polymer sensors, surface acoustic wave (SAW) sensors, field-effect gas sensors, pellistors, and fibre-optic sensors.

1.3 Types of Sensors

Among the different types of sensors, conducting polymers, bulk acoustic devices and MOS are most commonly used.

a) Conducting Polymer Sensors:

An active material of conducting polymer of the family like polypyrolles, thiophenes, indoles, or furans is used in this type of sensors. These polymer sensors change their size and conductance to varying degrees under the influence of different gases. The polymer material is electropolymerized between two electrodes with a gap of about 10μm to 20μm. On application of odourants, the bonding of the molecules changes and affect the transfer of electrons along the polymer chain, causing a change in the conductivity. Conducting polymer sensors can work at ambient temperature and they do not need heaters like MOS gas sensors. However, the major disadvantage of such sensors is that the manufacturing of sensors by electro polymerization is difficult, time consuming and prone to be affected by humidity. Fig 1.1 shows a conducting polymer sensor.

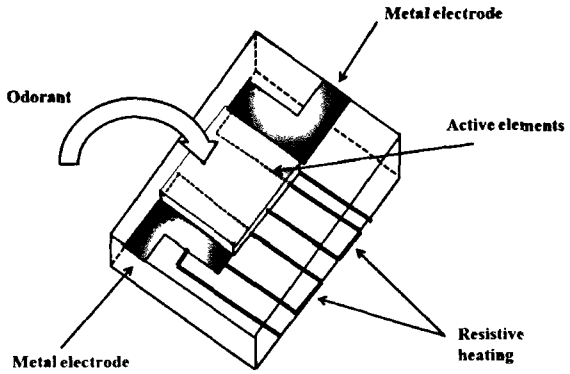

Fig. 1.1: Conducting Polymer Sensor.

b) Acoustic Sensors:

The most common acoustic sensors are- quartz crystal microbalance (QCM) and surface acoustic wave (SAW) devices as shown in Fig. 1.2 (a) and 1.2 (b) respectively. These sensors are operated by a mass changing principle. When exposed to the odourant, the surface of these sensors absorbs the gas molecules decreasing the resonance frequency of a resonating disc. On exposing to a reference gas the resonance frequency of the sensor comes back to its original value. The selectivity and sensitivity of the QCM sensor depends on the type of the polymer material coating. The size and mass of the quartz crystal can control the response and recovery time of the sensor. The SAW sensor operates at much higher frequency than the QCM sensor; hence the change in resonance frequency is also much higher in this sensor. A typical SAW sensor produces a resonant frequency of several hundred megahertz. Due to higher operating frequency, the signal-to-noise ratio is found to be less in SAW sensors. The only drawback of these types of sensors is that they require more complex electronic processing circuits compared to conductivity sensors.

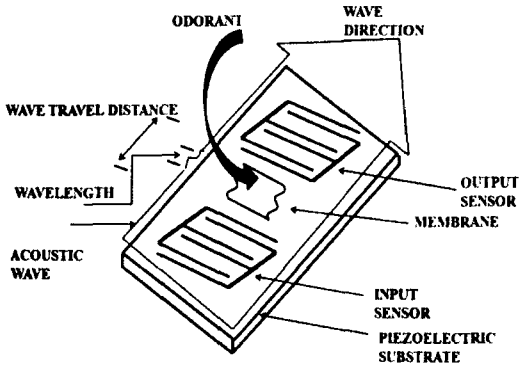

Fig. 1.2 (a) SAW sensor.

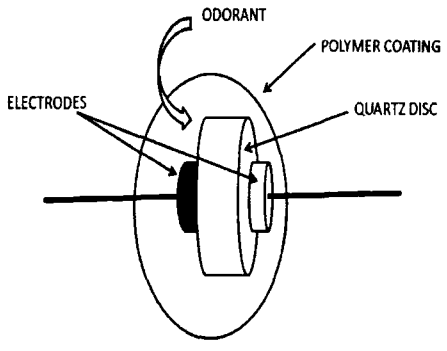

Fig. 1.2 (b) QCM sensor.

c) Metal Oxide Semiconductor (MOS) Sensors:

MOS gas sensors have been more widely used to make arrays for odour measurement than any other class of gas sensors. Although the oxides of many metals such as SnO_2, TiO_2, ZnO etc. show gas sensitivity under suitable conditions, the most widely used material is tin dioxide (SnO_2) doped with a small amount of a catalytic metal such as palladium or platinum. These sensors are based on change of resistance when exposed to volatile organic compounds. The cause of the change of sensor resistance is due to an ionosorption process and explained in terms of electron transfer from the semiconductor to adsorbed surface species. The adsorption process that is responsible for the sensor signal is strongly influenced by the presence of the pre-adsorbed species (like ionosorbed oxygen, hydroxyl groups, carbonates, etc.) and by only measuring the change of resistance upon exposure to the target gas the electrical effect of quite complex surface reactions is measured. MOS gas sensors are the most popular in E-Nose applications because of their low-cost and flexibility associated to their production, simplicity of their use, higher discriminating power and robustness. Upon exposure to an oxidizing substance, the surface of the MOS gas sensor undergoes a chemical reaction, which translates into a measured change in conductance across the sensor. The value of interest during the collection of data from the sensor is the change in voltage over a period of time. Although MOS gas sensors respond to a broad range of volatiles, they have higher affinity for aldehydes, alcohols and ketones and they are less responsive to molecules like terpenes, aromatic compounds or organic acids.

The basic principle of the device is that it allows gaseous compounds to react with the catalytic metal and produce species that are able to diffuse through the metal film and absorb onto a metal insulator. A reversible reaction occurs where the analyte binds to the surface of the sensing material. The binding is determined by the intermolecular forces between the analyte and the sensing material but is usually characterised by a hydrogen bonding. When the odour concentration is removed the analyte does not change but will dissociate from the sensing material. This type of reaction is similar to the interaction between odours and receptor proteins in biological systems. When an analyte undergoes a chemical change at the sensor surface, i.e. catalysis, irreversible reaction occurs. Sensors exhibiting such reactions are mostly the SnO_2 sensors having high sensitivity to specific odours. The change in the properties of the sensors causes

the change in conductivity. A typical response of a MOS gas sensor is shown in Fig. 1.3.

MOS gas sensors operate by binding molecules to the device surface through one or more mechanisms including adsorption, absorption, and chemisorption and co-ordination chemistry. The choice of binding mechanism has important implications for the selectivity and reversibility of the sensing system. Chemisorption is preferred when a highly selective system is required. The high binding strength will, however, result in poor reversibility. Chemisorption of oxygen molecules in the air environment takes place in the forms of O^{2-}, O^{-} and O^{2}. An equilibrium state exists among the chemisorbed species on the surface of SnO_2 at constant temperature. During the interaction of the sensing material with gas molecules to be detected, the conductance of the gas sensors varies. The surface reactions occur at low temperatures

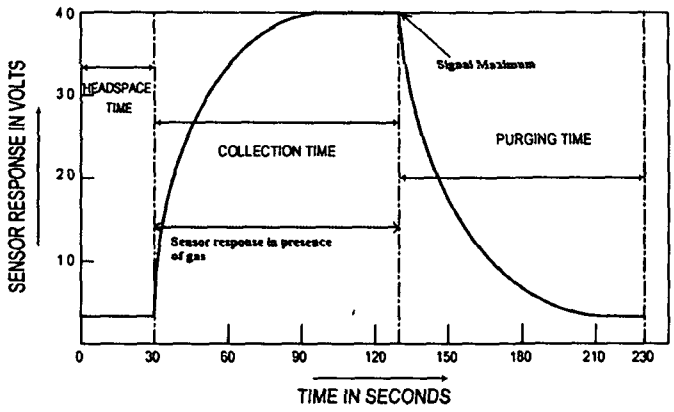

Fig 1.3: Response curve of E-Nose to the odourant molecules.

while at higher temperatures bulk reactions between point defects in the SnO_2 lattice and gaseous oxygen molecules takes place. Therefore the sensor material is heated upto a temperature of the order of 400°C to 600°C with the help of a heater mounted in the sensor module. In both cases, adsorption at active sites occurs first followed by some surface catalytic reactions. Similar reactions also occur at grain boundaries or at three-phase boundaries (i.e. at metallic contacts on surface metallic clusters). The differences in response patterns between the sensors are subjected to multivariate analysis and other statistical data processing, and classification of odour types are performed.

MOS gas sensors have attracted the attention of many researchers interested in gas sensing under atmospheric conditions due to the: low-cost and flexibility; simplicity of their use; large number of detectable gases/possible application fields[3–6]. The initial research on metal oxide-gas reaction effects was conducted by Heiland[7], Bielanski *et al.*[8] and Seiyama *et al.*[9] and the decisive step was taken when Taguchi brought semiconductor sensors based on metal oxides TiO_2, WO_3, SnO_2 and Ga_2O_3 powders and thick-films in particular to an industrial product Taguchi-type sensors[10]. Nowadays, there are a number of manufacturers producing this type of sensors, such as Figaro, Fast Ion Sensor (FIS), Magnetospheric Ion Composition Sensor (MICS), Underground Storage Tank(UST), CityTech, Applied- Sensors, New Cosmos, etc. The MOS gas sensors are typically used in ventilation control, combustible gas leak warning, and combustion control and breathe alcohol detection applications etc.

Recently MOS gas sensors are based on the micro hot plates (Fig.1.4(a)) fabrication using advanced silicon technology while conventional Taguchi gas sensors are based on ceramic fabrication processes (Fig.(1.4(b)). The advantages of micro hot plate MOS gas sensors are- faster start-up, faster response, lower power consumption, more accurate temperature control and more accurate detection and identification characteristics.

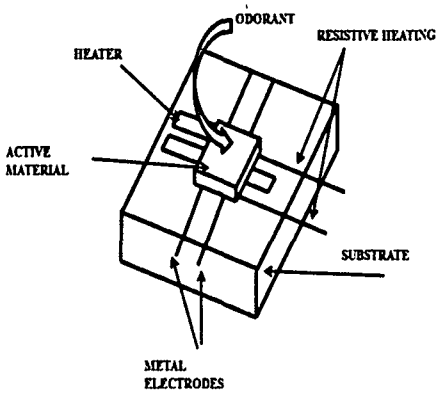

Fig. 1.4 (a) Micro-hotplate type MOS gas sensor.

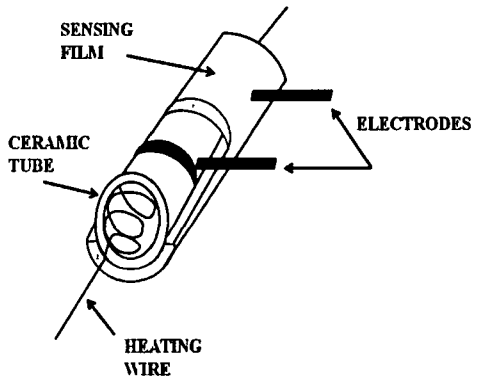

Fig. 1.4 (b) Ceramic type MOS gas sensor.

a) Field Effect Transistor Sensors:

Field Effect (FE) transistor operating in the diode coupled mode are also recently been used as gas sensors. The gas sensitive properties are achieved by depositing a catalytic metal stack on the device and the gate attains a gas sensing sensitivity. The

sensitive layer can be designed to be specific and sensitive to hydrogen containing toxic gases, such as NH_3, HCN and H_2S. Combinations of the dual device used are-

a) One FE sensor and one MOS gas sensor on the same header

b) Two different MOS gas sensors

The ideal gas sensor would exhibit reliability, robustness, sensitivity, selectivity and reversibility. As high selectivity with high reversibility in the sensors is difficult to attain, either a compromise is necessary or the sensor's detection layer must be regenerated. Today, the use of chemical sensors to measure and analyze odours is a growing field that attracts interests from the sensor and pattern recognition communities. A variety of sensing technologies are available and presently there are several different kinds of commercial electronic noses which use gas sensors for different applications.

1.4 Selectivity enhancement in MOS gas sensors:

The ideal MOS gas sensor would exhibit reliability, robustness, sensitivity and reversibility however; they are poorly selective and are prone to response drift[11]. Each metal-oxide sensor is primarily selective to one certain gas but it shows a small but non-zero cross sensitivity to other gases also [12]. Furthermore, it is also known from previous research work of different groups that the performance of almost all types of SnO_2 sensors is sensitive to the change in operating temperature[13, 14]. This property of sensitivity to operating temperature has been exploited by researchers to improve the selectivity of the sensor. This will be discussed in section 1.4.1. Hence, these properties of metal oxide sensors have to be taken into consideration when designing a gas measuring system. Moreover, they are influenced by water vapour, so changes in the moisture content of the atmosphere being monitored interfere with gas sensing.

In this thesis we have analysed two very important sensor characteristics-Noise features and Sensor dynamics based on temperature modulation to enhance the classification percentage of different gases.

1.4.1 Temperature Modulation

To improve the selectivity of sensor, the operating temperature of the MOS gas sensors have been widely investigated in many works. Researchers have also explored different ways to achieve selectivity either by enhancing gas adsorption or promoting specific chemical reactions via catalytic or electronic effects using bulk dopants, surface modification methods and by the addition of metallic clusters or oxide catalysts[15, 16]. The selectivity of chemical sensors can also be strongly influenced by the addition of metal clusters like platinum and palladium. These materials increase the sensor selectivity for reducing gases, e.g. CO[17]. Apart from material selection, one of the most established ways of enhancing the selectivity of MOS gas sensors is by periodically varying the sensors' operating temperature. Temperature modulation alters the kinetics of the sensor through changes in the operational temperature of the device. As the sensor response changes at different working temperatures, measuring the sensor response at different temperatures is similar to have an array of different sensors. Researchers have reported on the advantage of temperature modulation on a ceramic metal oxide sensor at two different temperatures to detect the presence of carbon mono-oxide [18-20]. Work has been carried on the temperature modulation using square wave to quantify hydrogen sulphide[21, 22]. To discriminate between different gases, modulating patterns of temperature such as sawtooth, triangular and square waves were also applied to the sensors[23]. The sinusoidal variation in the temperature also enhanced the classification of different gases. A number of works on the cyclic variations of the sensor heater voltage have been reported by many authors[24, 25]. The response of the gas sensors to modulating temperature primarily depends on the analytical model which is based on the physical and chemical properties of the sensor material. The development of micromachined substrates for MOS gas sensors ensured operating temperature modulated in a more efficient way. Cavicchi *et al* introduced the use of micromachined tin oxide gas sensors in temperature modulation applications[26-28]. In many works[29] quantitative analyses of gases with temperature modulated gas sensors have been reported.

1.5 Noise in MOS gas sensors:

The temperature profile of the MOS gas sensor surface greatly influence the response behavior due to rapid thermal fluctuations in respect of its noise and stability. The interference and noise in sensors and circuits may present a substantial source of errors and should be seriously considered. Noise in MOS gas sensor seriously influences the sensitivity and selectivity causing misclassification of gases. It has already been mentioned in section 1.4 that the MOS gas sensor dynamics basically consists of the thermal dynamics and the reaction kinetics. Therefore, the noise features are greatly influenced by the mentioned two factors-the thermal model and the chemical model inherent to the sensor. There are two basic classifications of noise for a MOS gas sensor: *inherent noise*, which is noise arising within the sensor, and *transmitted noise*, which is noise picked up from outside the sensor such as the measuring circuit.

1.5.1 Various kinds of Noise and Noise Sources

The odour recognition process in artificial nose begins in the senor system which is responsible for the measurement of the odourant stimulus through the sensitivity of its sensors. This odour classification process involves the data preprocessing which may give rise to a number of problems such as the disturbance of noise, and contamination of sensor signals by interfering signals present in the environment. Noise can arise at various stages in the measurement process, including the quantity under measurement itself; the sensors, the analog processing system, the data acquisition stage and the digital signal processing system. The noise developed during the early measurement stages is most harmful since it propagates and can be amplified during the later stages of the signal pathway. Several types of noise sources such as *thermal noise*, *popcorn noise*, *white noise*, *pink noise*, *shot noise* exists in MOS gas sensors. Other types of noise such as *transmitted noise*, *noise due to improper electric shielding*, *improper magnetic shielding*, *noise due to ground loops*, *quantization noise* and *seebeck noise* also exist in gas sensors.

1.5.1.1 Inherent noise

The different types of inherent noises are described as follows:

i) Thermal noise:

This type of noise arises from the thermal fluctuations in the electron density within a conductor. It is also known as Johnson or Nyquist noise and arises in any medium that dissipates energy. The charge carriers have thermal energy and they vibrate randomly with time and with respect to each other. As the charges move close together, the repulsion increases the potential energy of the electrons. A conductor with unoccupied electron shells, tend to lose electrons easily during reactions. The unfilled electron shells allow a higher energy electron to enter and be easily transferred across the lattice but with an occasional collision with an impurity atom. These collisions produce electrical resistance that varies with the change in temperature. At absolute zero condition, a pure metal forms a perfect lattice with no vibration. Hence, the electrical resistance is zero resulting in zero thermal noise. Thermal noise has a flat power spectral density (PSD) and is often termed as white noise. In addition to it, the amplitude distribution of thermal noise is Gaussian. In a resistor, these thermal motions cause thermal noise. The mean-square value of noise voltage can be calculated from the charge as:

$$\overline{e_n^2} = 4kTR\Delta f\left(\frac{V^2}{Hz}\right) \tag{1.1}$$

where k =1.38×10^{-23} J/K (Boltzmann constant), T is the temperature (in K), R is the resistance , and Δf is the bandwidth over which the measurement is made (in Hz). For practical purposes, noise density per $\sqrt{Hz}$ generated by a resistor at room temperature may be estimated from a simplified formula: $\overline{e_n} \approx 0.13\sqrt{R}$ in $nV\sqrt{Hz}$. A simple resistor can also be a source of noise. It behaves as a perpetual generator of electric signal. Naturally, relatively small resistors create extremely small noise. In some sensors, Johnson noise must also be taken into account. To reduce the noise, the bandwidths of the interfacing circuits must be just wide enough to pass the minimum required signal. The noise voltage should be proportional to the square root of the bandwidth. It means that reducing the bandwidth to 100 times, the noise voltage will be reduced by a factor of 10.

ii) Popcorn noise:

It is a type of electronic noise that arises in semiconductors. It is caused by defects that are dependent on the integrated-circuit manufacturing techniques. It is also termed as impulse noise, bi-stable noise, or random telegraph signal (RTS) noise. It consists of sudden step-like transitions between two or more discrete voltage and current levels, as high as several hundred microvolt, at random and irregular times. Each shift in offset voltage or current often lasts from several milliseconds to seconds. Its sound resembles like that of popcorn popping if hooked up to an audio speaker. Popcorn noise was first observed in contact diodes, and then re-discovered during the commercialization of one of the first semiconductor op-amps. The most common cause of popcorn noise is the random trapping and release of charge carriers at thin film interfaces. In cases where these charges have a substantial impact on transistor performance the output signal can be noteworthy. These defects can be caused by manufacturing processes, such as heavy ion implantation, or by unintentional side-effects such as surface contamination. Individual op-amps can be monitored for popcorn noise with peak detector circuits, to curtail the amount of noise in a specific application.

iii) White noise:

Since the spectral density of Johnson noise is constant over a broad range of frequencies, it is often called ***white noise*** because it is similar to white light. White noise is a random signal with a flat power spectral density. In other words, the signal contains equal power within a fixed bandwidth at any centre frequency. In statistical sense, a time series r_t is characterized as having weak white noise if $\{r_t\}$ is a sequence of serially uncorrelated random variables with zero mean and finite variance. Strong white noise is also independent and identically distributed, which implies no autocorrelation. In particular, if r_t is normally distributed with zero mean, the series is called a Gaussian white noise. The bandwidth of white noise is limited in practice by the mechanism of noise generation, by the transmission medium and by finite observation capabilities. A noisy random white noise is shown in Fig.1.5.

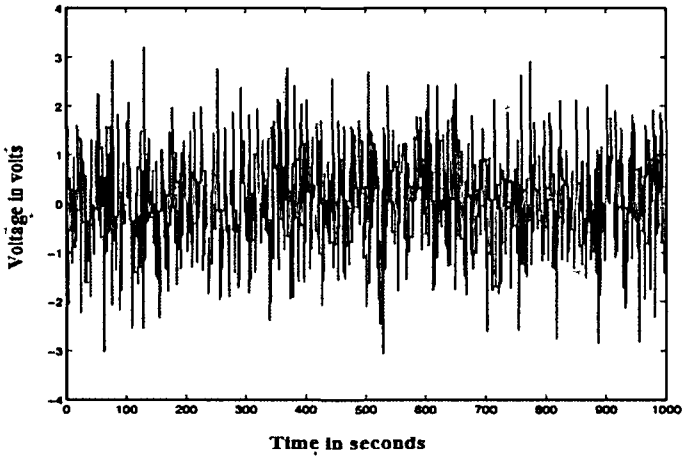

Fig.1.5: Gaussian white noise.

iv) Shot noise:

Another type of noise that arises from the random fluctuations in the number of charge carriers that cross a potential barrier in the charge flow is the Shot or Schottky noise. Shot noise is always associated with direct current flow. It is the result of dc currents across the potential barriers, such as in transistors or vacuum tubes. The noise results from the emission of electrons from the base of a transistor. It is also spectrally white Gaussian noise. Its value becomes higher with the increase in the bias current. This is the reason that field-effect transistor (FET) and CMOS semiconductors current noise is quite small. A convenient equation for shot noise is,

$$i_{sn} = 5.7 \times 10^{-4} \sqrt{I \Delta f} \qquad (1.2)$$

where I is a semiconductor junction current in picoamperes and Δf is a bandwidth of interest in hertz.

v) Pink noise:

Pink noise has a spectral envelope which is not flat with frequency but gradually decreases at higher frequencies. It contains a greater relative proportion of low frequency energy than white noise. Both the noise voltage and noise current sources have a spectral density roughly proportional to $1/f$. This type of noise occurs in all conductive materials and hence associated with resistors. At extremely low frequencies, it is impossible to separate the $1/f$ noise from dc drift effects. This noise is also called as flicker noise and usually prominent at frequencies below 100 Hz, where

many sensors operate and become barely noticeable at frequencies above a few hundred KHz where the white noise becomes more prominent. It may dominate Johnson and Schottky noises and becomes a main source of errors at these frequencies. The magnitude of pink noise depends on current passing through the resistive or semiconductive material. This type of noise can be reduced significantly. Fig.1.6 shows the spectral distribution of "pink noise".

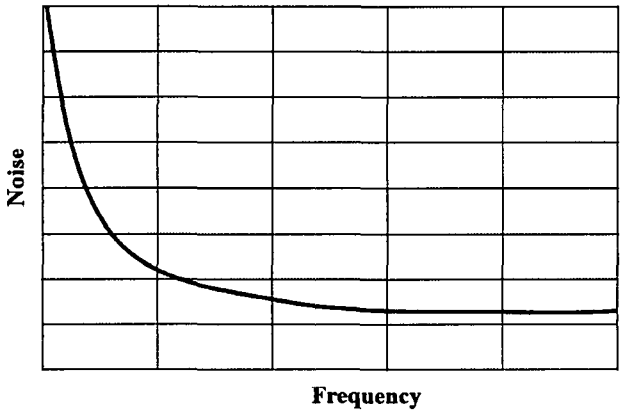

Fig.1.6: Spectral distribution of pink noise.

vi) Seeback noise

This noise is a result of the '*Seebeck effect*' which is actually the generation of an electromotive force (e.m.f.) when two dissimilar metals are joined together. The Seebeck e.m.f. is small and, for many sensors, may be simply ignored. The noise must be taken into account when absolute accuracy of the order of 10–100 μV is required. In a sensor the connection of any two dissimilar metals produces a temperature sensor which is a spurious signal. In electronic circuits, the connection of dissimilar metals can be found everywhere: connectors, switches, relay contacts, sockets, wires, and so on. In most cases, Seebeck e.m.f. may be eliminated by a proper circuit layout and thermal balancing. It is a good practice to limit the number of junctions between the sensor and the front stage of the interface circuit. Connectors, sockets, switches, and other potential sources of e.m.f. must be avoided as much as possible. When avoiding such connectors are not possible the number and type of junctions in the circuit's front stage should be such that differential cancellations occur.

1.5.1.2 Transmitted noise

A signal which is amplified and converted from a sensor into a digital form should be regarded both in terms of magnitude and spectral characteristics and also in terms of a digital resolution. In the measuring circuits, noise can be produced by the monolithic amplifiers and other components which are required for the feedback, biasing, bandwidth limiting, and so forth. Drift may be caused by input offset voltages and bias currents. Both noise signals (voltage and current) result from physical mechanisms within the resistors and semiconductors that are used in fabricating the circuits. In our measuring circuit, the transmitted noise arises out of the DAQ circuit, sensor biasing and potential divider circuit. The sources of this type of noise are voltage surges in power lines, lightning, and change in ambient temperature, sun activity, and so forth. These interferences propagate towards the sensor and the interface circuit, and finally appear at the output. However, they also affect the sensing element inside the sensor, its output terminals, or the electronic components in a circuit. The interferences are received by the sensor and the circuit. Transmitted noise can be classified depending on how it affects the output signal, how it enters the sensor or circuit, and onwards. Such noise can be either additive or multiplicative with respect to its relation to the output signals. Additive noise is added to the useful signal and mixed with it as a fully independent voltage (or current). Multiplicative noise affects the transfer function of the sensor or the circuit's nonlinear components as the voltage (or current) value. Transmitted noise may be periodic, or random, and it ordinarily may be reduced substantially by taking precautions to minimize electrostatic and electromagnetic pickup from power sources at line frequencies and their harmonics, radio broadcast stations, arcing of mechanical switches, and current and voltage spikes resulting from switching in reactive (having inductance and capacitance) circuits as discussed below:

1.5.1.3 Mechanical Noise:

Vibration and acceleration effects are also sources of transmitted noise in sensors. These effects may alter transfer characteristics (multiplicative noise) or they may result in the generation of spurious signals (additive noise) by a sensor. If a sensor incorporates certain mechanical elements, the vibration along some axes with a given frequency and amplitude may cause resonant effects. For instance, most pyroelectric

detectors also possess piezoelectric properties. The main function of the detector is to respond to thermal gradients; however, such environmental mechanical factors as fast changing air pressure, strong wind, or structural vibration cause the sensor generate an interference signal that is added to normal stimuli.

Transmitted noise may be reduced by proper shielding described below:

1.5.1.4 Electric shielding

Interferences attributed to electric fields can be significantly reduced by appropriate shielding of the sensor and circuit. It is very important to identify the noise source and how it is coupled to the circuit. Each shielding problem must be analyzed separately and carefully. A shielding affects in two ways. First, it limits noise to a small region which will prevent noise from getting into nearby circuits. However, the problem with such shields is that the noise captured by the shield can still cause problems if the return path that the noise takes is not provided through the ground system and making the connections correctly. Second, if noise is present in the circuit, shields can be placed around critical parts to prevent the noise from getting into sensitive portions of the detectors and circuits. These shields may consist of metal boxes around circuit regions or cables with shields around the center conductors.

1.5.1.5 Magnetic shielding

Noise resulting from electrostatic and electrical fields may be reduced by proper shielding. It is much more difficult to shield against magnetic fields because it penetrates conducting materials. A typical shield placed around a conductor and grounded at one end has little effect on the magnetically induced voltage in that conductor. As a magnetic field penetrates the shield, its amplitude drops exponentially. For improving low-frequency magnetic field shielding, a shield consisting of a high-permeability magnetic material should be used. However, noise still persists at higher frequencies and strong magnetic fields. An effective magnetic shielding can be accomplished with thick steel shields at higher frequencies. Since magnetic shielding is not very successful, the most effective approach at low frequencies is to minimize the strength of magnetic fields, minimize the magnetic loop area at the receiving end,

and select the best geometry of conductors. Magnetic fields are much more difficult to shield against than electric fields because they can penetrate conductive materials.

1.5.1.6 Ground loops and ground isolation

A circuit itself may generate enough noise when it is used for low-level input signals causing substantial measurement inaccuracy. Usually, conductors between electronic components are quite specific. They may connect a capacitor to a resistor, a gate of a JFET transistor to the output of an operational amplifier, and so forth. However, there are at least two conductors which, in most cases, are common for the majority of the electronic circuit. These are the power-supply lines and the ground lines. Both may carry undesirable signals from one part of the circuit to another; specifically they may couple strong output signals to the sensitive input stages. Grounding at two or more points may form ground loops; which minimizes the undesirable signals.

Thus to summarize, noise due to interferences such as fluctuations in the dc power supply, changes in the ambient temperature, capacitive or inductive couplings, and ground loops can be transmitted. To reduce electromagnetic interference noise, careful design and construction of electronic circuits, with proper shielding and grounding must be done. Differential measurements are useful techniques to reduce low-frequency noise at the expense of amplifying high-frequency components.

The inherent drift and poor repeatability of the gas sensor responses can sometimes be significantly larger than most other noise sources which effectively reduce the sensitivity of the electronic nose systems. The noise generated in E-Nose may result in an inaccurate classification of the tested odours. Some noise also comes from factors related to the MOS gas sensors themselves such as sensor age, exposure to water and excess voltage, the bulk dissolution of surface atoms, mechanical wear and fatigue, self-heating, poisoning, and oxidation. On the other hand, the impact on various gas sensors from environmental factors is not uniform, therefore, system parameters should be properly adjusted in the de-noise process[30].

The accuracy of a sensor depends on its noise floor. To attain the lowest noise floor and highest *S/N* ratio, component-level noise sources must be analyzed and considered when calculating the overall noise of the system. When a signal is measured through a

sensor, there is a tendency for the low amplitude part of the signal to be corrupted by sensor noise. Researchers have tried several attempts for the noise removal and signal recovery of the sensor systems using different filtering techniques[31-34].

Noise in gas sensors is considered to be any unwanted effect that obscures the detection of the desired gas. It can arise at various stages of the measurement process the sensors, the analog processing system, the data acquisition stage and the digital signal processing system out of which the noise in the sensors is most harmful as it propagates and can be amplified through the subsequent stages. In this thesis, we make the statistical and frequency analysis of noise under pulse modulated heater voltage of MOS gas sensor based electronic nose and noise compensation using amplitude demodulation technique.

1.5.2 Noise Parameters:

Random processes are best described by their statistical properties. Mostly, noise is characterised by its statistical parameters such as mean, standard deviation, Probability Distribution Function (PDF), histogram, Signal-to-Noise Ratio (SNR) etc. Many works have been reported on the modeling of noise using the statistical features of noise. In[35] the noise was modeled considering the statistical characteristics of the noise. The analysis of the noise showed that the distribution of the amplitude of the disturbance is nearly Gaussian. In most of the cases of image processing, we do not have a priori knowledge on the nature of the noise and its statistical parameters[36]. For this reason the statistical parameters of the noise must be estimated as they state the quality of the filtering or the analysis of the images[37]. The identification of the nature of the noise is possible by measuring the variations of statistical parameters such as the standard deviation computed in the homogeneous regions of the observed image[38]. The noise identification is possible by the estimation of the statistical parameters of noise. The PDF shows how the measured data depends on the parameters to be estimated, and how the data is corrupted by random errors or noise. Histograms, which show the probability distribution of parameter values shows the distribution of amplitude values of noise by plotting the number of values within fixed amplitude ranges or bins. Statistical analysis is often used to explore the data such as to examine the distribution of values for a particular aspect. This information is useful for defining

classes and ranges of data, reclassifying data, or analyzing data errors. Thus, statistical analysis reveals the characteristics of the noise features as a whole.

1.5.2.1 Probability Distribution Function (PDF)

The behavior of a random variable is characterized by its probability distribution, that is, by the way probabilities are distributed over the values it assumes. The fluctuations of a purely random signal, or the distribution of a class of random signals in the signal space, cannot be modeled by a predictive equation, but can be described in terms of the statistical average values, and modeled by a probability distribution function in a multidimensional signal space.

We specify a function $P_x(x)$, called the probability density function (PDF) of a random variable X, such that the probability that the random variable X takes a value in a set A (of real numbers) is given by-

$$P[X \in A] = \begin{cases} \Sigma_{x \in A} f(x) & \text{for all sets } A \text{ if } X \text{ is discrete} \\ \int_A f(x)dx & \text{for all intervals } A \text{ if } X \text{ is continuous} \end{cases} \quad (1.3)$$

If A be the set of all values that are less than or equal to a fixed value t (i.e., $A = (-\infty, t]$), the probability function $P[X \leq t]$, denoted by $F(t)$, is called the distribution function of X.

For the data range $-\infty \leq x \leq 1$, the probability lies between 0 to 1, given by,

$$0 \leq P_x(x) \leq 1 \quad (1.4)$$

The PDF of a signal always satisfies the condition that-

$$\int_{-\infty}^{+\infty} P_x(x)dx = 1 \quad (1.5)$$

If the PDF of a signal is known, the probability of the signal falling within a range can be determined by-

$$P(x_1 < x < x_2) = \int_{x_1}^{x_2} P_x(x)dx \quad (1.6)$$

For a sensor system which can develop a large number of noise data, its PDF can be assumed to be Gaussian, however such statistics may not be obtained for less number of data. The PDF of Gaussian function with mean μ and standard deviation σ can be represented by the Fig.1.7.

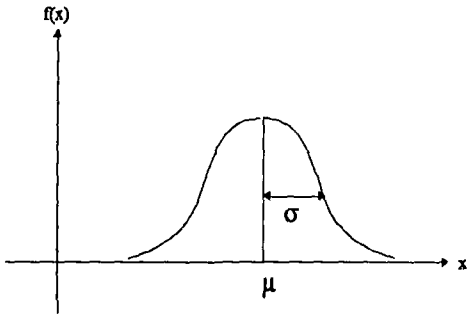

Fig.1.7: PDF of Gaussian distribution.

1.5.2.2 Histogram

When there are a large number of observed data, a histogram is an excellent graphical representation of the data, facilitating;

(a) an evaluation of adequacy of the assumed model,
(b) estimation of percentiles of the distribution, and
(c) estimation of the distribution parameters.

The vertical axis of a histogram can represent either the class frequency or the relative class frequency; in the former case the graph is called a frequency histogram and in the latter a relative frequency histogram. The construction of the histogram of a measured data is as follows. Let us denote a generic (univariate) dataset of size n by,

$$x_1, x_2, \quad , x_n$$

and then the range of the data is divided into intervals called bins denoted by,

$$B_1, B_2, \quad , B_m$$

The length of an interval B_i is denoted by $|B_i|$ and is called the bin width. The area under the histogram on each bin B_i reflects the number of elements in B_i. The histogram of a random data set results a Gaussian distribution when the number of samples is large. Hence from definition of histogram, the sum of all the values in the histogram must be equal to the number of data points N, in the signal given by,

$$N = \sum_{i=0}^{M-1} H_i \tag{1.7}$$

where H_i represent the histogram and i is an index from *0* to *M-1*, and M is the number of possible values that each sample can take. The histogram can be used to calculate the mean and standard deviation of a large data set. The mean μ and standard deviation σ are calculated from the histogram by the equations:

$$\mu = \frac{1}{N} \sum_{i=0}^{M-1} iH_i \tag{1.8}$$

$$\sigma^2 = \frac{1}{N-1} \sum_{i=0}^{M-1} (i-\mu)^2 \tag{1.9}$$

In this study the histogram of the sensor data was used to compute the mean, standard deviation and variance of the sensor noise for different pulse modulated heater voltage.

1.5.2.3 Signal-to-Noise Ratio

Signal-to-noise ratio (SNR) expresses the relationship between signal and noise powers, as well as between the root-mean-square (rms) values of signal and noise voltages given by:

$$\text{SNR (dB)} = 10 \log_{10} \left(\frac{P_s}{P_n} \right)$$

$$\text{SNR (dB)} = 20 \log_{10} \left(\frac{V_s(rms)}{V_n(rms)} \right)$$

where P_s and P_n are the power of the signal and noise respectively and V_s and V_n are the signal and noise voltage respectively.

The signal-to-noise ratio (SNR) is used to characterize the quality of the signal detection of a measuring system. It is an important characteristic of a system to express the quality of the output signal and that the best relation between it and the input signal is achieved when the ratio of the SNR at the output versus the input is highest.

1.5.2.4 Noise Modeling

Noise may be defined as any unwanted signal that interferes with the communication, measurement or processing of an information-bearing signal. Noise is present in various degrees in almost all systems and environments. The modeling of noise characterises the structures and the patterns of a noise process. To model noise accurately, a structure for modeling is required for both the temporal and the spectral characteristics of noise. Accurate modeling of noise statistics is the key to achieving high quality signals.

One of the most useful and vital tools for gaining insight into the structure of a noise process is the use of *Fourier transform* for frequency analysis. The FFT of noise reveals whether the noise is a low frequency noise or a high frequency noise and hence determines the type of noise. In current practice, the simplest method for noise modeling used is to estimate the noise statistics from the signal-inactive periods. In best Bayesian signal processing methods, a set of probability models are trained for the signal and the noise processes. The models are then used for the decoding of the underlying states of the signal and noise, and for noisy signal recognition and enhancement.

In measurement systems, it is often assumed that the noise is a stationary additive white Gaussian (AWGN) process. Although for some problems this is a valid assumption and leads to mathematically convenient and useful solutions, in practice the noise is often time-varying, correlated and non-Gaussian. This is particularly true for impulsive-type noise which is non-stationary and non-Gaussian and hence AWGN assumption is not valid. Non-stationary and non-Gaussian noise processes can be modeled by a Markovian chain of stationary sub processes. Most sensor noise is non-stationary in nature i.e. the statistical parameters of the noise, such as its mean, variance and power spectrum, vary with time and may be modeled using the *hidden Markov model*s (HMMs). An HMM is essentially a finite state Markov chain of stationary sub processes by which the noise can be modeled. For a non-stationary noise, a multistate HMM can model the time variations of the noise process with a finite number of stationary states. For non-Gaussian noise, a mixture Gaussian density model can be used to model the space of the noise within each state.

1.5.2.5 Noise Filtering and Compensation

Noise Filtering is a signal processing operation to retrieve the pure signal from the corrupted signal. In other words, a filter maps its input signal to another output signal facilitating the extraction of the desired information contained in the input signal. *Sensor noise compensation* mechanisms are important for improving sensor response. In case of time-invariant filters the internal parameters and the structure of the filter are fixed, and if the filter is linear the output signal is a linear function of the input signal. Noise removal or noise reduction can be done by filtering, by wavelet analysis, or by multifractal analysis. Conventional linear system adaptive filtering techniques have been widely used in adaptive noise reduction problems. However, because of the linearity of the operation, the filter cannot change the intrinsic property of the original noisy signal, such as regularity, etc. However, there are situations where the specifications are time varying. The solution in these cases is to employ a digital filter with adaptive coefficients, known as adaptive filters[39-45]. Adaptive filters are used for non-stationary signals and environments, the applications of which include multichannel sensor noise reduction, radar/sonar signal processing, and channel equalization for cellular mobile phones, echo cancellation, and low delay speech coding. Different adaptive filter schemes include:

a) State-Space Kalman Filters
b) Sample-Adaptive Filters
    i) Recursive Least Square (RLS) Adaptive Filters
    ii) The Steepest-Descent Method
    iii) The Least Mean Square (LMS) Filter

a) State-Space Kalman Filters

These types of filters can be used with time-varying as well as time-invariant processes. Kalman filter theory is based on a state-space approach in which a state equation models the dynamics of the signal process and an observation equation model for the noisy signal. For a pure signal $x(m)$ and noisy observation $y(m)$, the state equation model and the observation model are defined as-

$$x(m) = \Phi(m, m-1)x(m-1) + e(m) \tag{1.10}$$

$$y(m) = H(m)x(m) + n(m) \tag{1.11}$$

where, $x(m)$ is the n-dimensional state parameter of the signal, vector at time m, $\Phi(m, m-1)$ is an $n \times n$ dimensional state transition matrix that relates the states of the process at times $m-1$ and m,

$e(m)$ is an n-dimensional uncorrelated input excitation vector of the state equation,

$y(m)$ is the m-dimensional noisy and distorted signal observation vector,

$H(m)$ is the $m \times n$ channel distortion matrix,

$n(m)$ is the m-dimensional additive noise process.

The filter derivation assumes that the state transition matrix $\Phi(m, m-1)$, the channel distortion matrix $H(m)$.

The Kalman filter is the best estimator for a large class of problems and a very effective and useful estimator for an even larger class. With a few theoretical tools, this filter is very easy to use. The Kalman filter is essentially a set of mathematical equations that implement a predictor-corrector type estimator that is best in the sense that it minimizes the estimated error covariance provided some presumed conditions are met. The filter is relatively simple and robust in nature. For nonlinear systems it is not possible, in general, to implement the best state estimator in closed form, but various modifications of the Kalman filter can be used to estimate the state. One disadvantage of this approach is that the physical meaning of the state variables may be lost.

b) Sample-Adaptive Filters

They have a number of advantages over the block-adaptive filters, including lower processing delay and better tracking of non-stationary signals. These are essential characteristics in applications such as echo cancellation, adaptive delay estimation, low-delay predictive coding, noise cancellation, radar, and channel equalisation in mobile telephony. An adaptive filter starts at some initial state, and then the filter coefficients are periodically updated so as to minimise the difference between the filter

output and a target signal by recursive algorithm. In adaptive filtering the filter type model and the adaptation algorithm are as follows:

Filter type:

A filter can be a finite impulse response (FIR) filter, or an infinite impulse response (IIR) filter. FIR filters have good stability and convergence properties and hence often used in practice.

Filter order:

The maximum delay, in samples, used in creating each output sample is termed as the order of the filter. It can also be defined as the order of its transfer function. The filter order is either set by using a prior knowledge of the input and the desired signals, or it may be obtained by monitoring the changes in the error signal as a function of the increasing filter order.

Adaptation algorithm:

The two most widely used adaptation algorithms are the RLS error and the LMS methods. The factors influencing the choice of the adaptation algorithm are the computational complexity, the speed of convergence to best operating condition, the minimum error at convergence, the numerical stability and the robustness of the algorithm to initial parameter states. The following are the very common adaptation algorithm:

i) Recursive Least Square (RLS):

The RLS filter is a sample-adaptive, time-update, version of the Wiener filter. For stationary signals, the RLS filter converges to the same best filter coefficients as the Wiener filter. For non-stationary signals, the RLS filter tracks the time variations of the process. The RLS filter has a relatively fast rate of convergence to the best filter coefficients which is useful in applications such as speech enhancement, channel equalization, echo cancellation and radar where the filter should be able to track relatively fast changes in the signal process.

ii) The Steepest-Descent Method

The mean square error surface with respect to the coefficients of an FIR filter is a quadratic bowl-shaped curve, with a single global minimum that corresponds to the LSE filter coefficients. The steepest-descent search for the minimum mean square error coefficient is based on taking successive negative gradient of the error surface. Starting with a set of initial values, the filter coefficients are updated successively in the downward direction, until the minimum point, at which the gradient is reached at zero.

iii) The Least Mean Square (LMS)

A computationally simpler version of the gradient search method is the LMS filter, in which the gradient of the mean square error is substituted with the gradient of the instantaneous squared error function. The main advantage of the LMS algorithm is its simplicity both in terms of the memory requirement and the computational complexity. The LMS has a disadvantage that for signals with a large spectral dynamic range the convergence is uneven and slow.

The selection of the noise reduction technique is application dependent. So, it is necessary to learn and compare the filtering techniques to select the one that is appropriate for the application in which we are interested. If the features of the filtered signal are fed into a neural network pattern recognizer, then the rate of successful classification should determine the ultimate measure by which to compare various filtering techniques. Another filter is the moving average filter which is a very useful one for many applications. It is best for a common problem, reducing random white noise while keeping the sharpest step response. A Kalman filter works similar to a moving average, except that the lag is much less; and it works by adjusting itself to the level of noise, rather than a fixed averaging length. A number of works have been reported in recent years on the reduction of noise by various de-noising methods. A novel method of noise reduction is proposed for charge amplifiers in imaging and sensor systems[46], which are referred to as zero-pole modulation and demodulation. Here, the input signal is passed through a zero-pole system without being modified, the output noise of the charge amplifier being reduced by the demodulation. In another work[47], numeric amplitude-demodulation based technique was employed to enhance

simple electromagnetic analyses. The analysis was based on amplitude demodulation and bandpass filtering processes. It led to the removal of the clock harmonics and some noise sources hence allowing the efficient disclosing of the leaking information. In[48], a new modulation technique that is based on switching on and off the power supply voltage of the amplifier is employed which can also be applied also to self-generating sensors. Here, the chopping of the amplifier gain via the power supply voltage is done. To reduce the flicker noise, the amplified signal was then synchronously demodulated and low-pass filtered. A modulation / demodulation system is also proposed in[49] to modulate the $1/f$ noise in capacitive sensors, to a higher frequency and then the noise modulated sensor signal is low-pass filtered. However, the recovery of the original signal from the noisy signal by the amplitude demodulation (AD) technique in case of MOS gas sensors has not been reported so far.

1.6 Sensor Dynamics

The dynamic behavior of the sensors determines the performance of the sensor. The sensor response to a variable input is different from that exhibited when the input signals are constant. The response of gas sensors to odourants is generally regarded as a first order time response. When the sensor is exposed to the odorant, a change in its output signal occurs steady-state is reached. After removing the odour the sensor returns back to its baseline as shown in Fig. 1.8. The time during which the sensor is exposed to the odorant is referred to as the response time while the time it takes the sensor to return to its baseline resistance is called the recovery time. The sensor dynamics gives information about the important parameters i.e. response and recovery time of the sensor. In fact the reason for dynamic characteristics is the presence of analogous energy-storing elements such as inertial masses, inductances, electrical and thermal capacitances. By analyzing the response of the sensor to different variable input waveforms such as impulse, step, ramp, sinusoidal the dynamic characteristics are determined.

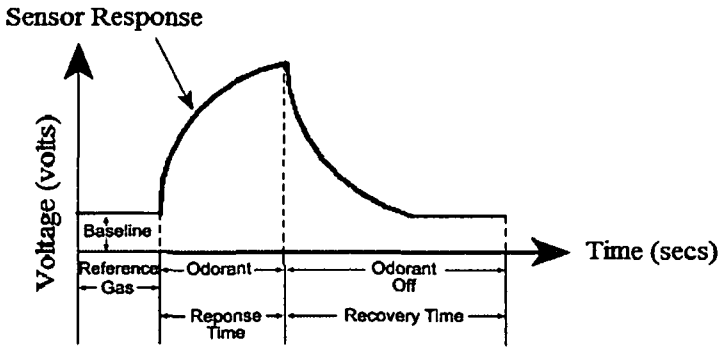

Fig.1.8: Sensor response to an odourant.

1.6.1 Adsorption Kinetics

To understand the dynamics of a MOS gas sensor, it is necessary that we analyse how the sensor works with gas adsorption kinetics which is discussed here.

A MOS gas sensor comprises of a sensitive metal-oxide layer deposited on a substrate with Pt or Au electrodes for measuring the electrical characteristics of the device. The sensors posses an in-built heater, separated from the sensing layer and the electrodes by an electrically insulating layer. The heater elevates the operating temperature of the sensor to 200°C–400°C. We have used Taguchi MOS gas sensors in our work which consist of an electrically heated ceramic pellet, onto which a thin porous film of SnO_2 doped with metal ions has been deposited[50]. The doped SnO_2-film behaves as an n-type semiconductor and due to chemisorption of oxygen at the sensor surface results removal of electrons from the conducting band, takes place. The resistance change of the oxide layer happens due to combustion reactions within the lattice oxygen species on the surface of metal oxide particles. Fig. 1.9 shows typical changes in conductivity of n-type MOS gas sensors for O_2 and CH_4. In (a) when oxygen dissolves in the sensors surface, the resistance increases to the reference or background level. In (b), the reaction of a volatile compound with the surface is shown that creates a decrease in resistance.

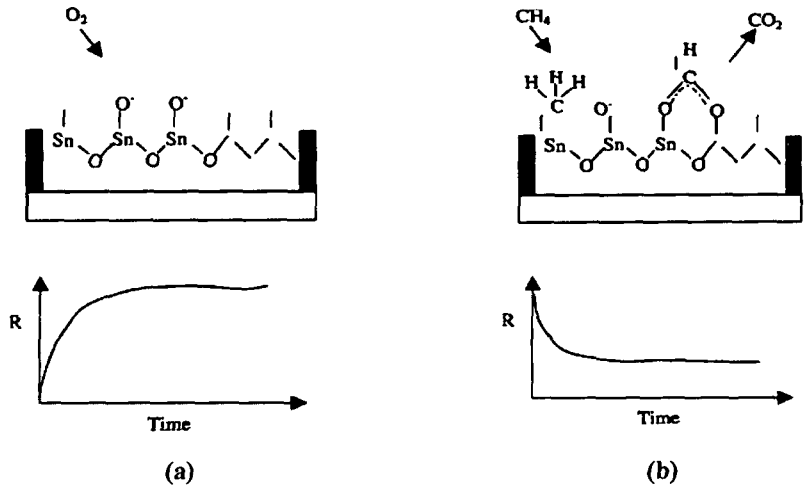

Fig. 1.9: Resistance changes due to the interaction of a volatile compound with the surface of a MOS gas sensor (a) for O_2 and (b) CH_4.

The MOS gas-sensing materials are typically n-type semiconductors that develop an electron-depleted surface layer. This depletion layer is caused by atmospheric oxygen and at high temperature oxygen adsorbs electrons from the MOS film surface to form reactive O^{-2} or O^- species. The gas molecules in the applied gas react with the reactive oxygen species at the MOS surface and affect the depletion layer thickness leading to measurable changes in the resistance of the material. Reducing gases like CO and H_2 react with the highly sensitive MOS surface and remove some of the chemisorbed oxygen as a result electrons are injected back into the MOS, which reduces the thickness of the depletion layer. Oxidizing gases such as NO_2, on the other hand, draw even more electrons from the sensor surface, thereby increasing the thickness of the depletion region[51]. Any such infinitesimal changes in the depletion layer thickness affect the overall resistance of the MOS material, which is measured using simple and inexpensive electrical circuitry.

The sensing unit of the MOS gas sensor features a heating element that provides the desired temperature for adsorption and desorption of oxygen gas and for reaction of the analyte gases with those reactive adsorbed oxygen species. This heating element which can be a platinum or platinum alloy wire, a resistive metal oxide, or a thin layer of deposited platinum, is used to regulate the sensor temperature, since the sensors exhibit different gas response characteristics at different temperature ranges. The sensor is then elevated at a specific high temperature which determines the specific

characteristics of the sensor. When the heater is elevated to a sufficient temperature, the oxygen is adsorbed on the surface with a negative charge. The donor electrons are transferred to the adsorbed oxygen thus leaving a positive charge in the layer. The reactions at the heated MOS surface change the concentration of electrons in the MOS film depletion layer. This in turn changes the conductance of these devices as a function of the concentration of the gases. In the presence of gases, the metal oxide causes the gas to dissociate into charged ions or complexes which results in the transfer of electrons. The built-in heater, which heats the metal oxide material to an operational temperature range that is best for the gas to be detected, is regulated and controlled by a specific circuit. These gas-induced resistance changes are influenced by many material-related factors such as the type of semiconductor oxide material, oxide film thickness, grain size, porosity, material sintering temperature and time, catalyst type and catalyst particle distribution.

1.6.2 Sensor Models

System Identification aims to determine particular models for dynamical systems based on observed inputs and outputs. Although dynamical systems in the physical world are naturally described in the continuous-time domain, most system identification schemes have been based on discrete-time models without concern for the merits of natural continuous-time model descriptions. System Identification has been extensively studied in the past, and is of major importance in diverse fields of signal processing[52-60]. The major advantage of system identification technique is how easily stability and transient response information could be extracted from them. In other words, the theory and methods to determine pole location (root locus, lead-lag blocks) in order to shape a systems response and to determine the system stability were well understood. There are three basic models used for system identification:

i) Autoregressive with exogenous inputs (ARX)

ii) Autoregressive moving average model (ARMAX)

iii) State-space (SS) model.

i) Autoregressive with exogenous inputs (ARX) models:

The ARX model is the simplest model that incorporates the stimulus signal. However, this model captures some of the stochastic dynamics as part of the system dynamics. A multivariable linear, stochastic model is represented by a linear differential equation as:

$$Y(k) = \sum_{i=1}^{n_a} a_i y(k-i) + \sum_{i=1}^{n_b} b_j u(k-i) + \sum_{i=1}^{n_c} c_k e(k-i) \tag{1.12}$$

where n_a, n_b, and n_c are, respectively, AR, X, and MA orders. The function a_i is the pulse response function from the past outputs to the present output $y(k)$, and b_i and c_i are the pulse response from the past and present inputs $u(k)$ and noise $e(k)$, respectively, to the present outputs. ARX is a parametric models with $c_i = 0$ and with exogenous inputs (ARX). The linear regression can be used for model parameters estimation. The identification method for the ARX model is the least squares error (LSE) method, which is a special case of the prediction error minimization (PEM) method described later in this chapter.

i) Autoregressive moving average models with exogenous inputs (ARMAX):

Autoregressive moving average models with exogenous inputs (ARMAX) models are used for the estimation of the order and the model structure of the system using all relevant information such as the measurable input/output variables, internal variables of the system, measurable disturbance, and even the phenomenological information of the system. For eqn. (1.12), ARMAX is an autoregressive moving average model with (ARMAX) and all the coefficients a_i, b_i, and c_i are estimated. There are various estimating methods of ARMAX models such as pseudo linear regressive, correlation methods, subspace methods, etc.[61].

iii) State-Space (SS) models:

The state-space model of a continuous-time dynamic system can be derived either from the system model given in the time domain by a differential equation or from its

transfer function representation. The state space form is a powerful way to represent a system[62]. Let us consider the state space system:

$$\begin{aligned} \dot{x}(t) &= Ax(t) + Bu(t) \\ y(t) &= Cx(t) + Du(t) \end{aligned} \tag{1.13}$$

This system of first-order differential equations is known as the state equation of the system and $x(t)$ is the *state vector* and $u(t)$ is the *input vector*. The second equation is the *output equation*. Here,

A= state matrix; B=input matrix; C=output matrix; D=direct transition matrix.

The state-space model is useful for the analysis of nonlinear systems. The state equations may be obtained from an n^{th} order differential equation or directly from the system model. Since the system identification has been performed from the discrete data of input-output, the discrete state space model is more relevant than continuous time model. The discrete state-space model is given by:

$$x(KT+T) = Ax(KT) + Bu(KT) \tag{1.14}$$

$$Y(KT) = Cx(KT) + Du(KT) \tag{1.15}$$

where K is the sampling instant and T is the sampling interval.

Representing $x(KT)$ as $x(k)$ Eqn.(1.14) and (1.15) reduces to,

$$x(k+1) = Ax(k) + Bu(k) \tag{1.16}$$

$$y(k) = Cx(k) + Du(k) \tag{1.17}$$

Let us consider a scalar differential equation:

$$y(k+n) + a_1 y(k+n-1) + a_2 y(k+n-2) + ...a_{n-1} y(k+1) + a_n y(k) = bu(k) \tag{1.18}$$

where k denotes the k^{th} sampling instant, $y(k)$ is the system output at the k^{th} sampling instant and $u(k)$ is the input at the k^{th} sampling instant. Here $bu(k)$ is termed as the forcing function.

Defining the terms as,

$$x_1(k) = y(k)$$
$$x_1(k+1) = x_2(k)$$
$$x_2(k+1) = x_3(k)$$
.....
$$x_{n-1}(k+1) = x_n(k)$$
$$x_n(k+1) = -a_1 x_n(k) - a_2 x_{n-1}(k) - ..... - a_n x_1(k) + bu(k)$$

Then eqn.(1.18) can be written as-

$$\begin{bmatrix} x_1(k+1) \\ x_2(k+1) \\ \vdots \\ x_{n-1}(k+1) \\ x_n(k+1) \end{bmatrix} = \begin{bmatrix} 0 & 1 & \cdots & 0 & 0 \\ 0 & 0 & \cdots & 0 & 0 \\ \vdots & \vdots & \cdots & \vdots & \vdots \\ 0 & 0 & \cdots & 0 & 1 \\ -a_n & -a_{n-1} & & -a_2 & -a_1 \end{bmatrix} \begin{bmatrix} x_1(k) \\ x_2(k) \\ \vdots \\ x_{n-1}(k) \\ x_n(k) \end{bmatrix} + \begin{bmatrix} 0 \\ 0 \\ \vdots \\ 0 \\ b \end{bmatrix} [u(k)]$$

$$y(k) = \begin{bmatrix} 1 & 0 & \cdots & 0 \end{bmatrix} \begin{bmatrix} x_1(k) \\ x_2(k) \\ \vdots \\ x_{n-1}(k) \\ x_n(k) \end{bmatrix}$$

or
$$x(k+1) = Ax(k) + Bu(k)$$
$$y(k) = Cx(k)$$

where, $x(k) = \begin{bmatrix} x_1(k) \\ x_2(k) \\ \vdots \\ x_{n-1}(k) \\ x_n(k) \end{bmatrix}$, $A = \begin{bmatrix} 0 & 1 & \cdots & 0 & 0 \\ 0 & 0 & \cdots & 0 & 0 \\ \vdots & \vdots & \cdots & \vdots & \vdots \\ 0 & 0 & \cdots & 0 & 1 \\ -a_n & -a_{n-1} & & -a_2 & -a_1 \end{bmatrix}$, $B = \begin{bmatrix} 0 \\ 0 \\ \vdots \\ 0 \\ b \end{bmatrix}$,

$C = \begin{bmatrix} 1 & 0 & \cdots & 0 \end{bmatrix}$

The Linear Time Invariant (LTI) system can be represented in continuous time transfer function as-

$$y(t) = Hu(t) \tag{1.19}$$

where the transfer function H in Laplace domain can be represented using state-matrices as-

$$\hat{H}(s) = C(sI - A)^{-1}B + D \tag{1.20}$$

where I is the identity matrix. This eqn.(1.21) can be reduced to a form,

$$\hat{H}(s) = \frac{b_0 s^m + b_0 s^{m-1} + ... + b_m}{s^n + a_1 s^{n-1} + ... + a_n} \tag{1.21}$$

Further the z-transform of the LTI model can be represented as-

$$\hat{H}(z) = \frac{b_0 z^m + b_1 z^{m-1} + ... + b_m}{z^n + a_1 z^{n-1} + ... + a_n} \tag{1.22}$$

State space model provides a suitable starting point for identification of the nonlinear dynamics of the system.

1.6.3 Stability and Transfer Functions

An LTI system is stable if the output eventually comes back to its equilibrium state when the system is subjected to an initial condition. To analyze the stability, the poles are determined and if the poles lie in the left half of the complex frequency plane and have negative real parts, the system is stable. The most important characteristic of the dynamic behavior of a system is its stability. An LTI system is stable if the output eventually comes back to its equilibrium state when the system is subjected to any input or disturbance.

1.6.3.1 Step and Impulse Response

Step Response: The *step* responses are used in practice to capture the transient responses of a system. It describes how the system reacts to disturbances and, qualitatively, about the system stability. The response of an LTI system to a unit step is given by[63]:

$$h_{-1}(t) = h(t) * u(t) = \int_{-\infty}^{\infty} h(\tau)u(t-\tau)d\tau = \int_{-\infty}^{\infty} h(\tau)d\tau \tag{1.23}$$

which shows that the response at any time t of an LTI system stimulated by a unit step is the integral of the impulse response. If any excitation is changed to its integral, the response also changes to its integral. Since the first derivative is the inverse of integration, if the excitation is changed to its first derivative, the response is also changed to its first derivative as shown in Fig.1.10.

The response of a system to a complex exponential e^{st} is given by:

$$y(t) = h(t) * e^{st} = \int_{-\infty}^{\infty} h(\tau) e^{s(t-\tau)} d\tau = \int_{-\infty}^{\infty} h(\tau) e^{-st} d\tau \tag{1.24}$$

where s is any complex constant. The integral $\int_{-\infty}^{\infty} h(t) e^{-st} dt$ is called the Laplace transform of $h(t)$.

Let us consider an input equal to a discrete-time step with magnitude α, i.e.,

$$u(t) = \begin{cases} 0, t < 0 \\ \alpha, t \geq 0 \end{cases} \tag{1.25}$$

and let $y(t)$ be the corresponding output, which is called the *step response.*

Impulse Response: The *impulse* response function is the response of a linear system to a unit-impulse input when the initial conditions are zero. Applying a continuous-time impulse to the LTI system we have-

$$u(t) = \delta(t) = \begin{cases} 1, t = 0 \\ 0, t \neq 0 \end{cases} \tag{1.26}$$

The corresponding output y (t) is called the impulse response and its z-transform is specifically the system's transfer function:

$$H_d(z) = \sum_{k=0}^{\infty} z^{-k} y(k) \tag{1.27}$$

For a first-order system, the differential equation is-

$$\frac{dy(t)}{dt} + ay(t) = x(t) \tag{1.28}$$

where 'a' is a constant and the initial condition is, $y(0) = 0$ and $x(t)$ is the input.

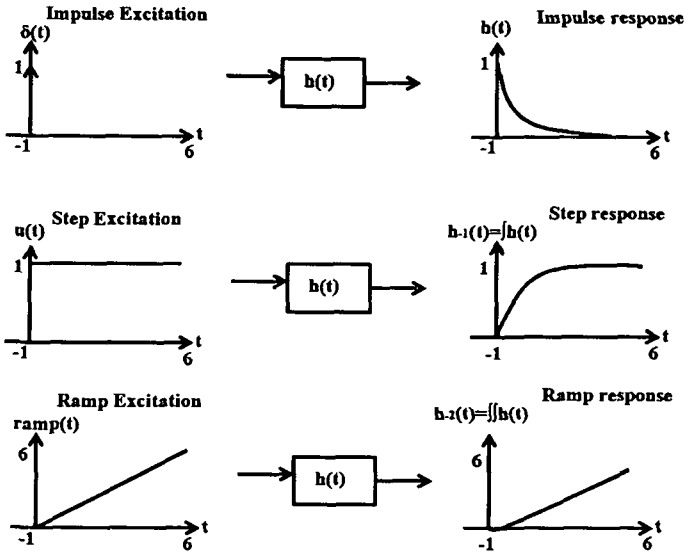

Fig.1.10: Relations between integrals and derivatives of excitations and responses for an LTI system.

Taking Laplace transform with impulse input, we get from (1.28)-

$$sY(s) - y(0) + aY(s) = X(s) \tag{1.29}$$

The transfer function in s-domain is given by:

$$G(s) = \frac{Y(s)}{X(s)} = \frac{1}{(s+a)} \tag{1.30}$$

In time-domain, the system response is-

$$y(t) = e^{-at} \tag{1.31}$$

From Eqn.(1.30) three cases can be considered as-

i) If $a > 0, y(\infty) = 0 \rightarrow$ then the system is *stable.*

ii) $a = 0, y(\infty) = 1 \rightarrow$ then the system is *marginally stable.*

iii) $a < 0, y(\infty) = \infty \rightarrow$ then the system is *unstable.*

Graphically the three cases can be represented as shown in Fig.1.11 with polar plots and impulse response.

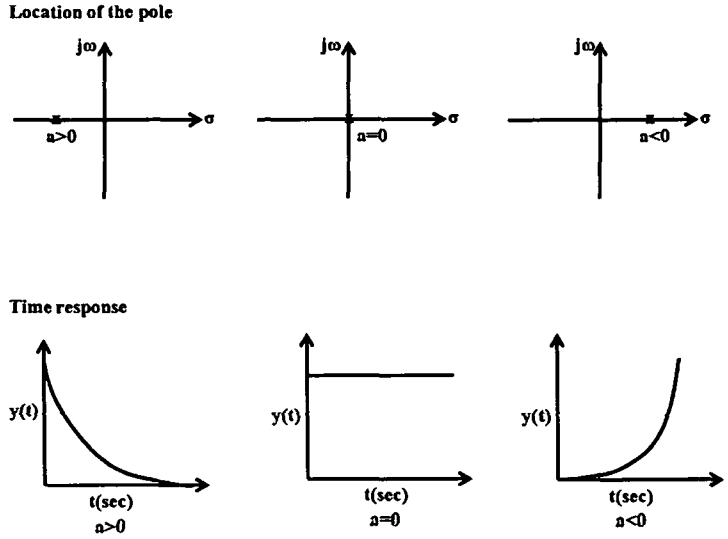

Fig.1.11: Graphical representation of the stability criterion.

The response curves of a first-order system to pulse inputs and impulse inputs are shown in Fig.1.12.

Considering a first-order system, response to a pulse input of amplitude $1/t_1$ and duration t_1, two cases can be assumed:

i) If the time duration $0 < t < t_1$ of the input is sufficiently small compared with the system time constant T, then the response is approximately a unit-impulse response.

ii) If, $t_1 < 0.1T$, the response of the system is identical to the unit-impulse response.

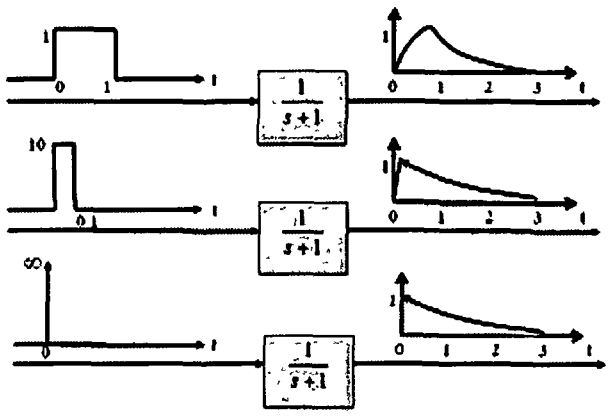

Fig.1.12: Response curves of a first-order system subjected to pulse inputs and impulse input.

1.6.3.2 Pole-Zero Plot

An important feature is the strong influence of the choice of boundary conditions on the dynamics of a system such as pole and zero locations. Stability of a system can be defined in two ways:

i) A system is *stable* if a system is subjected to a bounded input and the response is bounded in magnitude[64].

ii) A system is *unstable* if the natural response approaches infinity as time goes to Infinity[65].

The pole locations of the system give insight into the natural response of a system and, thus, its stability. For the state-space system as already described is given by,

$$\begin{aligned} \dot{x} &= Ax + Bu \\ y &= Cx \end{aligned} \tag{1.32}$$

Taking the Laplace Transform ignoring initial conditions and solving for $X(s)$ we obtain,

$$X(s) = (sI - A)^{-1} BU(s) \tag{1.33}$$

where I is the identity matrix. Using this relation for $Y(s)$ and then simplifying we get,

$$Y(s) = CX(s) = C(sI - A)^{-1} BU(s) \tag{1.34}$$

$$\Rightarrow \frac{Y(s)}{U(s)} = C(sI - A)^{-1} B \tag{1.35}$$

Or the transfer function, $$H(s) = C(sI - A)^{-1} B \tag{1.36}$$

Solving linear time-invariant systems by the Laplace Transform method we get,

$$Y(s) = \frac{K(s + z_1)(s + z_2).....(s + z_m)}{(s + p_1)(s + p_2).....(s + p_n)} \tag{1.37}$$

where $m < n$ (for limited response at high frequency).

The constants z_i are called the zeros of the transfer function or signal, and p_i are the poles. When viewed in the complex plane, the magnitude of $Y(s)$ will go to zero at the zeros, and to infinity at the poles. To determine stability of a system the denominator of the transfer function is factorized and it is seen if the poles were in the left half of the complex frequency plane. A system is stable if and only if all of the poles occur in the left half of the complex plane as shown in Fig.1.13. The marginally stable parts

correlate with a zero real part, and unstable parts to a positive real part. The equilibrium state of a *continuous-system* with constant input is *stable* if all poles of the transfer function $H(s)$ have non-positive real parts and all poles with zero real parts are single. The equilibrium state is asymptotically *stable* if and only if all poles of the transfer function $H(s)$ have negative real parts; that is, all poles are in the left half of the s-plane. Similarly, the equilibrium state of a *discrete-system* with constant input is *stable* if all poles of $H(z)$ have absolute values less than or equal to one and all poles with unit absolute values are single. The equilibrium state is asymptotically *stable* if and only if all poles of $H(z)$ have absolute values less than one; that is, the poles are all inside the unit circle of the z-plane. Fig.1.13(a) and (b) shows the pole-zero plots of a stable and unstable system respectively.

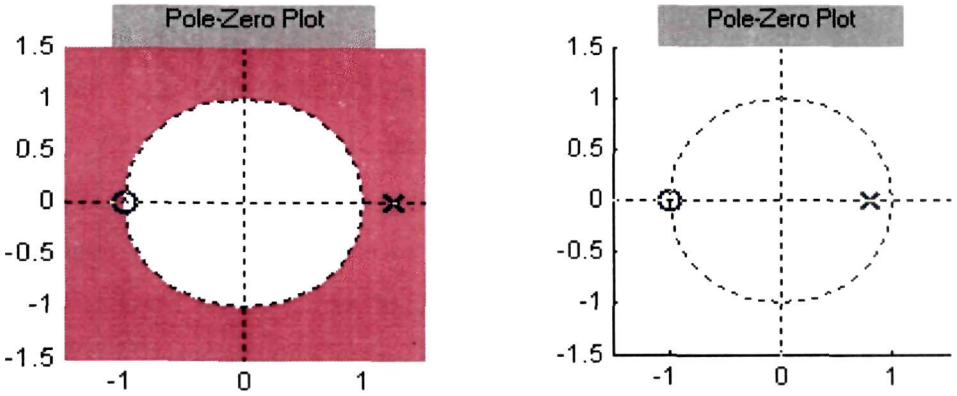

(a) (b)

Fig.1.13: Pole-zero plots for (a) an unstable system; (b) a stable system.

In this work, the best transfer function is selected based on the pole-zero plots. The distance of the poles from the unit circle is calculated and the frequency that gives the least distance is considered to be stable.

1.6.4 System Identification

Sensor system identification and modeling is an important area due to its potential scope for performance analysis, comparison, calibration and compensation. A number of works have been carried out in the past for modeling sensor dynamics through system identification. In[66] a useful method for improving sensors' dynamic characteristics and realizing sensors' dynamic compensation has been proposed. The

model parameters were estimated from the differential equation based on numerical integrals, without iterations. The method was useful in removing to a great extent measurement noise in the output and also achieving lower model order and higher accuracy. In another work[67] the response of the acceleration sensor was reconstructed using various modeling methods. The reconstructed signal from distorted acceleration signal also had higher level of accuracy. A least square method based on Walsh function was also employed for studying the force sensor's dynamic modeling[68]. This method determined the coefficient of either differential equation or transfer function directly based on the time-domain sensor data. The efficiency of the method was tested by the identification of the emulating data and the force sensor's pulse respond curve is modeled by using the method.

Work on the dynamic model identification of sensors based on support vector machine (SVM) model was also performed in[69]. The method has prominent advantages as compared with conventional model identification methods. Simulations and experimental results show the efficiency and high precision of this dynamic model identification method. An identification method based on support vector regression (SVR) for Hammerstein model was also investigated to analyze the nonlinear dynamic system of transducer[70]. In this model, the nonlinear dynamic characteristic of pressure transducer was expressed by a nonlinear static subunit followed by a linear dynamic subunit. Compared with conventional identification methods, the proposed method determines the analytic expressions of nonlinear dynamic transducer and only one dynamic calibrating experiment was needed. Further, the order of Hammerstein model built by this method provided a better way for identification for nonlinear dynamic transducer system. Work has also been carried on the application of the nonlinear model based on the orthonormal function in dynamic compensation of sensors[71]. The structure of this model and the corresponding algorithm compensated sensor ideal output and input properties. From experimental results the effectiveness of dynamic model method was determined.

In another work[72], the force without expensive force sensor using the pressure transducer on each cylinder is studied with system identification method. In[73] the problem of carrying out dynamic measurements when the multicomponent gas mixture undergoes changes with the same time-scale than the gas sensors time-constants is

studied. To overcome such problems inverse models which allow the reconstruction of the gas concentrations presented to the gas sensor array are built. Different model structures, including linear and non-linear, have been tested for verification of the approach. Further, the experimental identification and modeling of the nonlinear dynamics of a high performance hydraulic actuator was performed in[74] where an analytical model of the system is formulated. The nonlinear elements of the actuator model obtained through simulation are shown to predict the behaviour of the real system's very accurately. In another work[75] the output signals obtained from the pressure sensors are analyzed using the auto-regressive exogenous (ARX) system identification and the common pole–zero principle. The important dynamic characteristics including frequency response, transfer function, resonant frequency and damping ratio of the pressure sensors are revealed. Therefore, system identification is an essential requirement in instrumentation for obtaining a model of a sensor or transducer of interest or a new sensor to be developed, for sensor performance analysis, fault diagnosis, etc.

Although a considerable amount of research has been carried out for identification of transfer function and modeling of different sensor, very little attempt has been made for MOS gas sensors. In this research an attempt has been made to determine the MOS gas sensor transfer function by identification method so that the stability of the response can be analyzed. Most of the dynamical system behavior can be obtained exploiting system identification techniques. Among other factors like noise behavior, obtaining a quasi-isothermal condition of the sensor surface and sensor stability are also important criterions when the sensor is operated by pulse modulated heater voltage. A quasi-isothermal state provides a slow change in sensor adsorption kinetics which on the other hand, determines the stability of the response. Since attainment of a proper isothermal sensor state is determined by the heater pulse fluctuation, a study on stability of the sensor will lead to a method of selection of suitable heater pulse frequency and duty cycle. Depending upon input-output relation, the identification of systems can be divided into two groups:

i) Static System Identification:

In this type of identification the output at any instant depends upon the input at that instant. These systems are described by the algebraic equations. The system is memory less and mathematically it is represented as-

$$y(n) = f[x(n)] \tag{1.38}$$

where $y(n)$ is the output at the n^{th} instant corresponding to the input $x(n)$.

ii) Dynamic System Identification:

In this type of identification the output at any instant depends upon the input at that instant as well as the past inputs and outputs. Dynamic systems are described by the difference or differential equations. These systems have memory to store past values and mathematically represented as-

$$y(n) = f[x(n), x(n-1), x(n-2).....y(n-1), y(n-2),....] \tag{1.39}$$

where $y(n)$ is the output at the n^{th} instant corresponding to the input $x(n)$.

The process of system identification deals with the determination of the complete characteristics of an unknown system from its output with the input being known. The characteristic of the unknown system can be determined in terms of its impulse response. Least Square Error (LSE) is one of the methods for performing system identification. In this method, a model is assumed for the system and the parameters of the model that minimizes the error energy between the outputs of the actual system and that of the model. This provides the best parameters of the model for identification. In general, the mean square error (MSE) is minimized. The method of linear prediction is a special case of system identification. This method enables the prediction of future samples based on the present samples. In other words, the future samples are expressed as the weighted sum of the present samples, the weights of which are selected such that the prediction error energy is minimum. The prediction co-efficients form an IIR or Autoregressive (AR) model. Let us consider an unknown system $H(z)$. By system identification the structure of the system can be determined using the knowledge of its input $x(n)$ and output $y(n)$ as shown in Fig. 1.14. The

structure of the unknown system can be quantified in terms of its impulse response $p(n)$, which is time-invariant.

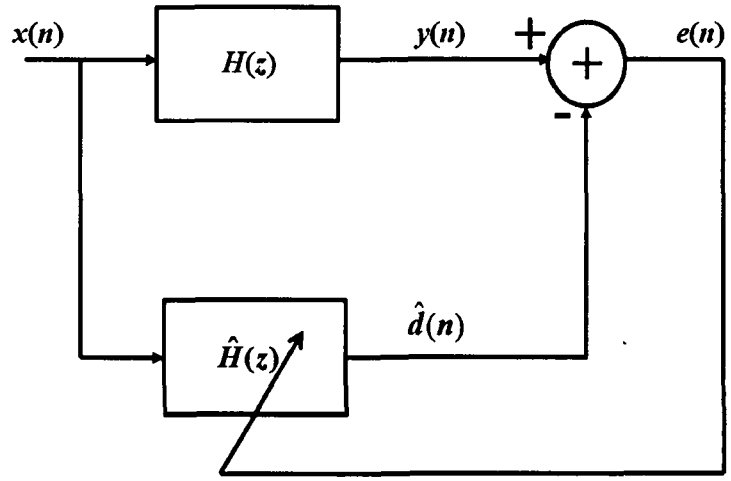

Fig.1.14: Block diagram of System Identification.

1.6.4.1 Least-Square Error Algorithm (LSE):

In parametric system identification a finite number of unknown parameters can be determined that characterizes the model of the system. In *least squares criterion* algorithm the sum of squares of error between actual observed outputs and estimated output values of the identified model is minimised. The criterion of the LSE algorithm has a unique minimum point, provided that the model is not over-parameterized[76]. It produces the estimated parameters with the highest probability (maximum likelihood). Parametric identification using the method of least-squares involves three steps:

i) Formulation of the parametric transfer function identification problem
ii) Line fitting using the least-squares method
iii) Surface fitting using the least-squares method

i. Parametric Identification

The co-efficients a_i and b_i of the z-transfer function (Eqn.1.23),

$$\hat{H}(z) = \frac{b_0 z^m + b_1 z^{m-1} + \ldots + b_m}{z^n + a_1 z^{n-1} + \ldots + a_n}$$

are determined, assuming that the no. of poles n and the number of zeros m are known. This can be done using the methods of least-squares which is introduced next, starting from a simple line fitting.

ii. Least-squares line fitting

The method can be used for solving linear equations:

$$y_i = ax_i + b, \quad \forall\{1,2,.....,N\} \tag{1.40}$$

The values for parameters a and b can be found for which the left- and the right-hand-sides of (1.40) differ by the smallest possible error. More precisely, the predicted values of a and b leads to the smallest possible sum of squares for the errors over the N experiments. The values for a and b are determined that minimize the following SSE:

$$SSE = \sum_{i=1}^{N}(ax_i + b - y_i)^2 \tag{1.41}$$

iii. Vector least-squares

Let us consider a linear equation of the form:

$$y = \sum_{j=1}^{m} z_j\theta_j = z\cdot\theta \tag{1.42}$$

where y is a scalar, $z = [z_1 \quad z_2 \quad \cdots \quad z_m]$ an m-vector, and $\theta = [\theta_1 \quad \theta_2 \quad \cdots \quad \theta_m]$ is also an m-vector whose values are to be determined.

To determine the parameter vector θ, N experiments are conducted from which measurements $(z(i), y(i)), i \in \{1,2,....,N\}$, are obtained where each $z(i)$ denotes one m-vector and each $y(i)$ a scalar. The values for θ are formulated that minimize the following Sum-of-Squares Error (SSE):

$$SSE = \sum_{i=1}^{N}(z(i)\cdot\theta - y(i))^2 \tag{1.43}$$

Least squares and similar techniques have a distinct advantage as compared to nonlinear search methods. The advantage of least squares methods is that it avoids the risk of convergence to sub–best minima of the criterion function[77]. The least squares

criterion has important statistical relationship with estimation probability. If appropriate probabilistic assumptions about underlying error distributions are made, LSE algorithm produces the maximum-likelihood estimate of the parameters.

Another method of identification involves estimation of model parameters which minimizes the optimally determined one-step-ahead output prediction error called the prediction error minimization method.

1.6.4.2 Prediction Error Minimization (PEM)

This method is used for estimating the parameters of a dynamic model based on measured input-output data. It considers the accuracy of the predictions computed for the observations, rather than the model mismatch. This technique is perhaps the most closely connected to systems theory as it explicitly exploits the dynamical structure of the studied system.

The general properties of PEM are:

1. Prior information on the model structure (model type and orders of each term) is needed.
2. The structural inconsistency may lead to biased parameter estimates. The bias is revealed differently for different input excitation.
3. To find a parsimonious model, trial and error procedure with different orders is usually necessary.
4. Generally, nonlinear equation should be solved to find an estimate.

In principle all systems are stochastic, which means that the output $y(t_k)$ at time k cannot be determined exactly from data available at the time k-1. It is thus important to know at the time k-1 what the output $y(t_k)$ of the stochastic process is likely to be at time k. Therefore, it is necessary to determine the model parameter vector θ, so that the prediction error defined as,

$$\varepsilon(t_k,\theta) = y(t_k) - \hat{y}(t_k|t_{k1};\theta) \quad (1.44)$$

is as small as possible. $\hat{y}(t_k|t_{k1};\theta)$ is the predicted response at the time k based on the parameters θ, given by-

$$\hat{y}(t_k|t_{k1};\theta) = L(q,\theta)y(t_k) \tag{1.45}$$

where $L(q,\theta)$ is a p-variate prediction filter having a pure time delay between $y(t_k)$ and $\hat{y}(t_k|t_{k1};\theta)$. This filter can be constructed in a number of ways, but it will always be based on the model parameters θ. Once the model structure and this filter have been chosen, the prediction errors are calculated from (1.45). Once the model structure is chosen, it is necessary to make the following choices to define a prediction error method for minimization of $\varepsilon(t_k,\theta)$

a) To choose the prediction filter parameter $L(q,\theta)$.
b) To choose a scalar-valued function that can assess the performance of the predictor.
c) To choose the procedure for minimization of this performance function.

The PEM algorithm uses numerical optimization to minimize the cost function defined as a weighted norm of the prediction error. For scalar outputs, the cost function is defined as:

$$V_N(G,H) = \sum_{t=1}^{N} \varepsilon^2(t) \tag{1.46}$$

where $\varepsilon(t)$ is the difference between the measured output and the predicted output of the model.

Model validation is the final stage of the system identification procedure. In fact it overlaps with the model structure selection. Statistical tests on the prediction errors $\varepsilon(t_k,\theta)$ are also typically used numerical indicators for model validation. If the statistical distribution of $\varepsilon(t_k,\theta)$ matches the assumed distribution then it can be concluded that the system dynamics is indeed well represented by the model. Any different trend in the statistical characteristics, from the original one, is an indication that either the model or the noise is incorrectly assumed or that the parameters are incorrectly estimated.

System identification includes the following steps:

a) **Experiment design:** It includes the choice of the measured variables and of the character of the input signals. Its purpose is to obtain good experimental data.
b) **Selection of model structure:** A suitable model structure is chosen using prior knowledge and trial and error.
c) **Choice of the criterion to fit:** A suitable function is chosen, which shows how well the model fits the experimental data.
d) **Parameter estimation:** An optimization problem is solved to obtain the numerical values of the model parameters.
e) **Model validation:** The model is tested in order to reveal any inadequacies.

1.7 Detection and Classification of Gases

The idea to portray the natural human senses with artificial systems has been a dream of human kind. Efforts have been made to develop artificial systems reproducing the five senses of human beings[78]. From this point of view, sensors play an important role in the reproduction/simulation of the five senses possessed by human beings. The fact of being able to unbiased analysis and getting results in real time, has propitiated the research and development of techniques to get better accuracy, in classifying gases. The ability to mimic the human sensory response led to the development of E-Nose. As defined by Persaud and Dodd in the early 1980''s: "An electronic nose is an instrument, which comprises an array of electronic chemical sensors with partial specificity and an appropriate pattern-recognition system, capable of recognizing simple or complex odours". Currently, E-Nose systems have applications such as quality assurance of food and drugs, medical diagnosis, and environmental monitoring[79]. The E-Nose has become a key element in the food quality analysis of many industries that manipulate the aroma properties of their manufactured foods. E-Nose offers an efficient way to analyze and compare different odours. However, developing artificial olfaction systems is quite complex and more analytical approach is required for the comparison and classification of odours.

1.7.1 Biological Olfaction

Human olfaction begins with sniffing, which moves air samples that contain molecules of odours to the thin mucus layer lining the olfactory epithelium in the upper portion of the nasal cavity. A simplified schematic view of the human olfactory system is shown in Fig 1.15. Odour receptors of the human nasal cavity can detect and discriminate up to 10,000 different chemical traces. The olfactory region of each of the two nasal passages in humans is an area of about 2.5cm^2 holding about 50 million primary sensory receptor cells. Each olfactory receptor consists of 8-20 cilia in the olfactory epithelium projecting down into a layer of mucus about 60 microns thick. The mucus lipids help the transportation of the odourant molecules to the olfactory receptors and produce the signals that our brain receives to interpret the odour. Information about the stimulus causes a distinctive neuron signal pattern and such patterns allow discriminating between a vast numbers of different odours. Odourant particles are polar and can be detected by humans at concentrations below 1ppb. The detection levels of different materials are different such as rose-0.29ppm, lemon-10ppb, off-flavor in fish-0.01ppb; grapefruit-0.00002ppb. The human olfactory system has the limitation of discriminating mixtures of more than three to four components. The electronic nose technology involves a device that mimics the human olfactory system with the analogy to an array of olfactory receptors, signal excitation by neurons, and pattern classification in the brain. The brain then performs processing and classification operation, resulting in a suitable decision for the next course of action. This process of classification appears to be a learning process, with new smells having to be sampled, recognized and remembered subconsciously in the memory of the individual.

A gas detecting instrument with a single sensor element features the ability to provide measurement results immediately on-site and to conduct continuous monitoring. However, such single sensor elements are not able to classify an odour from a group; rather they can measure the strength or ppm level only of a single odour. To match the sensitivity of the nose, the E-Nose sensor requires intelligent classification and discrimination ability.

Our understanding of biological olfaction has increased rapidly during the past decades[80] and attempts have been made to model this process[81]. Even though conventionally the human nose is used to assess odours such as tea, wines or perfumes, by nature it is subjective and biased. Moreover it is not practical to use the conventional human testing for industrial applications where dangerous components are present in the gas or when it is needed to monitor certain volatile compounds for prolonged periods of time. E-Nose is the alternate technique in such situations.

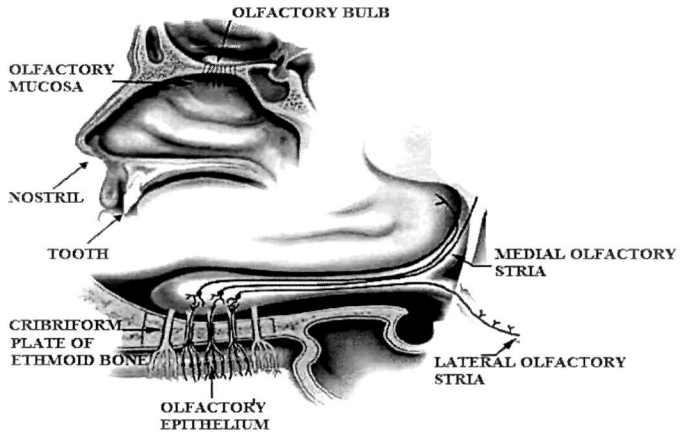

Fig. 1.15: The Human Olfactory System

1.7.2 Electronic Nose

In the artificial olfactory system, the olfactory receptor cells are replaced by a chemical sensor array. Employing chemical sensors in an array form with pattern recognition capability provides a higher degree of selectivity leading to an extensive range of applications. The basic principle of E-Nose is that each odour leaves a characteristic pattern or fingerprint on each sensor array. The degree of selectivity and the type of odours that can be detected largely depend on the choice and number of sensors in the sensor array. The sensors are often mounted in an air tight chamber containing gas inlets and outlets to control the gas flow. The signals from each sensor are measured and processed, usually by an analogue to digital conversion that is performed by a computer. After the signal processing, the data is transformed by a variety of pre-processing techniques designed to reduce the complexity of the multi-sensor response. As shown in Fig. 1.16 the headspace generation ensures the concentration of volatiles of organic solvents before and during sampling. During the

collection time, the sensors are exposed to constant flow of gases through pipelines inside the electronic nose and the response begins. During the purging operation, sensor heads are cleared with a blow of fresh air so that the sensors go back to their baseline values.

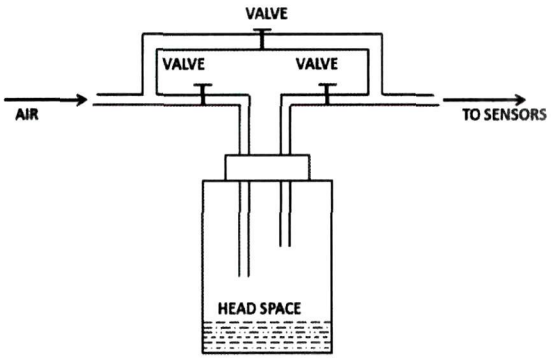

Fig 1.16. A headspace sampling system.

The E-Nose system, comprises of three functional components that works in tandem-

i) an integrated chemical sensor array,
ii) an interfacing electronic circuitry and
iii) a pattern recognition (PARC) software paradigm.

Sensor electronics convert the chemical signal into an electrical signal and also amplify and condition it. Interfacing electronics circuitry is used to digitize and store the response signal for processing. Patterns from known odours are used to build a database and train a pattern recognition system so that unknown odours can subsequently be classified and identified. The degree of selectivity and the type of odours that can be detected largely depend on the choice and number of sensors in the sensor array. Hence the E-Nose is a combined chemical sensing and data analysis system.

An E-Nose, as the human olfactory system, discriminates new patterns and associates them to specific odours by training the system using a set of known data samples. Sample delivery systems are used to transfer the odour from the source (typically by a miniature pump) to a sensor chamber in which an array of selected gas sensors is installed. The process of odour delivery can be summarized as follows:

At the beginning of a sampling process, the odour delivery system drives each sensor to a known reference state by applying a reference gas (for example, fresh air) to the sensor chamber. The responses of the sensors in this state are known as baseline level. Then, the delivery system exposes the sensors to a given odour, producing first a transient response as the compounds starts interacting with the surface and bulk of the sensor's active material. After a few seconds to a few minutes, the sensors reaches a steady state and, finally, the odour is removed from the system and the sensor is brought back to the baseline level by pumping the reference gas to prepare the system for a new measurement cycle. The above mentioned steps are known in the E-Nose literature as a "three phase sampling process" and they are usually carried out in chambers where humidity, temperature and exposure to the analyte are controlled[82]. Fig. 1.17 shows a typical response of a given array of gas sensors to a three-phase sampling process. The three phase sampling process has been widely used in laboratory-based applications with an important amount of success. Many articles on this subject have been published over the last years, mainly in relation to the food and beverage industry[83-86]. Commercial E-Nose systems also invariably employ these basic stages of operation. Fig.1.18 shows the comparison between the three basic elements that comprise and electronic nose and a human nose.

Many of these sensing technologies are explored in the research and have also been implemented on commercially available electronic noses[87-91]. The sensing technologies of gas sensors have certain advantages and disadvantages over their counterpart to choose the right kind of gas sensor, depends on the type of application. Among the desired applications of E-Nose, they should be able to react to and recover from an exposed odour within an acceptable time frame. This is especially important in applications that integrate E-Nose with a robotic system as in[92].

Another important aspect is that the power consumption of the sensors should be relatively low. The headspace, containing the sensor array is likely to involve other electrical equipment such as pumps and valves which often share the same power supply. Also smaller the sensor sizes higher the possibility of integration of sensors in a variety of platforms, including portable E-Nose[93].

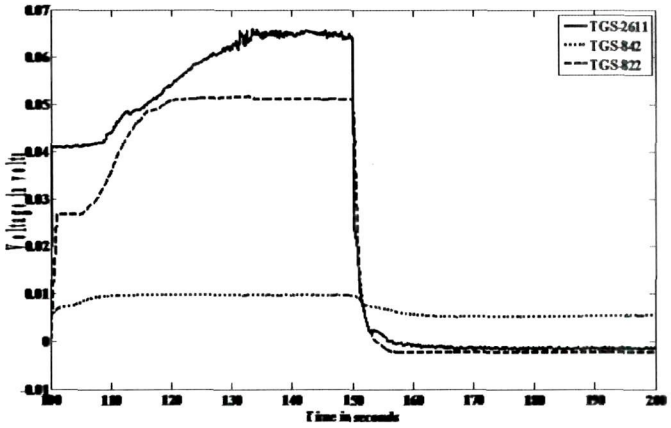

Fig.1.17 Measured response of an array of E-Nose (TGS-2611, TGS-842 and TGS-822).

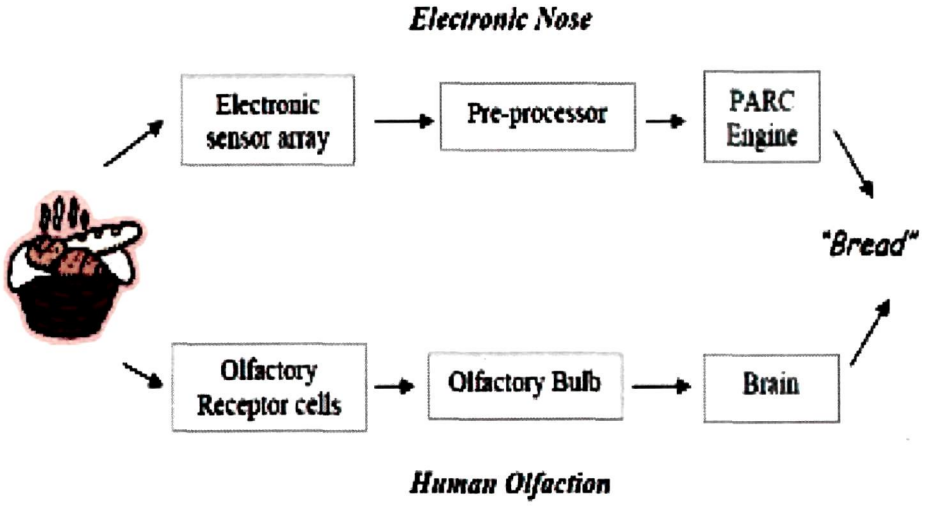

Fig 1.18.Comparison between the three basic elements that comprise and E-Nose and a human nose .

1.8 Signal processing and Pattern Recognition:

It has already been mentioned that the odour classification and discrimination is performed by MOS gas sensors with the help of algorithms supported by learning, training and decision making. These algorithms are basically data and signal processing that work sequentially. The four sequential stages of E-Nose signal processing and pattern recognition are as follows:

a) Pre-processing

b) Feature extraction

c) Classification

d) Decision making

Fig.1.19 shows the different stages of the E-Nose signal processing stages.

The sensor response in terms of variation of resistance in the case of chemoresistive type and polymer sensors, or variation of mass and resonance frequency in the case of piezoelectric sensors is converted to a variation in voltage or current using an electronic circuit. Sensor drift is one of the factors that have to be compensated for in this stage.

One of the most important functions of this stage is the sensor output normalization. Since the sensors in the array have different sensitivities, the voltage levels of the output signals from the sensors will be different. The process of separating individual samples from universal samples space is called classification. The classification helps to sort out samples to the nearest matching class or even to the absolute class of the sample as per the flexibility of algorithm rules. When the sensor response data are projected on an appropriate low-dimensional space, the classification stage is used to identify the patterns that are representative of each odour. The classification stage is able to assign to the data a class label to identify the odourant by comparing its patterns with those compiled during training. The decision making stage makes judgement to the classification and even determines that the unknown sample "does not belong" or "it belongs" or "it nearly belongs to" any one of the database.

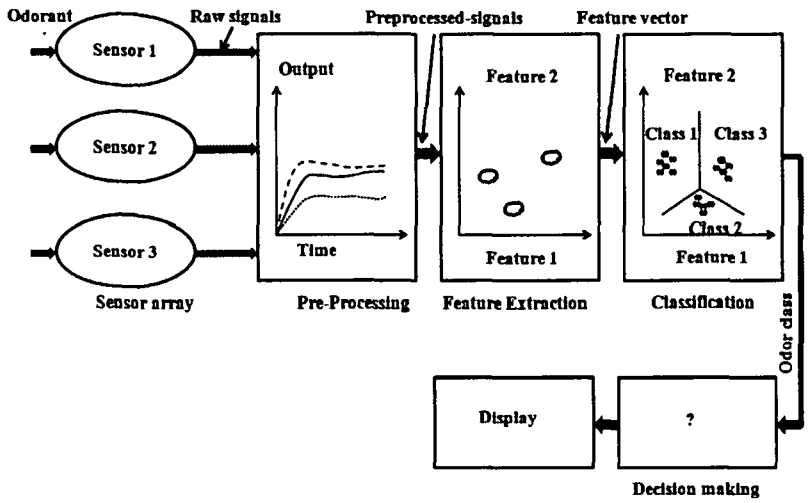

Fig.1.19. Block diagram of various stages of odour classification.

1.8.1 Feature Selection

Feature is the best subset of measurements based on an evaluating criterion. During the recent years many works related to feature extraction, feature construction, space dimensionality reduction, sparse representations have been performed by most of the researchers, the applications of which includes bio-informatics, chemistry, text processing, pattern recognition, speech processing, vision perception, flavour discrimination and quality prediction. Feature selection is a preprocessing step to machine learning and is useful in data visualization and data understanding, reducing the measurement and storage requirements, reducing training and utilization times, defying the curse of dimensionality to improve prediction performance. Feature selection based on static performance data, which are used as the training set, may not always provide the best classification results in dynamic environments. Hence, to enable the feature selection to adapt to the dynamic operation, it requires the system to be able to dynamically update the training set data. Selecting the most relevant variables is usually subsets for building a predictor, particularly if the variables are redundant. Conversely, a subset of useful variables may exclude many redundant, but relevant, variables.

Feature selection is a process of choosing a subset of original features so that the feature space is reduced according to a certain evaluation criterion. The building of a feature representation is an opportunity for incorporating domain knowledge into the data and can be very application specific. Nonetheless, there are a number of generic feature construction methods such as clustering; basic linear transforms of the input variables as *Principal Component Analysis* (PCA), *Linear Discriminant Analysis* (LDA); more sophisticated linear transforms like spectral transforms (Fourier transforms), wavelet transforms or convolutions of kernels; and applying simple functions to subsets of variables, like products to create monomials. Feature selection has been a fertile field of research and development since ages and has proved to be very efficient in removing irrelevant and redundant features, increasing efficiency in learning tasks, improving learning performance like predictive accuracy, and enhancing comprehensibility of learned results[94-96].

Feature selection algorithms fall into two broad categories, the filter model or the wrapper model[97, 98]. The filter model relies on general characteristics of the training data to select some features without involving any learning algorithm whereas the wrapper model requires one predetermined learning algorithm in feature selection and uses its performance to evaluate and determine which features are selected. As for each new subset of features, the wrapper model needs to learn a classifier. It tends to find features better suited to the predetermined learning algorithm resulting in better learning performance, but it also tends to be more computationally expensive than the filter model[99]. The filter model is usually chosen when the number of features becomes very large because of its computational efficiency. For the purpose of feature selection, usually the data sets are chosen to span a wide variety of domains. The data sets that had sufficiently large experimental measurements to create a large enough test set are chosen.

Temperature affects the dynamic characteristics of the gas sensors, particularly when they employ viscous damping. In the works[100-102], the authors described techniques for extracting and using the steady-state, the slope as well as the transient response information from the sensor's response. The dynamic signal extraction techniques and best array configuration were used to improve the classification performance in[103]. The sensor response curves were determined using six features which represented the differences of dynamic behaviour of sensors to different sample gases, in phase space. The degree of difference was used to evaluate how much information was extracted from the response curves by the proposed method[104].

In this work it was found that when the adsorption process becomes short, the reacting time i.e. the reaction between the sensor and the sample gets reduced. Research has been carried out on feature extraction on recovery responses which shows that the shape of the recovery curves did not change much with the reaction time[105]. The recognition time and response recovery time of sensors were determined and the feature extraction was done based on these[106]. In our experiment, all the responses from the gas sensor data were formatted for this purpose. Each dataset is split into training, validation and test set.

After checking some simple feature statistics, a subset is selected and then trained using Neural Networks. Further, a feature subset is selected which is then trained by ANN with full parameter selection. Hence, better classification of data is achieved by using these algorithms.

1.8.2 Pattern Recognition

Dimensionality reduction and feature subset selection are two techniques for reducing the attribute space of a feature set, which is an important component of pattern recognition. Classification is a supervised learning algorithm in contrasts with clustering, which are unsupervised learning algorithm[107]. In general, supervised classification is applied due to higher accuracy level achieved and more robust methods exist, compared to the unsupervised approach. It maps a data into one of several predefined classes. Data classification is a two-step process. In the first step, a model is built describing a predetermined set of data classes or concepts. Typically the learned model is represented in the form of classification rules, decision trees, or mathematical formulae. In the second step the model is used for classification. Classification techniques including decision tree[108, 109], *Artificial Neural Network* (ANN)[110], *Support Vector Machine* (SVM)[111, 112] , *Rough Set Theory* (RST)[113] and other rule based classification systems have been proposed in many works. ANN classification, which is supervised, has been proved to be a practical approach with lots of success stories in several classification tasks. Neural classifiers operate directly on the training data taking each individual pattern into consideration. The classification stage is able to assign to the data a class label to identify the odourant by comparing its patterns with those compiled during training. The different tools used for performing classification work are shown in Fig.1.20.

The judgement to the classification is made by the decision making stage which even determines that the unknown sample "does not belong" or "it belongs" or "it nearly belongs to" any one of the database.

In the conventional ANN classification, a sample from the original data set is mapped to a space between 0 and 1 (recognition space) by the neural network. The sample is marked as class 0 if it is more close to 0 than to 1. Otherwise, the sample belongs to

class 1. If this space can be divided into partitions, then the mapped sample can get close to these partitions freely, and the mapping relationship could be formed easily using neural network. Based on this idea, the performance of ANN classification including training speed and accuracy could be improved. For the conventional statistical classifiers, the size of training data is an important factor for the success of an ANN

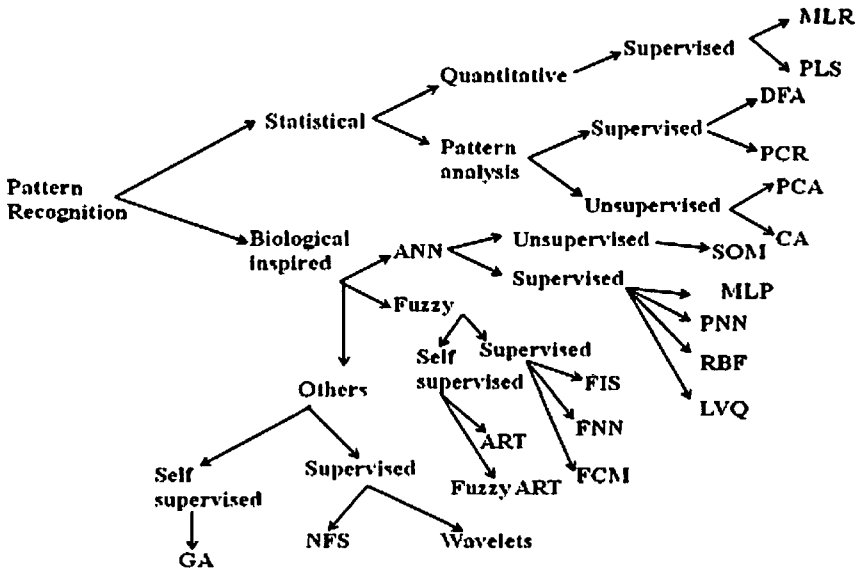

Abbreviations

ANN-Artificial Neural Network
ART-Adaptive Resonance Theory
DFA-Discriminate Function Analysis
GA-Genetic Algorithm
LDA-Linear Discriminant Analysis
MLR-Multiple Linear Regression
NFS-Neuro Fuzzy System
PCA-Principal Component Analysis
PCR-Principal Component Regression
PLS-Partial Least Square
RBF-Radial Basis Function
SOM-Self Organizing Map

Fig.1.20. Tree diagram showing various classification schemes.

classification. Fewer training samples are not sufficient for networks to derive the characteristics of the classes and also the use of too large number of training samples may cause networks to overfit to the data, as well as requires more learning time. However, it should be pointed out that a larger number of training data should be always preferred as opposed to a smaller number.

In this thesis, ANNs were used for the classification of MOS gas sensor data. Two ANN paradigms namely MLP and RBF were used for the training of the data and the classification accuracy was determined.

1.9 Artificial Neural Network:

An ANN is man's attempt to mimic the brain computationally. The most commonly used pattern recognition technique is the ANN. They are highly parallel mathematical constructs that have been inspired by the biological nervous system. ANN consists of a number of processing elements called '*neurons*' which represent the biological neurons, and their interconnections, the synaptic links. The strengths of these connections are called '*weights*' and are determined either during a training phase (or learning phase) for supervised ANN, or by an algorithm for unsupervised ANN. There are many different types of ANN structures that have been applied to solve odour classification problems such as *multi-layered perceptron* (MLP), *radial basis function* (RBF), *linear vector quantization* (LVQ) etc. In artificial neurons, this signal transfer is simulated by multiplication of the input signal, x, with the synaptic weight, w, to derive the output signal y. The artificial neuron is the heart of every neural network. A single neuron receives input signals, x_i, from n neurons, aggregates them by using the synaptic weights, w_j, and passes the result after conversion by a *transfer function* (activation function) as the output signal Y_i (Fig. 1.21). Some important activation functions are given in Table 1.1. A general neural network consists of an *input layer*, one or more *hidden layer*(s), and an *output layer* and these layers are fully connected. Fig.1.22 shows an ANN architecture of 3-6-10 neurons. The Fig. shows that the output signals (y_i) of the neurons of one layer act as the input signals (x_i) for the neurons of the following layer.

The input layer of the ANN interface the signals from the external world to the ANN. Hidden layers are the real classifiers that works for the classification algorithm of ANN. The output layer is considered a collector of the features detected and producer of the target or result.

The main advantages of neural networks are its adaptability in terms of learning, self-organisation, training, and noise tolerance. ANN is the most commonly used pattern

recognition techniques with E-Nose. ANNs enable to detect a greater number of classes than the number of unique sensor types, and the

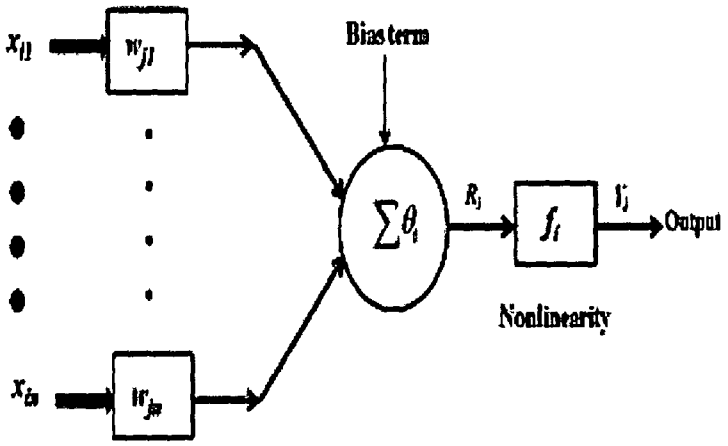

Fig.1.21. Operation of a single neuron.

less selective sensors can be rendered much more selectivity when used in conjunction with an ANN.

Table 1.1: Important transfer functions for neural networks:

Step function	Sigmoid function	Linear function
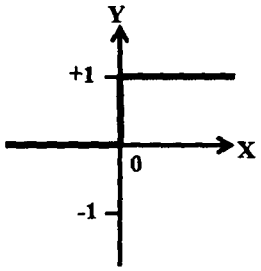	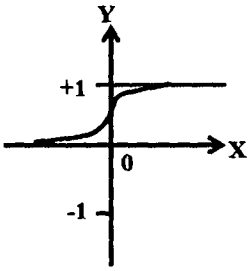	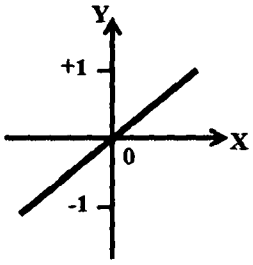
$Y^{step} = 1, X \geq 0$ $Y^{step} = 0, X < 0$	$Y^{sigmoid} = \frac{1}{1+e^{-X}}$	$Y^{linear} = X$

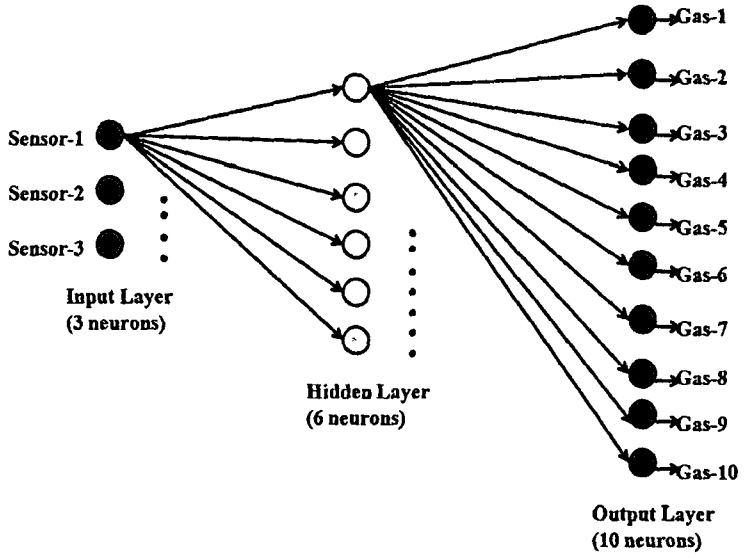

Fig. 1.22: Architecture of a neural network.

This is because, once a network is trained for a particular odour, the consecutive recognition process can occur rapidly and effectively. Learning in a neural network is accomplished through an adaptive procedure, known as '*learning rule*'. The weights of the network are incrementally adjusted so as to improve the performance over time. The basic learning rules are the supervised learning, unsupervised learning and reinforcement learning.

i. Supervised Learning:

In the supervised learning, the output response is compared to a desired target response. If the actual response differs from the target response, the network generates an error signal which is then used to calculate the adjustment that should be made to the synaptic weights, so that the actual output matches the target output. The most common types of networks used to detect odours are the multi-layered perceptron (MLP) network and radial basis function (RBF).

a. Multi Layered Perceptron (MLP)

Perceptrons are fast and reliable networks especially suited for simple problems in pattern classification. An understanding of the operations of the perceptron provides a good basis for understanding more complex networks. A multilayer perceptron

(MLP) is a *'feedforward'* ANN model that maps sets of input data onto a set of appropriate output. Feedforward means that data flows in one direction from input to output layer (forward). This type of network is trained with the backpropagation learning algorithm. MLPs are widely used for pattern classification, recognition, prediction and approximation. Fig.1.23 shows a single layered perceptron architecture. It (x_1, x_2,..., x_n) represents a vector of real-valued inputs weighted with (w_1, w_2...,w_n). The linear combination of these inputs is given by-

$$\sum_{i=0}^{n} w_i x_i = w_0 x_0 + w_1 x_1 + ... + w_n x_n \qquad (1.47)$$

where w_0 denote the threshold bias value and x_0 is always 1. The output is 1 if the result is greater than 1, otherwise −1. MLP using a 'backpropagation' algorithm are the standard algorithm for any supervised learning pattern recognition process and the subject of ongoing research in computational neuroscience and parallel distributed processing. They are useful in research in terms of their ability to solve problems stochastically.

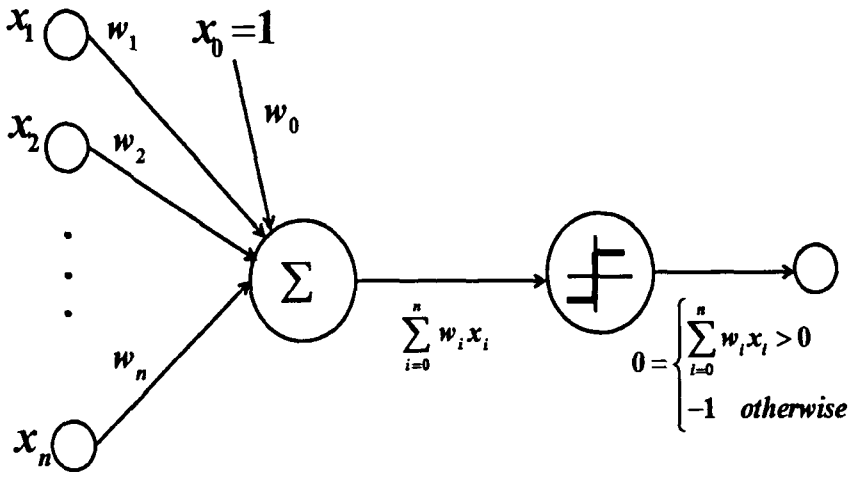

Fig. 1.23: Single layered perceptron architecture.

b. Radial Basis Function (RBF)

Radial basis networks require more neurons than other feed-forward networks. In principle, they could be employed in any sort of model and any sort of network. Radial functions are a special class of function. Their characteristic feature is that their

response decreases (or increases) monotonically with distance from a central point. The centre the distance scale, and the precise shape of the radial function are parameters of the model, all fixed if it is linear. Fig. 1.24 shows a radial basis network.

A typical radial function is the Gaussian function which in the case of a scalar input is given by:

$$h(x) = \exp-\left(\frac{(x-c)^2}{r^2}\right) \tag{1.48}$$

where c is the centre and r is the radius. A Gaussian RBF monotonically decreases with distance from the centre. A multiquadric RBF in the case of scalar input is given by:

$$h(x) = \frac{\sqrt{r^2+(x-c)^2}}{r} \tag{1.49}$$

It monotonically increases with distance from the centre. For a single layer RBF network with inputs (x_1, x_2,..., x_n) and weights (w_1, w_2...,w_n) the output is given by:

$$f(x) = \sum_{i=1}^{n} w_n h_n(x) \tag{1.50}$$

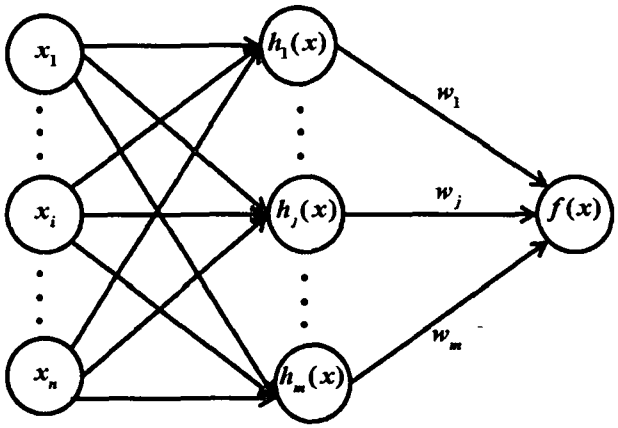

Fig. 1.24: Radial basis network.

ii. Unsupervised Learning:

In unsupervised learning there is no feedback path. Unsupervised learning algorithm is favoured in sampling odours when the number of possible outputs is unknown. This type of learning does not require a target output. During the training session, the neural

net receives the input excitations or patterns and it arbitrarily organizes them into categories. When a stimulus is later applied, the network provides an output response indicating the class to which the stimulus belongs. If a class cannot be found for the input stimulus, a new class is generated. This type of learning ensures the optimization of some criterion or performance function defined in terms of the output activity of the units in the network. Here, the weights and the outputs of the network are usually expected to converge to representations that capture the statistical regularities of the input data.

iii. Reinforcement Learning:

In this type of learning, the network's weights are updated in response to an evaluative teacher signal. It differs from supervised learning, where the teacher signal gives the correct value. Here the algorithm learns a policy of how to act when given an observation of the world. This type of learning rules may be viewed as stochastic search a mechanism that maximizes the probability of positive external reinforcement for a given training set.

Pattern recognition and classification can be observed as a function approximation problem. The stage of pattern recognition and classification determines the relationship between a set of independent variables (the feature vector) and a set of dependent classes (odour classes). The data may be qualitative, quantitative or both. There are two types of data structures in pattern recognition:

i) **Object data**: This type of data are the numerical vectors of n features, represented by a set of N feature vectors in the n-dimensional measurement space i.e, $x=\{x_1,x_2,x_3,.....x_n\}$.

ii) **Relational data**: This type of data bears a numerical relationship of N^2, say $\{r_{ij}\}$, between different pairs of objects. In other words, r_{ij}, represents the extent upto which the objects i and j are related in the sense of some binary relationship.

The interpretation of a vast data set is difficult and the analysing of such multivariate data sets is a multi-step process including data pre-processing, visualising relevant information, and finally classification of samples. This multi-step process is

collectively known as pattern recognition. A key concept in the field of pattern recognition is that of uncertainty which arises both through noises on measurements, as well as through the finite size of data sets. Probability theory provides a consistent framework for the quantification and manipulation of uncertainty and forms one of the central foundations for pattern recognition. In pattern recognition, features are the individual measurable properties of the phenomena being observed. The E-Nose raw data might not be the most useful input variables for statistical analysis due to noise, sensor drift or inconsistency. To obtain better results, data pre-processing is done which modifies existing raw data with the hope to obtain more quality input variable. Patterns from known odours are used to construct a database and train a pattern recognition system so that unknown odours can subsequently be classified and identified. For achieving better classification results, the choice of discriminating and independent features is an important criterion. The most commonly used data pre-processing techniques are normalisation, mean centering and scaling. Normalisation eliminates quantitative information concentration from a data set; mean centering eliminates constant drift from a data set and range scaling helps to eliminate the influence of absolute values by scaling them to values between zero and one. Different areas of pattern recognition have different features and once the features are recognized, they are classified into smaller set of algorithms. Classification techniques are divided in statistical approaches and neural network approaches. The most common are Bayesian classifiers, KNN classifier. Support vector machines and multi layer perceptrons.

The process of separating individual samples from universal samples space is called classification. The classification helps to sort out samples to the nearest matching class or even to the absolute class of the sample as per the flexibility of algorithm rules. There are many available statistical techniques that can be applied.

a) Multiple Linear Regression (MLR),–

It is a statistical technique that uses the independent variables or in this case, the sensor responses to predict the dependent variables by performing least-squares fit of the data. For E-Nose data, the goal of MLR is to calculate the regression coefficients.

Despite of many applications of MLR, few drawbacks such as the sensitivity to noise, and the treatment of co-linearity in then gas sensing array exists.

b) Partial Least Squares (PLS) –

This is another linear regression technique that is based on both MLR and principal component analysis. PLS is also more precise than MLR. This is because unlike MLR, in PLS the variables do not need to be orthogonal. Instead PLS can partly contain the same information, or be collinear and extracts the latent structures in the data which have the character of the weighted averages.

c) Cluster Analysis (CA) –

CA helps in finding the natural grouping in the individual observations within a data set. Cluster analysis is unsupervised technique and can be further subdivided as agglomerative and divisive cluster analysis depending on how the clustering algorithm is performed. Agglomeration means that each point is initially considered as a cluster and then joined with neighbouring clusters to form larger groupings whereas in divisive the entire data set is considered as one cluster than further divided to form smaller groupings of data.

d) Principal Component Analysis (PCA) –

PCA is an unsupervised data reduction method. It performs a principal component or eigenvector analysis of the data and projects the samples into a new co-ordinate system. The most useful feature of PCA is that it describes major trends in the data by reducing the dimensionality of the data. During the process the original data set is reduced in dimensions with as little loss of information as possible. This is achieved by filtering out the noise in the original data matrix, without removing essential information described in the variance of the data. As a result, PCA can be used as a preprocessing technique.

Different nonlinearity functions are used depending on the ANN paradigms and the algorithms use out of which the two most important nonlinearities are hard limiter and sigmoid. The details about these will be explained in the later chapters.

1.10 Outline of the Thesis

The principal aim of this doctoral thesis is to study the noise feature in MOS based gas sensors by the process of frequency and duty cycle under pulsed modulated heater voltage. The reduction of noise in sensors by Amplitude Demodulation technique was also performed in this research. Further the study was extended for best frequency selection by System Identification followed by the modeling of MOS gas sensor.

The thesis is organized into 5 chapters. *Chapter* 1 gives a brief introduction on the research work and comprehensive literature. A comparative study of biological and artificial olfaction is presented. It reviews the different methods proposed by other research groups, which have conducted research in the temperature modulation field, in order to increase sensors selectivity. Further various noise and noise sources; the compensation techniques; the dynamic behaviour of the sensors is also presented. The sensor dynamics was explained and system identification technique was introduced. Additionally, this chapter reviews the feature extraction and pattern recognition methods implemented in the analysis of experimental data from temperature modulated gas sensors.

Chapter 2 gives a detailed procedure for the design and development of the sensor set-up. Three types of MOS gas sensors are explored and explained. The design of Printed Circuit Board (PCB) and interfacing with a PC is also shown. The statistical and frequency analysis of noise in MOS gas sensors is described and best frequency and duty cycle is selected for further analysis. The classification for different gas samples was performed using ANN and results before and after selection of frequency is compared. Results, discussions and reference list are presented at the end of the chapter.

Chapter 3 gives a brief explanation of the various kinds of noise in gas sensors followed by the noise reduction using amplitude demodulation. The wavelet filtering method was applied to reconstruct the signal from the original extracted sensor signal. The spectral analysis of the responses obtained from the amplitude demodulation technique and wavelet filtering were done and the bandwidth was compared for both

the cases. The results, discussions and reference list are presented at the end of the chapter.

Chapter 4 introduces the system identification technique for best frequency selection purpose. Different sensor models are explained and stability criterion for the MOS gas sensors is presented based on the pole zero plot and the overshoot percentage. After frequency selection the sensor data was used in the classification by ANN paradigms (MLP and RBF) and the results before and after selection of frequency was compared henceforth. At the end the results, discussions and conclusions and reference list are presented.

Chapter 5 is presented with the detailed procedure of determination of the MOS gas sensor model by both theoritical and experimental technique. The model dynamics of the sensor is studied and stable transfer function is determined. Validation of the model was done by comparing the results with that of the theoretical results of the system model. The chapter is concluded with the results, discussions, conclusions and reference list.

1.11 Publication on this chapter

1. Dutta, N., & Bhuyan, M. Chapter 3, Measurement of Odour by Sensor Arrays, *Odour Impact Assessment Handbook*, Wiley Publisher. (In Press).

CHAPTER 2

CHAPTER 2

NOISE FEATURE ANALYSIS OF MOS GAS SENSORS

2.0 Introduction:

Electronic nose uses an array of gas sensors with different selectivities towards the various classes of compounds, and the composite signal of the array is used in conjunction with chemometrics for the classification and identification of classes of the samples. There exist several materials to build gas sensors as discussed in **Chapter 1**.

MOS gas sensors are one of the most widely spread devices used for E-Nose applications due to their low cost, acceptable response, low recovery times and robustness. Electronic noses are more widely used in environmental monitoring, food quality detection and medicine. The odour recognition process in electronic nose begins in the sensor system which is responsible for capturing or measurement of the odourant stimulus through the sensitivity of its sensors. Each odourant is presented to the sensor system, which generates a pattern of resistance values that characterize the odour. This pattern is presented to the recognition system, which in turn classifies the odour.

The preprocessing of the data is done before the classification of odour. The data preprocessing is important because a number of different problems can compromise the performance of the sensor system which are as follows:

i) The odour signal can present disturbance or noise,
ii) The data acquisition may be unstable,
iii) The signal propagation through the communication channel between the sensor and pattern recognition systems can be contaminated by the interference signals from the environment.

The odour responses must be analyzed before the pattern recognition process to compensate for the concentration drifts in the response arrays, eliminate noise and normalize data.

Noise in gas sensors is considered to be any unwanted effect that obscures the measurement of the desired signal. Noise can arise at various stages in the measurement process, including the sensor signal under measurement, the sensors, the analog processing system, the data acquisition stage and the digital signal processing system out of which the noise in the early measurement stages is most harmful as it propagates and can be potentially amplified through the subsequent stages in the signal pathway. Noise can also arise in the latter stages of the signal pathway, primarily during the analog-to-digital conversion, when the continuous sensor signals are converted into a discrete subset of values and stored in the computer memory. On the other hand, the inherent drift and poor repeatability of sensor responses can also sometimes be significantly larger than most of the other noise sources effectively limiting the sensitivity of electronic nose systems.

2.1 Temperature Modulation:

The selectivity of MOS gas sensors is greatly influenced by the operating temperature of the device, since the reaction rates for different volatile compounds and the stability of adsorbed oxygen species are a function of surface temperature. The performance of the MOS gas sensors can be enhanced by improving the temperature-selectivity dependence. The temperature of the sensor may be cycled during the exposure to an odourous compound to obtain multivariate dynamic responses. Several approaches have been explored for deriving higher numbers of features by applying modulated temperature to the sensor instead of applying a fixed temperature[114-117]. Application of periodic heating voltage to MOS gas sensors has several advantages:

i) Because of different rates of reaction of various gases at different temperatures, a cyclic variation of temperature gives a unique signature for each gas.
ii) Sensitivity and selectivity may be enhanced.

Usually it is seen that applications such as pattern recognition and multi-component analysis are done with fixed temperature of the sensor heater, which leads to lack of selectivity and discrimination capability of the sensor. Many authors have indicated that modulation of the sensor temperature[114-116] provides more information from a single sensor than in isothermal operation, allowing improved research works in gas detection. Authors have reported on the advantage of temperature modulation of MOS gas sensor at two different temperatures to detect the presence of carbon mono-oxide[19, 118, 119]. Work has been carried on the temperature modulation using square wave to quantify hydrogen sulphide by many researchers[21, 22]. To discriminate between different gases, modulating waveforms such as sawtooth, triangular and square were also applied to the sensors[23]. The sinusoidal variation in the temperature also enhanced the identification of different gases. A number of works on the cyclic variations of the sensor heater have been reported by many authors [120, 121]. In the temperature cycling technique, the heating element of the gas sensor is connected to a waveform generator that periodically changes the working temperature of the device.The development of micromachined substrates for MOS gas sensors ensured operating temperature modulated in a more efficient way. Cavicchi *et al* introduced the use of micromachined tin oxide gas sensors in temperature modulation applications[26-28]. The temperature profile of the sensor surface greatly influence the response behavior due to rapid thermal fluctuations in respect of its noise and stability. Researchers have tried to improve selectivity by modulating the heater voltage however analysis of noise and stability of the sensor responses under modulated heater voltage has not been explored so far. Therefore the aim of this research is to analyse the baseline noise behavior and stability of MOS gas sensors by applying pulse voltages to the heater with different frequencies and duty cycles.

2.1.1 Experimental set-up:

In this research work, noise feature analysis of MOS gas sensors under pulse temperature modulation is achieved. Three MOS gas sensors, TGS-2611, TGS-822 and TGS-842 of FIGARO INC, Japan (Table 2.1) are used to carry out the experiments for noise feature analysis. Based on its sensitivity to different odours such as alcohol, volatile organic compounds (VOCs) etc the sensors are selected. The three MOS gas sensors are supplied with the gases through the teflon pipes. The different gases used in the experiment are *ethyl acetate, acetonitrile, ethanol, kerosene, petroleum ether,*

chloroform, methanol, isopropyl alcohol, acetone and *hexane*. The description of each of the gases is tabulated in Table 2.2.

Table 2.1: Details of the Sensors used in Experiments

Sensors Range	Manufacturer	Specific Use	Detection Range
TGS-2611	Figaro Engineering Inc.	Combustible gas detection. Sensitive to Methane, Acetonitrile, Kerosene, Petroleum ether, Chloroform, Methanol, Acetone, Hexane etc.	500 to 10,000 ppm
TGS-822	Figaro Engineering Inc.	Organic solvents such as alcohol (ethanol, isopropylalcohol, methanol etc.), toluene etc.	50 to 5,000ppm
TGS-842	Figaro Engineering Inc.	Combustible gas detection. Sensitive to acetonitrile, chloroform, methanol, acetone hexane etc.	500ppm to 10,000ppm

Table 2.2: Composition of the ten sample gases:

Sl. No.	Gases Used	Description
1.	Ethyl-acetate ($CH_3COOCH_2CH_3$)	It is an organic compound and is the ester of ethanol and acetic acid.
2.	Acetonitrile (CH_3CN)	It is the simplest organic nitrile and also termed as methyl cyanide.
3.	Ethanol (CH_3CH_2OH)	It is a 2-carbon alcohol and also termed as ethyl-alcohol.
4.	Kerosene	It is a combustible hydrocarbon liquid constituting of n-dodecane, alkyl benzenes, and naphthalene and its derivatives.
5.	Petroleumether	It is a light hydrocarbon comprising of a mixture of alkanes, e.g., pentane, hexane, and heptanes.
6.	Chloroform ($CHCl_3$)	It is an organic compound produced by heating a mixture of chlorine and either chloromethane or methane.
7.	Methanol (CH_3OH)	It is the simplest alcohol and also termed as methyl-alcohol.

8.	Isopropylalcohol (C_3H_8O)	It is the simplest example of a secondary alcohol, where the alcohol carbon is attached to two other carbons. It is a structural isomer of propanol.
9.	Acetone ($(CH_3)_2CO$)	It is also termed as dimethyl-ketone and is produced directly or indirectly from propylene.
10.	Hexane (C_6H_{14})	It is a hydrocarbon or an alkane with six carbon atoms.

The sensor TGS-2611 has a very high sensitivity to methane gas. The target gases for this type of sensor are methane and natural gases. So the sensor has sensitivity towards gases such as *acetonitrile*, *kerosene*, *petroleum ether*, *chloroform*, *methanol*, *acetone* and *hexane*. TGS-822 has high sensitivity to the vapors of organic solvents as well as other volatile vapors. It also has sensitivity to a variety of combustible gases. Hence the sensor has good sensitivity towards the gases such as *ethanol*, *isopropylalcohol*, and *methanol*. Similarly, TGS-842 has high sensitivity and selectivity to methane and natural gases (naturally occurring hydrocarbon gas mixture). The gases such as *acetonitrile*, *chloroform*, *methanol*, *acetone* and *hexane* therefore are sensitive to this sensor.

Diaphragm pumps are used to direct the sample gas and the clean air flow into the sensor headspace. The pumps are controlled by the PC through a driver circuit consisting of relays and transistor switches. The sequence of 'purging' and 'refreshing' with proper time duration was controlled through the DAQ card by the PC using LabVIEW programming. The sensors used are shown in Fig.2.1. The experimental set-up consists of these three sensors and a diaphragm pump system with flow control devices.

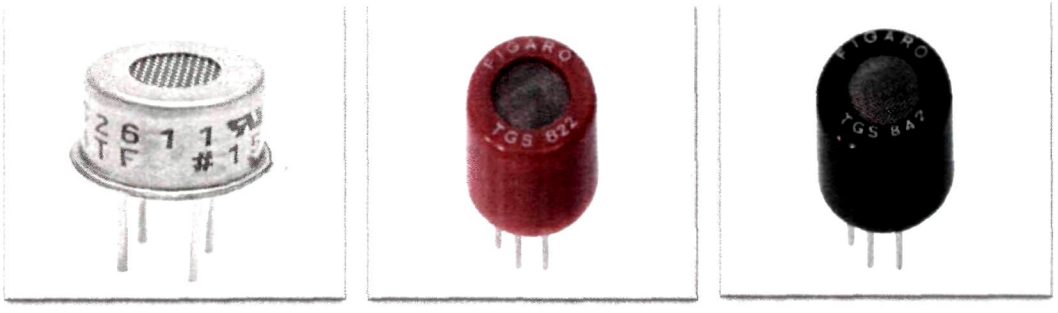

TGS-2611 TGS-822 TGS-842

Fig. 2.1. Three Taguchi Gas Sensors from Figaro Inc. Japan, used in this Research Work.

The experiment is conducted on the MOS gas sensors for different pulse modulating temperature. The modulation patterns of heater voltage (frequency and duty cycle) of the sensors are controlled by a PC through a Data Acquisition (DAQ) card PCI6024E, National Instruments) and data acquisition software-LabVIEW. Analog output of the card was applied to the gate of a MOSFET which supplies the pulse modulating voltage to the heaters of the sensors. Therefore, the heater voltage ($+V_H$) accordingly followed the pulse signal to excite the sensor. The sensor output was interfaced to the PC through the DAQ card. The sensors are kept inside a sensor head chamber away from interfering gas so that the baseline is established with clean air. Before each run of data acquisition, the baseline was verified and when found deviated, it was corrected by applying clean air. It was found in each run of experiment that on application of clean air the sensor baseline settles to a fixed level ensuring absence of any interfering gas. When the pulse signal generated by the PC switches on the MOSFET, the heater voltage is switched on to +5 V with the same frequency as that of the pulse applied. As a result the sensor temperature becomes pulsating with different frequencies. Fig 2.2 shows few typical signals used for modulating the heater temperature; however the pulse (b) signal was used for the experiment.

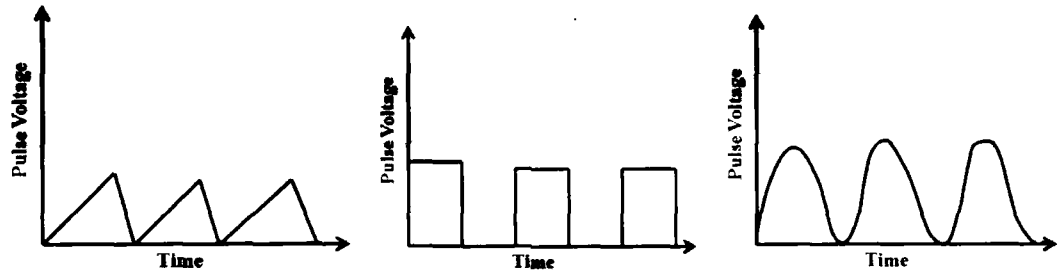

Fig. 2.2 Typical signals (a) ramp, (b) pulse and (c) sinusoidal used for modulating the heater temperature .

Ideally, the reference and sample vessels are placed in controlled room environment at about 25°C temperature and 65% humidity with deviation less than ±2%. The switching circuits are developed using 12 V relay (**Series 511, SPDT**) for alternately switching between reference vessel and sample vessel. The sequence of 'purging' and 'refreshing' with proper time duration was controlled through the DAQ card by the PC using LabVIEW programming. The two transistors used for switching are **BD139**. Two diaphragm pumps (**SB-548A**) are used for constant supply of sample vapour and room

air as desired by the programmed options. Data acquisition of the sensor signals is performed by High Performance data Acquisition Card (PCI-6024E, National Instruments). The card has also been used to condition the data in required format and convert into digital form to make it compatible with computer processing. The photograph of the sensor set-up is shown in Fig.2.3.

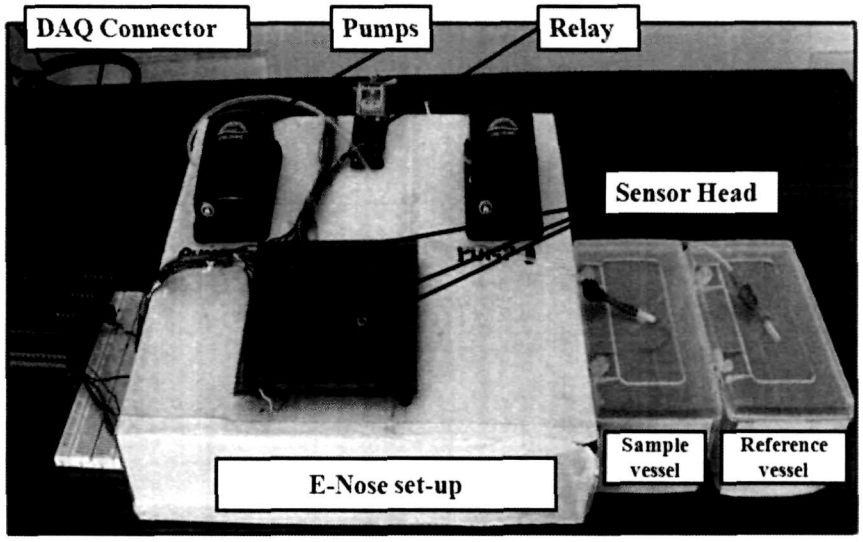

Fig. 2.3: MOS Gas sensor Experimental set-up, Department of Electronics & Comm.Engg., Tezpur University, India.

2.2 Noise parameters analysis:

Research has been carried out on the noise in sensors[122, 123] and different techniques have been developed for selectivity detection of gases[124]. Determination of noise features such as Probability Distribution Function (PDF) and power density spectrum estimation has been performed for several typical gas sensors[125]. The noise feature analysis for typical gas sensors have been performed by many researchers during the past years. Fengchun Tian et al[126] determined the noise features of gas sensors due to fixed sensor temperature; however noise analysis under modulated temperature has not yet been performed. The reason for analyzing the sensor noise behavior at different frequencies and duty cycles is that we need to know a suitable pulse frequency and duty cycle at which the sensor can be used with the best signal to noise ratio (SNR). This is important in circumstances where a sensor has to discriminate or classify odours in a noisy environment. In this work, pulse modulated heater voltage with different frequencies and

duty cycles were applied to the heater of the MOS gas sensor heater to achieve the modulation in the sensor temperature for studying the type of noise. The frequency spectrum of noise was determined by FFT analysis and noise dependency was verified by PDF, histogram and SNR under different frequencies and duty cycles of pulse heater voltage. Fig.2.4 shows the pulse modulating and DAQ system.

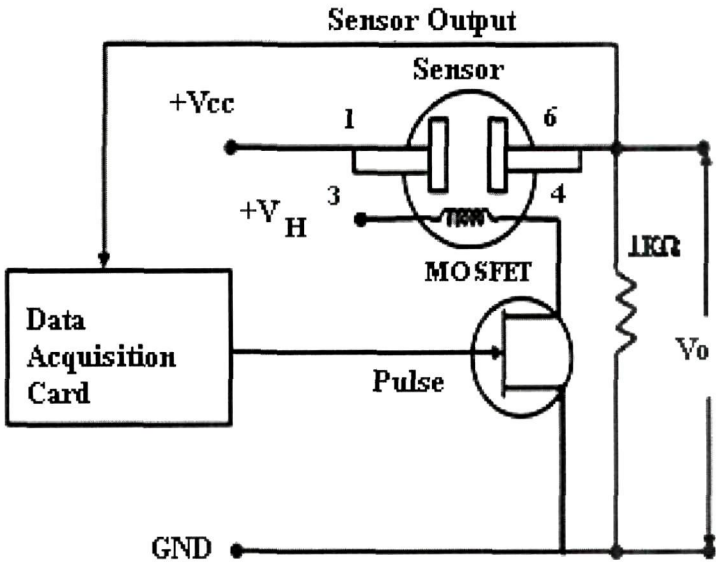

Fig. 2.4. Pulse modulating and DAQ system.

2.2.1 Data Acquisition:

In this research, we have conducted sensor noise analysis by two different experiments-

a) In the first part of the experiment, the data acquisition and storage was done without the application of any input odour to the MOS gas sensor.
b) Based on the experiment (a), the best selected frequency and duty cycles are used to show the classification efficiency. The analysis is conducted on the acquired signals by applying ten different gases- acetone, acetonitrile, chloroform, ethanol, ethyl acetate, isopropylalcohol, kerosene, methanol, n-hexane and petroleumether.

The flow rates are kept constant for both of the two experiments. The schematic diagram for the flow control and alternate switching for sample and reference gases is shown in Fig.2.5. The gases were selected based on the fact that the MOS gas sensors used (TGS-

2611, TGS-822 and TGS-842) have good sensitivities to the families of the gases as described in *Section 2.1.1.*

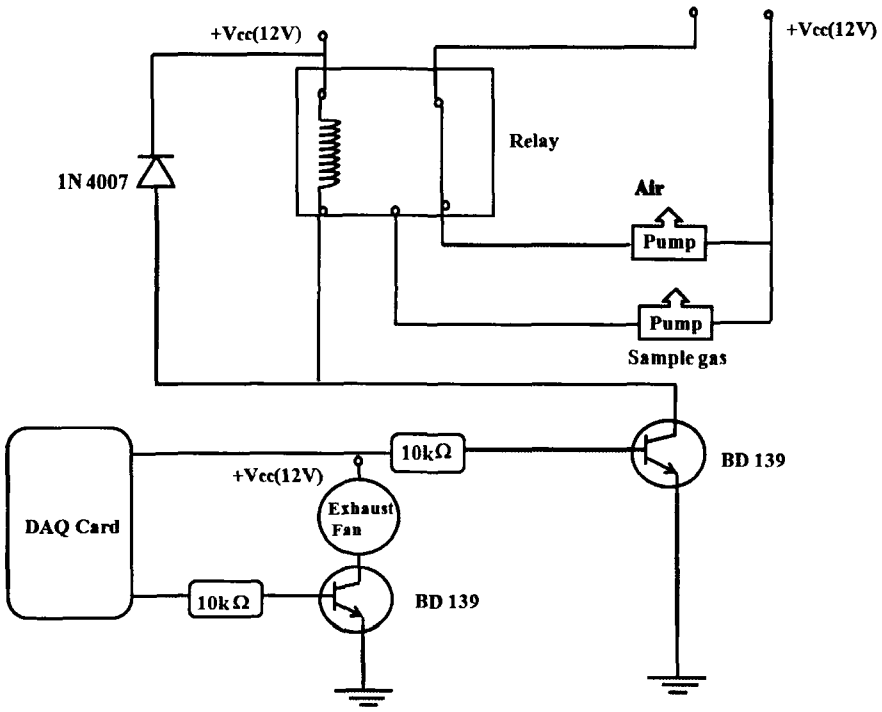

Fig. 2.5. Pump control driver circuit for switching between sample and reference vessels.

2.2.1.1 LabVIEW Environment

LabVIEW features interactive graphics, a state-of-the-art user interface, and a powerful graphical programming language. In the LabVIEW DAQ VI Library, a series of virtual instruments for using LabVIEW with National Instruments DAQ hardware, is included. The devices have three different input modes—non referenced single-ended (NRSE), referenced single-ended (RSE), and differential (DIFF) input. The single-ended input configurations provide up to 16 channels while the DIFF input configuration provides up to eight channels. Input modes are programmed on a per channel basis for multimode scanning. Connection of these analog input signals to the device depends on the type of input signal source and the configuration of the analog input channels used. When configuring the input channels and making signal connections, we determine whether

the signal sources are floating or ground-referenced. A ground-referenced signal source is connected to the building system ground and is, therefore, already connected to a common ground point with respect to the device, assuming that the computer is plugged into the same power system. In our case we configure the input channel in the RSE mode. The devices have a bipolar input range that changes with the programmed gain. The devices can scan multiple channels at the same maximum rate as their single-channel rate. They supply two channels of analog output voltage at the I/O connector. The bipolar range is fixed at ±10 V. Data written to the digital-to-analog converter (DAC) is interpreted in two's complement format. The block diagram configured in LabVIEW is shown in Fig 2.6. For measurement task, the simulated signal was configured as 'Output to DAQ assitant2'. The 'Write to Measurement file' was configured for storing the data which was saved as LVM files. The sensor responses were observed in the front panel.

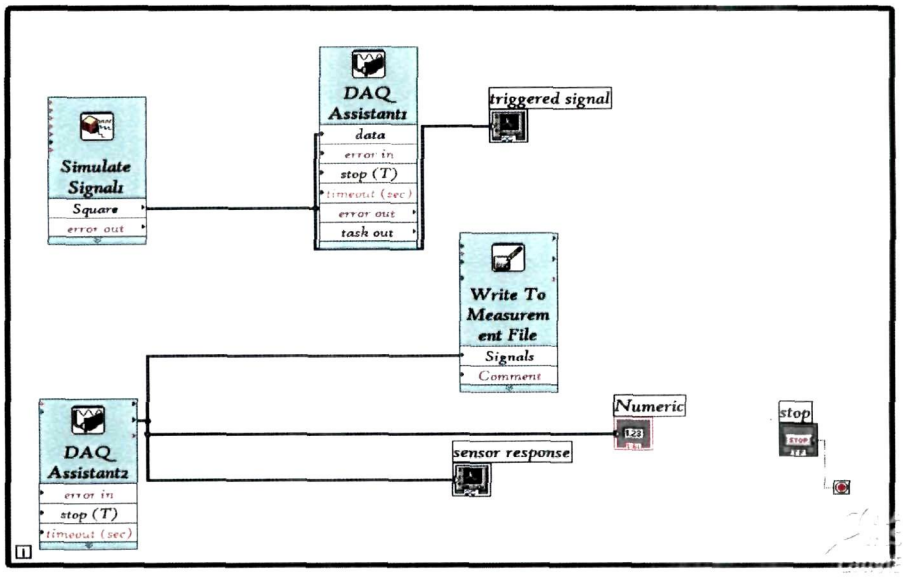

Fig. 2.6 Block diagram configured in LabVIEW.

2.2.1.2 Heater Voltage Modulation

A pulse signal whose duty cycle and frequency can be controlled was generated in the LabVIEW environment and applied to the sensor heater through a MOSFET. As a result the sensor temperature becomes pulsating with different 'on' and 'off' durations. The sensor output signal captures noise developed inside the sensor which is mostly thermal

noise. The sensor response was analyzed without applying any gas for noise with the pulsed heater voltage applied. The frequency and the duty cycle of the heater 'on'/ 'off' sequence was varied to analyze the noise behavior.

The sensor temperature was pulsed at four selected frequencies of 10mHz, 40 mHz, 80 mHz and 120 mHz to generate noise. Further the noise behavior was analyzed with two different 'on' and 'off' time durations i.e. duty cycle of the pulse signal- 50 % and 75 % duty cycles without the application of any gas. The MOS gas sensor noise analysis under signal inactive period i.e. without application of gas is important to determine suitable time duration of the pulsed heater voltage at four different heater pulse frequencies. Therefore the frequency and duty cycle of the heater pulse voltage is required to be correlated to severity of noise. The sensor responses were acquired at a sampling frequency of 1 kHz over duration of about 15 min, so that sufficient data is available for analysis. The pulse frequency and duty cycle were varied for each experiment after correcting the baseline. In order to avoid non-uniformity, data for a single pulse cycle was extracted and analyzed in MATLAB.

Normalization of data was performed to highlight the noise spectrum over a positive scale. FFT, PDF, histogram, other statistical parameters (mean, standard deviation and variance) and SNR were calculated. The total data points for the signals with frequencies of 10 mHz, 40 mHz, 80 mHz and 120 mHz were 100×10^3, 25×10^3, 12.5×10^3, 8×10^3 respectively at the sampling frequency used in the experiments.

2.2.1.3 Measuring Circuit

The application circuit diagram for measuring the MOS gas sensors response is shown in Fig.2.7. The resistances and power supplies indicated in Fig.2.7 are as follows:

i) Sensor Resistance (R)

This is the characteristic resistance of the sensor surface normally defined by the manufacturer in a range under standard ppm of certain sample and other circuit conditions of load resistance and power supply (V_c). The value R changes on exposure to different sample vapors. The typical values are (1-5)kΩ for TGS-2611, (1-10)kΩ for

TGS-822 and (3-15)kΩ for TGS-842. The output response is generated by the change in the resistance of the sensor surface on application of a gas.

ii) Load Resistance (R_L)

The load resistance is selected based on the condition that the power dissipation does not exceed the limit specified by the manufacturer for the sensors. The resistance values are calculated for the three sensors based on the maximum current under minimum sensor resistance (R). The values are indicated in the circuit diagram of Fig.2.7 and listed in Table 2.3.

iii) Circuit Power Supply (V_c)

The maximum circuit power supply specified by manufacturer for the three sensors is 24V. In this circuit, the used value of V_c is 12V.

iv) Heater Voltage (V_H)

The heater voltage is a uniform value of 5V for all the three sensors which keeps the sensors at elevated temperature of 200 to 400°C (approx.) to have better response.

v) Output Voltage (Vo)

The output voltage is measured as the sensor response across the load resistance R_L which varies from a fraction of a volt to few volts.

vi) Power Dissipation (P_S)

The maximum power dissipation takes place when the sensor resistance (R) is minimum for chosen load resistance and power supply. The power dissipation is given by -

$$P_S = (V_C^2 \times R_S)/(R_S + R_L)^2$$

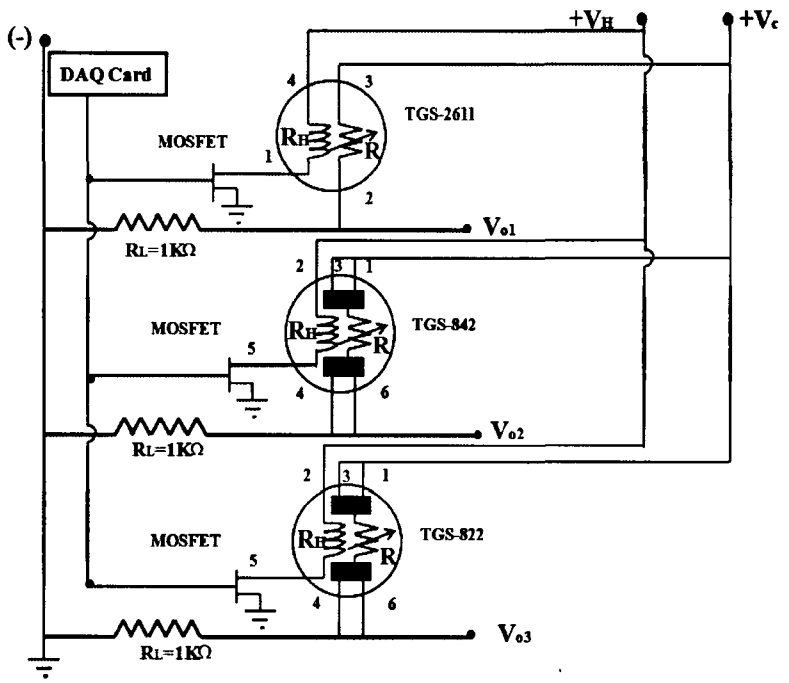

Fig. 2.7 Measurement Circuit for MOS gas sensor responses.

2.2.1.4 E-Nose set-up

The E-Nose system of this work comprises of three MOS gas sensors namely TGS-2611, TGS-822 and TGS-842. The interfacing with the PC is done in order to achieve the online acquisition of E-Nose sensor responses in real time and providing control signals to the E-Nose electronic circuits for various operations such as switching and time setting. The E-Nose set up interfacing with PC is shown in Fig.2.8.

2.2.2 Data Pre-processing:

The pre-processing of the data is done for the following reasons-

i) to reduce the amount of data which are irrelevant to the study;
ii) to enhance sufficient information within the data to achieve the desired goal;
iii) to transform the data to a form suitable for further analysis.

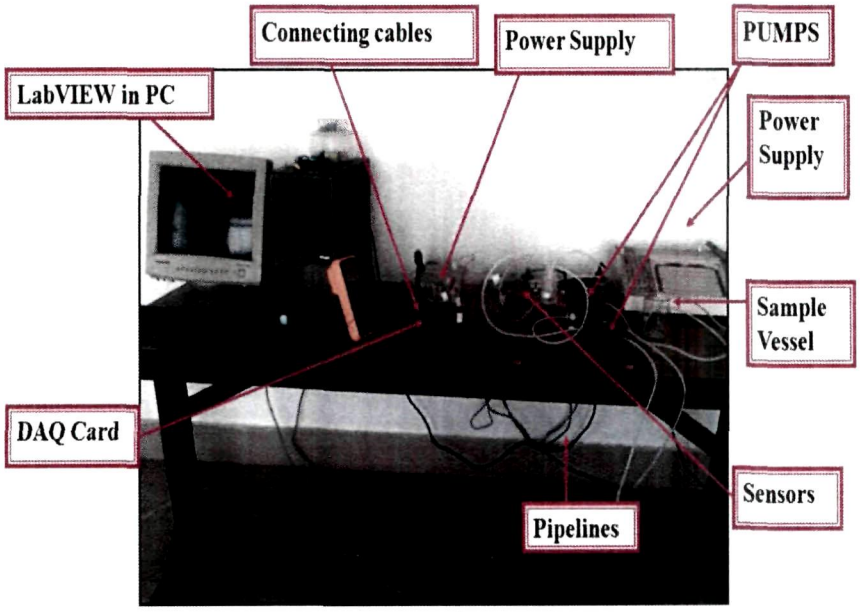

Fig. 2.8 E-Nose set up interfacing with PC.

Various analytical methods are used for the pre-processing of data out of which the common one is the vector normalization method. Since the sensors in the E-Nose array have different sensitivities, the voltage levels of the output signals from the sensors will be different. Hence the signal levels need a standardization or normalization. Normalization removes sample-to-sample absolute variability and transforms vector length to be one. It assumes that the extracted features linearly correlate with signal intensity. Various methods of normalizations are available such as-

a) Liberalization:

$$X_{ij} = \log\left|(Y_{ij}^{\max} - Y_{ij}^{\min})\right| \tag{2.1}$$

$$X_{ij} = \sqrt{(\left|(Y_{ij}^{\max} - Y_{ij}^{\min})\right|)} \tag{2.2}$$

b) Vector Normalization:

$$R_{ij} = X_{ij} / \sum (X_{ij})^2 \tag{2.3}$$

c) Sensor Normalization:

$$R_{ij} = X_i / \max(X) \tag{2.4}$$

d) Sensor Auto Scaling:

$$R_{ij} = \left|(X_{ij} - X_{ij}^{mean})\right| \sigma_i \tag{2.5}$$

where σ is the standard deviation. X's are the calculated or preprocessed values and Y's are the observed or measured values for sample odour and Y_{ij}^{max} and Y_{ij}^{min} are its maximum and minimum values.

Table 2.3: MOS gas sensor parameters.

Sensor	V_H (V)	V_c (V)	Sensor Resistance R(k Ω)	Heater Resistance R_H (Ω)	Heater Current I_H (mA)	R_L (k Ω)	Max.Power Dissipation (P_s), for R (min) (Worst condition)	Target Gases
TGS-2611	5	5	0.68 to 6.8 in 5000 ppm	59	56 ± 5	1	12.5mW	Methane, Natural Gas
TGS-822	5	5 or 10	1 to 10 in 300ppm	38	132	1	12.5mW	Alcohol Organic solvents
TGS-842	5	5 or 10	5 to 20 in 1,000ppm	30	167	1	4.68mW	Methane Natural gas

The normalised data are stored in the memory for pattern recognition. Most widely used normalization technique is the vector normalization where each feature vector is divided by its mean so that it is transformed to lie on a hyper-sphere of unit value. We have used sensor normalization technique (eqn.2.4) to normalize the sensor data for noise feature analysis.

2.3 Statistical analysis:

The MOS gas sensor noise analysis under signal inactive period i.e. without application of gas is important to determine a suitable time duration of the pulsed heater voltage at four different heater pulse frequencies. Therefore the frequency and duty cycle of the heater pulse voltage is required to be correlated to severity of noise. Here we have tried to observe and analyse the noise in the MOS gas sensors with the sensor excited by its power supply (V_c) and pulse modulated heater voltage (V_H) without applying any gas.

From the sensor data response, a single data set X is constructed for all the four different frequencies i.e. 10mHz, 40mHz, 80mHz and 120mHz and two duty cycles of 50% and 75%. The LabVIEW display of sensor TGS-822 for 10mHz and 50% duty cycle is shown in Fig. 2.9. The noisy responses of the gas sensors TGS-822, TGS-842 and TGS-2611 for all the four frequencies and two duty cycles, in MATLAB are shown in Fig.2.10.

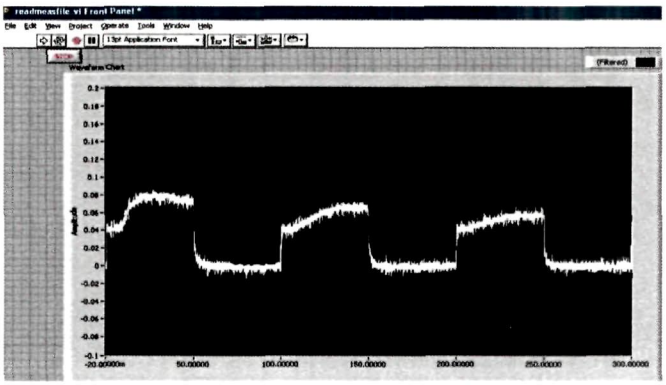

Fig. 2.9. Noisy response shown by sensor TGS-822 in LabVIEW at 10mHz and 50% duty cycle.

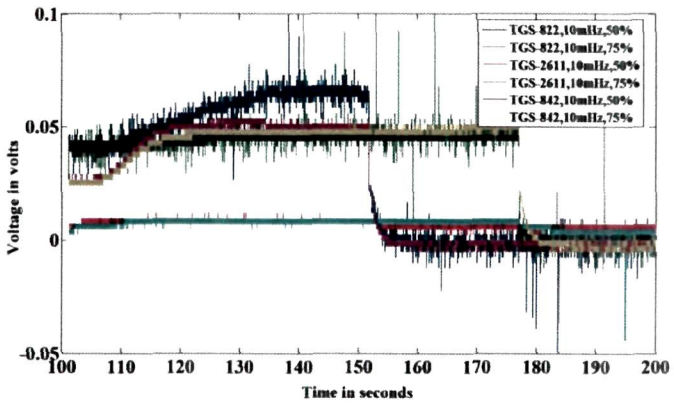

(a)

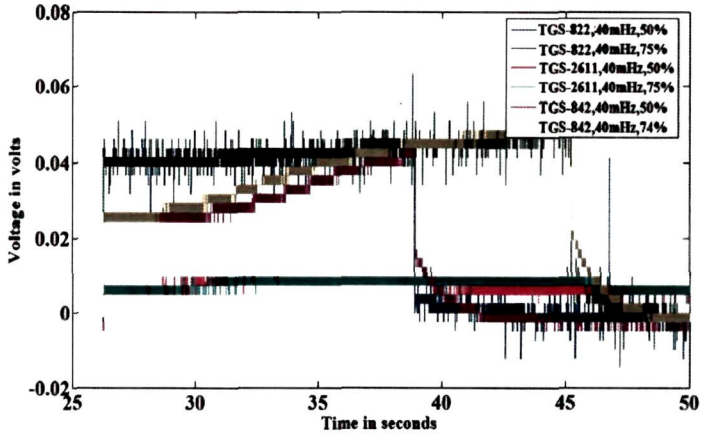

(b)

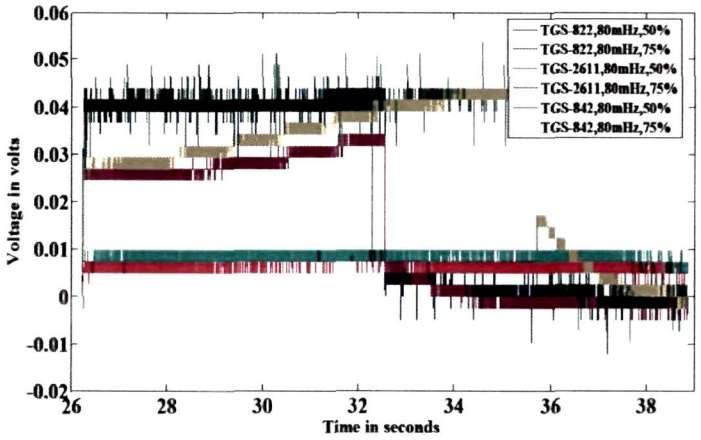

(c)

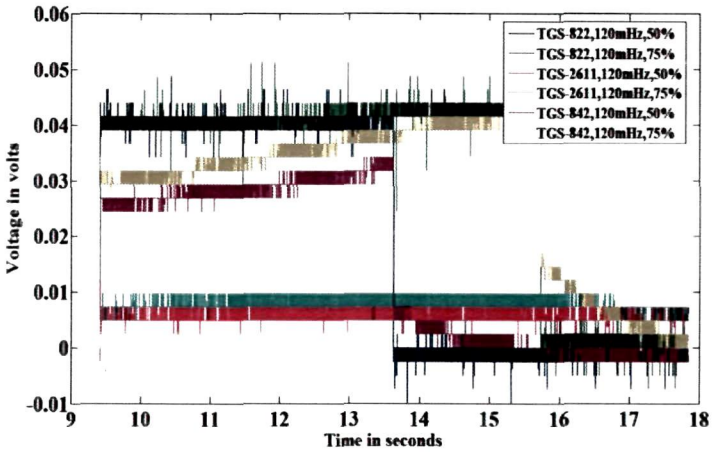

(d)

Fig. 2.10. Noisy responses of TGS-822, TGS-2611 and TGS-842 at 50% and 75% duty cycles for (a) 10mHz, (b) 40mHz, (c) 80mHz and (d) 120mHz.

The data vector has been constructed for each sensor comprising of two columns- the time-column (x-axis) and the sensor voltage (y-axis). The y-column vector was used to compute the FFT of the sensor data in MATLAB.

2.3.1 Probability distribution function (PDF):

PDF is an important statistical tool to analyze the noise characteristics of a sensor signal. The theory of probability gives us the basic tools for constructing and analyzing mathematical models for random phenomena such as noise.

In this chapter, noise analysis under modulated temperature is performed. Pulse modulated heater voltage with different frequencies and duty cycles are applied to the MOS gas sensor heater to achieve the modulation in the sensor temperature for studying the type of noise. The frequency spectrum of noise is determined by FFT analysis and noise dependency is verified by PDF, histogram and Signal-to-Noise Ratio (SNR) under different frequencies and duty cycles of pulse heater voltage. The normalized data from the sensors is used to compute the PDF estimation and histogram. The noise PDF shows that for all cases of pulses, the distribution is Gaussian however with different mean, variance and standard deviation. The PDF for the sensor noise signals satisfies the requirement for the noise to be coloured i.e. with non-zero mean. Fig. 2.11 shows the PDF of TGS-822, TGS-842 and TGS-2611 at 10mHz, 40mHz, 80mHz and 120mHz each at 50% and 75% duty cycles respectively.

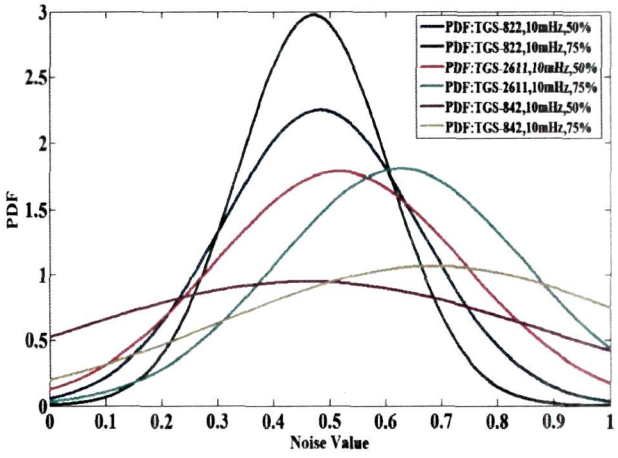

(a)

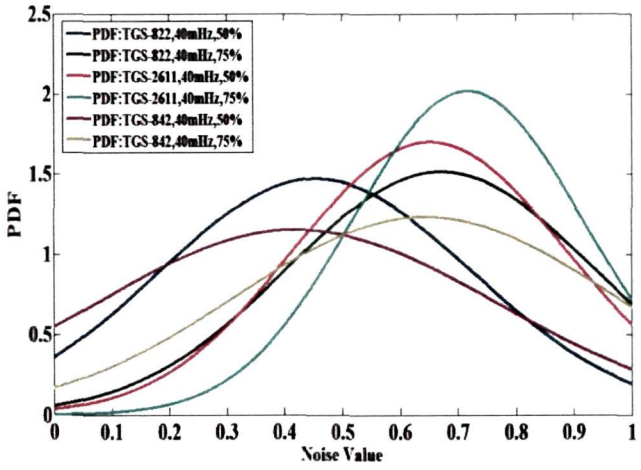

(b)

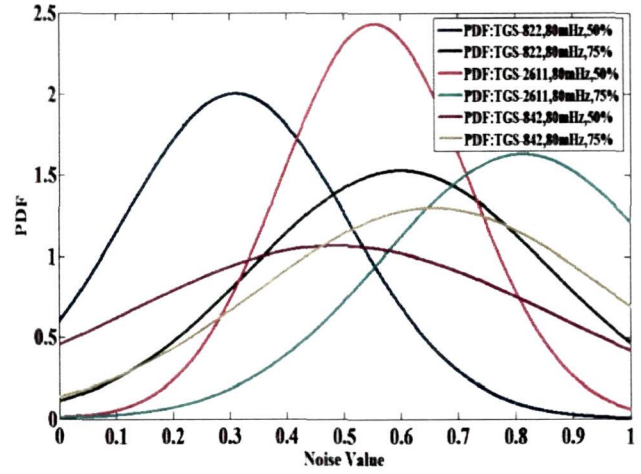

(c)

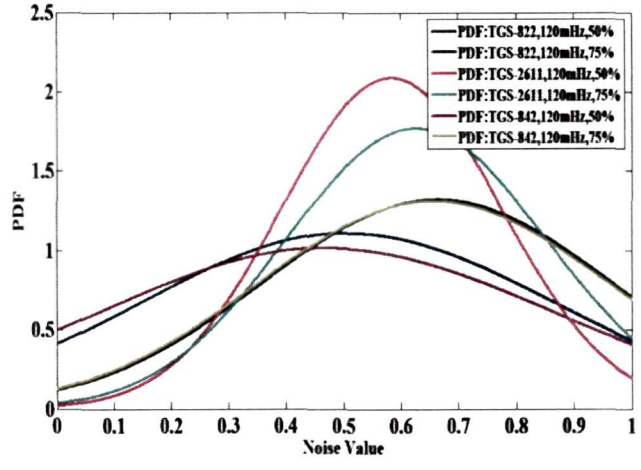

(d)

Fig. 2.11. The PDF of TGS-822, TGS-2611 and TGS-842 sensor noise signals at 50% and 75% duty cycles for (a) 10 mHz , (b) 40 mHz, (c) 80mHz and 50% duty cycle, and (d) 120mHz.

2.3.2 Histogram:

Histogram is a graphical representation showing a visual interpretation of the distribution of data. The histogram is used to group sensor response voltages together that have the same value. The histogram method, which has been proved to be an unbiased estimation for a random variable, is used to estimate the PDF of noise[127]. Typically, the histogram results a Gaussian distribution when the number of samples is large. Hence from definition of histogram, the sum of all the values in the histogram must be equal to the number of points N, in the signal given by eqn.1.7.

The histogram is used to calculate the mean and standard deviation of very large data sets. The mean (μ)and standard deviation (σ) are calculated from the histogram by the equations (1.8) and (1.9).

Mathematically, a histogram is a mapping m_i that counts the number of observations that fall into various disjoint categories (known as bins), whereas the graph of a histogram is merely one way to represent a histogram. Thus, if n is the total number of observations and k be the total number of bins, the histogram m_i meets the following conditions:

$$n = \sum_{i=1}^{k} m_i \tag{2.6}$$

Fig. 2.12, Fig. 2.13 and Fig. 2.14 shows the histograms of the sensor TGS-822, TGS-842 and TGS-2611 for the same respective frequencies and duty cycles.

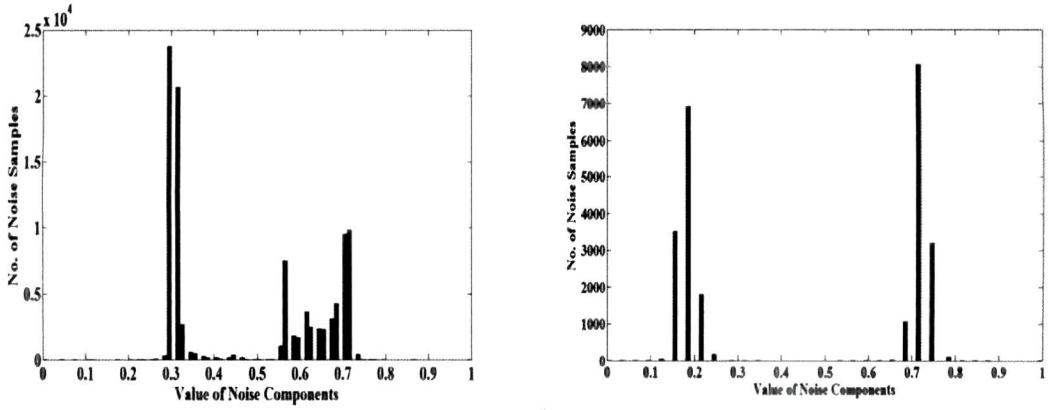

(a) (b)

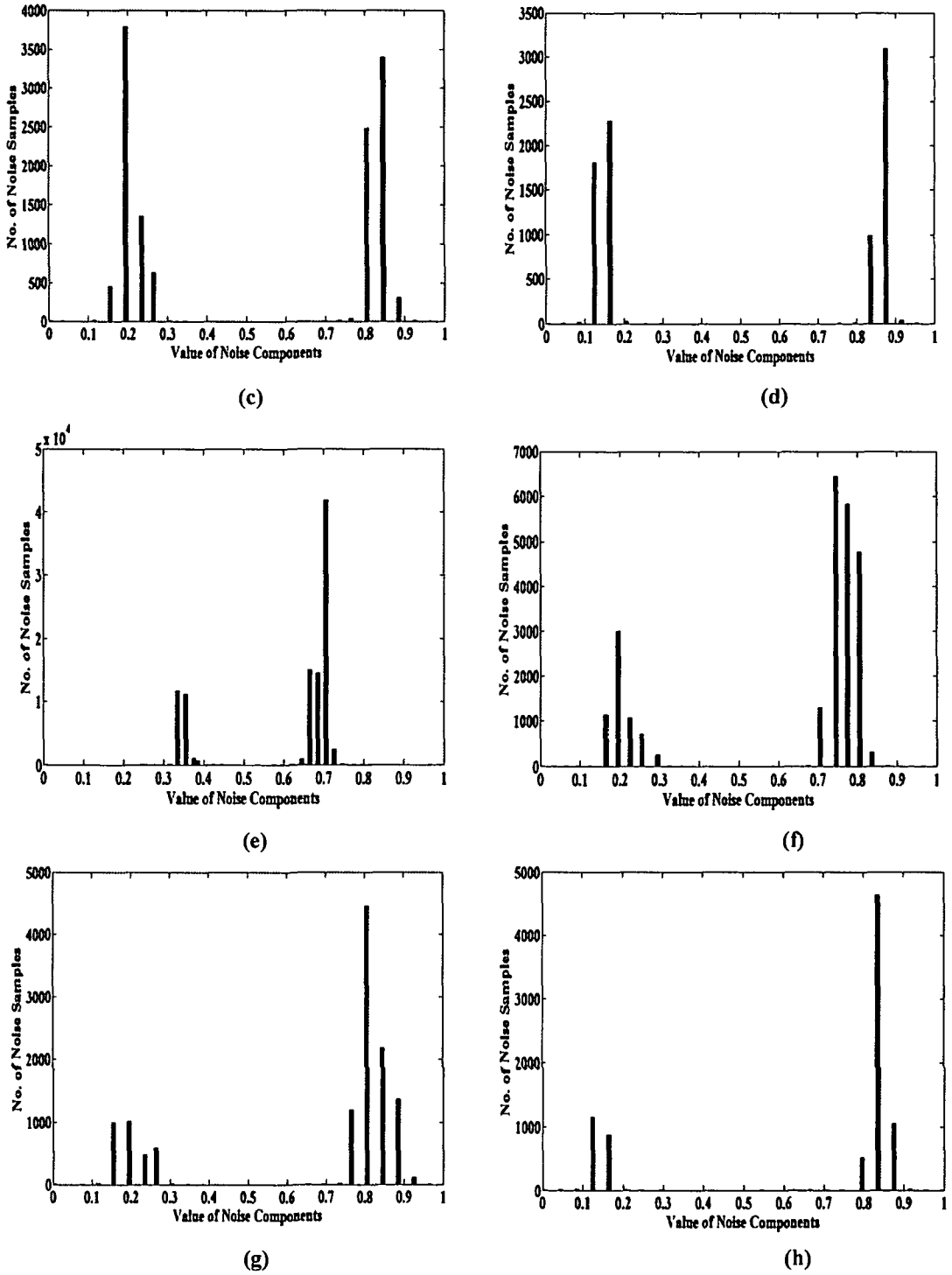

Fig. 2.12. The histogram of TGS-822 sensor noise signals at (a) 10 mHz and 50% duty cycle, (a) 40 mHz and 50% duty cycle, (c) 80mHz and 50% duty cycle, (d) 120 mHz and 50% duty cycle, (e) 10 mHz and 75% duty cycle, (f) 40 mHz and 75% duty cycle, (g) 80mHz and 75% duty cycle, (h) 120 mHz and 75% duty cycle

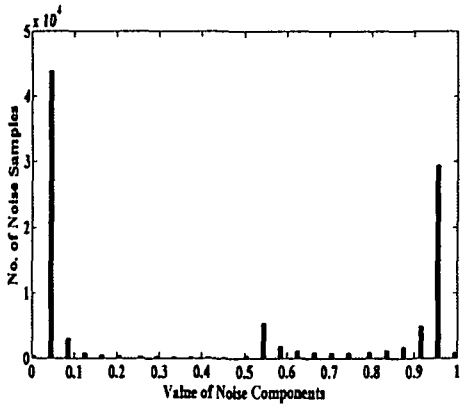
x 10^4
No. of Noise Samples
Value of Noise Components

(a)

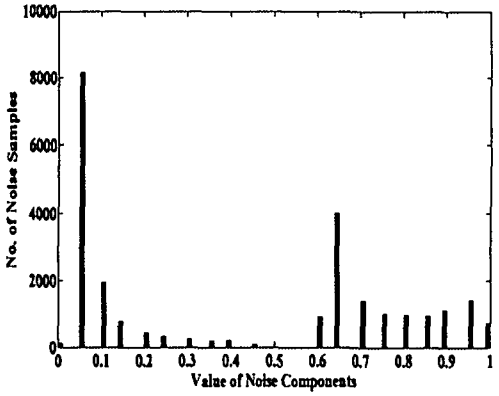
No. of Noise Samples
Value of Noise Components

(b)

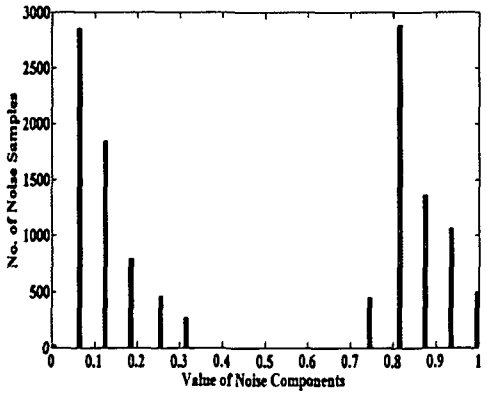
No. of Noise Samples
Value of Noise Components

(c)

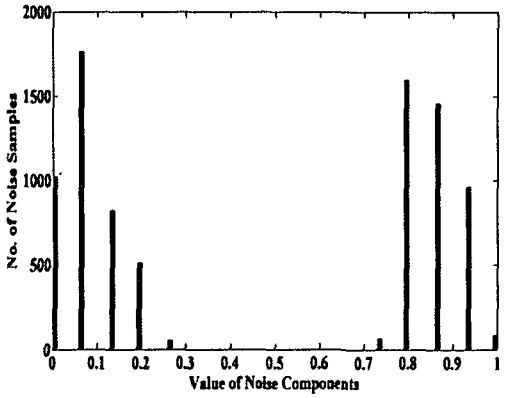
No. of Noise Samples
Value of Noise Components

(d)

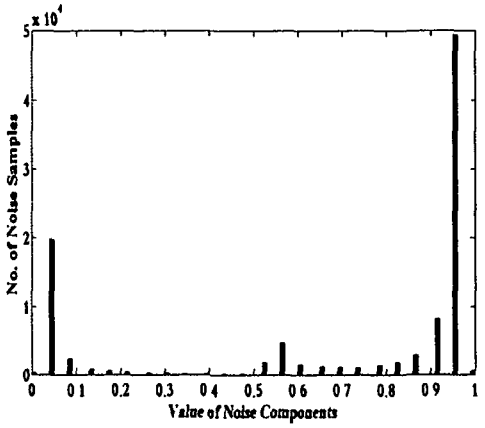
x 10^4
No. of Noise Samples
Value of Noise Components

(e)

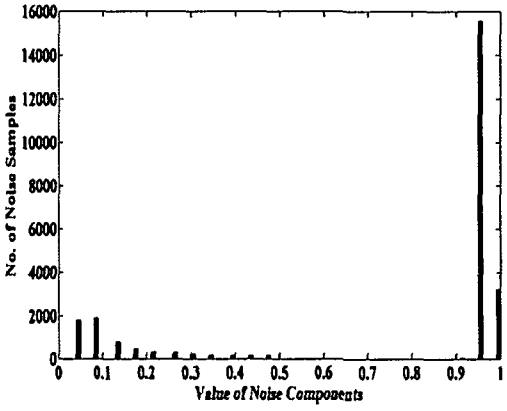
No. of Noise Samples
Value of Noise Components

(f)

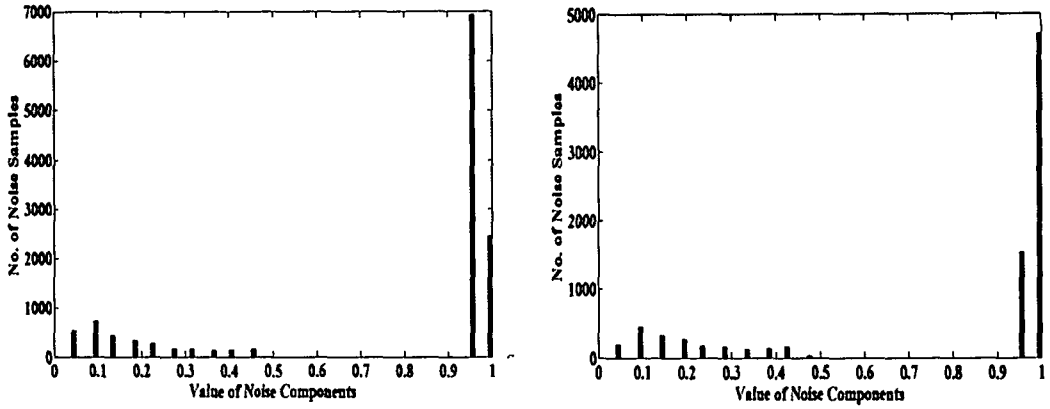

Fig. 2.13. The histogram of TGS-842 sensor noise signals at (a) 10 mHz and 50% duty cycle, (a) 40 mHz and 50% duty cycle, (c) 80mHz and 50% duty cycle, (d) 120 mHz and 50% duty cycle, (e) 10 mHz and 75% duty cycle, (f) 40 mHz and 75% duty cycle, (g) 80mHz and 75% duty cycle, (h) 120 mHz and 75% duty cycle.

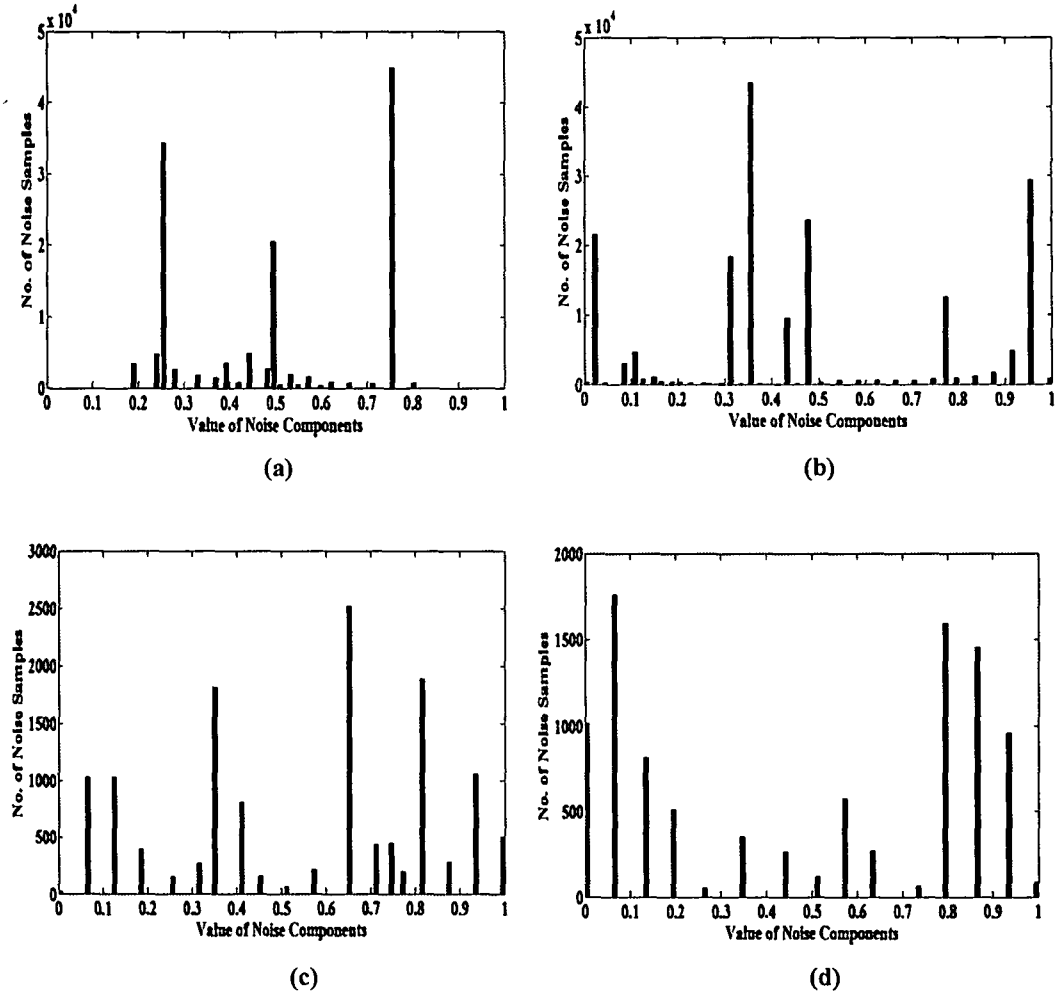

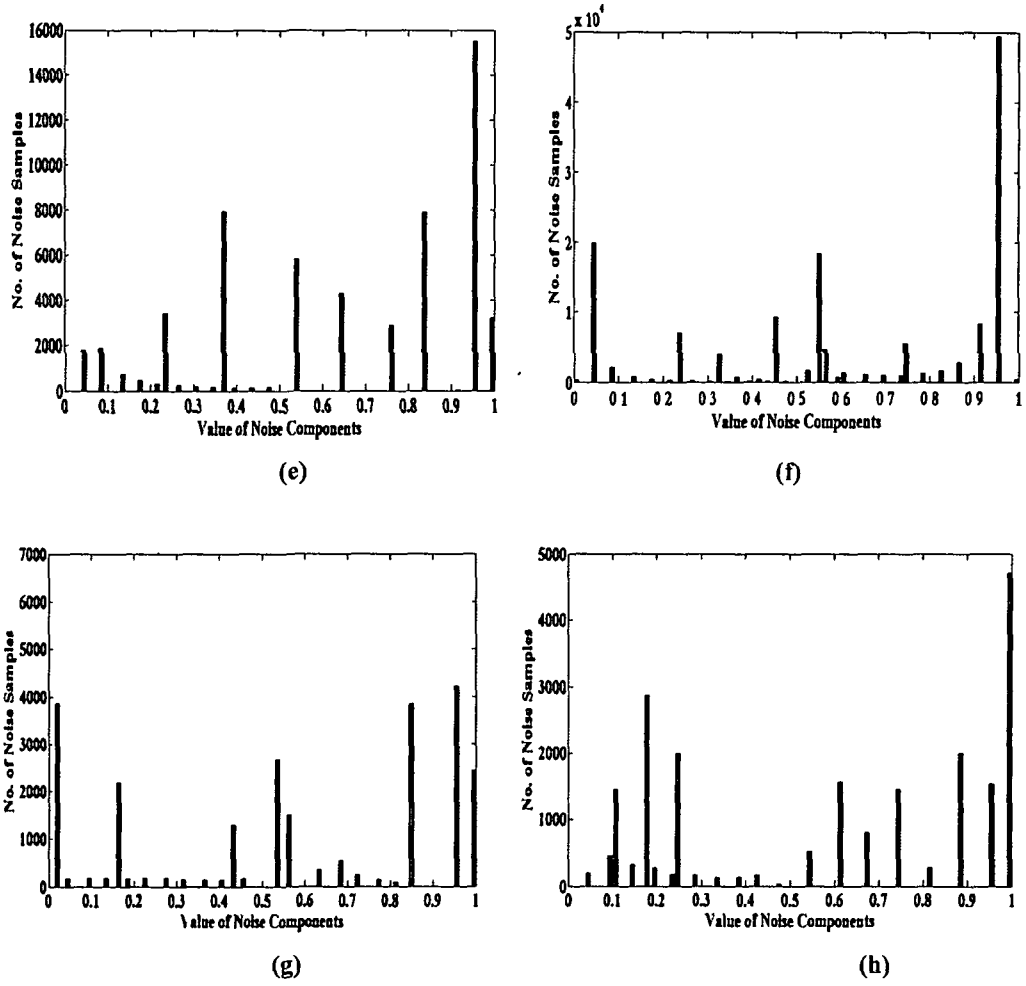

Fig. 2.14. The histogram of TGS-2611 sensor noise signals at (a) 10 mHz and 50% duty cycle, (a) 40 mHz and 50% duty cycle, (c) 80mHz and 50% duty cycle, (d) 120 mHz and 50% duty cycle, (e) 10 mHz and 75% duty cycle, (f) 40 mHz and 75% duty cycle, (g) 80mHz and 75% duty cycle, (h) 120 mHz and 75% duty cycle.

The mean value of the noise data showed that it is non-zero, depicting that the noise is colored and $1/f$ type. Higher standard deviation and variance was observed when the pulse frequency was increased which showed that the signal becomes noisier for the three sensors when pulsed heater voltage frequency is increased. The duty cycle of the pulse also changes the noise level with reverse dependency i.e. noise level increases when duty cycle is reduced. Table.2.3 shows the mean, variance and standard deviation calculated for various frequencies and duty cycles for all the three sensors. From Table 2.3 it is observed that for all the three sensors, the most convenient results i.e. lowest noise is obtained at 10mHz frequency and 75% duty cycle.

2.3.3 Signal-to-Noise Ratio (SNR):

The *signal-to-noise ratio* (SNR) is the ratio of the signal amplitude to the noise signal amplitude at a given point in time. SNR is usually expressed in dB and in terms of peak values for impulse noise and root-mean-square values for random noise. When a signal is constant or periodic and the noise is random, it is possible to enhance the SNR by averaging the measurement. In this research, the ratio of the sensor response signal for pulsed heater voltage to the noise in the average power level is termed as the Signal-to-Noise ratio (SNR) of the sensor given by-

$$SNR = \frac{P_S}{P_N} \tag{2.7}$$

where P_S is the power of the sensor response signal and P_N is that of the noise present in the signal. Measuring the SNR usually requires that the noise be measured separately, in the absence of signal. Depending on the type of experiment, it may be possible to acquire readings of the noise alone, for example on a segment of the baseline before or after the occurrence of the signal. However, if the magnitude of the noise depends on the level of the signal, then the experimenter must try to produce a constant signal level so as to measure the noise on the signal. In a few cases, where it is possible to model the shape of the signal exactly by means of a mathematical function, the noise may be estimated by subtracting the model signal from the experimental signal.

In this work, the SNR is calculated for all the three sensors during signal inactive period i.e. without application of gas and is tabulated in Table 2.3. It can be seen, that at a particular frequency of 10mHz and 50% duty cycle, the SNR of sensor TGS-822 and TGS-842 ranges from about 45.63dB to 56.88dB. Within this particular range for the said frequency and duty cycle, the two sensors produces noise differently which is same as in the case for a different set of frequencies and duty cycle. Therefore, this analysis can be used for comparing the noise immunity of the two sensors. Similar is the case when we compare all the three sensors. From Table 2.4 it can be seen that at a frequency of 10mHz and 75% duty cycle, TGS-2611 shows the highest SNR with a value of 59.22dB as compared to TGS-822 and TGS-842.

2.3.4 Noise spread and population behavior:

In this study, two newly introduced noise characteristics are analyzed with the help of the histogram components of the signal and the corresponding histogram ratios. This study is found to be an additional statistical noise feature to confirm the noise dependency on the frequency and the duty cycle of the pulse modulated heater voltage.

2.3.4.1 Signal spread and population behavior of MOS gas sensor

A histogram is a mathematical tool that gives only the number of samples for different signal levels. However, it is not possible to compare two histograms in terms of spread and population of the samples. In this study a new characteristic has been defined which determines the noise behavior of the three sensors at different sensor signal levels. We have introduced two terms namely Noise Spread Figure (NSF) and Noise Population Figure (NPF) with the help of various histogram components. The noise characteristics of the sensors are therefore studied with the help of the following histogram components of the signal and their ratios as depicted in Fig.2.15.

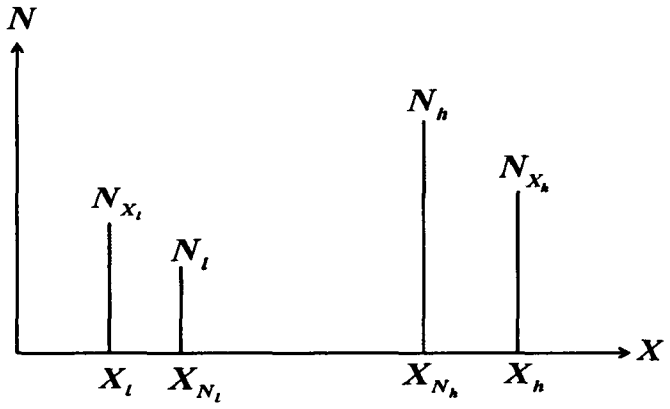

Fig. 2.15. Histogram showing signal spread and population.

The following histogram components can be defined as –

X_h = Highest value of signal component.

X_l = Lowest value of signal component.

Table 2.4. Bandwidth, mean, variance , standard deviation and SNR of sensor data for different frequencies and duty cycles (best suitable values are shown in bold).

Sensor	Duty cycle	Pulse Frequency (mHz)	Mean	Variance	Standard deviation	Signal-to-Noise Ratio(dB)	Noise Bandwidth (mHz)
TGS-822	50%	10	0 4830	0 0316	0 1777	45 63	7
		40	0 4542	0 0735	0 2711	41 90	19
		80	0 5189	0 0989	0 3145	34 29	38 3
		120	0 5067	0 1290	0 3592	27 32	70
	75%	**10**	**0.6057**	**0.0230**	**0.1515**	**52.04**	**3.63**
		40	0 6270	0 0606	0 2461	45 84	16 3
		80	0 6683	0 0743	0 2726	44 88	32 7
		120	0 6632	0 0911	0 3018	29 18	64
TGS-842	50%	10	0 4603	0 0776	0 3214	56 88	dc
		40	0 4275	0 1241	0 3523	48 05	
		80	0 4893	0 1403	0 3746	44 03	
		120	0 4700	0 1540	0 3924	27 82	
	75%	**10**	**0.6846**	**0.0605**	**0.3149**	**57.50**	dc
		40	0 6454	0 1058	0 3252	55 49	
		80	0 6699	0 1201	0 3465	49 76	
		120	0 7028	0 1287	0 3545	46 61	
TGS-2611	50%	10	0 5267	0 0492	0 2218	48 30	dc
		40	0 5398	0 0543	0 2330	41 03	
		80	0 5221	0 0582	0 2374	33 52	
		120	0 5188	0 0605	0 2413	30 79	
	75%	**10**	**0.8270**	**0.0458**	**0.2110**	**59.22**	dc
		40	0 8239	0 0489	0 2139	49 53	
		80	0 8312	0 0566	0 2279	39 99	
		120	0 8463	0 0576	0 2336	33 75	

X_{N_h} = Signal value corresponding to the highest number.

X_{N_l} = Signal value corresponding to the lowest number.

N_h = Signal population for highest signal spread.

N_l = Signal population for lowest signal spread.

N_{X_h} = Samples corresponding to highest signal value.

N_{X_l} = Samples corresponding to lowest signal value.

The following ratios are also defined as follows-

$\frac{X_h}{X_l}$ = Spread ratio of the highest to lowest components of signal value level in the histogram. (2.8)

$\frac{X_{N_h}}{X_{N_l}}$ = Spread ratio of the signal values corresponding to the highest to lowest numbers. (2.9)

$\frac{N_h}{N_l}$ = Ratio of the highest to lowest signal population. (2.10)

$\frac{N_{X_h}}{N_{X_l}}$ = Ratio of signal population for highest to lowest signal spread (2.11)

To analyze the signal spread and population behaviour, the following two terms are defined as:

$$\text{Noise Spread Figure (NSF)} = \frac{X_h/X_l}{X_{N_h}/X_{N_l}} \tag{2.12}$$

$$\text{Noise Population Figure (NPF)} = \frac{N_{X_h}/N_{X_l}}{N_h/N_l} \tag{2.13}$$

To explain the two figures introduced in eqn. (2.12) and (2.13), we consider a pure and a noisy signal as shown in Fig. 2.16 (a) and (b) and the components of the pure and noisy signal in 2.16 (c) and (d) respectively.

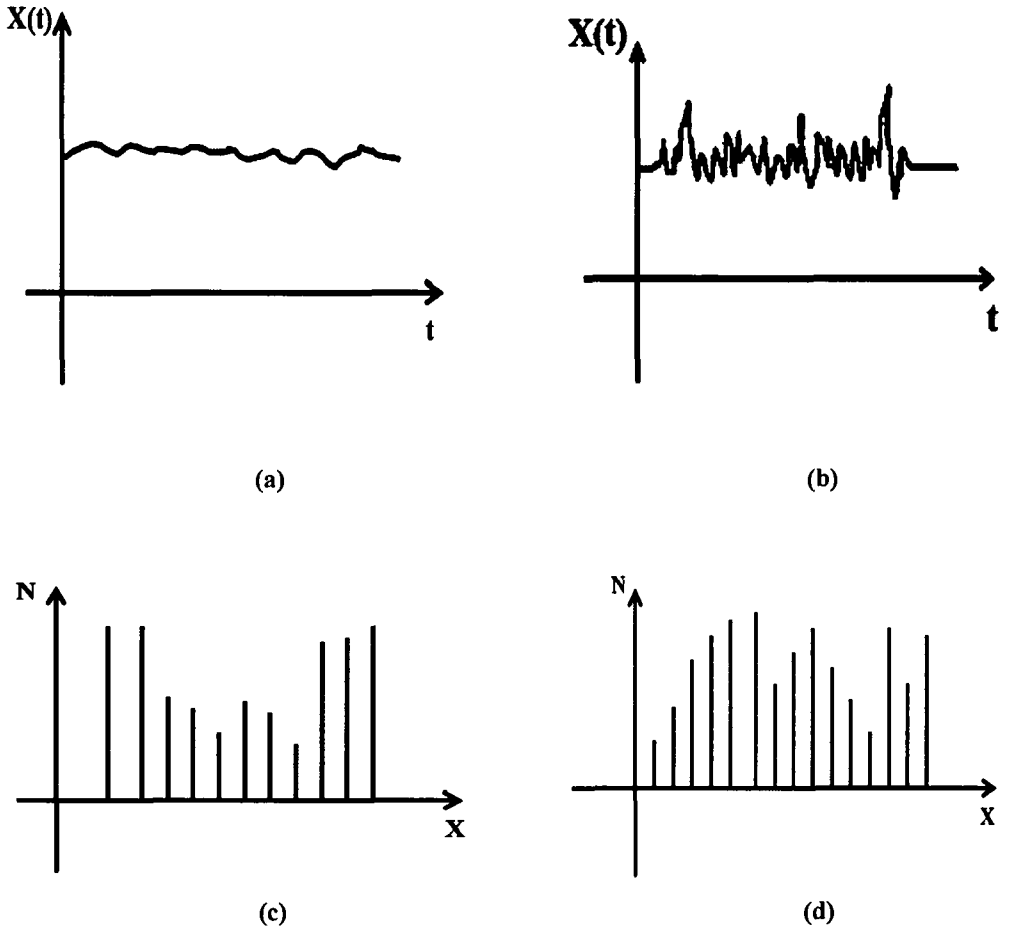

Fig. 2.16. (a) Pure Signal, (b) Noisy Signal, (c) Histogram components of a pure signal and (d) Histogram components of a noisy signal.

Four cases can be considered for the two cases of signals shown above:

- Case I: For a pure signal, $X_{Nh} >> X_{Nl}$, so from eqn. (2.12) *NSF* will tend to zero.
- Case II: For a noisy signal, $X_h >> X_l$ and $X_{Nh} \supset X_{Nl}$, so from eqn. (2.12) *NSF* will be high.
- Case III: For a pure signal, $Nx_h \supset Nx_l$ and $Nh >> Nl$ so from eqn. (2.13) *NPF* will tend to zero.
- Case IV: For a noisy signal, $N_h \supset N_l$ and $Nx_h >> Nx_l$, so from eqn. (2.13) *NPF* will be high.

Again let us consider two histograms shown in Fig.2.12 (e) and (h). Fig.2.17 (a) and (b) represent two histograms at frequency 10mHz and 75% duty cycle and at 120mHz and

75% duty cycle respectively for sensor TGS-822. These two histograms were taken because from the experimental results the histogram given by Fig. 2.12 (e) for 10mHz and 75% duty cycle provided the best suitable results in the statistical noise feature analysis whereas the histogram given by Fig. 2.12 (h) for 120mHz and 75% duty cycle yielded more noise than at other frequencies and duty cycles.

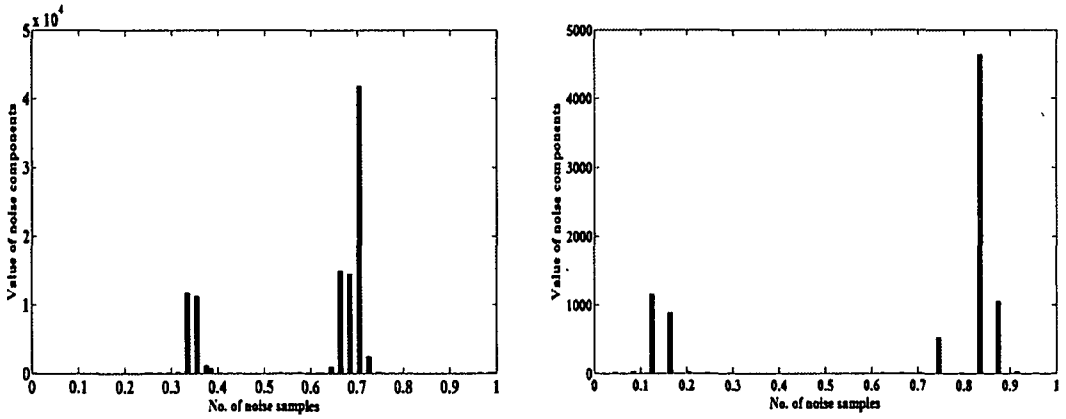

(a) (b)

Fig. 2.17. Histogram of sensor TGS-822 (a) at frequency 10mHz and 75% duty cycle and (b) at frequency 120mHz and 75% duty cycle.

The two ratios NSF and NPF for the two figures are calculated as follows:

For better accuracy we consider a threshold size of histogram as 200 samples and signal value as 0.34 i.e. we discard the values below these threshold levels. The histogram components for Fig. 2.17(a) are-

$X_h = 0.73$; $X_l = 0.34$; $X_{N_h} = 0.71$; $X_{N_l} = 0.38$; $N_h = 41850$; $N_l = 686$; $N_{X_h} = 3000$; $N_{X_l} = 11000$

Therefore, $\frac{X_h}{X_l} = 2.1$; $\frac{X_{N_h}}{X_{N_l}} = 1.8$; $\frac{N_h}{N_l} = 61$; $\frac{N_{X_h}}{N_{X_l}} = 0.2727$

Hence, $(\text{NSF})_{10\text{mHz},\,75\%} = \frac{X_h/X_l}{X_{N_h}/X_{N_h}} = 1.17$

and $(\text{NPF})_{10\text{mHz},\,75\%} = \frac{N_{X_h}/N_{X_l}}{N_h/N_l} = 0.004$

The histogram components for Fig. 2.17(b) are-

$X_h = 0.88$; $X_l = 0.12$; $X_{N_h} = 0.84$; $X_{N_l} = 0.74$; $N_h = 4633$; $N_l = 480$; $N_{X_h} = 1200$; $N_{X_l} = 1300$

Therefore, $\frac{X_h}{X_l} = 7.3$; $\frac{X_{N_h}}{X_{N_l}} = 1.135$; $\frac{N_h}{N_l} = 9.652$; $\frac{N_{X_h}}{N_{X_l}} = 0.923$

Hence, $(NSF)_{120mHz,\,75\%} = \frac{X_h/X_l}{X_{N_h}/X_{N_l}} = 6.43$

and $(NPF)_{120mHz,\,75\%} = \frac{N_{X_h}/N_{X_l}}{N_h/N_l} = 0.095$

Thus comparing the values of NSF and NPF for both, Fig. 2.17 (a) and 2.17 (b) we find that at 10mHz and 75% duty cycle, the values of NSF and NPF are higher than at 120mHz and 75% duty cycle indicating that the noise spread is high and with high population i.e. signal is less noisy in case of the former. It is also observed that the high spread with more population as given in Fig. 2.17 (b) is noisier than low spread with high population.

Hence, for a particular noise or noisy signal, as the noise level increases, the spread ratios shown in eqns. (2.8), (2.9), (2.10) and (2.11) increases and as a result the NSF of eqn. (2.12) and NPF of eqn. (2.13) increases. Hence these two noise figure terms can be used to indicate the noise level of a signal. The NSF and NPF calculated from eqn. (2.12) and (2.13) respectively are tabulated in Table 2.4 for all the four different frequencies and duty cycles. From Table 2.5 it is observed that the NSF and NPF ratios for all three sensors increase as the pulsed heater voltage frequency is increased. Also for higher duty cycle, the NSF and NPF ratios decrease. This conforms to the results of other statistical features obtained from Table 2.4. It is observed that at low heater pulse frequencies the noise spread and noise population is smaller.

Table 2.5 Noise Spread Figure and Noise Population Figure variation with pulse frequency and duty cycle (best suitable values are shown in bold).

Sensor	Duty cycle	Pulse Frequency (mHz)	NSF	NPF
TGS-822	50%	10	2 80	0 0067
		40	4 49	0 0115
		80	5 74	0 125
		120	6 46	2 818
	75%	**10**	**1.17**	**0.004**
		40	1 65	0 026
		80	1 85	0 065
		120	6 43	0 095
TGS-842	50%	10	2 67	0 012
		40	3 12	0 014
		80	3 66	0 0164
		120	4 52	0 032
	75%	**10**	**1.32**	**0.01**
		40	2 59	0 025
		80	2 89	0 03
		120	3 56	0 44
TGS-2611	50%	10	1 315	0 017
		40	1 492	0 019
		80	1 97	0 16
		120	2 04	0 287
	75%	**10**	**1.08**	**0.011**
		40	1 12	0 209
		80	1 4	0 261
		120	1 98	1 313

2.4 Frequency analysis:

The frequency spectrum of a time-domain signal is a representation of that signal in the frequency domain which is determined by FFT analysis.

2.4.1 Fast Fourier Transform (FFT):

A fast Fourier transform (FFT) is an efficient algorithm for computing the discrete Fourier transform (DFT) and its inverse. Fourier's representation of functions as a

superposition of sines and cosines are common in the analysis of communication signals and systems. The usefulness of Fourier Transform (FT) lies in its ability to analyze a signal in the time domain for its frequency content. The DFT estimates the Fourier Transform of a function from a finite number of its sampled points. The FFT can be used only when the samples are spaced uniformly. When a continuous-time signal such as the sensor response is sampled at a uniform rate, the resulting sample values may be treated as a discrete-time signal and processed using the FFT. The applications of FFT include systems analysis, digital filtering, simulation, power spectrum analysis, communication theory, etc.

For a response sequence x of length n, the DFT is a vector X of length n, whose elements are defined as:

$$X(k) = \sum_{p=0}^{n=1} x(p) e^{-j2\pi kp/n} \tag{2.14}$$

where k=0,1,....,n-1.

A common use of FFT is to find the frequency components of a signal buried in a noisy time domain signal. It gives the spectrum of the signal. The measurement of noise levels depends on the bandwidth of the measurement. The noise floor of a power spectrum is actually the narrowband noise level in each FFT bin.

2.4.2 Random White Noise Behavior

White noise is a random signal with a flat power spectral density containing equal power within a fixed bandwidth at any center frequency as shown in Fig.2.18. It shows equal amount of fluctuations at all frequencies and its fluctuation at any instant of time is independent of the fluctuations at other times.

A noise signal $x[n]$ is white if it has zero mean; $E(x[n]) = 0$ for all n, with $E(x[n])$ being the expected value of the random variable $x[n]$. Further, white noise have unit variance; $E(x[n]x[n]) = 1$, for all n, and lastly it can be said that the noise signal $x[n]$ is white if it is independent from sample to sample, i.e. not correlated in time; $E(x[n]x[n-k]) = 0$, for $k \neq 0$ and for all n. The analysis of a white noise signal in the frequency domain poses

several problems such as it is not periodic, has no finite extent and has infinite energy. Power spectral density function can be used to handle such problems.

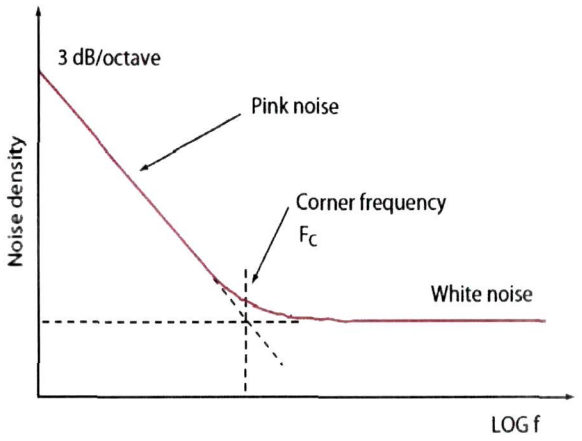

Fig. 2.18. White noise power spectral density.

The power spectrum of white noise is homogeneously distributed across the frequencies. Since random signals are non-periodic in nature their spectra varies from time to time and a large number of samples or a long time period is necessary to characterize their average spectral properties. A white noise signal may have Gaussian amplitude distribution or it may have some other distribution i.e. the statistical properties do not determine the shape of the spectrum. The spectra of white noise become flatter with frequency as larger number of samples is used to compute it.

In this study, the frequency spectrum of the sensor signal falls off steadily into the higher frequencies as depicted in Fig.2.18 and the flat part of the noise graph i.e. the noise floor becomes constant over a frequency termed as white noise.

2.4.3 Bandwidth

In general, bandwidth is the difference between the upper and lower frequencies in a continuous set of data typically measured in hertz. The characteristic of bandwidth is that a band of a given width can carry the same amount of information, regardless of where that band is located in the frequency spectrum. Most commonly, bandwidth is measured as the 3-dB bandwidth, that is, the frequency range within which the spectral

density is above half its maximum value or the spectral amplitude is more than 70.7% of its maximum.

In this work the noise bandwidth of the sensor response is determined for four different frequencies and two duty cycles of the pulsed heater voltage. FFT was performed for the determination of the bandwidth as tabulated in Table 2.4. Fig. 2.19 shows the FFT of TGS-822, TGS-842 and TGS-2611 at 10 mHz, 40mHz, 80mHz and 120 mHz each at pulsed duty cycles of 50 % and 75 % respectively. The frequency component of noise in case of the sensors TGS-842 and TGS-2611 is smaller at higher frequencies and the noise bandwidth is close to dc as seen from the table.

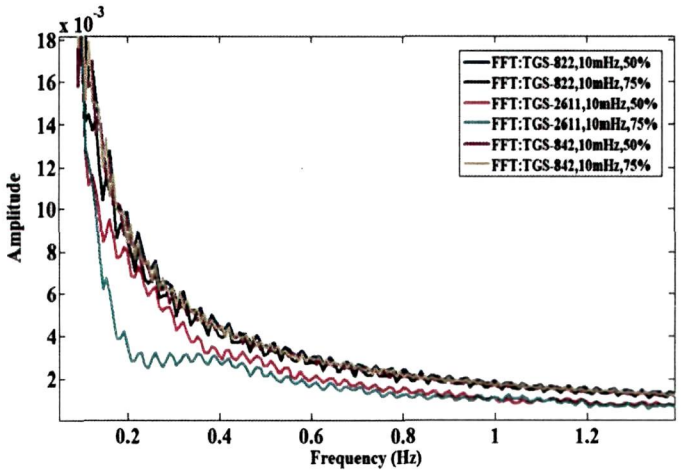

(a)

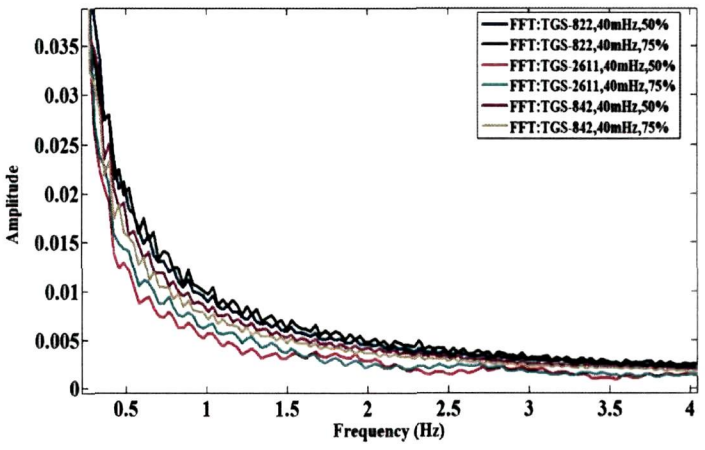

(b)

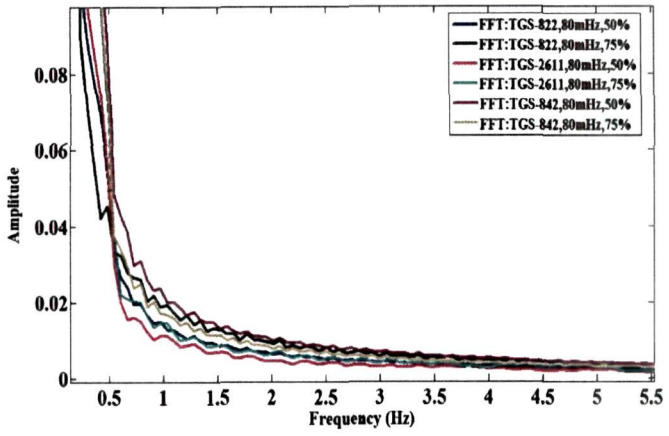

(c)

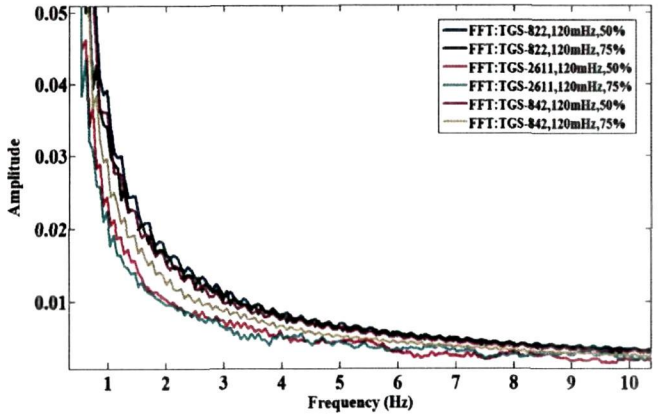

(d)

Fig. 2.19. The FFT of TGS-822, TGS-2611 and TGS-842 sensor noise signals at 50% and 75% duty cycles for (a) 10mHz , (b) 40mHz , (c) 80mHz and (d) 120mHz.

From the FFT a higher noise bandwidth was observed when pulse frequency was increased. Similarly it is seen that the duty cycle of pulse also contributes to the noise bandwidth with reverse dependency i.e. noise bandwidth decreases as duty cycle increases.

2.5 Discussions

In this study, the noise features of MOS gas sensor applying pulse modulated temperature with different frequencies and duty cycles are analyzed. To verify the noise dependency on the frequency and duty cycle of the modulated heater voltage, the PDF, SNR, histogram and FFT of the MOS gas sensor noise was performed. The statistical

analysis reveals that - the noise floor level decreases as the duty cycle of the pulsed modulated heater voltage is increased and pulse frequency is decreased. The same observation is evident for the FFT of the sensor responses that produces higher noise-bandwidth at higher heater pulse frequency however at lower duty cycle. The sensor noise is found to be $1/f$ or pink and it increases with the increase in pulsed heater voltage frequency and vice-versa. The PDF for the sensor noise signals satisfies the requirement for the noise to be coloured i.e. with non-zero mean. This part of the research deals with the study of noise in the MOS gas sensors without application of gas but under application of pulsed heater temperature. It was observed in this experiment that the characteristics show different behaviour for different patterns of pulsed heater voltage (i.e. heater temperature) with variable frequency and duty cycle.

The noise behavior of the three MOS gas sensors TGS-2611, TGS-822 and TGS-842 was studied with the help of the two newly introduced characteristic figures- NSF and NPF at four different frequencies namely 10mHz, 40mhz, 80mHz and 120mHz and at two different duty cycles namely 50% and 75%. NSF and NPF ratios also conforms to our previous statistical and FFT results i.e. decrease at lower frequency and higher duty cycle. Hence we are able to conclude that the heater pulse frequency and duty cycle considerably influences the noise behavior of the sensor.

The study confirms that the noise immunity of the sensors is more at higher pulse frequency but less at higher duty cycle. This is because a comparatively fast change in temperature produces spurious output signals. Recently, researchers are trying to extract higher degree of features by applying pulsed heater temperature; there must be a compromise between the highest heater pulse frequency and lowest duty cycle to get the best SNR for a particular sensitivity of the sensor.

This analysis facilitates that for improving the classification efficiency of the sensor array, sensor responses can be generated by using a suitable pulse frequency and duty cycle. The method for improvement of classification efficiency by using the best frequency and duty cycle is discussed in the next section. The best frequency and duty cycle for all the three sensors TGS-822, TGS-842 and TGS-2611 is found to be 10mHz and 75% duty cycle.

2.6 Gas classification with the best heater pulse frequency using dynamic features:

In the first part of this research work (*Section 2.3* and *Section 2.4*), the noise characteristics of an E-Nose array consisting of the same MOS gas sensors TGS-822, TGS-842 and TGS-2611 are studied at four different frequencies and two duty cycles for ten gas vapours. This study determined the best suitable heater pulse frequency and duty cycle for a particular sensor which was used as the operating temperature for the second part of the experiment.

In the second part of this study, the dynamic behavior of the MOS gas sensors are studied at these best selected temperatures and duty cycle and the classification of gas is performed using artificial neural network (ANN) to compare the results before and after the frequency selection.

2.6.1 Dynamic analysis of MOS gas sensors

Dynamic behavior of sensor is the criterion on the basis of which the performance of the sensor can be judged. The faster the dynamic response of the sensor the better is the performance of the sensor. Under static conditions, a sensor is fully described by its static sensitivity and signal amplitude, however, when we vary a stimulant say the heater voltage, the sensor response generally does not follow with perfect fidelity. The reason is that both the sensor and its coupling with the source of stimulus cannot always respond instantly. In other words, a sensor may be characterized with a time-dependent characteristic, which is called a *dynamic characteristic.*

2.6.2 Effect of pulse modulation frequency on noise behavior

By operating the MOS gas sensors in dynamic mode and characterizing their transient responses the selectivity of MOS gas sensors can be increased[128]. The dynamic operation of a sensor can be done by – AC operation mode modulation of the gas concentration and modulation of the sensor operating temperature. A periodic waveform is applied to the sensor input in the AC operation mode instead of a fixed DC power supply, while the sensor heater voltage (V_H) is kept constant. Gutierrez et al. [129, 130] have found that the peaks appearing in the impedance plots of tin oxide gas sensors in the presence of

reducing gases are a function of the nature of the adsorbed species. Amrani et al.[131] have found that for a single sensor element, characteristic patterns can be found over a very wide frequency range. The modulation of the gas takes place when analyte molecules interact (adsorption/desorption) with the sensor surface. This process consists in the controlled modulation of the gas concentration which produces an output signal containing information on the dynamic adsorption and desorption processes taking place in the sensor surface. Because of this, the transient signals carry information about these processes that are generated when the controlled modulation of a sensor input parameter is performed. The frequency spectrum of these transient signals can be a source of information containing details on the dynamics of the interaction process and have the potential for gas identification. The transient response of gas sensors in gaseous concentration have been performed by many researchers[132-135]. It has been shown that the dynamic sensor response increases the selectivity of a sensor array[101, 136, 137].

Research has also been conducted combining both effects simultaneously, analyte concentration modulation and working temperature modulation[138]. This process increases the resolving power of metal oxide sensors. Furthermore, its simplicity makes it especially suited for low-cost applications.

Metal Oxide materials such as SnO_2 and ZnO are widely used as sensitive layer for gas sensors in electronic nose. The electronic nose technology with MOS based gas sensors have been widely applied in odour analysis[139-141] as well as in industries focusing on the improvement of performance. Accordingly, the development of gas sensors for the detection of single gases has seen an increasing interest within the research community. Besides such advantages, gas sensors exhibit a series of unpleasant characteristics such as cross-sensitivity, drift and humidity effects, ageing, poisoning etc. Temperature also affects the dynamic characteristics, particularly when they employ viscous damping. A comparatively fast temperature change may cause the sensor to generate a spurious output signal. Feature extraction using both the steady state and dynamic response of the sensor has been widely used for gas sensors applications. In[100-102], the authors described techniques for extracting and using the steady-state, the slope as well as the transient response information from the sensor's response. In[142], dynamic signal extraction techniques and optimal array configuration were used to improve the classification performance. In[104] the sensor response curves were determined using six features which

represented the differences of dynamic behaviour of sensors to different sample gases, in phase space. The degree of difference was used to evaluate how much information was extracted from the response curves by the proposed method. In this work it was found that when the adsorption process becomes short, the reacting time i.e. the reaction between the sensor and the sample gets reduced. In[105] research has been carried out on feature extraction on recovery responses which shows that the shape of the recovery curves did not change much with the reaction time. In[106] recognition time and response recovery time of sensors were determined and the feature extraction was done based on these.

In all the research works mentioned above, analysis were performed on the dynamic responses of the gas sensors. Similar to *response time*, *recovery time* etc. *time constant* is also an important parameter that describes the response behaviour of a MOS gas sensor to a particular gas. Fig. 2.20 shows the dynamic characteristics of a sensor response.
In this part of the research work, we have made an analysis on odour classification using time constants of the sensor response as a feature. The time constant, τ , is a measure of the sensor's inertia. In analogous electrical systems, it is equal to the product of capacitance and resistance: $\tau = CR$. In thermal terms, it is equal to the product of thermal capacity and thermal resistance. In a first-order system, the response is given by,

$$y(t) = y_m(1 - e^{-t/\tau}), \tag{2.15}$$

where y_m is steady-state output, t is time. Substituting $t = \tau$, we get,

$$\frac{y}{y_m} = 1 - \frac{1}{e} = 0.6321 \tag{2.16}$$

In other words, after an elapse of time equal to one time constant, the response reaches about 63% of its steady-state level. To explain the relation between the dynamic features- slope, response-time and time-constant we consider Fig. 2.21 as shown below:

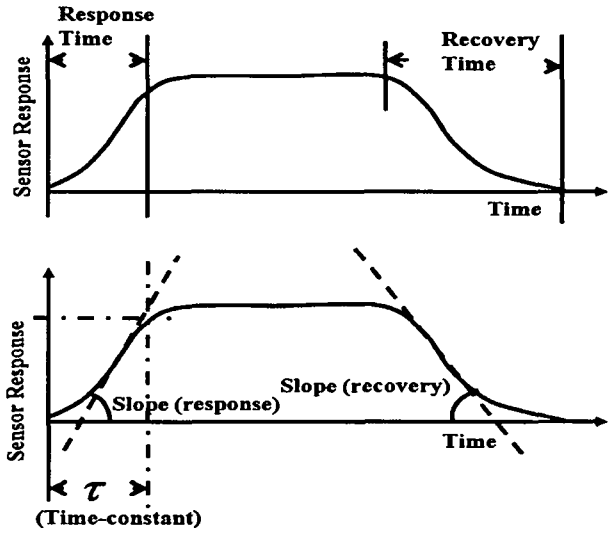

Fig. 2.20: The dynamic features of sensor response.

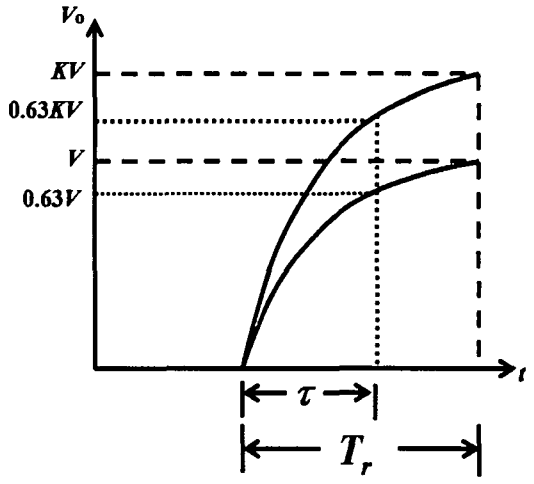

(a)

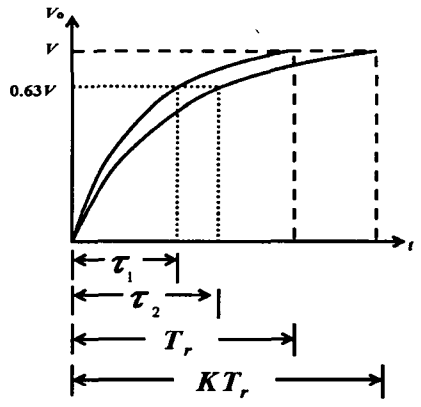

(b)

Fig. 2.21: Typical sensor response (a) with constant response time and (b) with constant response voltage.

where V = Response voltage

T_r = Response time

K = A constant

Now From Fig. 2.21 (a) where the response time T_r is same but response voltages are different, the slope and time-constant can be written as-

$$Slope = \frac{V}{T_r} \text{ (for response voltage } V) \quad (2.17a)$$

and $$Slope = \frac{KV}{T_r} \text{ (for response voltage } KV) \quad (2.17b)$$

Time- constant ,

$$\tau = \frac{0.63V}{T_r} = \frac{0.63V}{V} T_r = 0.63T_r \text{ (for response voltage } V) \quad (2.17c)$$

and $$\tau = \frac{0.63KV}{T_r} = \frac{0.63KV}{KV} T_r = 0.63T_r \text{ (for response voltage } KV) \quad (2.17d)$$

Similarly from Fig. 2.21 (b) where the response time T_r is different but response voltages are same, the slope and time-constant can be given as-

$$Slope = \frac{V}{T_r} \quad \text{(for response time } T_r) \quad (2.18a)$$

and $$Slope = \frac{V}{KT_r} \quad \text{(for response time } K\,T_r) \quad (2.18b)$$

Time-constant,

$$\tau_1 = \frac{0.63V}{T_r} = \frac{0.63V}{V} T_r = 0.63T_r \text{ (for response time } T_r) \quad (2.18c)$$

and $$\tau_2 = \frac{0.63V}{V} = \frac{0.63KV}{V} KT_r = 0.63KT_r \quad \text{(for response time } K\,T_r) \quad (2.18d)$$

Case I: When the response time is same but response voltages are different, the time-constant is same as given by eqn. (2.17c) and (2.17d). In such cases, the time-constant cannot be a feature for classification.

Case II: When the response time is different but response voltages are same, the time-constant is different although with different slopes as given by eqn. (2.18). In such cases, the time-constants can be used as a feature for classification.

Hence time-constant is an important parameter that can be used as a feature for classification of different gases using MOS gas sensors. In our study we have considered the time-constants for each of the ten sample gases as shown in appendix A2.1. These time constants depend on the dynamic behaviour of the sensor responses. During the adsorption process, the sensor response reaches up to a steady state from which the time constants could be determined.

The technique involves pre-processing and feature extraction and of the sensor response, principal component analysis (PCA) and then classification using ANN. The experimental procedures, data acquisition and analysis, results and discussions are described in this chapter. The time constants vary with different sample gases due to the different gas adsorption and heater thermal behaviour. On exposure to the organic gas, the conductance of the sensing element changes while the response time is dependent on the kind of sample gases. The selectivity of MOS gas sensors is greatly influenced by temperature modulation since the rate of reaction for different volatile compounds and the stability of adsorbed oxygen species are dependent on surface temperature. Since the optimum oxidation temperatures vary from gas to gas, a sensor operated at different temperatures behaves as different sensors. The average power consumed by the sensor with the modulated temperature can also be lowered in comparison to sensors working at a constant temperature.

2.6.3 Experimental Procedure

The dynamic analysis of MOS gas sensors (TGS-822, TGS-842, TGS-2611 of Figaro, Japan) was conducted for different pulse modulating temperature in the presence of the gases. The experimental set-up has already been described in *Section 2.1.1*.Two vessels were used as gas sample and room air vessels as shown in Fig.2.2. The sample gas and the clean air flow were directed into the chamber containing the sensors through two pumps, which were connected by teflon pipes. The gases from the sample vessel

containing sample gas and the fresh room air were sampled in a sequence for the pre-defined time duration.

The experiment was conducted on the MOS gas sensors with the application of ten different gas samples- ethylacetate, acetonitrile, ethanol, kerosene, petroleum ether, chloroform, methanol, isopropyl alcohol, acetone and n-hexane. Measurements were performed for 100 complete cycles (response and recovery) and a total of 100 data vectors were obtained for each of the 10 sample gases for the three sensors. The measurement was performed for 10 minutes for response followed by 25 minutes for recovery. The heater voltage was modulated at a frequency of 120mHz and 50% duty cycle and then at 10mHz and 75% duty cycle during the sample measurement cycle. The sensor response to fresh air was used as the baseline response for the experiments. Any variations in the baseline, which may occur due to various volatiles present in the room air, were monitored. It was found in each run of experiment that on application of clean air the sensor baseline settles to a fixed level ensuring absence of any interfering gas. The time constants were determined for each cycle and these time responses were used as the sample vectors for the odour classification. The sample measurements were stored in the data file in LabVIEW for further processing in MATLAB.

In the first part of experiments, the sensor temperature was pulsed at an arbitrary selected frequency of 120mHz and duty cycle of 50% to generate the sensor responses in the presence of the ten gases and then the time constants were determined. The sensors were then operated at the best selected pulse modulated frequency and duty cycle i.e. 10mHz and 75% duty cycle to generate the sensor responses in the presence of the 10 gases. The best selected frequency and duty cycle determination was based on the noise analysis as discussed in *Section 2.5*. The classification of data was performed using ANN. Fig2.22 shows an example of the sensor response in LabVIEW for ethanol and acetonitrile showing different response time.

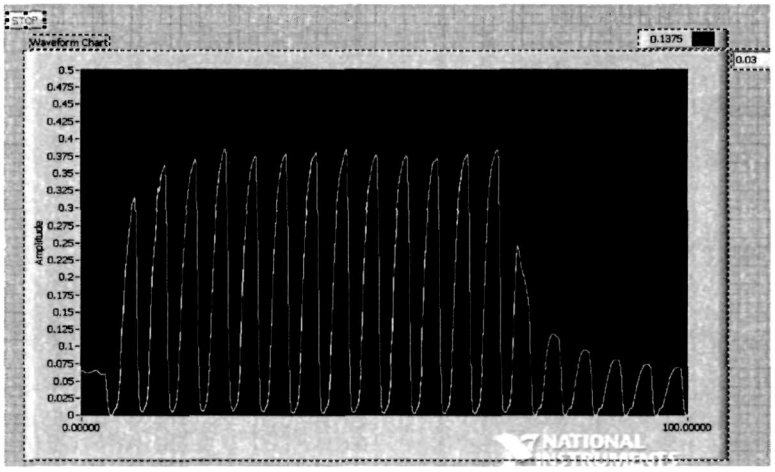

(a)

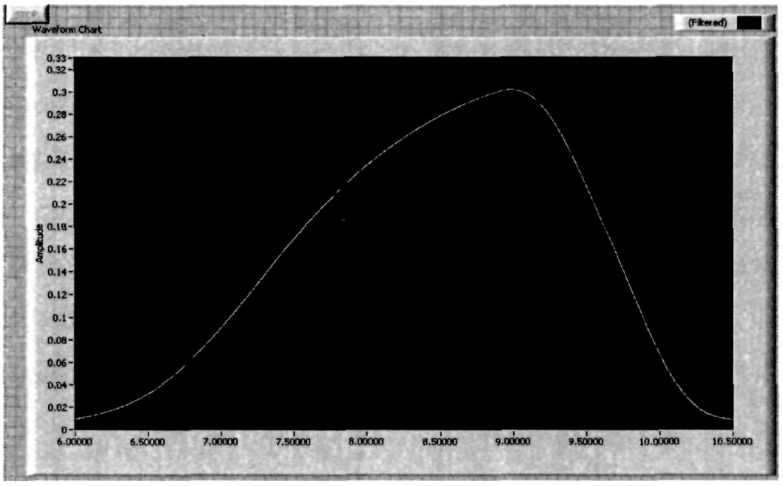

(b)

Fig. 2.22. The sensor response (TGS-822) in LabVIEW in presence of (a) ethanol and (b) acetonitrile for showing different response time.

2.6.4 Data Acquisition

Data acquisition refers to the process of recording sensor response in a prescribed format at a predefined rate. In this research sufficient amount of data sets were acquired in the long series of experiments. For the sensor data collection, a total time of 175 hrs was required for 100 data vectors from 10 measurement cycles.

2.6.5 Data Cluster Analysis

The cluster analysis of sensor data was applied to explore the existence of clusters in feature space within the datasets.

2.6.5.1 Feature Extraction Using Principal Component Analysis

PCA is a linear method that has been shown to be effective for the discrimination of sensor data [143]. PCA is a method consisting of expressing the sensor response vectors in terms of linear combination orthogonal vectors. Each principal vector accounts for a certain amount of variance in the data, with a decreasing degree of importance. This was done to reduce the dimensionality of the measurement space, and to extract relevant information for 'pattern recognition'. This dimensionality reduction stage projects the initial feature vector onto a lower dimensional space in order to avoid potential problems associated with high-dimensionality, sparse datasets and so on. Moreover, optimum feature extraction helps in removing a major portion of redundant data, which may be perceived as noise in the signal. The resulting low dimensional feature vector was then used for the classification of the data. It reduces the vector dimension of the dataset and thus makes it possible to identify the most important, or the principal, components. In particular, the first significant component explains the largest percentage of the total variance, the second one, the second largest percentage, and so forth. It is useful for visualizing any patterns existing in the response of a multisensory array data, hence facilitating the detection of odours[144].

In this analysis, PCA was used to observe the correlation of the sensor data to the classification of the gases. The results of the PCA, using the normalized data vectors at arbitrary frequency of 120mHz and 50% duty cycle is shown in Fig.2.23. The first three principal components were considered for analysis because they accounted for 95.6563% of the variance in the data set.

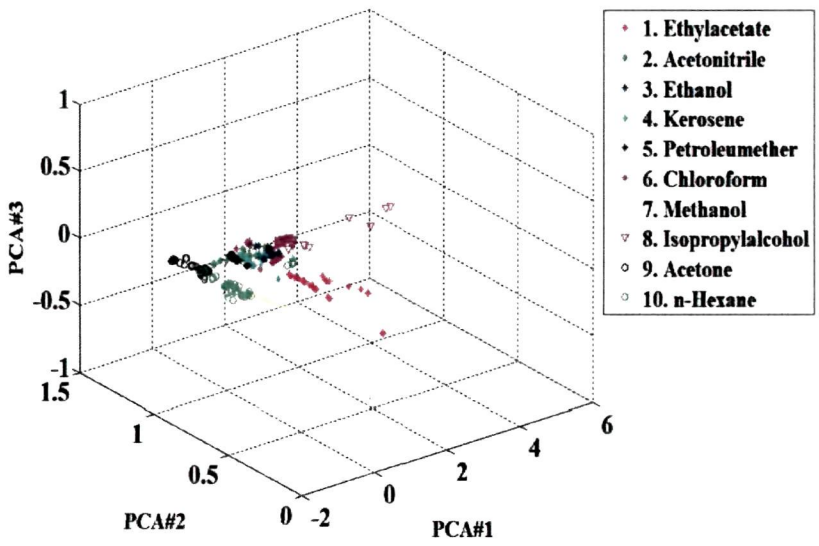

Fig. 2.23. PCA plot for the time constants for one gathering cycle of 100 data vectors with heater pulse frequency 120mHz and 50% duty cycle.

The variance and load values for each of 3 principal components (Fig. 2.23) are shown in Table 2.6.

Table 2.6 The results of PCA for the time constants before selection of frequency and duty cycle.

PC	% Variance	Eigen Values	Principal Components		
			$Sensor_1$	$Sensor_2$	$Sensor_3$
PC_1	95.6563	0.3143	-0.9826	0.1538	0.1040
PC_2	3.1172	0.2999	-0.1784	-0.9370	-0.3002
PC_3	0.2269	0.0152	0.0513	-0.3136	0.9482

It was observed that some samples were easily separated from the rest and form distinct clusters. But some other samples are not easily separable and overlap with other samples. This may be due to the variations of differentiability which are characteristic of the odour of these gas samples. Such results reveal the performance of the gas sensors in finding both the similarity as well as dissimilarity of aroma profiles for the different gas samples.

The results of the PCA, using the normalized data vectors for the selected frequency (10mHz frequency and 75% duty cycle) is shown in Fig.2.24.

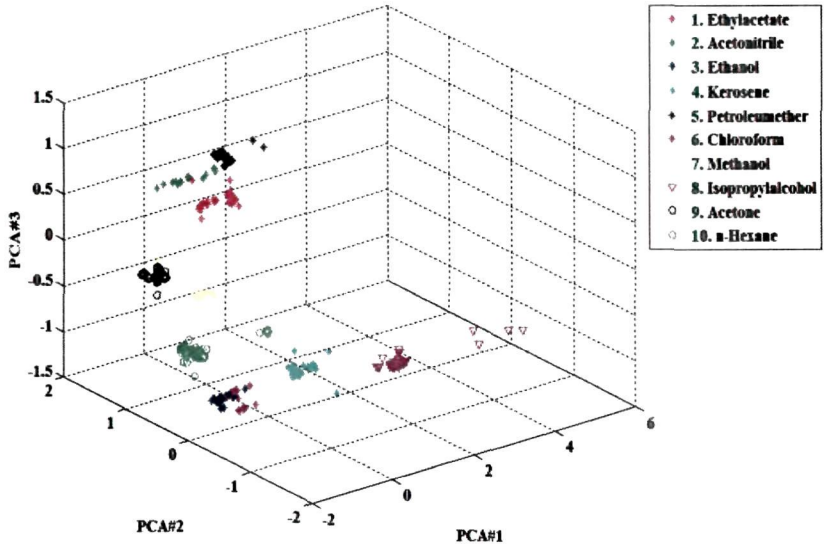

Fig. 2.24. PCA plot for the time constants for one cycle of 100 data-vectors with heater frequency 10mHz and 75% duty cycle.

The first three principal components were considered for analysis after selection of frequency and duty cycle because they accounted for 97.4176% of the variance in the data set. The variance and load values for each of 3 principal components (Fig. 2.24) are shown in Table 2.7.

Table 2.7 The results of PCA for the time constants after selection of frequency and duty cycle.

PC	% Variance	Eigen Values	Principal Components		
			$Sensor_1$	$Sensor_2$	$Sensor_3$
PC_1	97.4176	0.3761	-0.1023	-0.5411	-0.2133
PC_2	1.0112	0.2719	-0.0117	-0.6129	0.3422
PC_3	0.8399	0.0554	0.8210	0.0544	-0.0128

The results of PCA data visualization after selection of frequency and duty cycle indicate that there are ten distinctly separable clusters in the dataset and the sensor data has a better correlation.

2.6.5.2 Gas Classification Using Artificial Neural Network

Pattern recognition techniques based on artificial neural networks (ANN) approaches are very widely used for gas sensors[145]. During the learning phase of this approach, sensor response patterns are first trained and presented to the ANN along with respective class affiliations. Performance is then measured as the percentage of odours classified correctly when presenting a test set of new patterns to the ANN. Neural networks learn from examples through iteration, without requiring a priori knowledge of the relationship among variables under investigation. Two different ANN structures namely MLP and RBF were adopted for this stage of data classification. Training of the neural networks was performed with 50% of the whole data set and the rest 50% of the data sets were used for testing the neural network paradigms. A total of 30 data sets of dimensions (1×100) for each sensor were formed, thus 15 data sets were used for training and remaining 15 data sets were used to test the performance of the ANN paradigm. The two ANN paradigms were used for the analysis of the comparative results of the sensor data. The structures of the two ANNs are shown in Fig.2.25 (a) and Fig.2.25 (b) and the architecture of the two ANNs used in this experiment is tabulated in Table 2.8.

Table 2.8 Architecture of the two ANN paradigms (MLP and RBF):

Neural Networks	Architecture
Multi-layer Perceptron (MLP)	3 input neurons, 6 hidden neurons, 10 output neurons, 0.5 adaptive learning rate with momentum 0.42 (one for each sample type).
Radial Basis Function(RBF)	3 input neurons, 10 neurons in the output layer, spread constant 0.8.

a) Multi Layer Perceptron (MLP):

An MLP network was programmed in MATLAB environment with an adaptive learning rate of 0.5 and a momentum equal to 0.42. The architecture is shown in Fig.2.24 (a). It has 3 input neurons, from the three sensors, 6 hidden neurons and 10 output neurons chosen for the ten sample gases. The activation function for the neurons in the hidden layers employed is the '*logsig*' function and for the input and output neurons the

activation function is also the '*logsig*' function. The weights were trained with the back propagation algorithm. The network was able to reach a classification rate of 51.9% before the selection of frequency and duty cycle i.e. at 120mHz and 50% duty cycle. After the selection of frequency and duty cycle i.e. at 10mHz and 75% duty cycle the network achieved the classification percentage of 58.21% was obtained.

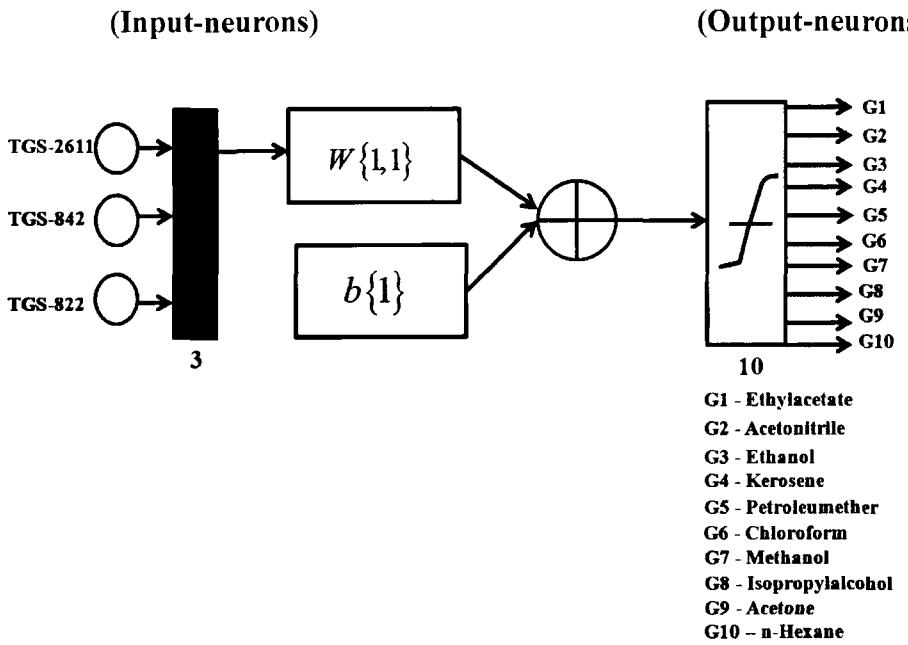

Fig. 2.25 (a). The architecture of MLP for ten sample gases.

The MLP network completed its training for approximately 3000 epochs taking about 1hour training time. Since MLP is poor in adapting the uneven distribution of samples, the classification by MLP was less in comparison to RBF. Table 2.9 shows the training and testing of the data sets on MLP network and its correct classification results for ten sample gases.

Table 2.9 Training and testing of sensor data on MLP network after the selection of frequency and duty cycle:

Sample Gases	Data vectors for training	Data vectors for testing	% Classification(for 100 data-vectors)
Ethyl Acetate	15(3×300)	15(3×300)	58.21%
Acetonitrile			
Ethanol			
Kerosene			
Petroleum Ether			
Chloroform			
Methanol			
Isopropyl Alcohol			
Acetone			
N-Hexane			

b) Radial Basis Function (RBF):

The RBF network has been found to be an efficient approach for interpolating scattered data and has been applied in various fields[146]. It has a similar architecture to the MLP, exhibiting fully inter-connected layers. It differs structurally from the MLP in that the hidden layer employs a different type of neuron, called the Radial Basis (RB) neuron. Like MLP, RBF also adopts the supervised learning method, being presented with the input patterns and the associated targets. The RBF network architecture is shown in Fig.2.25 (b). The neurons are added to the network until the sum-squared error (SSE) reduced to a specified error goal which was set as 10×10^{-6}. The spread constant was set at 0.8. The network was able to reach a classification rate of 75.9% before the selection of frequency and duty cycle. After the selection of frequency and duty cycle the network performed the classification of 85.62% was obtained. The training was completed in 100 epochs with a training time of approximately 26 minutes, hence showing better performance and less training time than MLP.

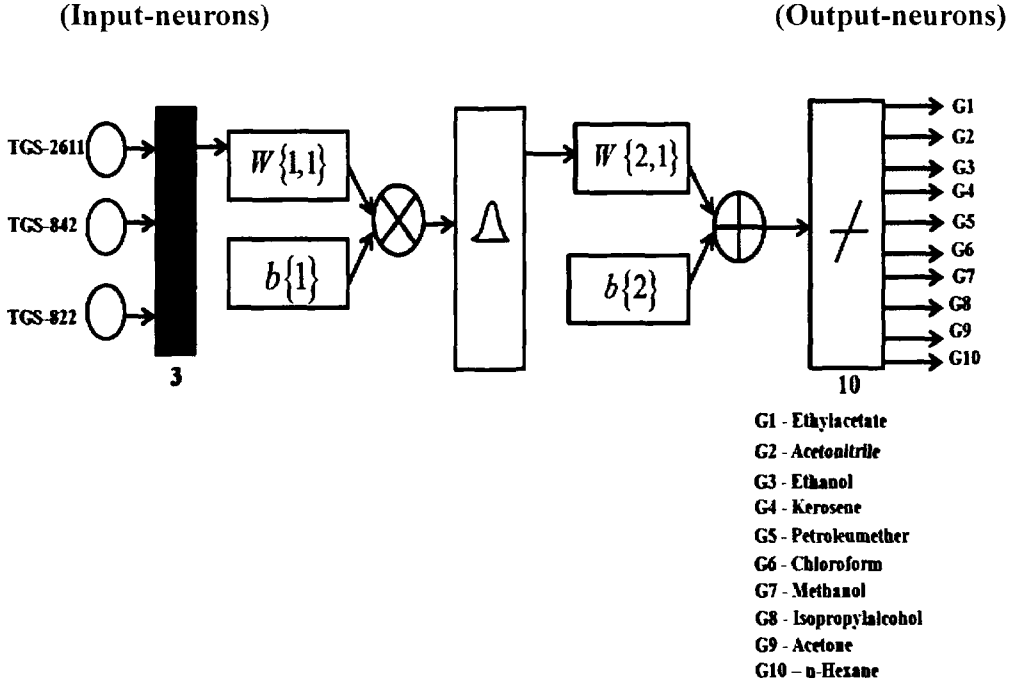

Fig. 2.25 (b). The architecture of RBF for ten sample gases.

2.6.5.3 ANN Performance and Classification Enhancement Results

The training performances of MLP and RBF used in the experiments are shown in Table 2.10. The time required to complete the iterations in case of MLP was more (1 hr approx.) than that for RBF (26 minutes).

Table 2.10 Training performance of Artificial Neural Network paradigms:

Neural Networks	Training time
Multi-layer Perceptron (MLP)	1 hour
Radial Basis Function(RBF)	26 minutes

The classification of the sensor data (time constants) was performed using the two ANN paradigms. It is seen that the classification is higher in case of RBF than in case of MLP. The classification also improved after selection of the frequency and duty cycle. Table 2.11 shows the classification results of the sensor data for the two ANNs.

From Table 2.11 it is seen that the results of classification improves considerable after the selection of frequency and duty cycle. The classification percentage enhances upto 85.62% using best selected frequency and duty cycle of 10mHz and 75% duty cycle for RBF. Also, the classification with RBF is much higher than that using MLP which improves from 58.21% to 85.62% using the former.

Table 2.11 Classification results in percentage before and after pulsed frequency selection:

Classification mode	MLP	RBF
Before selection of frequency and duty cycle	51.9%	75.9%
After selection of frequency and duty cycle	58.21 %	85.62 %

2.6.6 Results and Discussions

In this part of experiments on the dynamic analysis of MOS gas sensors under pulsed modulated heater voltage, it was found that different sample gases could be classified with the utmost accuracy when the classification of the data was done using best selected temperature i.e. best selected frequency and duty cycle of 10mHz and 75% duty cycle. This frequency was chosen because as per the analysis done in the first part of the experiments, out of the four chosen frequencies of 10mHz, 40mHz, 80mHz and 120mHz and duty cycles of 50% and 75%, the noise was found to be lowest at 10mHz and 75% duty cycle.

It is also concluded that the sensor responses are linearly correlated. A reasonable correlation exists between different sample gases (ten gases used in this case), hence showing that the odour established by PCA is consistent with different sample gases.

The results are tabulated in the Table 2.10. The experiments were performed to classify ten sample gases based on the time constants of the sensors i.e. using time constant as the feature for classification. The classification results of the gases were then compared for data extracted before selection of frequency and duty cycle and for data extracted

after selection of frequency and duty cycle. The classification methods used were PCA, MLP and RBF. From these results (Table 2.7 through Table 2.10), it is evident that the three MOS gas sensors are capable of discriminating the odour of ten sample gases analyzed by the data processing ANN techniques. An accuracy of 85.62% was reached in the classification using RBF network compared with 58.21% using an MLP, thus showing that RBF was much better compared to MLP.

2.7 Conclusion:

This part of the research focuses on the development of a heater pulse frequency and duty cycle selection technique that relies on the fact that frequency and duty cycle of the heater influences the noise behavior of the sensor response and thereby the classification efficiency also. Different data preprocessing and data analyzing techniques were employed. In the first part of experiments-both statistical and frequency spectrum of MOS gas sensor applying pulse modulated temperature with different frequencies and duty cycles are analyzed to study the noise feature. Under statistical analysis-PDF, mean and standard deviation, SNR and histogram was determined. Two new noise characteristic figures- NSF and NPF were introduced at four different frequencies namely 10mHz, 40mhz, 80mHz and 120mHz and at two different duty cycles namely 50% and 75%. It is observed that for a rapid temperature change of sensor temperature, the NSF and NPF ratios increases indicating the rise in the noise level of the signal. Also, it is observed that with the increase in the duty cycle, the NSF and NPF ratios decreases indicating that the level of noise falls off in comparison to the signal level.

Under frequency analysis of sensor data, the FFT analysis of the MOS gas sensor noise is performed to verify the noise dependency on the frequency and duty cycle of the modulated heater voltage by the determination of the noise bandwidth. The study determined the best selected frequency and duty cycle at which the noise was minimum. In the second part of the experiments, the dynamic analysis of the sensor data was done and the discrimination of ten different sample gases was performed using two sets of frequency and duty cycle. At first, the analysis was done using a frequency of 120mHz and 50% duty cycle and then the data was extracted using the best selected frequency and duty cycle of 10mHz and 75% duty cycle. The time constant was used as the feature in this case. LabVIEW (National Instruments) was used to acquire and display the

results. The feature extraction was done using PCA. The PCA results using the normalized data vectors were encouraging, which accounted for upto 98.0004% (Table 2.6) of the variance in case of sensor data before selection and 99.2687% (Table 2.8) of the variance for data after selection of frequency and duty cycle.

Two different ANN structures namely MLP and RBF were adopted for this stage of data classification. Training of the data sets was performed with 50% of the datasets and the rest 50% of the datasets was used for testing the ANN paradigms. The time required for training with MLP was longer than that required for training the network with RBF. Also RBF resulted in a better classification percentage than MLP.

This study is helpful to determine the best suitable heater pulse frequency and duty cycle for a particular sensor. Also from the results of dynamic analysis, it can be concluded that odour classification based on the dynamic responses can be realized using neural networks using gas sensors. Hence, such an approach should have a major role to play in other similar areas of application.

2.8 Publication on this chapter

1. Dutta, N., & Bhuyan, M. Noise Feature Analysis in Pulse Temperature Modulated MOS Gas Sensors, *Sensors and Transducers* **120** (9), 107--118, 2010.
2. Dutta, N., & Bhuyan, M. Statistical Analysis of Noise in MOS Gas Sensor Based Electronic Nose with Pulsed Temperature Modulation, in Computational Vision and Robotics (ICCVR'2010), Bhubaneswar, India, 23-27.
3. Dutta, N., & Bhuyan, M. Dynamic Response Based Odour Classification Using MOS Gas Sensors, in Emerging Applications of Information Technology (EAIT'2011), Kolkata, India, 231-234.

CHAPTER 3

CHAPTER 3

NOISE REDUCTION BY AMPLITUDE DEMODULATION

3.0 Introduction:

Metal oxide gas sensors for gas sensing have been intensively used during the last decades[116]. Commercial MOS gas sensors are commonly used in electronic noses because of their low cost and high sensitivities inspite of their disadvantages such as lack of stability, low selectivity and are mostly affected by noise. The noise from the gas sensors comprises of several odorant gas sensors which may result in inaccurate cluster analysis of the tested odour[147]. The noise in MOS gas sensors and the various kinds of noises have already been discussed in **Chapter 1** (*Section 1.5*). Since, the impact of noise on various gas sensors is not uniform, therefore, system parameters should be properly adjusted in the de-noise process[148]. The commercial MOS gas sensors exhibit $1/f$ noise that dominates usually at low frequencies. The variation of temperature and humidity changes the baseline of the sensor signal with time which must be recovered at the time of data acquisition.

But before discussing noise in MOS gas sensors, noise in circuits and sensors are discussed in this chapter. Noises are classified into two types: **inherent** and **transmitted** noises as already discussed in *Chapter1*. Inherent noises are of different types such as popcorn, white, thermal, pink, shot, schottky noise whereas transmitted noise are either additive or multiplicative depending on the behavior of transmitted noise. For example –when noise propagates toward the sensors and interface circuit, they are added with the actual signals

and eventually appear at the output signals. When noises are multiplied with the actual signals, noises affect the transfer function of the sensors.

Different noise filtering techniques have been discussed in **Chapter 1** (*Section 1.5.2.5*). The selection of the noise reduction technique being application dependent, it is necessary to analyse and compare the filtering techniques to select the one that is appropriate for the application in which we are interested.

The moving average filter is one of the most commonly used filters in signal processing which is optimal for reducing random noise. It is a simple Low Pass Finite Impulse Response (FIR) filter used for smoothing a noisy signal. As the filter length increase the smoothness of the output improves, whereas the sharp transitions in the data are reduced increasingly implying that this filter has excellent time domain response but a poor frequency response. A moving average filter can be expressed as-

$$y(n) = \frac{1}{2N+1} \sum_{i=-N}^{N} x(n+i) \tag{3.1}$$

where $x(n)$ and $y(n)$ are input signal and output signal of the moving average respectively, and N specifies the number of data points and observation window length equal to $2N+1$. As the number of points in the filter increases, the noise becomes lower; however, the edges becoming less sharp. The moving average filter provides the lowest noise possible for a given edge sharpness. Different methods have been employed by researchers to eliminate noise in signals. Conventional linear system adaptive filtering techniques have been widely used in adaptive noise reduction problems. However, because of its linearity, the filter cannot change the intrinsic property of the original noisy signal, such as regularity, etc. The linear filter tends to remove or keep both noise and wideband components in the signal because both of them may have similar appearance in spectrum. The FIR filter based noise reduction techniques in the transform domain have also been investigated[149, 150] in many works. Several denoising techniques including wavelet thresholding methods have also proved to be powerful tools for noise removal[151-158]. Noise suppression in sensors tends to reduce the dimensionality of multichannel data, caused by various noise sources. In[159] it

is seen that to reduce noise in multiple-channel recordings such as magneto encephalography (MEG) or electroencephalography (EEG), each sensor is projected on the subspace spanned by its neighbours and replaced by its projection. In recent years, work has been carried on the elimination of noise in Electrocardiogram (ECG) signals[160]. Two methods were used to remove the signal noise: polynomial fitting and high-pass filtering. The first approach uses a polynomial interpolation to estimate the baseline which is fitted from some fiducially points that are determined from P-R intervals[161], whereas these points are difficult to locate accurately before noise is removed from the ECG signal. As a result, this approach was ineffective[162] if the ECG signal is contaminated by noise. In another work, moving average filter[163] and the ECG signal is contaminated by noise. In another work moving average filter[163] and wavelet translation[165] were used to construct a high-pass filter. However, the high-pass filter would inevitably introduce distortions in various parts of the ECG signal, especially in the ST segment. Also, there have been many ways to represent linear or nonlinear high-pass filters[165], such as infinite-impulse response (IIR) and FIR. The performance of IIR filters is generally undesirable due to a nonlinear phase response, which introduces distortion into an ECG signal. Though by sampling rate decimation FIR complexity could be reduced drastically, the time delay introduced by an FIR filter is still unacceptable, especially when FIR is applied in short-lasting signals. Therefore, both the moving average filter and wavelet package translation were used in this work[160]. In another work[166] a modified Bessel filter for amplitude demodulation of respiratory electromyogram (EMG) signals has been studied containing a rectifier and a low-pass filter called a modified third-order Paynter filter. A moving averager was constructed around the Paynter filter. The properties of this filter were studied and it was found that the filter had poor high-frequency attenuation which permitted higher frequency signal components to pass through to the output-demodulated waveform as interfering noise.

A high frequency resonance (HFR) technique involving bandpass filtering and amplitude demodulation (AD) prior to spectral analysis are used in many research fields. Researchers have developed efficient and robust methods to estimate the proper center frequency and optimum bandwidth of the bandpass filter. The minimal Shannon entropy was used in[167, 168]

by Qiu *et al* where a bandwidth was chosen and periodicity detection method was applied for center frequency selection. In[169] these parameters were selected based on a kurtosis maximization criterion. On the other hand, in method[170] smoothness index was applied to guide the selection of these parameters. An online resonance frequency estimation algorithm was also further developed[171] which was used as the center frequency of a wavelet based filtering method.

Although a number of works have been performed on signals for filtering using FIR, IIR, HFR techniques, but these methods may not be suitable in a rapidly changing temperature condition of sensor (due to pulse heater voltage) because these techniques involve filter parameters, namely center frequency and bandwidth which are situation dependent and their selection is knowledge demanding. Hence, the objective of this chapter is to explain two parameter free techniques developed - AD and wavelet transform (WT) technique to recover the original signal from the noisy sensor signal.

In our work we have tried to recover the original signal from the noisy signal by the AD technique. There are several ways of demodulation depending on how parameters of the base-band signal are transmitted in the carrier signal, such as amplitude, frequency or phase.

The process of demodulation is the act of extracting the original information-bearing signal from a modulated carrier wave. For example, for a signal modulated with a linear modulation, like AM (Amplitude Modulation), a synchronous detector can be used. Different kinds of circuits perform these functions. An AM signal encodes the information onto the carrier wave by varying its amplitude in direct approval with the analogue signal to be sent. There are two methods used in the demodulation of amplitude modulated signals:

i) The simplest method of demodulation is the envelope detector. It consists of a rectifier and a low-pass filter. The rectifier may be in the form of a single diode, or may be more complex.
ii) The product detector multiplies the incoming signal by the signal of a local oscillator with the same frequency and phase as the carrier of the incoming

signal. After filtering the original signal will be obtained. This method will decode AM.

An AM signal can be rectified without requiring a coherent demodulator. The output will follow the same curve as the input baseband signal. There are forms of AM in which the carrier is reduced or suppressed entirely, which require coherent demodulation.

3.1. Noise in MOS gas sensors

The temperature profile of the MOS gas sensor surface greatly influences the response behavior of the sensor due to rapid thermal fluctuations in respect of its noise and stability. We have observed that the noises in MOS gas sensors are additive where the noise magnitude does not change when the actual signal changes. The additive noise magnitude is totally independent of the signal magnitude as long as the sensor and interface electronics are linear. If the signal is equal to zero, the output noise will still be present. If we have a noise free signal V_s then the signal added by an independent ambient noise e_n is given by:

$$V_{out} = V_s + e_n \tag{3.2}$$

Fig. 3.1(b) shows an example of such a noisy signal corresponding to a pure signal 3.1 (a). It is seen that the noise magnitude does not change when the actual signal changes. As long as the sensor and interface electronics are linear, the additive noise magnitude is independent of the signal magnitude, and if the signal is equal to zero, the output noise will exist.

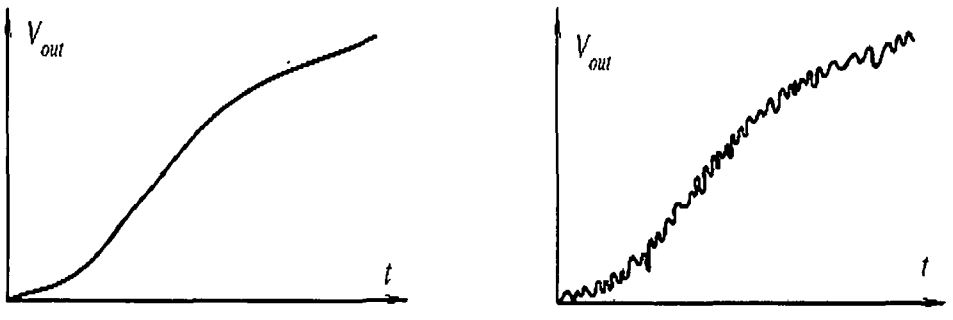

(a) (b)

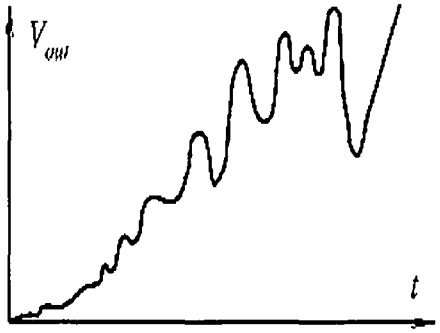

(c)

Fig. 3.1. Types of noise: (a) noise-free signal; (b) additive noise; (c) multiplicative noise.

Multiplicative noise affects the sensor signal or the nonlinear components of the circuit in such a way that the signal's value becomes altered or modulated by the noise given by:

$$V_{out} = [1 + N(t)]V_{\cdot} \tag{3.3}$$

where $N(t)$ is a function of noise. An example of such noise is shown in Fig. 3.1(c).

These types of noises at the output vanishes or becomes small or becomes additive when the signal's magnitude approaches zero. Multiplicative noise grows together with the signal's magnitude. Its name implies that it is a result of multiplication (which is a nonlinear operation) of two values where one is a useful signal and the other is a noise-dependent value.

Extrinsic noise is usually modeled as an unbounded white or colored Gaussian stochastic process, even though realistic stochastic perturbations are clearly bounded. Gaussian noise is evenly distributed over the entire signal. This type of noise has a Gaussian distribution, which has a bell shaped probability distribution function given by,

$$P_x(x) = \frac{1}{\sigma\sqrt{2\pi}} e^{-\frac{1}{2}\left(\frac{x-\mu}{\sigma}\right)^2} \tag{3.3}$$

where $P_{\cdot}(x)$ is the probability density function for Gaussian distribution of signal x, μ is the mean or average of the function, and σ is the standard deviation of the noise. Graphically, it is represented as shown in Figure 3.2.

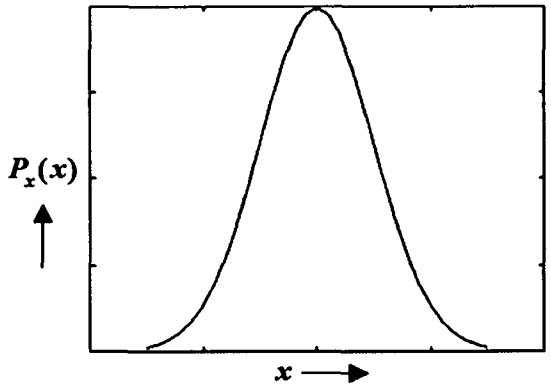

Figure 3.2: Gaussian distribution.

3.1.1 Experimental procedure

The low sensitivity signal from the MOS gas sensor (TGS-2611) was acquired for pulse modulating temperature by the data acquisition (DAQ) system. The MOS gas sensor signal was at first filtered in LabVIEW by a smoothing filter and then the experiment on noise analysis and filtering was performed without the application of any gas. The reason for choosing a low sensitivity sensor signal was that we wanted a signal completely buried in noise. The heater voltage was switched on to +5V when the pulse switches the MOSFET with the same frequency as that of the pulse applied. In our case, the pulse frequency used was 1Hz. The sensor output signal, without applying any gas, captures noise developed in the sensor due to various and mostly thermal related. The sensor was tested for noise with pulsed modulated heater voltage. The sensor temperature was pulsed at 1Hz frequency and 50% duty cycle to analyse the noise. The sensor noise signals were acquired at a sampling frequency of 1 kHz for time duration of about 15 min so that sufficient data is available for analysis. The data acquired was normalized to highlight the noise spectrum over a positive scale. The spectrum of the noisy signal was then analyzed and then by amplitude demodulating the signal-noise mixture, the envelope of the original signal could be determined and the spectrum analysis was performed. The original low sensitivity noisy signal of TGS-2611 filtered in LabVIEW is shown in Fig. 3.3.

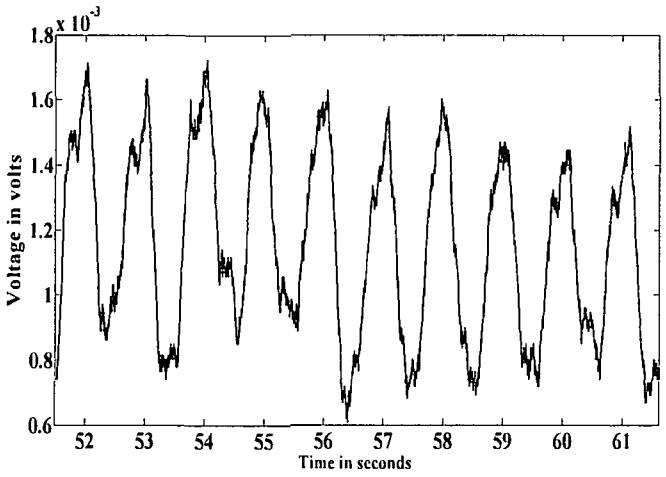

Fig.3.3: The original low sensitivity LabVIEW filtered sensor signal of TGS-2611.

3.1.2 White Gaussian noise addition

In order to analyse the efficiency of our proposed analog demodulation based noise filtering, we have used a MOS gas sensor of very low sensitivity so that the amplitude of the sensor signal is dominated by the noise i.e. the SNR ratio is deliberately made very low in the order of -14dB. The sensor signal was obtained by pulse modulating the heater voltage using a train of square pulses. This work emphasises on amplitude demodulation of the noisy sensor signal and recovery of the original low sensitivity sensor signal acquired by pulsed modulated temperature. After extracting the signal by using LabVIEW based smoothing filters, it was modulated with white noise as well as a low frequency sine signal. The resultant signal was then used for the analysis of noise reduction by the amplitude demodulation technique.

Continuous white noise has a correlation time of zero, a flat power spectral density (PSD), and infinite total energy. In practice, physical systems are never disturbed by white noise, although it is useful for theoretical approximation when the noise disturbance has a correlation time that is very small relative to the natural bandwidth of the system. Noise signals from two independent sources are uncorrelated. When white noise is added to a signal, the resultant signal will be the same form and size as the original signal but with Gaussian noise added. The addition of white noise to nanomechanical systems[172] showed a

marked amplification of the coherent signal strength. The determination of errors associated with frequency spectra produced by the CLEAN i.e. software based transformation of Roberts et al was performed by Monte Carlo based method that utilized three different types of simulation involving a data stripping operation and the addition of white and red noise to the analysed time series[173].

It is seen that noise in MOS gas sensor signal is generally spread uniformly across the spectrum. The amplitude of the noise varies randomly at different frequencies. The change in amplitude can actually modulate the sensor signal and be picked up in the AM system. In[174] a modulation / demodulation system is proposed to modulate the $1/f$ noise in capacitive sensors, to a higher frequency and then the noise modulated sensor signal is low-pass filtered. Also in another work, an AD based noise reduction technique was proposed which appeared at an instrumentation amplifier input[175]. A square-wave signal was used which was modulated with signal from sensor (input signal). The modulated signal was applied at instrumentation amplifier and then the amplified signal was modulated again with the same signal type. The noise and offset voltage which appeared due to the amplifier were modulated only once by the final multiplier and translated to the harmonics of the square-wave signal while, by using a low-pass filter, the filtered signal was obtained. The AD-based noise reduction algorithms are capable of increasing the SNR in the overall signal but not the SNR within a signal processing channel. These algorithms reduce noise interference by reducing the noise-dominant channels to the overall signal. These algorithms, therefore, do not enhance speech intelligibility in noise[176, 177]. If, however, the algorithm has more signal processing channels than the signal delivery channels, demodulation-based noise reduction algorithms can potentially increase the SNR within a signal delivery channel and improve speech intelligibility[178]. In another work[179], the adverse effects of the amplifier offset and flicker ($1/f$) noise of a differential low-noise high-resolution switched-capacitor readout circuit is minimized using amplitude modulation/demodulation. Since AD based techniques for noise filtering has been used in a number of multichannel sensor environment, it shows potential application in multisensor MOS gas array based E-nose.

Although a number of works have been performed on signals for filtering using Finite Impulse Response (FIR), Infinite Impulse Response (IIR) or High Frequency Response (HFR) techniques, these methods may not be suitable in a rapidly changing temperature condition of MOS gas sensor (due to pulse heater voltage) because these techniques involve filter parameters, namely center frequency and bandwidth which are situation dependent and their selection is knowledge demanding. Hence, the objective of this chapter 3 is to explain two parameter free techniques developed - AD and Wavelet transform (WT) technique to recover the original signal from the noisy sensor signal.

The sensor signal was at first filtered in LabVIEW by a smoothing filter and then it was modulated by adding -14dB white noise (Fig.3.4) and then both with white noise and a low frequency sine signal (Fig.3.5) so that we obtain a completely noise buried sensor signal for applying the AD technique. In our work, we have used the FFT analysis to confirm the validity of the AD process in the frequency domain.

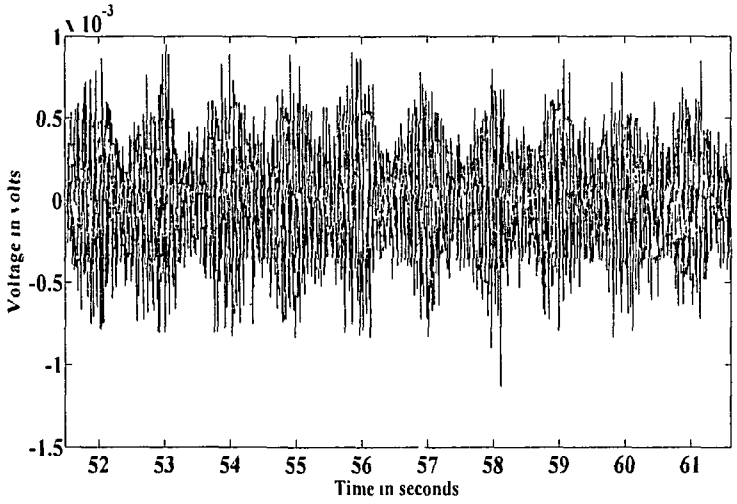

Fig.3.4: The noisy sensor response added with white noise of -14dB.

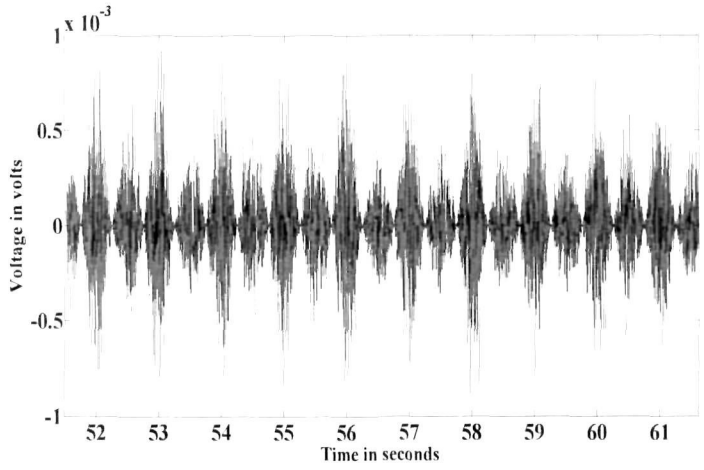

Fig.3.5: The noisy sensor response added with white noise of -14dB and a low frequency sine signal.

3.2. Amplitude Modulation and Demodulation

Modulation is an elementary requirement of communication system and can be defined as a process by which some characteristics of a signal termed as carrier is varied according to the instantaneous value of another signal known as the modulating signal. Modulation may be classified as continuous wave modulation and pulse modulation. If the carrier waveform is continuous in nature then the modulation process is termed as continuous wave modulation and if the carrier waveform is a pulse type waveform, then the modulation process is termed as pulse modulation. Amplitude Modulation (AM) is a type of continuous wave modulation.

AM is defined as a process in which the maximum amplitude of the carrier wave is made proportional to the instantaneous amplitude of the modulating signal. Let us consider a sinusoidal carrier wave $c(t)$ given as-

$$c(t) = A\cos\omega_c t \tag{3.4}$$

where A is the maximum amplitude of the carrier wave and ω_c is the fixed carrier frequency. Let

$m(t)$ be the modulating signal, then according to AM, the amplitude A of the carrier will have to be made proportional to the instantaneous amplitude of modulating signal $m(t)$. The amplitude modulated signal can be expressed as-

$$y(t) = m(t)\cos\omega_c t + A\cos\omega_c t \tag{3.5}$$

$$\Rightarrow y(t) = \left[A + m(t)\right]\cos\omega_c t \tag{3.6}$$

Fig.3.6 shows the block diagram of modulation and Fig. 3.7 shows the waveforms. The carrier signal given by eqn.(3.4) is a fixed frequency signal having frequency ω_c.

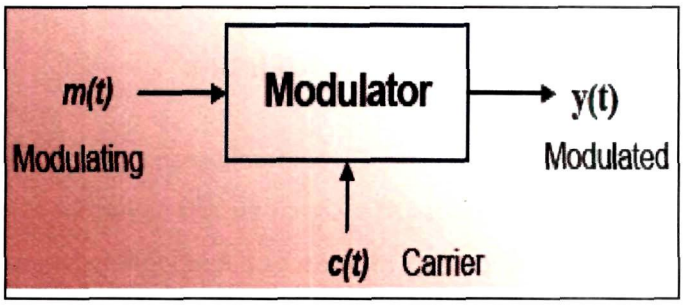

Figure 3.6: AM of the carrier signal $c(t)$ with the modulating signal $m(t)$.

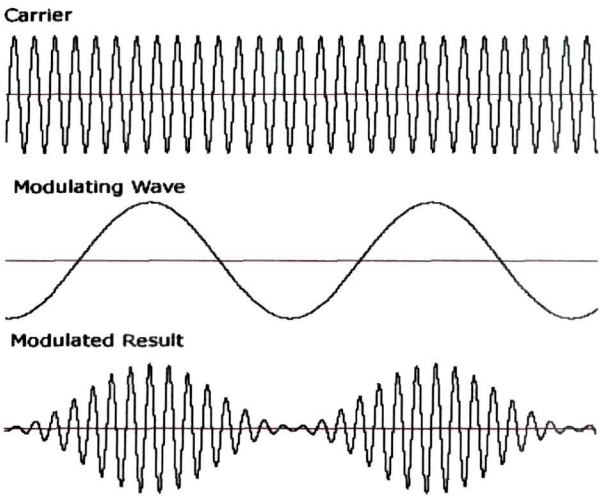

Figure 3.7: AM signal waveforms.

The AM signal of eqn.(3.6) has a constant frequency ω_c and amplitude $A+m(t)$ which implies that the amplitude of the signal changes around A in accordance with $m(t)$. The frequency of the AM signal remains unchanged and is equal to ω_c. The AM wave has time-varying amplitude called the envelope of the AM wave. The envelope of the modulated carrier has the same shape as the message signal $m(t)$. From eqn.(3.6) $A+m(t)$ represents the envelope of the AM wave containing the message signal $m(t)$. Hence, the modulated signal may be recovered from an AM wave by detecting the envelope.

In our analysis, the sensor signal is considered as the carrier signal $c(t)$ where the amplitude is modulated by the white Gaussian noise ($m_1(t)$) and a low frequency sine signal ($m_2(t)$). By adding noise to the sensor signal we obtain a completely noisy signal so as to perform the Amplitude Demodulation (AD) technique and obtain the accuracy of the noise reduction technique. The AM wave in this case can be expressed as-

$$y(t) = c(t) + m_1(t)c(t) \tag{3.7}$$

$$y(t) = c(t) + m_1(t)c(t) + m_2(t)c(t) \tag{3.8}$$

$$y(t) = \left[1 + (m_1 + m_2)\right]c(t) \tag{3.9}$$

where (m_1+m_2) represents the noise signal added to the sensor signal.

Demodulation is the process of extracting the message signal $m(t)$ from the modulated carrier signal $c(t)$. Demodulation rectifies the modulated wave i.e. negative half of the modulated wave is removed (Fig.3.8). The demodulation methods include envelope detection, square-law demodulation, and synchronous demodulation. A block diagram illustrating the various demodulation techniques is shown in Figure 3.9.

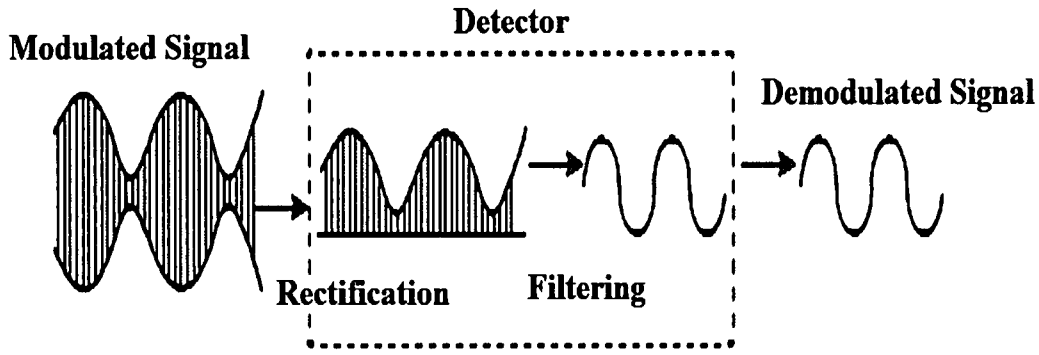

Figure 3.8: Demodulated signal output.

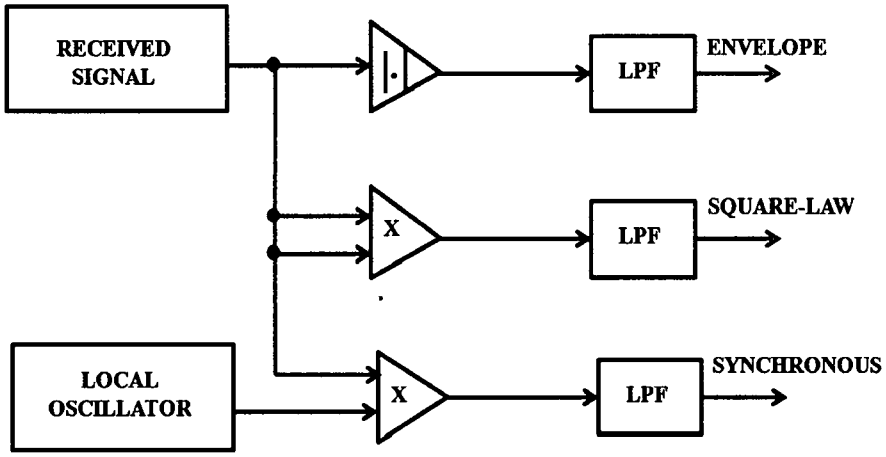

Figure 3.9: Methods of demodulation.

AM signals without overmodulation can be detected using the demodulator followed by a low-pass filter as shown in Fig.3.9. The square law detector is used for detecting modulated signal of small magnitude. A square-law demodulator squares the AM signal and then passes it through a lowpass filter as shown in Fig.3.9. To achieve better performance, a form of demodulation known as synchronous demodulation can be used. This system uses an oscillator signal to mix with the incoming signal to convert it down to the baseband signal. If the local oscillator signal has exactly the same frequency as the carrier within the AM signal, it will appear as a DC component at the output. The sidebands of the AM signal will appear relative to zero frequency, i.e. as the other modulating signal. Fig.3.10 shows

the block diagram of the AD technique used in our work to extract the noise free signal from the original sensor signal.

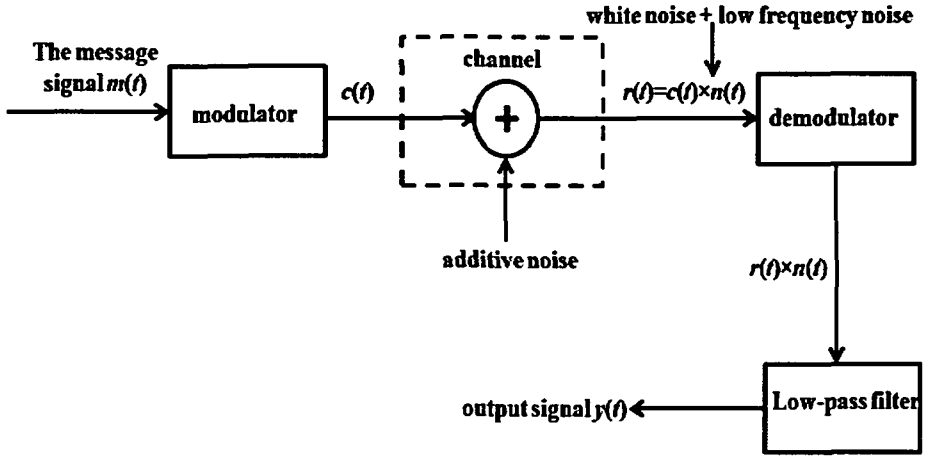

Figure 3.10: Block diagram showing the analog modulation-demodulation.

The demodulation process is explained by the flow diagram shown in Fig.3.11.

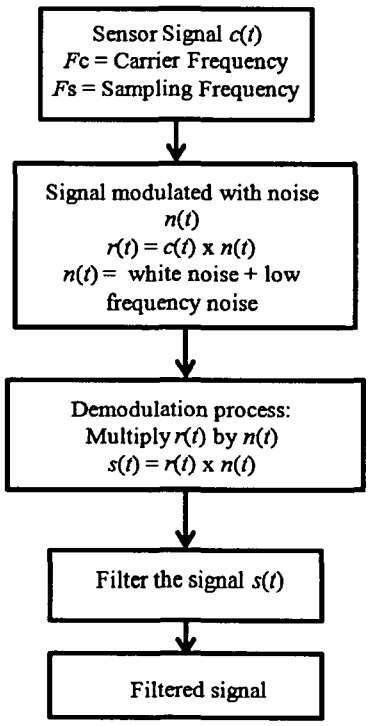

Figure 3.11: Flowchart showing the AD technique.

The original LabVIEW filtered signal recovered after amplitude demodulation is shown in Fig. 3.12. AD was also performed on white noise modulated sensor response and on the response added with both white noise and low frequency noise shown in Fig. 3.13 and Fig.3.14 respectively.

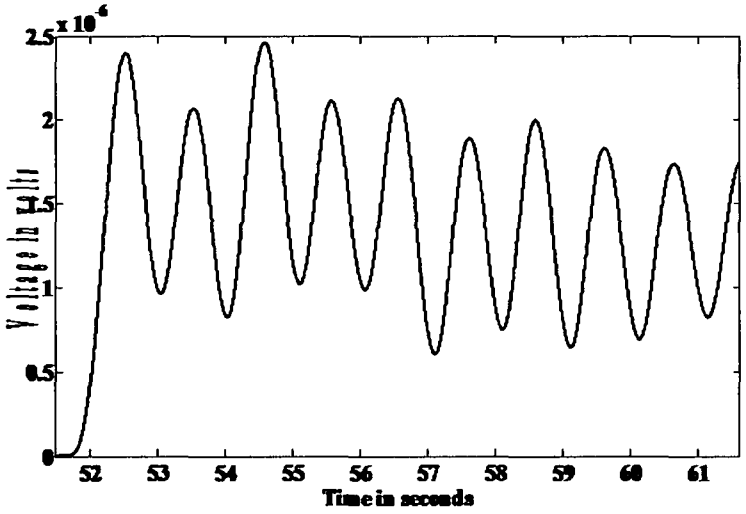

Figure 3.12: Amplitude Demodulated Signal of the original sensor signal.

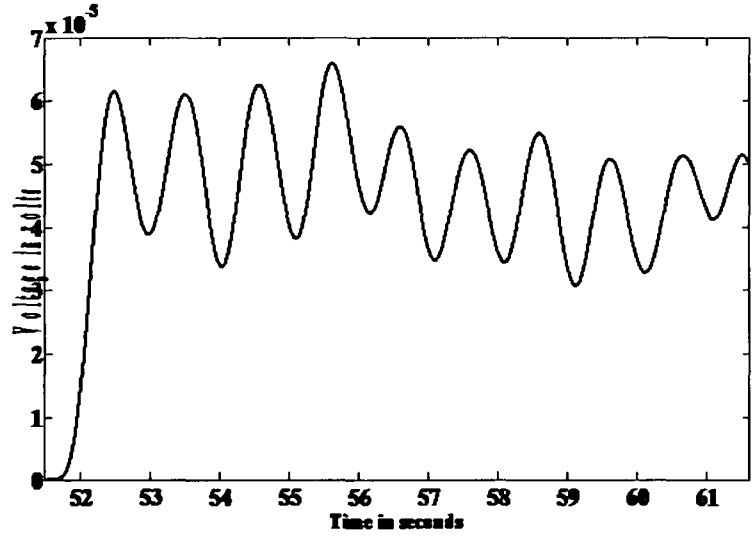

Figure 3.13: Amplitude Demodulated Signal of the white noise added signal.

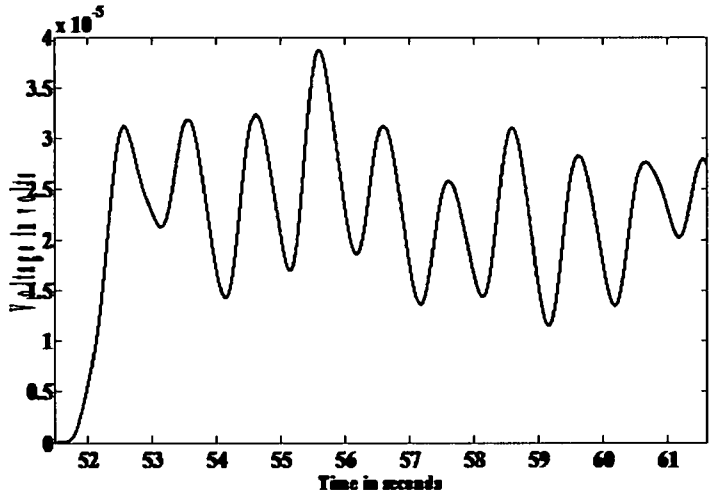

Figure 3.14: Amplitude Demodulated Signal of the white noise and low frequency noise added signal.

Applying the AD technique to the noise added signals as shown in Fig.3.4 and Fig.3.5, we obtain the filtered signals shown in Fig.3.13 and Fig.3.14 respectively.

3.2.1 Frequency Spectrum Analysis

To determine the accuracy of the AD technique the FFT analysis of the noisy and demodulated signals was performed. The bandwidth was compared for all the cases as tabulated in Table.3.1.

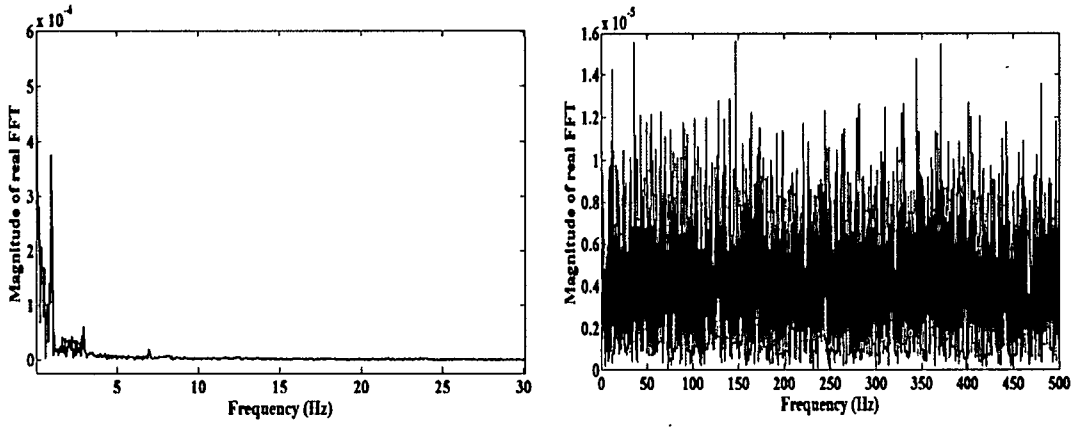

(a) (b)

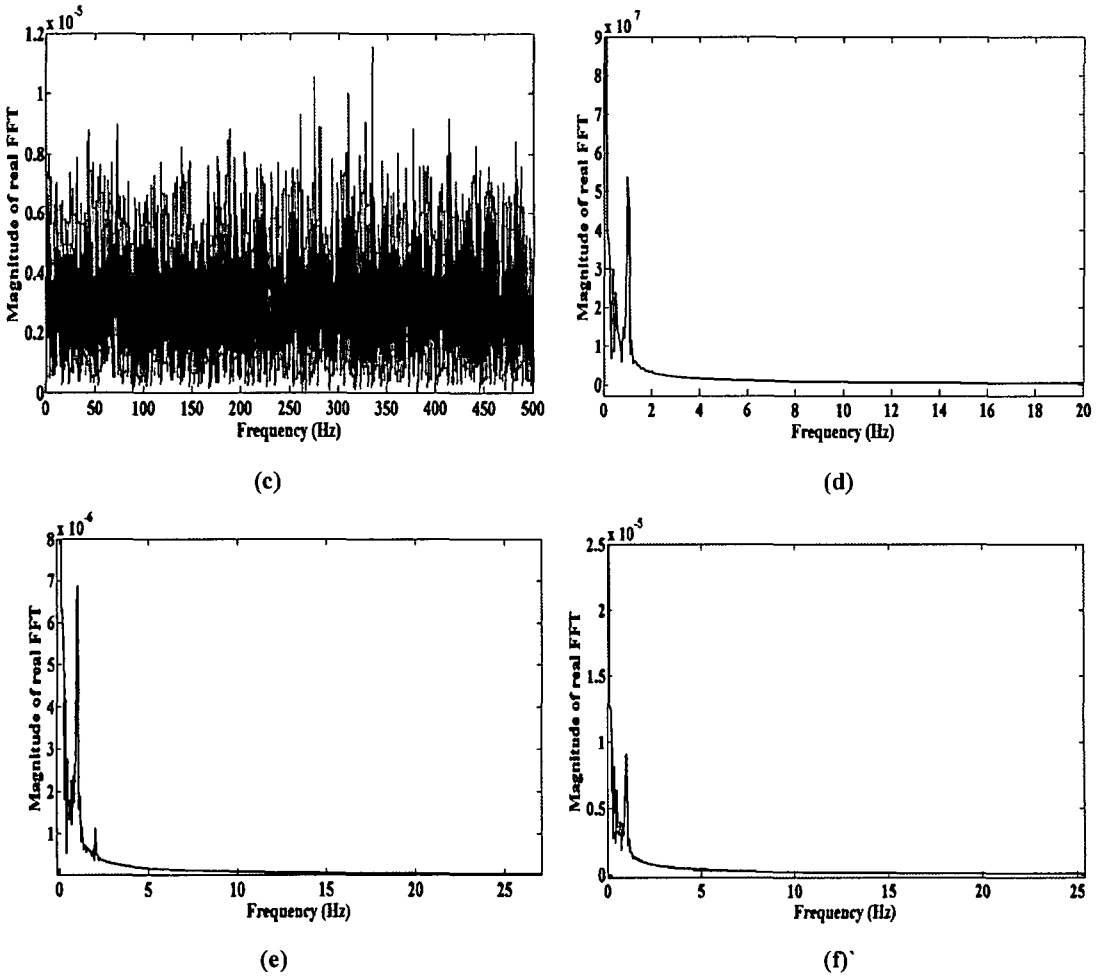

Figure. 3.15: The (a) FFT of original extracted sensor signal, (b) FFT of white noise added signal, (c) FFT of signal added with white noise and low frequency sine signal (d) FFT of amplitude demodulated signal of the original .signal, (e) FFT of amplitude demodulated signal added with white noise, and (f) FFT of amplitude demodulated signal added with white noise and low frequency noise.

Fig. 3.15(a) shows the FFT of the original sensor signal. It is seen that a sharp spectrum is observed at 1Hz. The FFT of sensor response added with white noise is shown in Fig. 3.15(b) while Fig. 3.15(c) shows the FFT of sensor response added with white noise and low frequency noise. The FFT was also performed for the verification of the demodulation technique applied to the noisy sensor response. Figure 3.15(d) shows the FFT for the amplitude demodulated signal of the original sensor signal. From Fig.3.15 (d) it is observed that the temperature pulse frequency component is observed at 1Hz. Fig. 3.15(e) shows the

FFT corresponding to the amplitude demodulated version of response added with white noise and Fig. 3.15(f) shows that of amplitude demodulated version of response added with white noise and low frequency sine signal where the 1Hz spectrum is reduced in amplitude.

Since the sensor response is a low frequency (1Hz) pulsed temperature signal, the signal bandwidth is mostly spread by noise. Hence, the signal bandwidth is important for predicting noise behavior. We have determined the bandwidth of all the six spectrums corresponding to Fig. 3.15 (a) to (f).

Table 3.1: Table showing the Bandwidth before and after the amplitude demodulation:

Sl. No	Sensor TGS-2611	Comparision of bandwidth		
		Bandwidth of sensor signal (Hz)	**Bandwidth of sensor signal with white noise added (Hz)**	**Bandwidth of sensor signal with white noise and low frequency noise added (Hz)**
1.	Before Amplitude Demodulation	0.0371	Very high	Very high
2.	After Amplitude Demodulation	0.0086	0.0383	0.0398

From Table 3.1 it is observed that the noise bandwidth is improved after the AD was performed. From this it can be concluded that the AD technique was able to remove the noise and recovers the original sensor signal. This parameter free technique could be very important as it helps in the removal of noise thus ensuring the proper use of the sensor in various gas detection applications. In addition to the AD technique, Wavelet filtering method is also applied to reconstruct the sensor signal.

3.3 Wavelet Transform Analysis

The wavelet transform (WT) is a time-scale representation successfully used in a number of applications. Its analyses the time–frequency analysis using a single transformation, which makes it feasible in applications such as signal de-noising, wave detection, data compression, feature extraction, etc. [180-183]. Wavelets can also model speech, music, video

and non-stationary stochastic signals in terms of time and scale distribution. In this work the WT was used as a filter for noise reduction of the signal generated by the MOS gas sensor system. The results of this wavelet filter were then used to perform the FFT and then the results were compared with the AD based spectral analysis.

The Fourier transform cannot provide any information of the spectrum that changes with respect to time because it assumes the signal to be stationary. Wavelets provide some advantages over Fourier transforms. They are effective in approximating signals with sharp spikes or signals having discontinuities. Unlike other traditional filtering methods, the WT preserve the temporal locality of sharp transitions within time-domain signals. The signal processing with wavelets decomposes the signal into its component elements. The basis functions in case of Fourier analysis are the sine and cosine waves. In wavelet analysis, the basis functions consist of the wavelet scale function, as well as scale and shifted versions of the mother wavelet function. The general information on the signal is captured by the wavelet scale function whereas the details of the signal are captured by the mother wavelet function. The wavelet transform is given by-

$$d_{0,0} = \langle g(t), \phi(t) \rangle \tag{3.15}$$

$$d_{j,k} = \langle g(t), \Psi_{j,k}(t) \rangle \tag{3.16}$$

$$j = 1, \ldots\ldots, N, \quad k = 1, \ldots\ldots 2^{j-1}$$

where $d_{j,k}$ are the wavelet coefficients, $g(t)$ is the signal to be transformed, $\phi(t)$ is the scale function and $\Psi_{j,k}(t)$ is the scaled and shifted version of the mother wavelet function $\Psi(t)$ which is given by-

$$\Psi_{j,k}(t) = 2^{j/2}\psi(2^j t - k) \tag{3.17}$$

and N is the number of wavelet scales over which the WT is generated. The inverse WT can be given by-

$$g(t) = d_{0,0}\phi(t) + \sum_{j,k} d_{j,k}\Psi_{j,k}(t) \tag{3.18}$$

3.3.1 Noise reduction Using Wavelets

The discrete wavelet analysis removes noise components from the signal through a de-noising approach. The procedure includes decomposing the signal into the detail components, identifying the noise components, and reconstructing the signal without these components. In this de-noising approach, the random errors in a signal are present in all co-efficients, while deterministic changes occur in a small number of relatively large coefficients. As a result a few larger coefficients representing the underlying signal is present in the non-linear thresholding function in the wavelet domain with the noise coefficients reduced to zero. The advantage of the wavelet de-noising method over classical linear filtering methods is that it removes all noise present and retains the signal present regardless of the frequency content of the signal. In such a de-noising process, a regular signal component can be accurately approximated by using a small number of approximation coefficients (at a suitably chosen level) and some of the detail coefficients. In de-noising and data compression process the choice of the mother wavelet plays a very significant role.

Wavelet analysis is a measure of similarity i.e. having similar frequency content between the basis functions and the signal itself. Therefore, in this case, the mother wavelets must be highly localized in time and frequency. One of the most popular orthonormal wavelets is Daubechies' wavelet. In such type of wavelets larger filter coefficients generate more localized wavelets in both time and frequency dimensions. In this work we have employed the order five wavelet transform of the Daubechies' family[184].

The wavelet filter was implemented through the multi-resolution pyramid decomposition technique[185]. The original extracted noisy signal is decomposed into two sets: a set of wavelet coefficients known as *details* and a set of coefficients known as *approximation*, using a bandpass and a lowpass filter for the decomposition. Thus, the pass band filtered signal is a detailed version of the signal and with high frequency components, while the other signal a low pass filtered with low frequency components. The low pass filtered signal is further decomposed into another set of high frequency and low frequency components and so on. The decomposition of the sensor signal can be described as:

$$s = a_m + \sum_{i=1}^{m} d_i \tag{3.19}$$

where a_m is the low pass filtered component and d_i is the high pass filtered component, m is the greatest decomposition level.

In this work we have performed wavelet decomposition on the original extracted noisy sensor signal (Fig. 3.3) using Daubechies' wavelet. The signals free of noise were found in the component of lowest frequency of a tree with five approximation levels ($a_1 - a_5$). The fifth order wavelet transform is employed in our case to recover the signal. The correlation of approximation level with original signal was analysed by Cross-correlation technique. We have found the cross correlation values at level 1 to level 8 and we have found that from level 6 the values decrease much abruptly as tabulated in Table 3.2. Therefore we have chosen the decomposition at level 5 for the analysis. Fig.3.16 (a) displays the decomposition tree of the analyzed signal and Fig.3.16 (b) shows the approximation components from level a_1 to a_5. Fig. 3.16 (c) shows the original noisy signal and wavelet filtered signal.

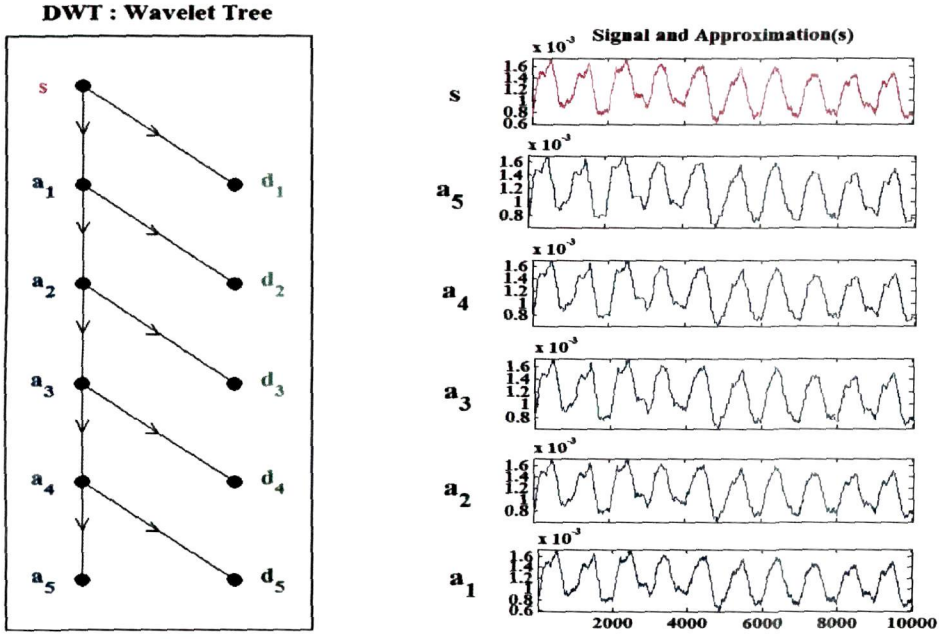

(a) (b)

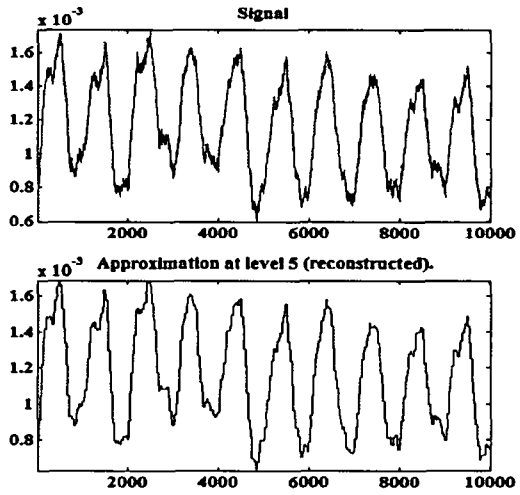

(c)

Fig. 3.16: (a) Tree of decomposition used to decompose and de-noise the sensor signal, (b) approximation components, a_1 to a_5 and (c) original noisy signal and wavelet filtered signal at level 5 (a_5).

Table 3.2: Cross-correlation coefficients:

Approximation coefficients	Cross correlation coefficients
a_1	0.9999
a_2	0.9997
a_3	0.9996
a_4	0.9993
a_5	0.9986
a_6	0.9971
a_7	0.9938
a_8	0.9696

From Table 3.2 it is seen that upto the level 5 (a_5), the values are consistent and from a_6 to a_8 the values decreases abruptly. Hence the signal at level 5 is selected for the analysis.

Further, the FFT analysis was performed and the bandwidth of the decomposed signals at all the levels was determined.

3.3.2 FFT Analysis of the Wavelet Filtered Signal

The performance of the wavelet technique was analysed by FFT analysis. Fig.3.17 shows the FFT of the wavelet filtered sensor signal. The bandwidth was determined for all the five detailed components and the bandwidth of all of them was calculated. The results of the bandwidth obtained by AD and wavelet analysis are tabulated in Table.3.3.

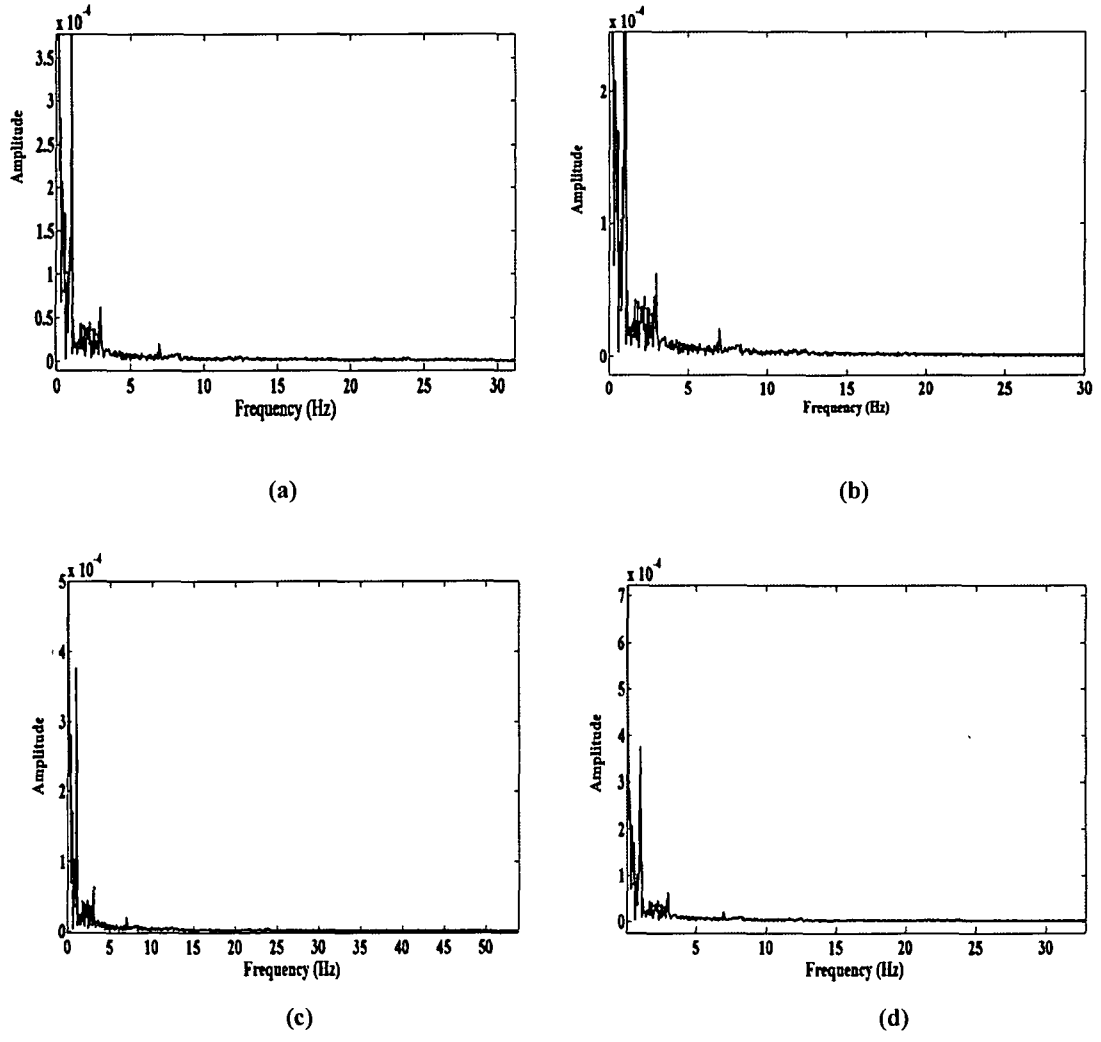

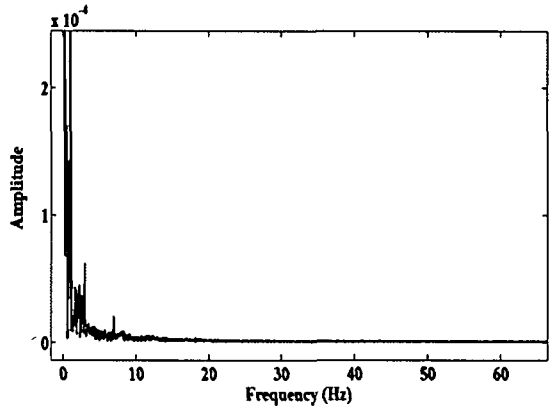

(e)

Fig. 3.17: The FFT of wavelet filtered sensor signal at (a) level-1 (a_1), (b) level-2 (a_2), (c) level-3 (a_3), (d) level-4 (a_4), and (e) level-5 (a_5).

Table 3.3: Table showing the Bandwidth of sensor signal with AD and Wavelet Transform analysis:

Sl. No	Comparision of bandwidth	
	Sensor TGS-2611	**Bandwidth of sensor signal (Hz)**
1.	By Amplitude Demodulation	**0.0086**
2.	By Wavelet Transform at level-1 (a_1)	**0.0373**
	at level-1 (a_2)	**0.0371**
	at level-1 (a_3)	**0.0371**
	at level-1 (a_4)	**0.0370**
	at level-1 (a_5)	**0.0369**

From Table 3.3 it is seen that the bandwidth of noise is more in case of wavelet filtered signal than the AD signal. The filtering by AD technique is therefore found to be better than the wavelet filtering method in our case, however the wavelet technique is better than AD filtering technique since it recovers the original information with minimal loss.

Wavelet analysis provides immediate retrieval of information that can be obscured by other time-frequency method analysis.

3.4 Conclusion

The AD technique is applied for the extraction of the original signal from the noise modulated sensor signal. The extracted low sensitivity signal was added to white noise and a low frequency sine signal. This was done so that the original signal was completely buried in noise. The AD was done on the signal and the original signal was recovered. Also spectral analysis of the signals before and after the amplitude demodulation was performed for the verification of the process.

The extracted noisy sensor signal was also decomposed using the wavelet filtering method. The reconstructed signal was analyzed by performing the FFT analysis. The bandwidth was determined and the results for AD and wavelet analysis were compared.

It is seen that the original signal was recovered without much loss of information after the amplitude demodulation was performed. The bandwidth of the sensor response before and after the AD shows that the noise could be removed effectively in this technique. The bandwidth of the signal using wavelet transform is found to be more than that performed using AD technique. Since AD based techniques for noise filtering has been used in a number of multichannel sensor environment, it shows potential application in multisensor MOS gas array based E-nose. Hence this work enumerate a novel technique of filtering MOS gas sensor responses using AD based algorithm which shows potential application in E-nose signal processing.

3.5 Publication on this chapter

1. Dutta, N., & Bhuyan, M. Amplitude Demodulation and Spectrum Analysis of Noise in *MOS Gas Sensor Based Electronic Nose, in International Conference on Advances in* Communication, Network, and Computing (CNC'2010), Calicut, 160-162.

CHAPTER 4

CHAPTER 4

HEATER PULSE FREQUENCY SELECTION BY SYSTEM IDENTIFICATION

4.0 Introduction:

In this chapter the basic issues of MOS gas sensor modeling by system identification and analysis of the MOS gas sensor stability criterion have been explained. Henceforth, based on the sensor stability, best suited transfer function was chosen for the MOS gas sensors and classification enhancement was done using Artificial Neural Network (ANN). The experimental procedures, and the modeling techniques with experimental results are the topics described in this chapter. The experiment was performed for three MOS gas sensors from Figaro (TGS-2611, TGS-842 and TGS-822) for two ranges of frequencies and the classification percentage for both the ranges of heater pulse modulating frequencies were determined.

The approach to system identification for a physical system using available data[186-189] is called a 'backward modeling' while modeling from system equations is called 'forward modeling'. Generally, identification is usually performed by finding the "best" set of parameters for a given model class, according to a chosen criterion such as least-squares error. If the resulting model is adequate for its stability analysis, predictions are made using this best model or else the model class is revised. System identification deals with building of mathematical models of dynamical systems based on the observed data from the system. To build mathematical models of dynamical systems from informative measured data for fitting such models system identification has been performed. A system can be linear or nonlinear and, depending on the type of the system, linear or nonlinear models can be estimated. In practice, linear models are very common and they are often used although the system is nonlinear. In these cases, the model can only give an approximate description of the system. This data-driven approach helps to observe the MOS gas sensor as a dynamic system and employ suitable methods so that its

behavior at different conditions can be modeled. We can interpret from the physical phenomenon of the sensor that the MOS gas sensor models rely on the following cascaded mechanisms-

i) adsorption of gas molecules by the sensor film,
ii) elevation of temperature of the sensor surface and
iii) the change in the electrical conductance of the sensor material.

The above stages, though looks distinct, physically it is difficult to distinctly segregate the whole model into such distinct stages.

System identification includes the following steps[190]: Firstly the experiment is performed to obtain good experimental data. Secondly, using a 'prediction error minimization' (PEM) technique a suitable model structure is chosen. Thirdly, a suitable input is chosen which shows how well the model fits into the experimental data. Finally, model validation is performed.

One of the most established ways of improving the selectivity of MOS gas sensors is by periodically varying the sensors' operating temperature and researchers have reported on the advantage of temperature modulation as discussed earlier. The response of the gas sensors to modulating temperature primarily depends on the analytical model which is based on the physical and chemical properties of the sensor material. By choosing the best heater modulating function with the best frequency to achieve a stable dynamics that follow the concentration of the analyte will be an important optimization strategy of MOS gas sensor.

The frequency of modulation is selected on trial and error method in many of the works based on temperature modulation[115, 191-198]. One of the methods of selecting most suited frequency was based on system identification through multilevel pseudorandom sequences[199] and pseudorandom binary sequences[200]. In these methods pseudorandom sequences (PRSs) and pseudorandom binary sequences (PRBSs) of maximum-length sequences (MLSs) was used to identify systems and how these method could be extended to systematically study temperature-modulated gas sensors, however the identification of systems using pulsed heater voltage for sensor stability analysis by system identification technique has not been explored so far. In this research we have

determined the transfer functions of the MOS gas sensors baseline model by system identification technique. The prediction error minimization (PEM) algorithm was used to derive the sensor Linear Time Invariant (LTI) model transfer function from measured input-output data without the application of any gas. Since pulse modulation is a popular method of feature extraction of MOS gas sensors, selection of parameters of pulse modulation will be a remarkable strategy in this area. To overcome the problem of choosing the best frequency of the temperature modulating signal of the MOS gas sensor, a new technique based on, system identification has been developed to select the sensor model that provides the most stable and desired sensor response. We have chosen a set of most suited frequencies for the first time in MOS gas sensors using system identification theory for sensor modeling[201, 202]. By using the system identification theory we determine the transfer functions of the MOS gas sensors during the signal-inactive period i.e. when the sensors were not exposed to any kind of gases. Based on the overshoot percentage of the step-response and the pole-zero plots the most stable transfer function was chosen. The aim is to find the stable transfer function that shows better percentage of fit than the other unstable transfer functions. Hence, the best fit stable transfer function obtained from the analysis was chosen to be optimum and the frequency and duty cycle at which this result was obtained was used for the classification of different gases.

The work therefore focuses on the most suitable temperature modulation based on the system identification technique. The most suitable transfer function was chosen for the MOS gas sensors based on the stability tests and then the sensors were operated at the respective best frequencies and duty cycles. The classification of various gases was performed by an array of gas sensors consisting three MOS gas sensors using Artificial Neural Network (ANN).

4.1 Experimental procedure

The photographic view of the experimental set-up connected to PC through DAQ card is shown in **Chapter 2** (*Section 2.2.1.4*, Fig.2.8).

4.1.1 Data Acquisition

Three MOS gas sensors (TGS-2611, TGS-842 and TGS-822 of Figaro, Japan) were used for acquiring data for different pulse modulating temperature. The heater voltage pulse modulation patterns (frequency and duty cycle) of the sensors were controlled by a PC through a Data Acquisition card (PCI6024E, National Instruments) and LabVIEW. The details have been explained in **Chapter 2** (*Section 2.2*).

In the first phase of this experiment the system identification was performed by using the sensor input-output data of the three MOS gas sensors without the application of any gases. For performing system identification using PEM algorithm, we have applied a large input-output pair of data set for two sensors (TGS-2611 and TGS-842) each operated by heater pulse of frequencies 10mHz, 40mHz, 80mHz and 120mHz and duty cycles of 50% and 75%. Moreover we have performed the same analysis for lower frequency range of frequencies 1mHz, 2mHz, 3mHz, 4mHz and 5mHz and duty cycles of 50% and 75% for two sensors (TGS-2611 and TGS-822). Lower frequency is preferred because of the following reasons-

i) To attain a quasi-isothermal state a slow change in sensor heater voltage is desirable such that the sensor dynamics is preserved[203].
ii) At lower frequencies, since the time-period is already high, smaller duty cycle may lead to attain the stable sensor dynamics.
iii) As the frequency is increased, the duty cycle has to be increased such that sufficient amount of heating takes place at the sensor surface in order to preserve the sensor dynamics.

The data-preprocessing was done as per the eqn. (2.4) as described in **Chapter 2** (*Section 2.2.2*).

4.2 Sensor Model Representation

The problem of building mathematical models of dynamical systems based on observed input-output MOS gas sensor data from the system is termed as system identification. This chapter presents system identification using the PEM method. As already described in **Chapter 1** (*Section 1.6.2*) there are three basic models for system identification:

i) Autoregressive with exogenous inputs (ARX)

ii) Autoregressive moving average model (ARMAX)

iii) State-space model.

The details of the above models are described in **Chapter 1** (*Section 1.6.2*).

In dynamic measurement, when the sensor temperature is modulated, the complicated response transients are considered to be related to different reaction kinetics of the gas molecules. At room temperature the gas molecules reacts with sensor surface of metal oxide while at elevated temperatures bulk reactions between point defects in the semiconductor lattice and gaseous oxygen molecules takes place. In both cases, the adsorption at active sites occurs first and then catalytic reactions take place. The oxygen adsorbates are partly consumed by oxidation of target gases on the semiconductor surface during the static measurement. The amount of chemisorbed oxygen decreases and hence the conductance increases. Therefore the resistance change of MOS gas sensors shows that the concentration of chemisorbed oxygen changes at the grain boundary. In the adsorption process the conductance increases with decrease in the concentration of chemisorbed oxygen.

The gradual variation of conductance of the sensor is a dynamic process governed by two factors:

i) thermal dynamics of the heater to sensor surface, and

ii) chemisorption kinetics.

The thermal dynamics of the heater is found to be mostly a stable process determined by the first-order transfer function[204], while the chemisorption kinetics is governed by reaction kinetics determined by various physical and chemical factors. From this aspect, the model of variation of conductance of the sensor is proposed with a combinational model as shown in Fig.4.1. The modeling of the MOS gas sensor dynamics has been performed and will be discussed in **Chapter-5.**

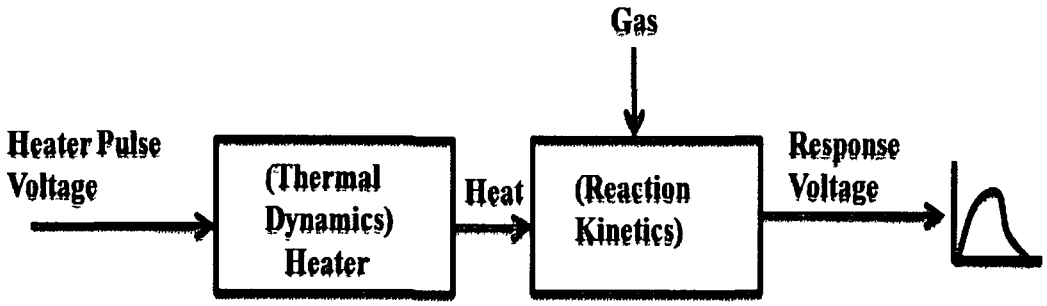

Fig. 4.1: Block diagram of metal-oxide gas sensor model.

4.3 Sensor System Identification

System identification deals with the mathematical modeling of dynamic systems based on measured input-output sensor data. The use of measured data makes the method inherently experimental whose objective is to obtain a model that describes the behaviour of the original sensor system sufficiently well for the model to serve its purpose. Work has been carried to model the gas sensor behaviour at different conditions as a dynamic system employing suitable system identification techniques[105, 106]. The model estimation from measured input and output signals is done using system identification. Parameter estimation of MOS gas sensor is employed to estimate the state-space structure from experimental input and output data. The reason for parameter estimation of the sensors is to determine best values of parameters for a numerical sensor model that predicts dependent variable outputs of the transfer function based on observations of measured inputs. This is necessary for the analysis of the various transfer functions of the three MOS gas sensors used in the experiment via system identification using sensor system input-output data at two different ranges of frequencies and duty cycles. The estimation of the various transfer functions was done using the prediction error method (PEM). The idea of PEM is to minimize the difference between the measured output and the prediction output based on past data. This method is described in details in **Chapter 1** (*Section 1.6.4.2*). The comparison between the simulated and the measured results are done and the percentage of the best fit was chosen as the most stable transfer function for that particular frequency and duty cycle.

As mentioned earlier, the sensor transfer functions have been derived for the following two ranges of pulse frequencies:

i) Lower frequency range of 1mHz, 2mHz, 3mHz, 4mHz and 5mHz and two duty cycles of 50% and 75% (for TGS-2611 and TGS-822).
ii) Upper frequency range of pulse frequencies of 10mHz, 40mHz, 80mHz and 120mHz, and two duty cycles of 50% and 75% (for TGS-2611 and TGS-842).

Thus, the system identification was performed for these two different ranges of frequencies at two different duty cycles using MATLAB.

The input signal of +5V was applied to the heater circuit. The input signal used in this work is the train of pulses. Fig.4.2 and Fig. 4.3 shows sample input and output responses of the two MOS gas sensors for lower frequency range and for upper frequency range respectively.

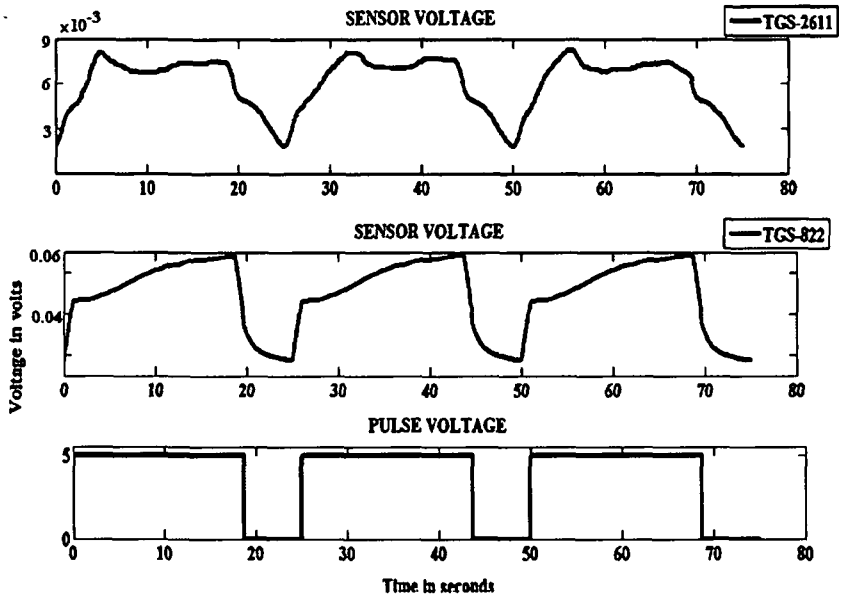

Fig 4.2: The input and output response of TGS-2611 and TGS-822.

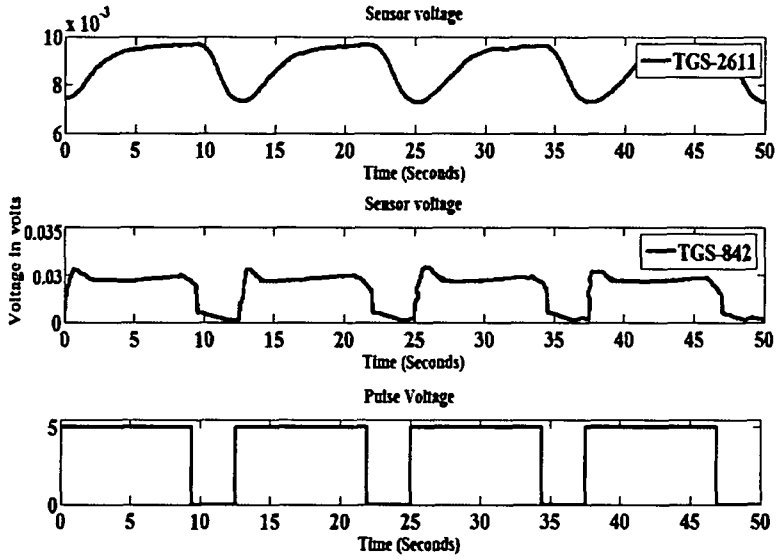

Fig 4.3: The input and output response of TGS-2611 and TGS-842.

Sensor input-output data:

The input heater pulse of +5V used for all the three sensors for a particular frequency and duty cycle is same for all the three sensors used in the experiment. A sample of the input and response for a lower frequency of 2mHz and 50% duty cycle and for a upper frequency of 40mHz and 75% duty cycle is shown Appendix A4.1 and Appendix A4.2 respectively. The data vector for each sensor is divided by the maximum response value for the corresponding sensor for normalisation using eqn. (2.4) given in **Chapter 2**. The new vector is called the normalized vector for the particular sensor. Total samples used for the lower frequency and upper frequency range are tabulated in Table 4.1.

Table 4.1: Data samples for lower and upper frequency range:

Range	Frequency (mHz)	(For TGS-2611, TGS-822 and TGS-842 for 50% and 75% duty cycles)		
		Total data samples	Samples for identification	Samples for simulation
Lower Frequency Range	1	700,000	1:500,000	600,000:700,000
	2	200,000	1:100,000	100,000:150,000
	3	135,000	1:66,666	99,999:133,332
	4	100,000	1:50,000	75,000:100,000
	5	80,000	1:40,000	50,000:70,000

Upper Frequency Range	10	600,000	1:300,000	400,000:500,000
	40	200,000	1:75,000	100,000:125,000
	80	100,000	1:50,000	75,000:87,500
	120	50,000	1:24,999	33,332:41,665

The system-identification flowchart is shown in Fig.4.4. The sequence of operation for system identification in MATLAB is as follows:

i) The input/output measurement data for the experiment performed is stored.

ii) The data structures are constructed as output-input for a particular sampling frequency.

iii) A continuous-time state-space model object is constructed containing all the information about a state-space model and specifying the parameters that are going to be estimated from given data.

iv) The parameter estimation is performed upon state-space objects, which requires both data (output data structure) and the state-space model.

v) The step response of the model is estimated for determining the stability of the model by calculating the overshoot percentage from the step response.

vi) To test the best fit of the estimated model, the model response is simulated and the model output is compared with measured output by selecting a portion of the original data that was not used in building the model.

vii) The pole-zero plots is then obtained to test the stability of the transfer function.

4.3.1 Transfer function determination

The most stable transfer function was selected by computing the pole-zero plots, the overshoot percentage and the best fit of the step response. The transfer functions thus obtained were proposed to work best with the specified frequency and duty cycle. The classification was then performed with the best chosen frequency and duty cycle and the classification enhancement results were obtained.

In the first part of the experiment, the heater pulse frequencies that were chosen are, 1mHz, 2mHz, 3mHz, 4mHz and 5mHz. Two duty cycles of 50% and 75% were chosen to generate the responses. Two MOS gas sensors namely TGS-822 and TGS-2611were used for conducting the experiment.

The estimated transfer functions of the two sensors (both in the s-domain and z-domain given by eqn. (1.21) and (1.22) respectively) for the above frequencies and duty cycles are tabulated in Table 4.2.

In the second part of the experiment, the frequencies chosen were-10mHz, 40mHz, 80mHz and 120mHz. Similarly two duty cycles of 50% and 75% were chosen to generate the responses. Two MOS gas sensors namely TGS-2611 and TGS-842 were used for conducting the experiment. The transfer functions of the MOS gas sensors (both in the z-domain and s- domain) for the above frequencies and duty cycles are tabulated in Table 4.3.

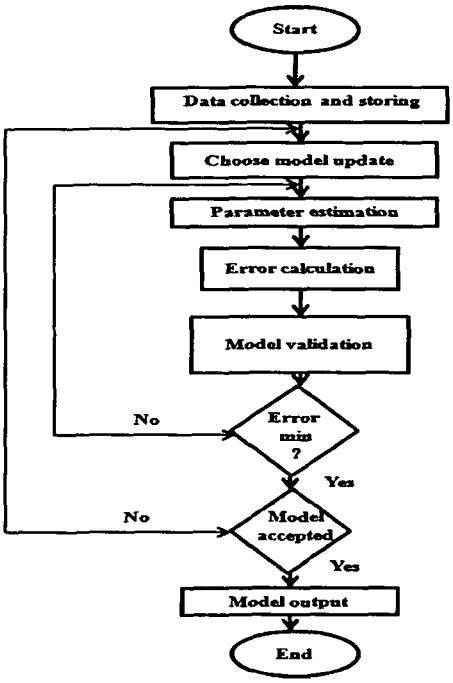

Fig 4.4: The system-identification flowchart.

System identification resulted the parametric models in transfer function for each of the sensors performed using MATLAB. The transfer functions were tested for their stability

analysis by determining the pole-zero plot and overshoot percentage as discussed in *Section 4.4.1*. This helps in finding the best transfer function at a specific frequency and duty cycle for each of the sensors.

4.4 Sensor Stability Analysis

The most important characteristic of the dynamic behavior of a system is its stability. An LTI system is stable if the output eventually comes back to its equilibrium state when the system is subjected to any input or disturbance, which is already described in **Chapter 1** (*Section 1.6.3*).

The MOS gas sensor stability under inactive period of the gas input is important to determine suitable time duration of the heater pulse voltage. The sensor transfer function is excited by the heater pulse either by a step pulse or an impulse determined by the frequency and duty cycle of the pulse. For short duration heater pulses when the frequency is high, the impulse response is more prominent than step response.

Hence, the dynamics of the sensor is greatly influenced by the frequency and duty cycle of the pulse temperature signal. Physically, this is because of the fact that the time for the reaction kinetics should match to the time for the sensor heating process. Fig 4.5 (a) and (b) shows two typical patterns of a MOS gas sensor responses where in (a) the sensor behaves as in transient mode with an overshoot before coming to a stable and equilibrium response level of 0.02 volt, whereas in (b) the sensor response is fairly stable.

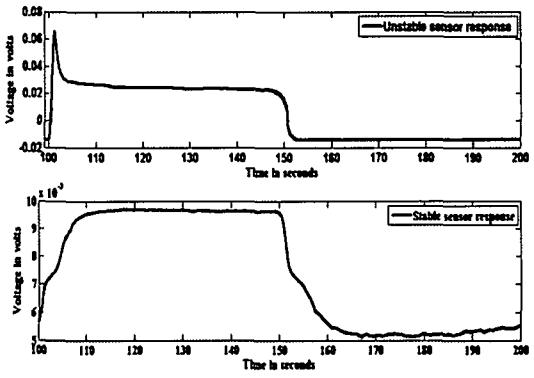

Fig4.5. Sensor baseline response on pulse temperature modulation (a) Unstable response with overshoots (b) Stable response (both without application of gas).

Table 4.2. Transfer function model parameters of the MOS gas sensors for different frequencies and duty cycles for lower frequency range:

Sensors	Frequency (mHz)	Duty Cycle (%)	Transfer Function $\hat{H}_f$; f indicates the heater pulse frequency	
			z-domain	s-domain
TGS-2611	1	50	$\hat{H}(z)_{1mHz} = \frac{(5.756\times10^{-7})(z-0.9984)}{(z-0.996)(z-0.9982)}$	$\hat{H}(s)_{1mHz} = \frac{(5.756\times10^{-4})(s+0.9984)}{(s+0.996)(s+0.998)}$
	2		$\hat{H}(z)_{2mHz} = \frac{(5.902\times10^{-7})(z-0.9989)}{(z-0.995)(z-0.996)}$	$\hat{H}(s)_{2mHz} = \frac{(5.902\times10^{-4})(s+0.9989)}{(s+0.9958)(s+0.9969)}$
	3		$\hat{H}(z)_{3mHz} = \frac{(9.0854\times10^{-8})(z-0.9977)}{(z-0.998)(z-0.9997)}$	$\hat{H}(s)_{3mHz} = \frac{(9.0854\times10^{-5})(s+0.997)}{(s+0.998)(s+0.9997)}$
	4		$\hat{H}(z)_{4mHz} = \frac{(2.0017\times10^{-8})(z-1.03)}{(z-0.9996)(z-0.9999)}$	$\hat{H}(s)_{4mHz} = \frac{(2.0017\times10^{-5})(s+1.03)}{(s+0.996)(s+0.999)}$
	5		$\hat{H}(z)_{5mHz} = \frac{(2.4379\times10^{-7})(s+1.001)}{(s+1.0008)(s+0.9998)}$	$\hat{H}(s)_{5mHz} = \frac{(2.4379\times10^{-4})(s+1.001)}{(s+1.0008)(s+0.9988)}$
	1	75	$\hat{H}(z)_{1mHz} = \frac{(5.7851\times10^{-7})(z-1)}{(z-0.999)(z-0.9998)}$	$\hat{H}(s)_{1mHz} = \frac{(5.7851\times10^{-4})(s+1)}{(s+0.999)(s+0.9998)}$
	2		$\hat{H}(z)_{2mHz} = \frac{(6.13\times10^{-7})(z-1.0001)}{(z-0.9998)(z-0.9999)}$	$\hat{H}(s)_{2mHz} = \frac{(6.13\times10^{-4})(s+1.0001)}{(s+0.9998)(s+0.9999)}$
	3		$\hat{H}(z)_{3mHz} = \frac{(7.2192\times10^{-8})(z-1.003)}{(z-0.999)(z-1.0003)}$	$\hat{H}(s)_{3mHz} = \frac{(7.2192\times10^{-5})(s+1.003)}{(s+0.9998)(s+1.0003)}$
	4		$\hat{H}(z)_{4mHz} = \frac{(8.5514\times10^{-8})(z-1.008)}{(z-0.9998)(z-0.9999)}$	$\hat{H}(s)_{4mHz} = \frac{(8.5514\times10^{-5})(s+1.008)}{(s+0.9998)(s+0.9999)}$

	5		$\hat{H}(z)_{5mHz} = \frac{(3.5997\times10^{-7})(z-1)}{(z-1.0002)(z-1.0005)}$	$\hat{H}(s)_{5mHz} = \frac{(3.5997\times10^{-4})(s+1.0001)}{(s+1.0002)(s+1.0005)}$
TGS-822	1	50	$\hat{H}(z)_{1mHz} = \frac{(2.791\times10^{-7})(z-1.00035)}{(z-0.992)(z-0.9938)}$	$\hat{H}(s)_{1mHz} = \frac{(2.791\times10^{-4})(s+1.0003)}{(s+0.992)(s+0.9938)}$
	2		$\hat{H}(z)_{2mHz} = \frac{(5.3083\times10^{-7})(z-1)}{(z-0.9993)(z-0.9997)}$	$\hat{H}(s)_{2mHz} = \frac{(5.3083\times10^{-4})(s+1.0001)}{(s+0.9993)(s+0.9997)}$
	3		$\hat{H}(z)_{3mHz} = \frac{(1.414\times10^{-7})(z-1)}{(z-0.9995)(z-0.9999)}$	$\hat{H}(s)_{3mHz} = \frac{(1.414\times10^{-4})(s+1)}{(s+0.9995)(s+0.9999)}$
	4		$\hat{H}(z)_{4mHz} = \frac{(4.039\times10^{-7})(z-1.001)}{(z-1)(z-0.9999)}$	$\hat{H}(s)_{4mHz} = \frac{(4.039\times10^{-4})(s+1.001)}{(s+1.0001)(s+0.9999)}$
	5		$\hat{H}(z)_{5mHz} = \frac{(4.4405\times10^{-7})(z-1)}{(z-1.0003)(z-1.0005)}$	$\hat{H}(s)_{5mHz} = \frac{(4.4405\times10^{-4})(s+1)}{(s+1.0003)(s+1.0005)}$
	1	75	$\hat{H}(z)_{1mHz} = \frac{(3.793\times10^{-8})(z-1)}{(z-0.9996)(z-0.9999)}$	$\hat{H}(s)_{1mHz} = \frac{(3.793\times10^{-4})(s+1)}{(s+0.9996)(s+0.9999)}$
	2		$\hat{H}(z)_{2mHz} = \frac{(6.0382\times10^{-8})(z-0.998)}{(z-0.996)(z-0.9998)}$	$\hat{H}(s)_{2mHz} = \frac{(6.0382\times10^{-5})(s+0.998)}{(s+0.996)(s+0.9998)}$
	3		$\hat{H}(z)_{3mHz} = \frac{(6.125\times10^{-8})(z-0.999)}{(z-0.999)(z-1.0002)}$	$\hat{H}(s)_{3mHz} = \frac{(6.125\times10^{-5})(s+0.999)}{(s+0.999)(s+1.0002)}$
	4		$\hat{H}(z)_{4mHz} = \frac{(4.8715\times10^{-8})(z-1.007)}{(z-0.999)(z-1.0009)}$	$\hat{H}(s)_{4mHz} = \frac{(4.8715\times10^{-5})(s+1.007)}{(s+0.999)(s+1.0009)}$
	5		$\hat{H}(z)_{5mHz} = \frac{(8.1379\times10^{-7})(z-1)}{(z-1.0005)(z-1.0009)}$	$\hat{H}(s)_{5mHz} = \frac{(8.1379\times10^{-4})(s+1)}{(s+1.0005)(s+1.0009)}$

Table 4.3. Transfer function model parameters of the MOS gas sensors for different frequencies and duty cycles for upper frequency range:

Sensors	Frequency (mHz)	Duty Cycle (%)	Transfer Function $\hat{H}_f$; f indicates the heater pulse frequency	
			z-domain	s-domain
TGS-2611	10	50	$\hat{H}(z)_{10mHz} = \frac{(3.612\times10^{-8})}{(z-0.999)}$	$\hat{H}(s)_{10mHz} = \frac{(3.612\times10^{-5})}{(s+0.999)}$
	40		$\hat{H}(z)_{40mHz} = \frac{(1.6313\times10^{-7})}{(z-0.999)}$	$\hat{H}(s)_{40mHz} = \frac{(1.6313\times10^{-4})}{(s+0.999)}$
	80		$\hat{H}(z)_{80mHz} = \frac{(1.3699\times10^{-7})}{(z-0.999)}$	$\hat{H}(s)_{80mHz} = \frac{(1.3699\times10^{-4})}{(s+0.999)}$
	120		$\hat{H}(z)_{120mHz} = \frac{(1.257\times10^{-8})}{(z-1)}$	$\hat{H}(s)_{120mHz} = \frac{(1.257\times10^{-5})}{(s+1)}$
	10	75	$\hat{H}(z)_{10mHz} = \frac{(4.903\times10^{-8})}{(z-1)}$	$\hat{H}(s)_{10mHz} = \frac{(4.903\times10^{-5})}{(s+1)}$
	40		$\hat{H}(z)_{40mHz} = \frac{(1.7\times10^{-7})}{(z-0.996)}$	$\hat{H}(s)_{40mHz} = \frac{(1.7\times10^{-4})}{(s+0.996)}$
	80		$\hat{H}(z)_{80mHz} = \frac{(1.599\times10^{-7})}{(z-0.999)}$	$\hat{H}(s)_{80mHz} = \frac{(1.599\times10^{-4})}{(s+0.999)}$
	120		$\hat{H}(z)_{120mHz} = \frac{(1.2567\times10^{-7})}{(z-0.999)}$	$\hat{H}(s)_{120mHz} = \frac{(1.2567\times10^{-4})}{(s+0.999)}$

TGS-842	10	50	$\hat{H}(z)_{10mHz} = \frac{(5.209\times10^{-6})(z-1.0007)}{(z-1)(z-1)}$	$\hat{H}(s)_{10mHz} = \frac{(5.209\times10^{-3})(s+1)}{(s+1)(s+1)}$
	40		$\hat{H}(z)_{40mHz} = \frac{(1.53\times10^{-7})(z-1.005)}{(z-1.001)(z-1)}$	$\hat{H}(s)_{40mHz} = \frac{(1.53\times10^{-4})(s+1.005)}{(s+1.001)(s+1)}$
	80		$\hat{H}(z)_{80mHz} = \frac{(5.2714\times10^{-6})(z-1)}{(z-1.005)(z-0.9995)}$	$\hat{H}(s)_{80mHz} = \frac{(5.2714\times10^{-3})(s+1)}{(s+1.005)(s+0.9995)}$
	120		$\hat{H}(z)_{120mHz} = \frac{(2.6915\times10^{-7})(z-0.963)}{(z-0.9995)(z-0.9996)}$	$\hat{H}(s)_{120mHz} = \frac{(2.6915\times10^{-4})(s+0.963)}{(s+0.9995)(s+0.9996)}$
	10	75	$\hat{H}(z)_{10mHz} = \frac{(5.2477\times10^{-6})(z-1)}{(z-1.002)(z-1.006)}$	$\hat{H}(s)_{10mHz} = \frac{(5.2477\times10^{-3})(s+1)}{(s+1.002)(s+1.006)}$
	40		$\hat{H}(z)_{40mHz} = \frac{(2.1647\times10^{-7})(z-0.9861)}{(z-1.005)(z-1.0006)}$	$\hat{H}(s)_{40mHz} = \frac{(2.1647\times10^{-4})(s+0.9861)}{(s+1.005)(s+1.0006)}$
	80		$\hat{H}(z)_{80mHz} = \frac{(5.2072\times10^{-8})(z-0.9986)}{(z-0.9995)(z-0.9997)}$	$\hat{H}(s)_{80mHz} = \frac{(5.2072\times10^{-5})(s+0.9986)}{(s+0.9995)(s+0.9997)}$
	120		$\hat{H}(z)_{120mHz} = \frac{(4.2481\times10^{-7})(z-0.9639)}{(z-0.9995)(z-0.9992)}$	$\hat{H}(s)_{120mHz} = \frac{(4.2481\times10^{-4})(s+0.9639)}{(s+0.9995)(s+0.9992)}$

4.4.1 Pole-Zero Plots and Step Responses

Lower Frequency Range:

Fig.4.6 and Fig. 4.7 shows the zoomed view of the position of pole-zero of the transfer functions that are tabulated in Table 4.2 for sensor TGS-2611 and TGS-822 respectively at all the frequencies and duty cycles. The distance of the poles from the unit circle is calculated from the transfer function and is tabulated in Table 4.4.

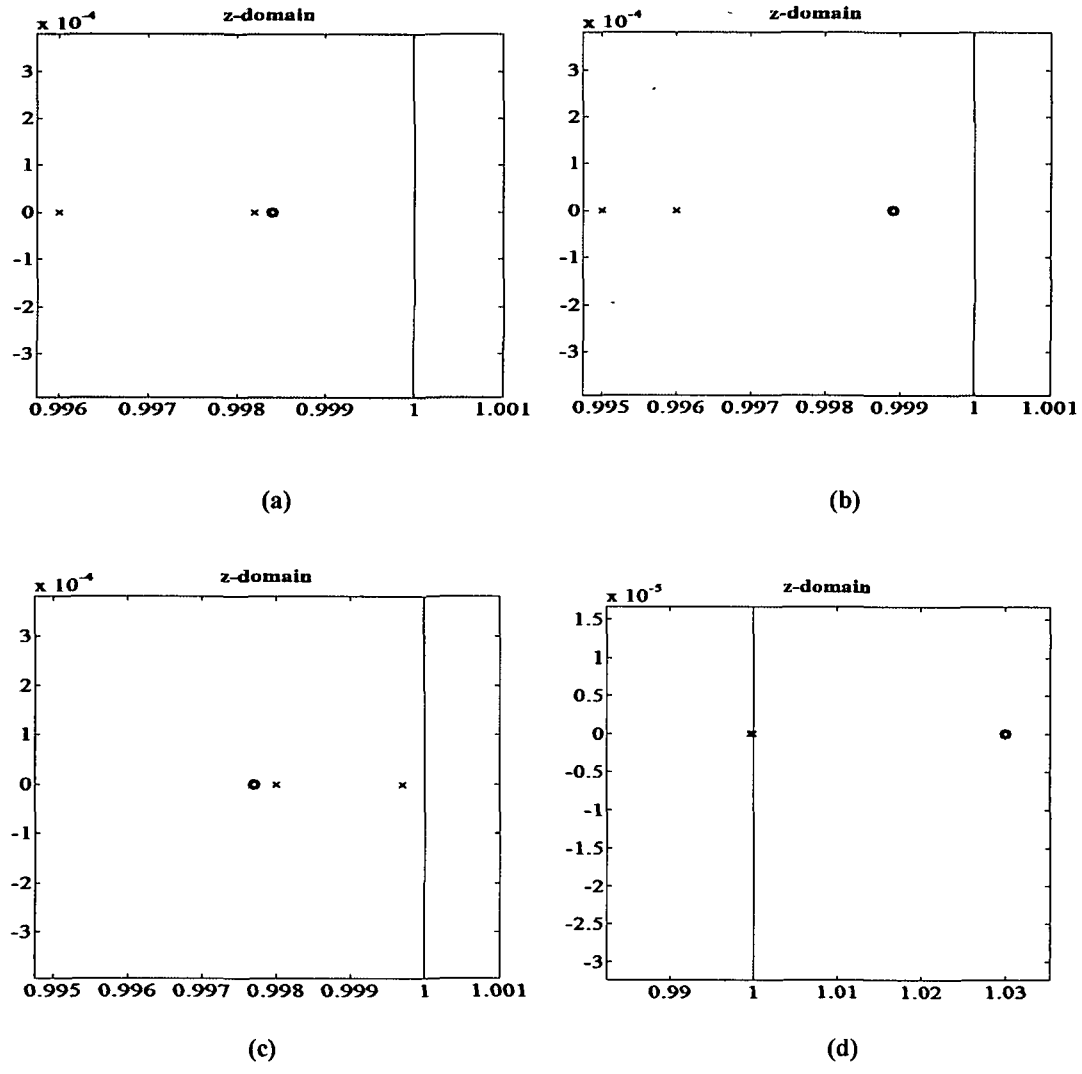

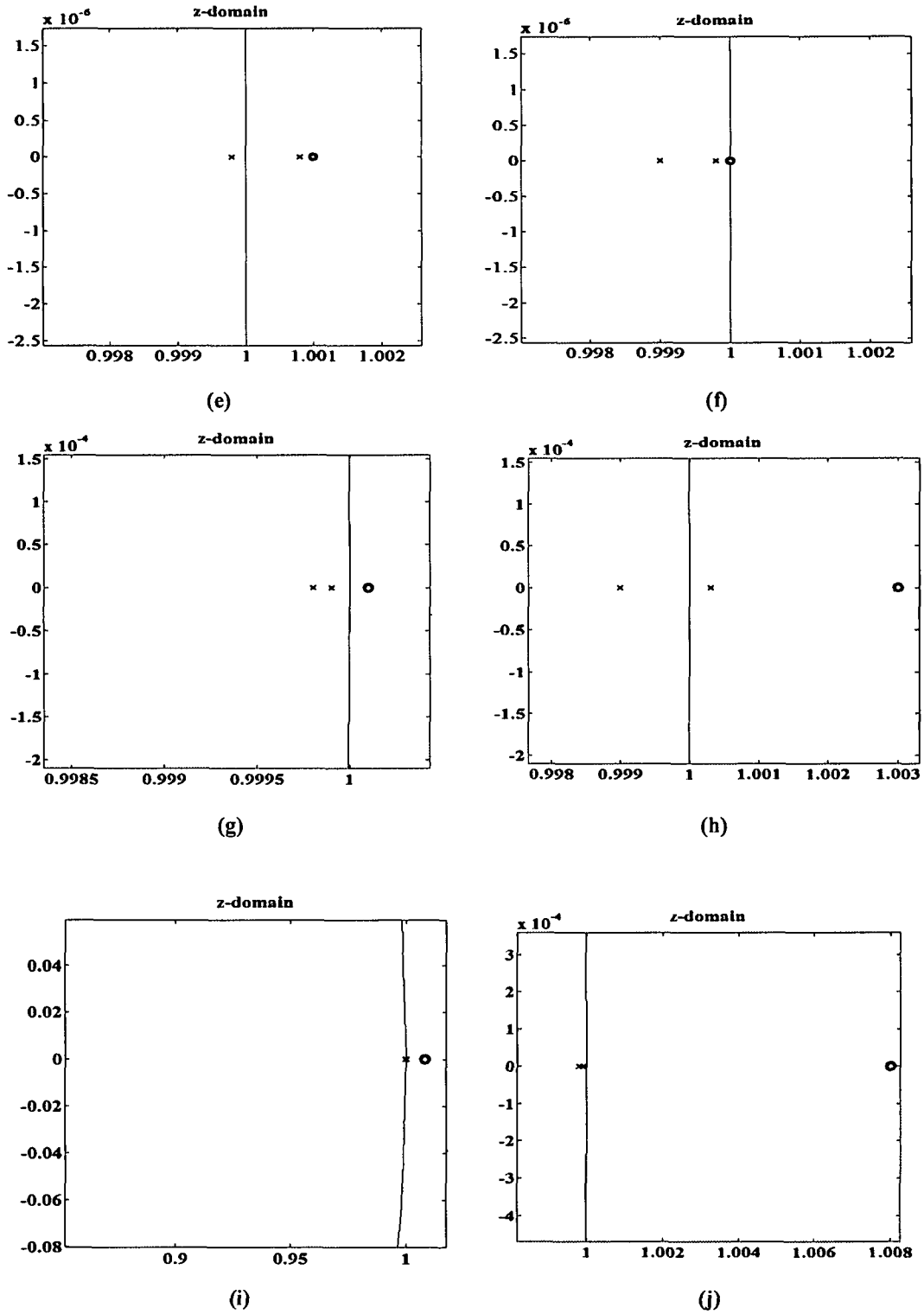

Fig4.6. Zoomed part of the pole-zero plot of transfer function in z-domain of sensor TGS-2611 at (a) 1mHz and 50% duty cycle, **(b) 2mHz and 50% duty cycle**, (c) 3mHz and 50% duty cycle, (d) 4mHz and 50% duty cycle, (e) 5mHz and 50% duty cycle, (f) 1mHz and 75% duty cycle, (g) 2mHz and 75% duty cycle, (h) 3mHz and 75% duty cycle, (i) 4mHz and 75% duty cycle, and (j) 5mHz and 75% duty cycle.

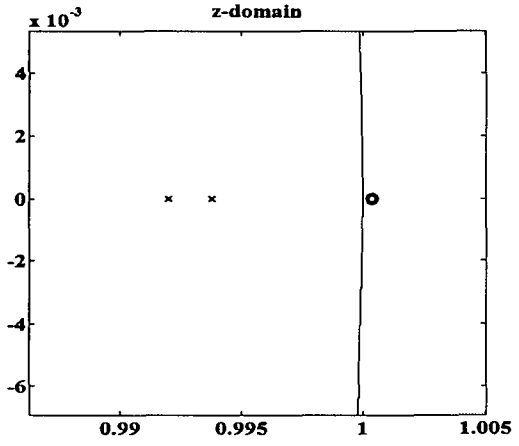
x 10^-3
z-domain
4
2
0
-2
-4
-6
0.99
0.995
1
1.005

(a)

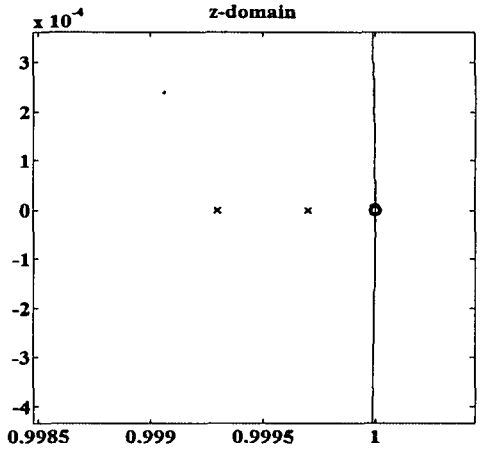
x 10^-4
z-domain
3
2
1
0
-1
-2
-3
-4
0.9985
0.999
0.9995
1

(b)

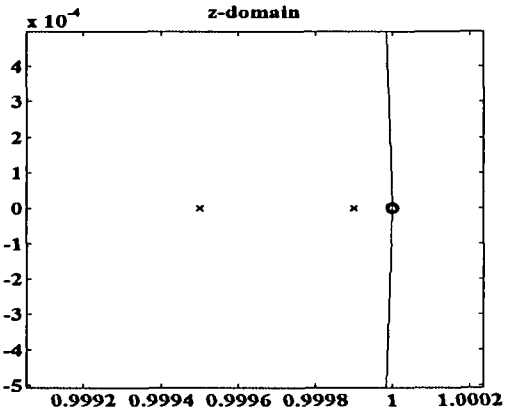
x 10^-4
z-domain
4
3
2
1
0
-1
-2
-3
-4
-5
0.9992
0.9994
0.9996
0.9998
1
1.0002

(c)

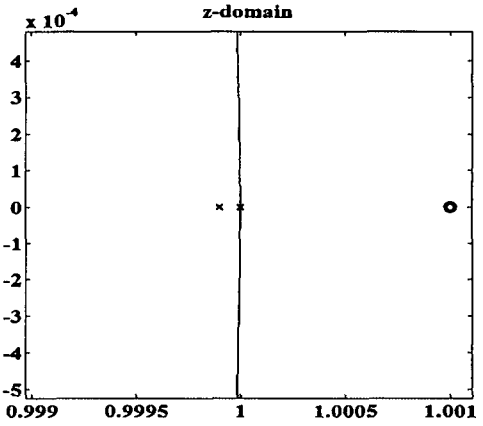
x 10^-4
z-domain
4
3
2
1
0
-1
-2
-3
-4
-5
0.999
0.9995
1
1.0005
1.001

(d)

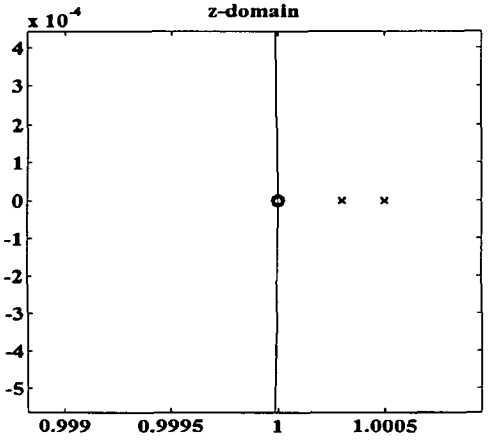
x 10^-4
z-domain
4
3
2
1
0
-1
-2
-3
-4
-5
0.999
0.9995
1
1.0005

(e)

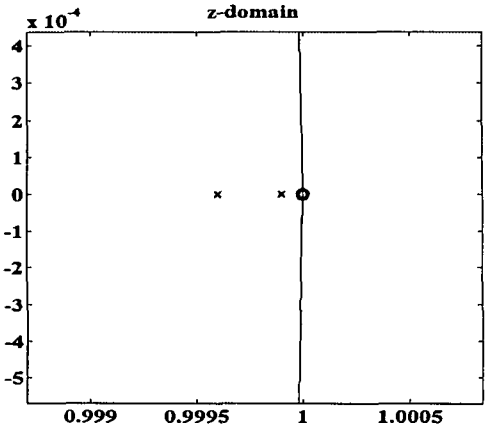
x 10^-4
z-domain
4
3
2
1
0
-1
-2
-3
-4
-5
0.999
0.9995
1
1.0005

(f)

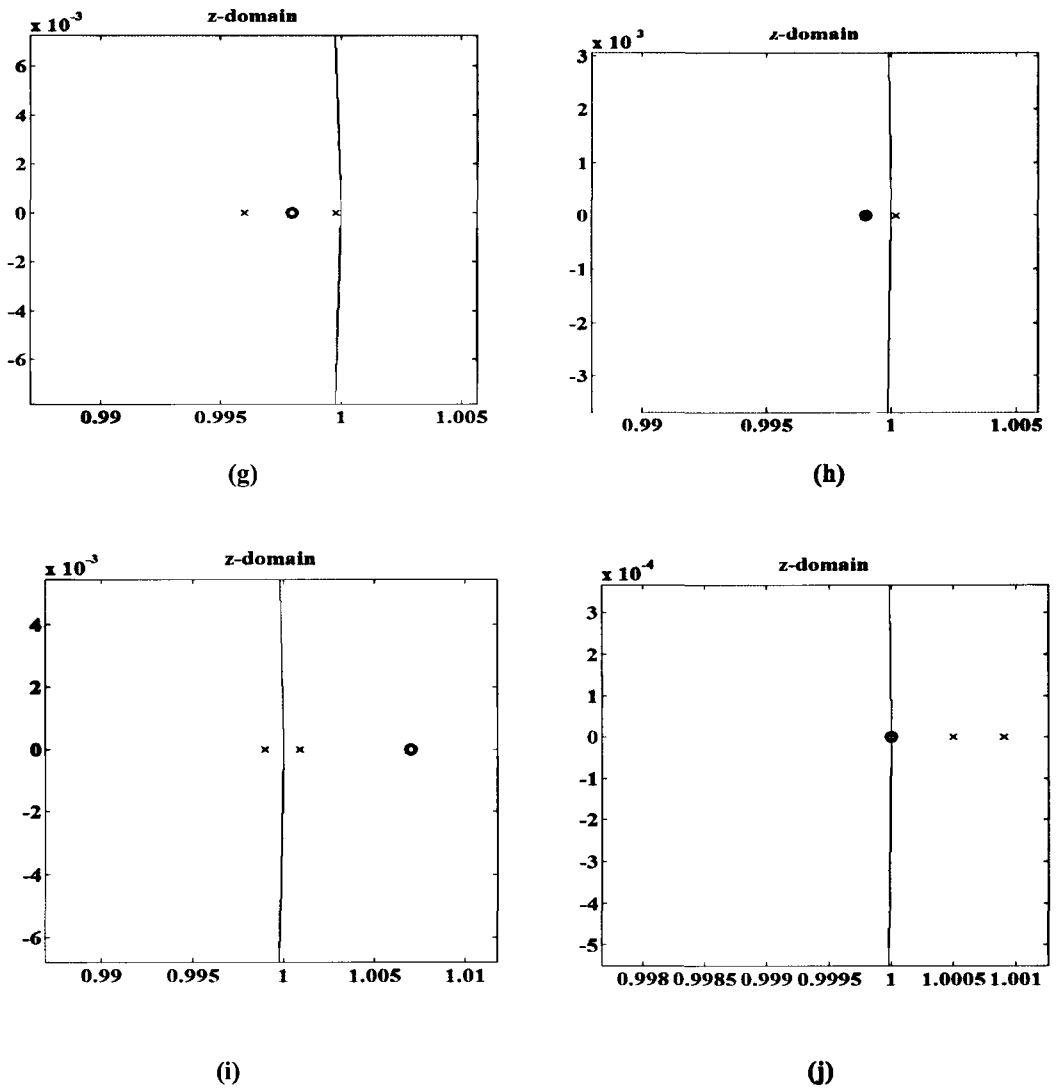

Fig4.7. Zoomed part of the pole-zero plot of transfer function in z-domain of sensor TGS-822 at **(a) 1mHz and 50% duty cycle**, (b) 2mHz and 50% duty cycle, (c) 3mHz and 50% duty cycle, (d) 4mHz and 50% duty cycle, (e) 5mHz and 50% duty cycle, (f) 1mHz and 75% duty cycle, (g) 2mHz and 75% duty cycle, (h) 3mHz and 75% duty cycle, (i) 4mHz and 75% duty cycle, and (j) 5mHz and 75% duty cycle.

One of the most important criterions for choosing the most stable transfer function is the overshoot percentage calculated from the step responses of the two sensors at the above mentioned frequencies and duty cycles. For the step response the overshoot percentage is shown in Table 4.4 and the step response diagrams are shown in Fig.4.8.

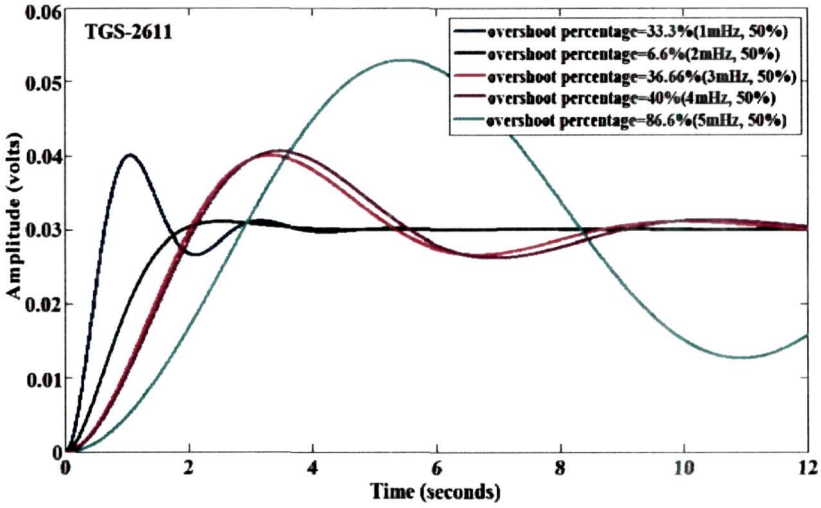
TGS-2611
overshoot percentage=33.3%(1mHz, 50%)
overshoot percentage=6.6%(2mHz, 50%)
overshoot percentage=36.66%(3mHz, 50%)
overshoot percentage=40%(4mHz, 50%)
overshoot percentage=86.6%(5mHz, 50%)
Amplitude (volts)
Time (seconds)

(a)

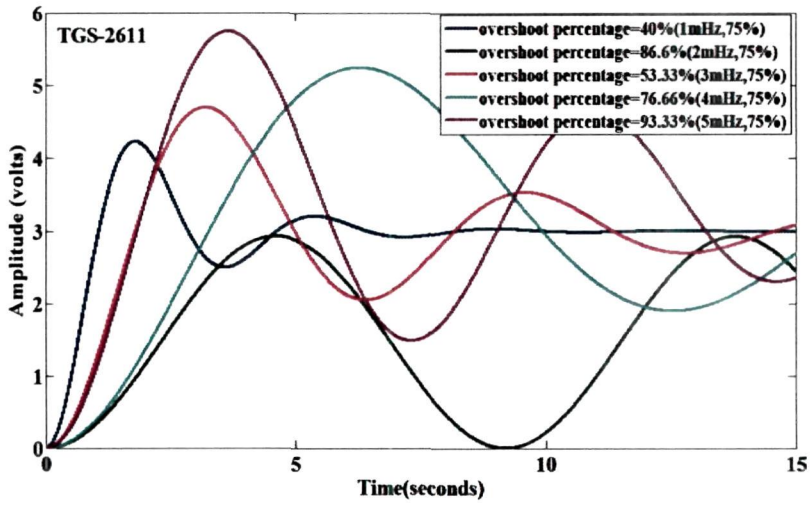
TGS-2611
overshoot percentage=40%(1mHz,75%)
overshoot percentage=86.6%(2mHz,75%)
overshoot percentage=53.33%(3mHz,75%)
overshoot percentage=76.66%(4mHz,75%)
overshoot percentage=93.33%(5mHz,75%)
Amplitude (volts)
Time(seconds)

(b)

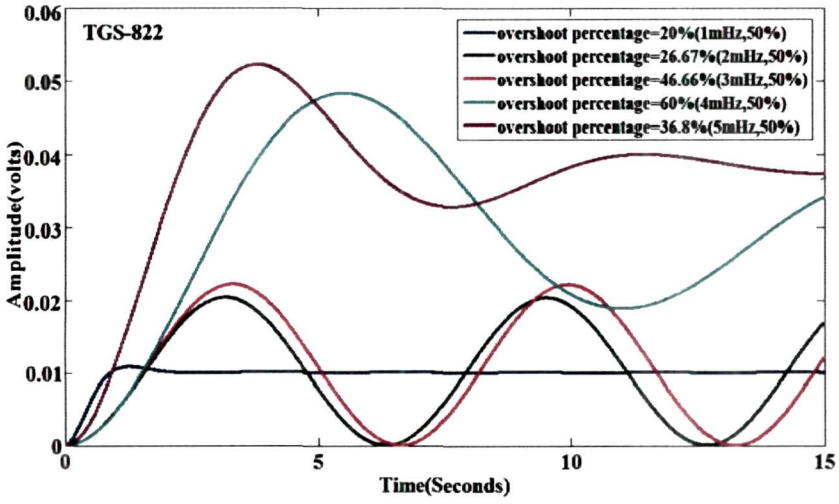
TGS-822
overshoot percentage=20%(1mHz,50%)
overshoot percentage=26.67%(2mHz,50%)
overshoot percentage=46.66%(3mHz,50%)
overshoot percentage=60%(4mHz,50%)
overshoot percentage=36.8%(5mHz,50%)
Amplitude(volts)
Time(Seconds)

(c)

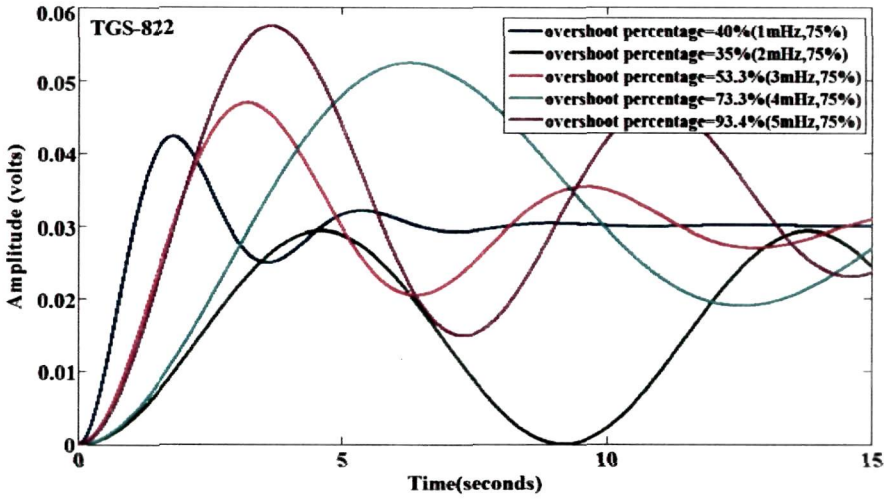

(d)

Fig4.8. Step response of frequencies 1mHz, 2mHz, 3mHz, 4mHz and 5mHz of (a) sensor TGS-2611 at 50% duty cycle, (b) sensor TGS-2611 at 75% duty cycle, (c) sensor TGS-822 at 50% duty cycle, (d) sensor TGS-822 at 75% duty cycle.

It is evident from Table 4.4 that the frequencies and duty cycles at which the transfer function was most stable for TGS-2611 and TGS-822 are **2mHz** and **50%** and **1mHz** and **50%** respectively on the basis of *two* observations:

i) The first observation was that the overshoot percentage was lowest (**6.6%**) for TGS-2611 at **2mHz** and **50%** duty cycle as shown in Fig.4.8 (a). Similarly for TGS-822 it was lowest (**20%**) at **1mHz** and **50%** duty cycle given in Fig.4.8 (c).

ii) The second observation was that the poles were inside the unit circles (having values **0.995**, **0.996**) at **2mHz** and **50%** duty cycle for TGS-2611 as shown in Fig.4.6 (b). Similarly, for TGS-822, the distance of the poles were inside the unit circle (having values **0.992**, **0.9938**) at **1mHz** and **50%** duty cycle as shown in Fig.4.7 (a).

Hence, the most stable transfer function selected for TGS-2611 is:

$$\hat{H}(z)_{2mHz} = \frac{(5.902\times10^{-7})(z-0.9989)}{(z-0.995)(z-0.996)}$$

Table 4.4. Transfer function model parameters of the MOS gas sensors (TGS-2611 and TGS-822) for different frequencies and duty cycles (The most stable model parameters are shown in bold):

Sensors	Frequency (mHz)	Duty Cycle (%)	Percentage of overshoot (%)	Position of pole from center	Stability	Stable Transfer Function (Based on percentage overshoot & pole-zero distance)
TGS- 2611	1	50	33.3	0.996,0.9982	Stable	$\tilde{H}(z)_{2mHz} = \frac{(5.902\times10^{-7})(z-0.9989)}{(z-0.995)(z-0.996)}$
	2		**6.6**	**0.995,0.996**	**Most Stable**	
	3		36.66	0.998,0.9997	Stable	
	4		40	0.9996,0.9999	Unstable	
	5		86.6	1.0008,0.9998	Unstable	
	1	75	40	0.999,0.9998	Stable	
	2		86.6	0.9998,0.9999	Stable	
	3		53.33	0.999,1.0003	Stable	
	4		76.66	0.9998,0.9999	Stable	
	5		93.33	1.0002,1.0005	Unstable	
TGS-822	**1**	50	**20**	**0.992,0.9938**	**Most Stable**	$\tilde{H}(z)_{1mHz} = \frac{(2.791\times10^{-7})(z-1.00035)}{(z-0.992)(z-0.9938)}$
	2		26.67	0.9993,0.9997	Stable	
	3		46.66	0.9995,0.9999	Stable	
	4		60	1,0.9999	Unstable	
	5		36.8	1.0003,1.0005	Unstable	
	1	75	40	0.9996,0.9999	Stable	
	2		35	0.996,0.9998	Stable	
	3		53.3	0.999,1.0002	Stable	
	4		73.3	0.999,1.0004	Stable	
	5		93.3	1.0005,1.0009	Unstable	

and that for TGS-822 is:

$$\hat{H}(z)_{1mHz} = \frac{(2.791\times10^{-7})(z-1.00035)}{(z-0.992)(z-0.9938)}$$

These transfer functions will be used for simulation later.

Upper Frequency Range:

Similarly for upper frequency range of frequencies and duty cycle the best transfer function is selected based on the overshoot percentage and pole-zero plots. Fig.4.9 shows the close view of the position of pole-zero of the transfer functions that are tabulated in Table 4.5 for sensor TGS-2611 at all the frequencies and duty cycles. Fig. 4.10 shows the zoomed visualization of the pole-zero diagrams of the transfer functions that are tabulated in Table 4.6 for sensor TGS-842 at all the frequencies and duty cycles. The distance of the poles from the unit circle is calculated from the transfer function and is tabulated in Table 4.5.

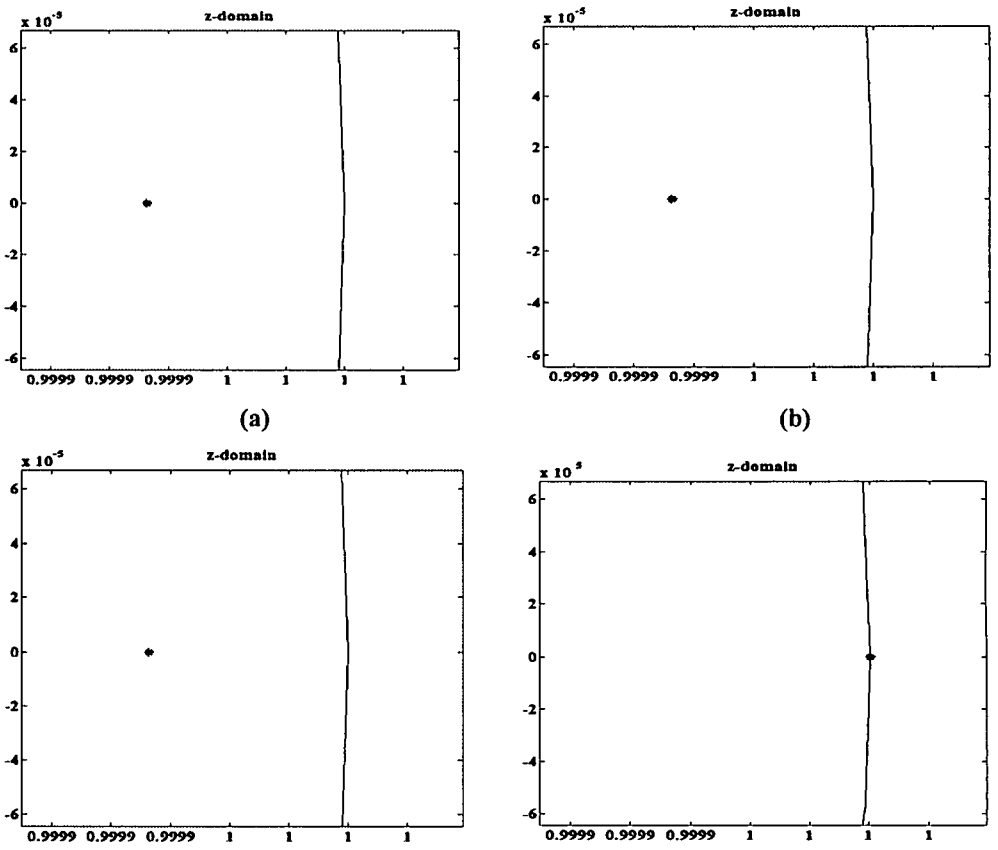

(a) (b)

(c) (d)

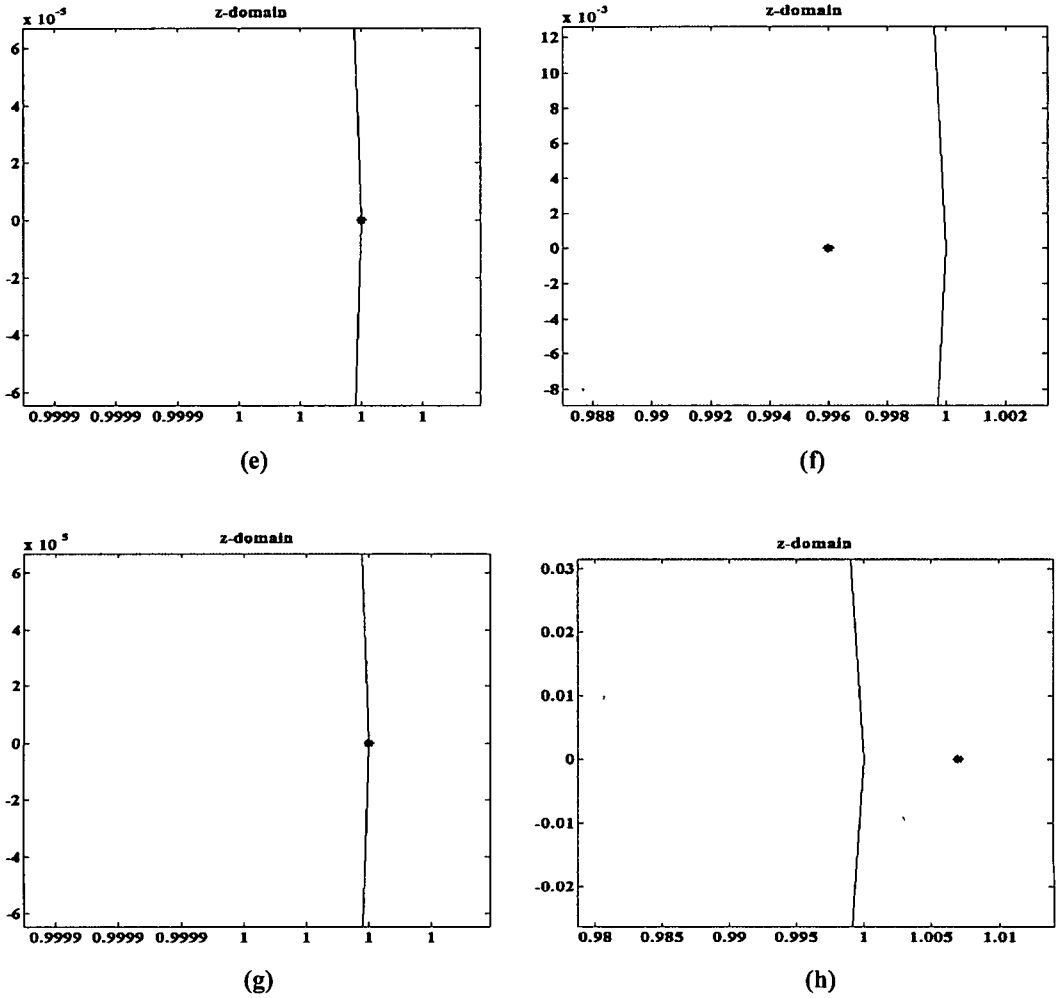

Fig4.9. Zoomed part of the pole-zero plot of transfer function in z-domain of sensor TGS-2611 at (a) 10mHz and 50% duty cycle, (b) 40mHz and 50% duty cycle, (c) 80mHz and 50% duty cycle, (d) 120mHz and 50% duty cycle, (e) 10mHz and 75% duty cycle, **(f) 40mHz and 75% duty cycle**, (g) 80mHz and 75% duty cycle, and (h) 120mHz and 75% duty cycle.

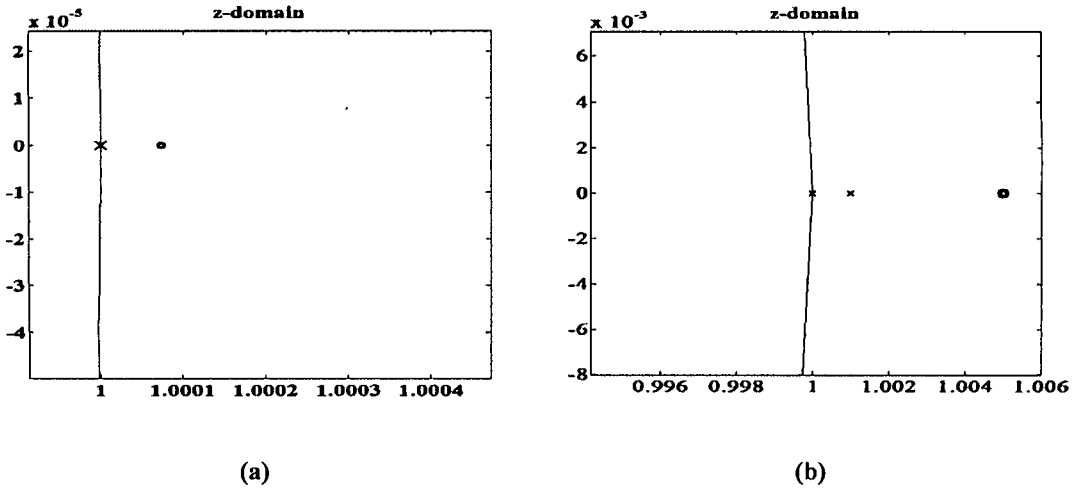

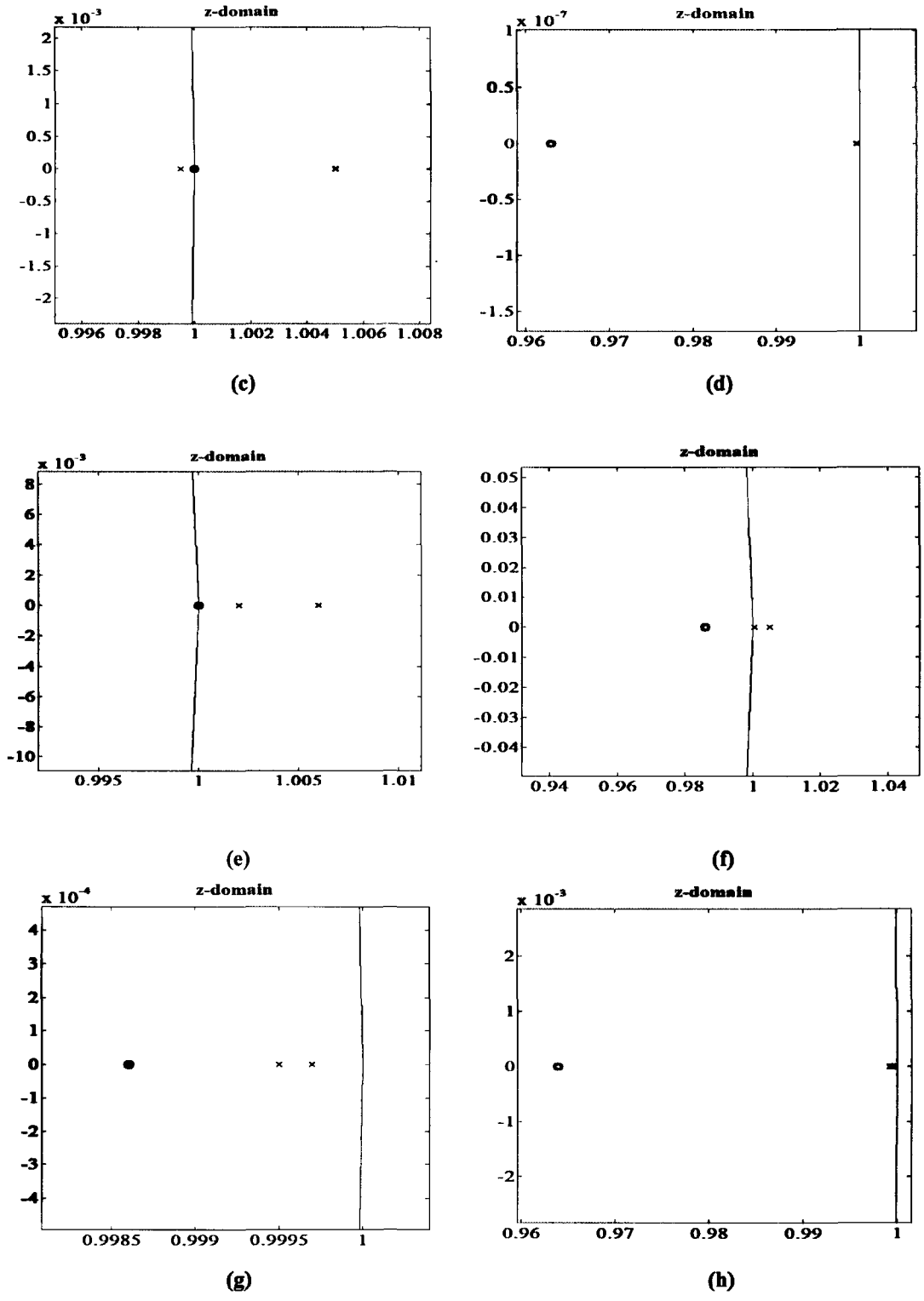

Fig4.10. Zoomed part of the pole-zero plot of transfer function in z-domain of sensor TGS-842 at (a) 10mHz and 50% duty cycle, (b) 40mHz and 50% duty cycle, (c) 80mHz and 50% duty cycle, (d) 120mHz and 50% duty cycle, (e) 10mHz and 75% duty cycle, (f) 40mHz and 75% duty cycle, (g) 80mHz and 75% duty cycle, and **(h) 120mHz and 75% duty cycle.**

The stable transfer function is again chosen from the overshoot percentage calculated from the step responses of the two sensors at the above mentioned frequencies and duty cycles. The overshoot percentage is shown in Table 4.5 and the step response diagrams are shown in Fig.4.11.

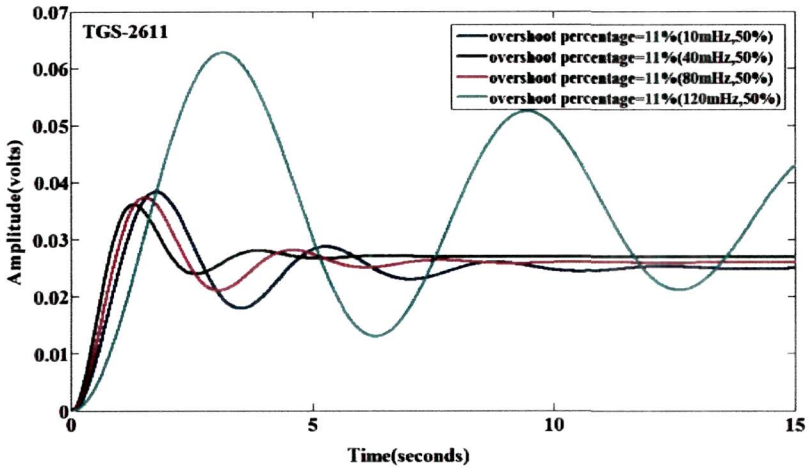

(a)

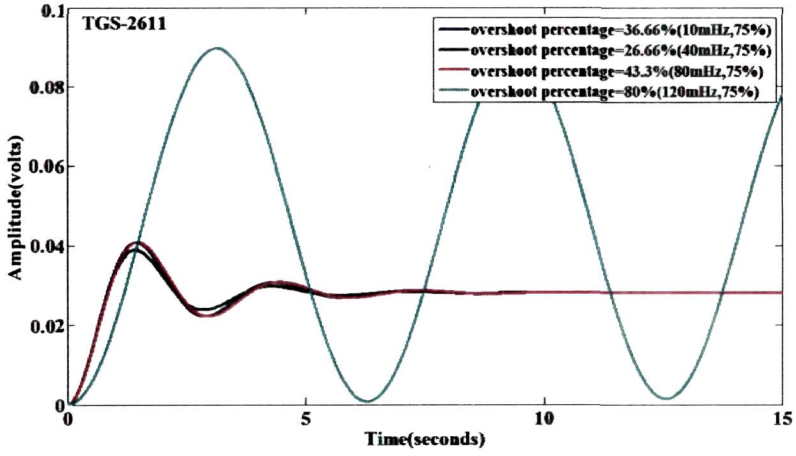

(b)

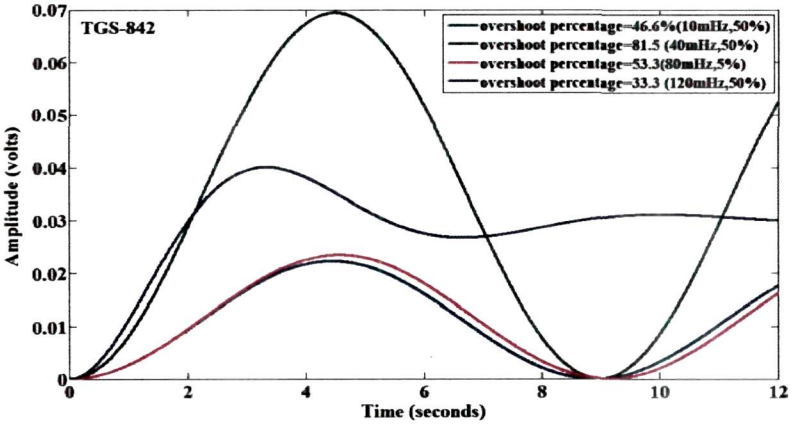

(c)

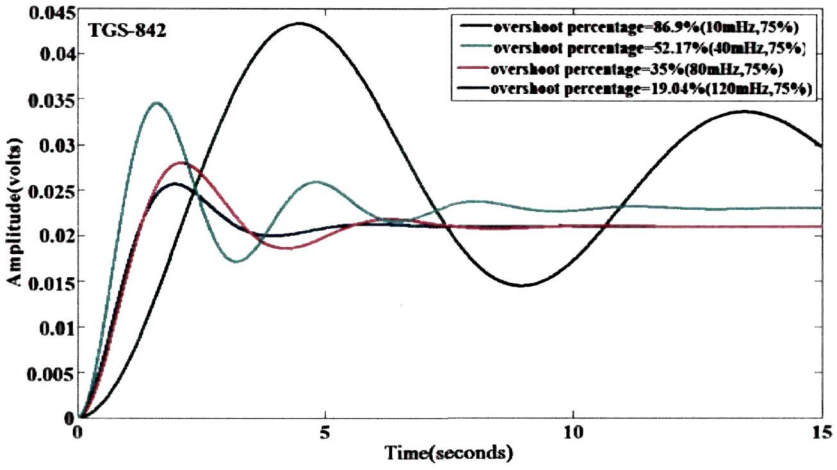

(d)

Fig4.11 Step response of frequencies 10mHz, 40mHz, 80mHz and120mHz of (a) sensor TGS-2611 at 50% duty cycle, (b) sensor TGS-2611 at 75% duty cycle, (c) sensor TGS-842 at 50% duty cycle, (d) sensor TGS-842 at 75% duty cycle.

For the upper range of pulsed frequencies, it is seen that the frequencies and duty cycles at which the transfer function was most stable for TGS-2611 and TGS-842 was obtained at **40mHz** and **75%** and at **120mHz** and **75%** respectively on the basis of *two* observations:

i) The first observation was that of the overshoot percentage which showed that the overshoot was lowest (**26.6%**) for TGS-2611 at **40mHz** and **75%** duty cycle. Similarly for TGS-842 it was lowest (**19.04%**) at **120mHz** and **75%** duty cycle.

ii) The second observation was that the poles were inside the unit circles (having values **0.996**) at **40mHz** and **75%** duty cycle for TGS-2611. Similarly, for TGS-842, the poles were inside the unit circles (having values **0.9992, 0.9995**) at **120mHz** and **75%** duty cycle.

The best transfer function selected for TGS-2611 was:

$$\hat{H}(z)_{40mHz} = \frac{(1.7\times10^{-7})}{(z-0.996)}$$

Table 4.5. Transfer function model parameters of the MOS gas sensors (TGS-2611 and TGS-842) for different frequencies and duty cycles (The most stable model parameters are shown in bold):

Sensors	Frequency (mHz)	Duty Cycle (%)	Percentage of overshoot (%)	Position of pole from center	Stability	Best transfer function
TGS-2611	**10**	50	58.3	0.999	Stable	$\bar{H}(z)_{40mHz} = \frac{(1.7\times10^{-7})}{(z-0.996)}$
	40		29.62	0.999	Stable	
	80		42.3	0.999	Stable	
	120		93.75	1	Unstable	
	10	75	36.66	1	Unstable	
	40		**26.6**	**0.996**	**Most Stable**	
	80		43.3	0.999	Stable	
	120		80	1.007	Unstable	
TGS-842	**10**	50	46.2	1,1	Unstable	$\bar{H}(z)_{120mHz} = \frac{(4.248\times10^{-7})(z-0.9639)}{(z-0.9995)(z-0.9992)}$
	40		81.5	1.001,1	Unstable	
	80		53.3	1.005,0.9995	Unstable	
	120		33.3	0.9995,0.9996	Stable	
	10	75	86.9	1.002,1.006	Unstable	
	40		52.17	1.005,1.0006	Unstable	
	80		35	0.9995,0.9997	Stable	
	120		**19.04**	**0.9992,0.9995**	**Most Stable**	

And that for TGS-842 was:

$$\hat{H}(z)_{120mHz} = \frac{(4.248\times10^{-7})(z-0.9639)}{(z-0.9995)(z-0.9992)}$$

After determining the best frequency and duty cycle, the best fit transfer function was selected by the simulation of the transfer function for both the ranges of frequencies and duty cycles.

The objectives for developing a technique for selection of heater pulse frequency and duty cycle based on stability criterion and system identification is achieved in this research. As stated earlier for chapter 2 we have found that the best pulse frequency and duty cycle for the three sensors are 10mHz, 75% duty cycle, which is based on noise analysis however, the stability analysis shows that this value is 40mHz, 75% duty cycle (TGS-2611) and 120mHz, 75% duty cycle (TGS-842) for upper frequency range and for lower frequency range the stability was found at 1mHz, 50% duty cycle (TGS-822) and 2mHz, 50% duty cycle (TGS-2611). Therefore selection of best operating frequency of heater pulse voltage is a trade-off between requirement of noise behavior and stability of the MOS gas sensor responses.

4.5 Transfer Function Selection

In this part of the analysis, the transfer functions shown in Table 4.2 and Table 4.3 were simulated for selection of the most stable transfer function. For simulation we have used the input data as shown in Table 4.1.

4.5.1 Best Fit Analysis:

In section 4.4 the most stable transfer functions were determined using percentage overshoot and pole-zero plot analysis. In addition to these tests, another test has been conducted by simulating the estimated models with a portion of the measured input and comparing the model responses ($\hat{y}$) with the measured responses (y).

The simulation results for different frequencies and duty cycles for lower frequency range of frequency are shown in Fig.4.12 and 4.13 for TGS-2611 and TGS-822 respectively.

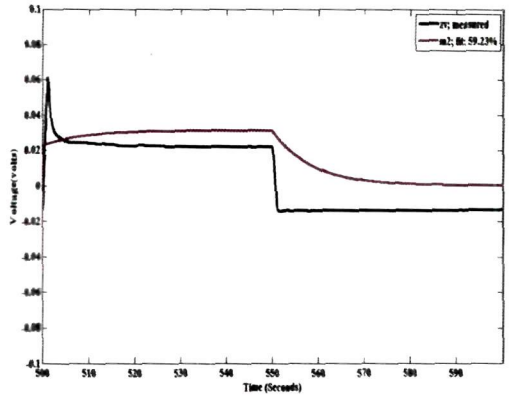
zv; measured
m2; fit: 59.23%
Voltage(volts)
Time (Seconds)

(a)

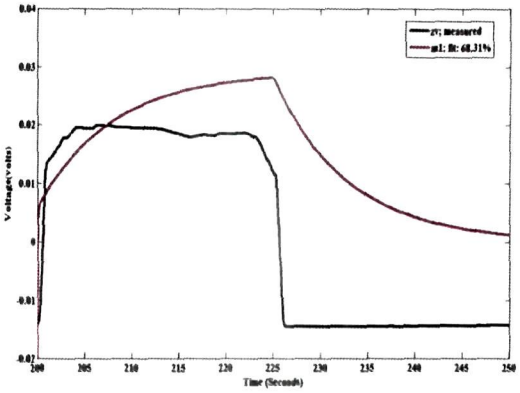
zv; measured
m1; fit: 68.31%
Voltage(volts)
Time (Seconds)

(b)

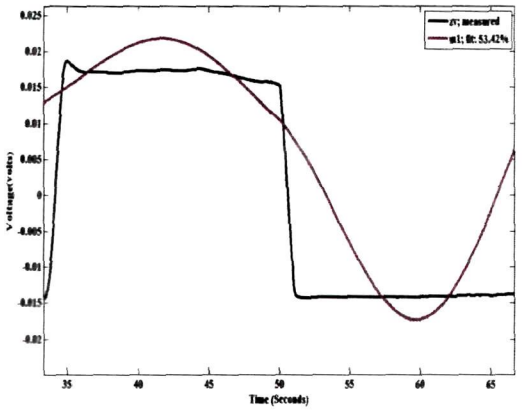
zv; measured
m1; fit: 53.42%
Voltage(volts)
Time (Seconds)

(c)

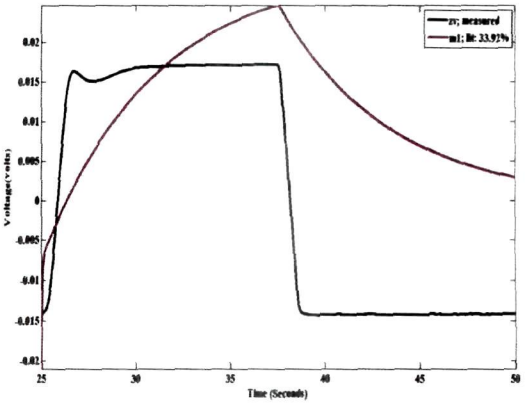
zv; measured
m1; fit: 33.93%
Voltage(volts)
Time (Seconds)

(d)

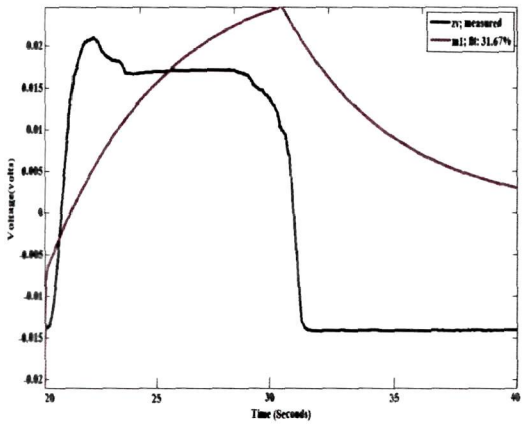
zv; measured
m1; fit: 31.67%
Voltage(volts)
Time (Seconds)

(e)

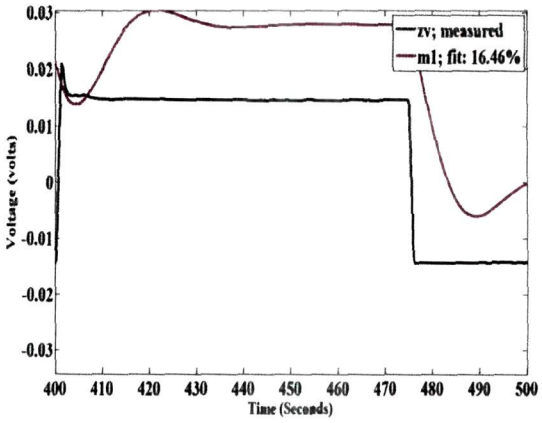
zv; measured
m1; fit: 16.46%
Voltage (volts)
Time (Seconds)

(f)

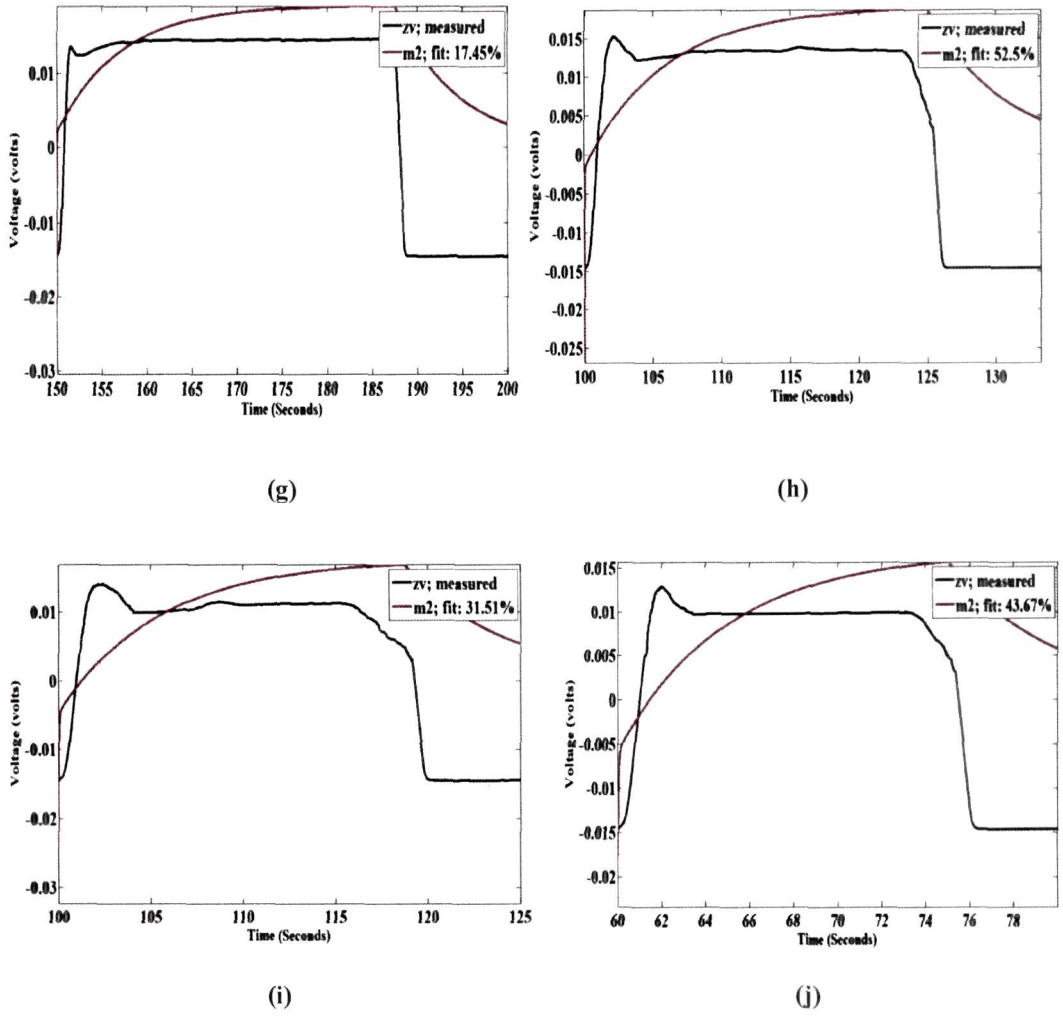

Fig. 4.12. Sensor responses measured and simulated for TGS-2611 at (a) 1mHz and 50% duty cycle, (b) 2mHz and 50% duty cycle, (c) 3mHz and 50% duty cycle, (d) 4mHz and 50% duty cycle, (e) 5mHz and 50% duty cycle, (f) 1mHz and 75% duty cycle, (g) 2mHz and 75% duty cycle, (h) 3mHz and 75% duty cycle, (i) 4mHz and 75% duty cycle, and (j) 5mHz and 75% duty cycle.

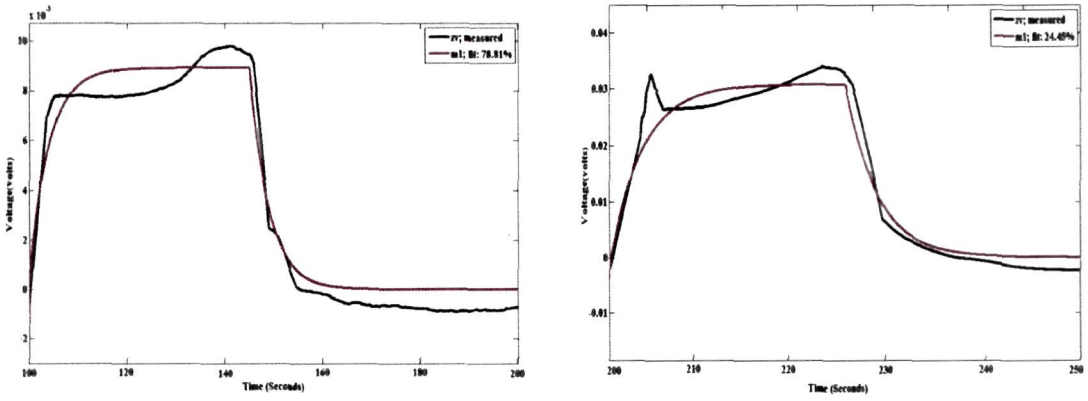

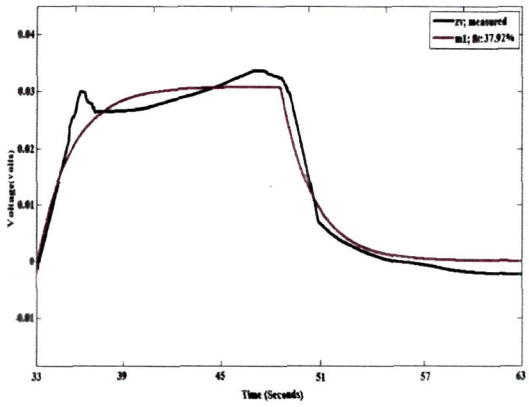
zv; measured
m1; fit:37.92%
Voltage(volts)
Time (Seconds)

(c)

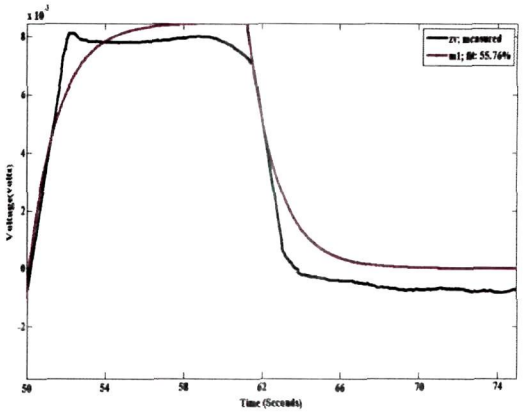
x 10^-3
zv; measured
m1; fit: 55.76%
Voltage(volts)
Time (Seconds)

(d)

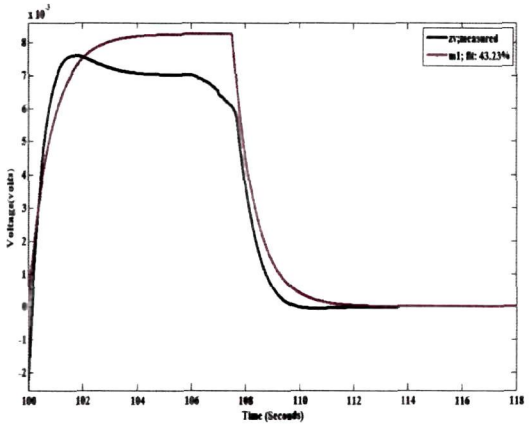
x 10^-3
zv;measured
m1; fit: 43.23%
Voltage(volts)
Time (Seconds)

(e)

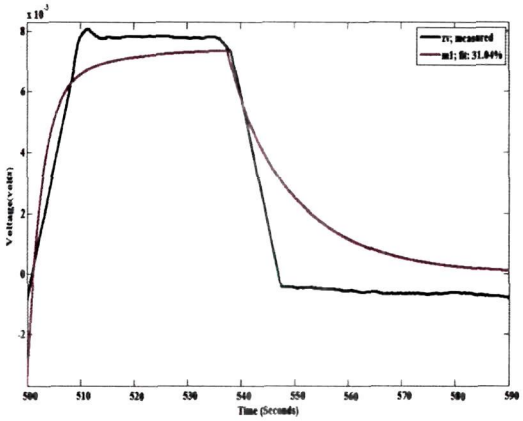
x 10^-3
zv; measured
m1; fit: 31.04%
Voltage(volts)
Time (Seconds)

(f)

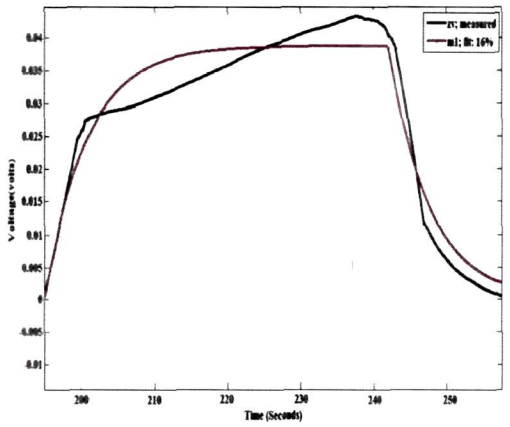
zv; measured
m1; fit: 16%
Voltage(volts)
Time (Seconds)

(g)

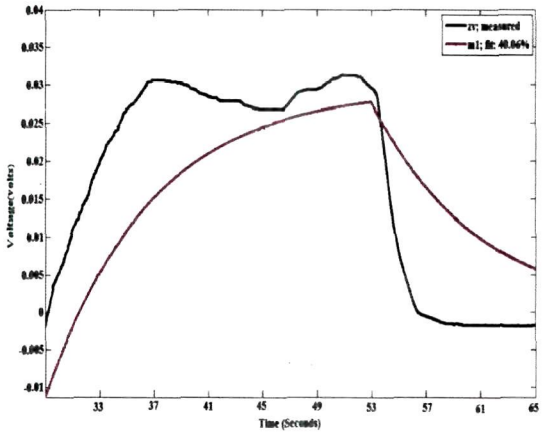
zv; measured
m1; fit: 40.06%
Voltage(volts)
Time (Seconds)

(h)

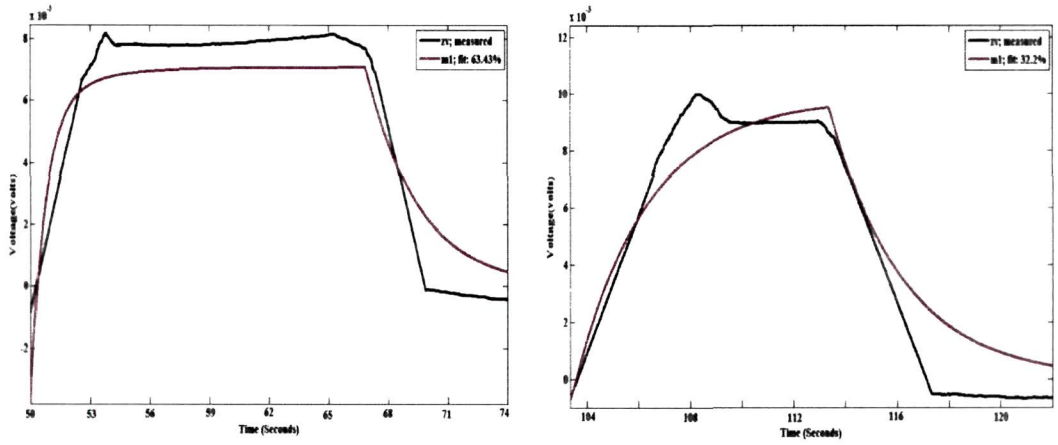

(i) (j)

Fig. 4.13. Sensor responses measured and simulated for TGS-822 at (a) 1mHz and 50% duty cycle, (b) 2mHz and 50% duty cycle, (c) 3mHz and 50% duty cycle, (d) 4mHz and 50% duty cycle, (e) 5mHz and 50% duty cycle, (f) 1mHz and 75% duty cycle, (g) 2mHz and 75% duty cycle, (h) 3mHz and 75% duty cycle, (i) 4mHz and 75% duty cycle and (j) 5mHz and 75% duty cycle.

The simulated and the measured results for sensor TGS-2611 and TGS-842 are shown in Fig.4.12 (a)-(j) and Fig.4.13 (a)-(j) respectively. The percentage of fit from the simulated results is tabulated in Table 4.6 and the best fit is computed for both the sensors. Fig. 4.12(b) and Fig. 4.13 (a) shows the best fit results the values for TGS-2611 and TGS-822 respectively which are shown in bold in Table 4.6.

Table 4.6: Table showing the percentage of best fit for low range of frequency:

Sensors	Frequency (mHz)	Duty Cycle (%)	Percentage of best fit (%)
TGS- 2611	1	50	59.23
	2		**68.31**
	3		53.42
	4		33.92
	5		31.67
	1	75	16.46
	2		17.45
	3		52.5
	4		31.51
	5		43.67
	1		**78.81**
	2		24.45

TGS-822	3	**50**	37.926
	4		55.76
	5		43.23
	1	75	31.04
	2		46
	3		40.06
	4		63.43
	5		32.2

From Table 4.6 it is evident that the fit percentage for TGS-2611 is best at **2mHz** frequency and **50%** duty cycle which is **68.31%**. Similarly, for TGS-822, the fit percentage is best at **1mHz** and **50%** duty cycle which is **78.81%**. Thus it is seen that the frequency and duty cycle at which the transfer function is most stable yields the best fit percentage. Using the respective best selected frequency and duty cycle for both the sensors the classifications of different gases have been performed as discussed in *Section 4.6*.

Similarly, for the upper frequency range of 10mHz, 40mHz, 80mHz and 120mHz and duty cycles of 50% and 75% the transfer functions were simulated to determine the best fit percentage. The simulation results for different frequencies and duty cycles for this range of frequency are shown in Fig.4.14 and 4.15 for TGS-2611 and TGS-842 respectively.

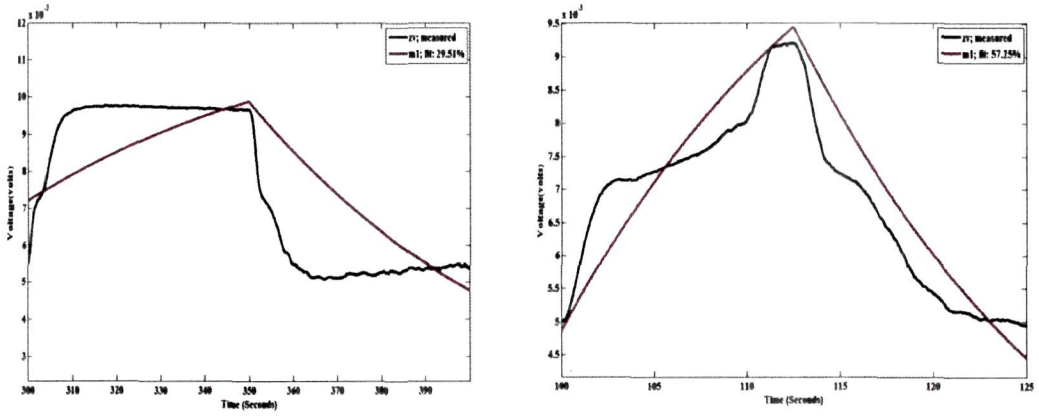

(a) **(b)**

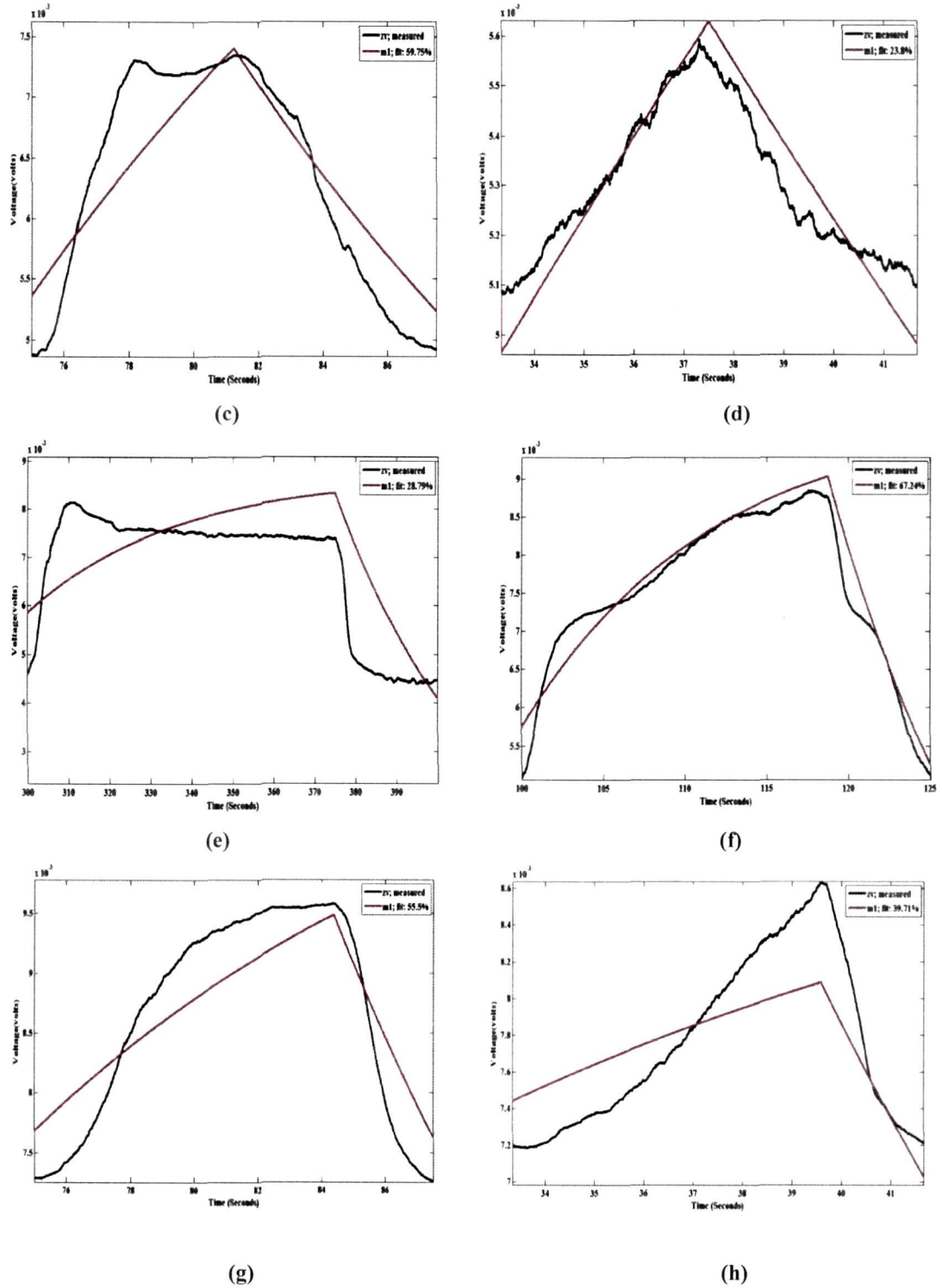

Fig. 4.14. Sensor responses measured and simulated for TGS-2611 at (a) 10mHz and 50% duty cycle, (b) 40mHz and 50% duty cycle, (c) 80mHz and 50% duty cycle, (d) 120mHz and 50% duty cycle, (e) 10mHz and 75% duty cycle, (f) 40mHz and 75% duty cycle, (g) 80mHz and 75% duty cycle, and (h) 120mHz and 75% duty cycle.

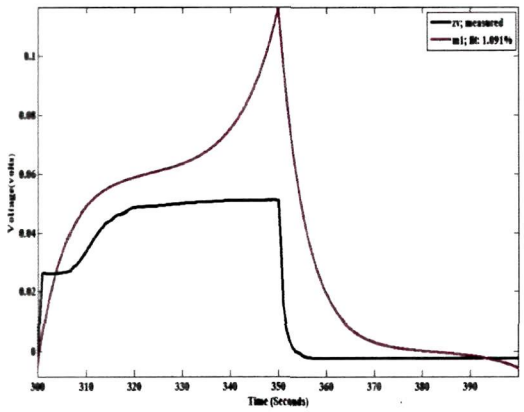
zv; measured
m1; fit: 1.091%
Voltage(volts)
Time (Seconds)

(a)

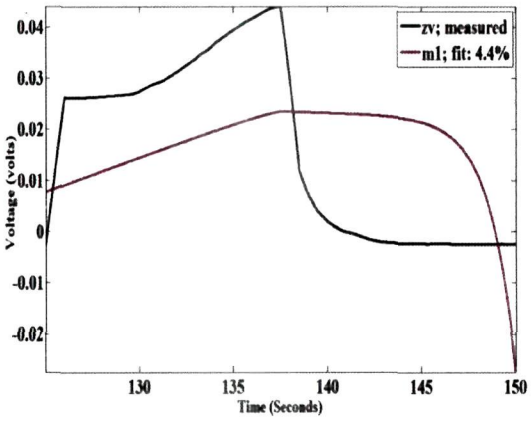
zv; measured
m1; fit: 4.4%
Voltage (volts)
Time (Seconds)

(b)

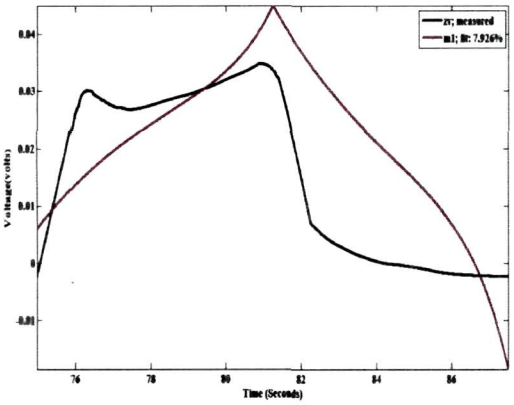
zv; measured
m1; fit: 7.926%
Voltage(volts)
Time (Seconds)

(c)

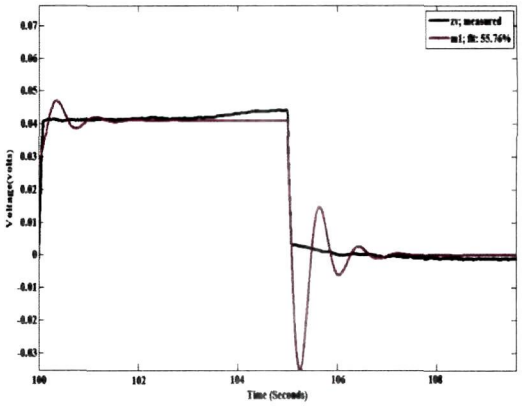
zv; measured
m1; fit: 55.76%
Voltage(volts)
Time (Seconds)

(d)

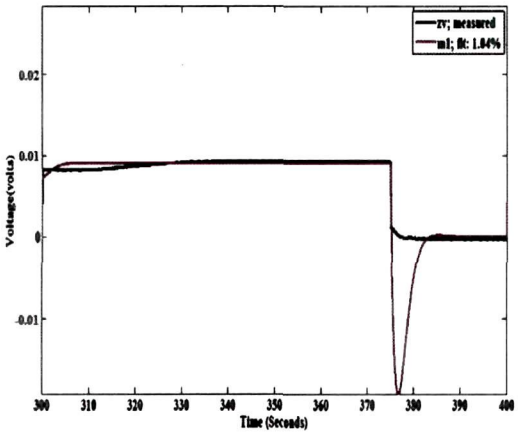
zv; measured
m1; fit: 1.84%
Voltage(volts)
Time (Seconds)

(e)

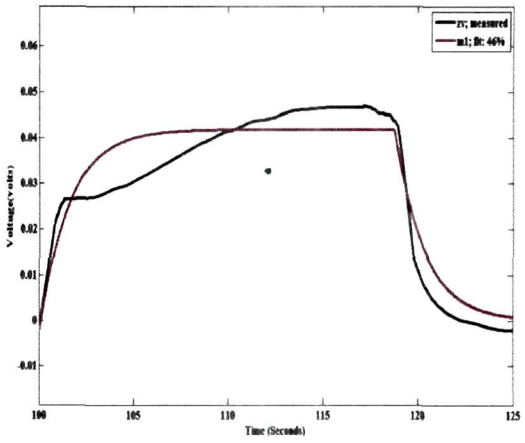
zv; measured
m1; fit: 46%
Voltage(volts)
Time (Seconds)

(f)

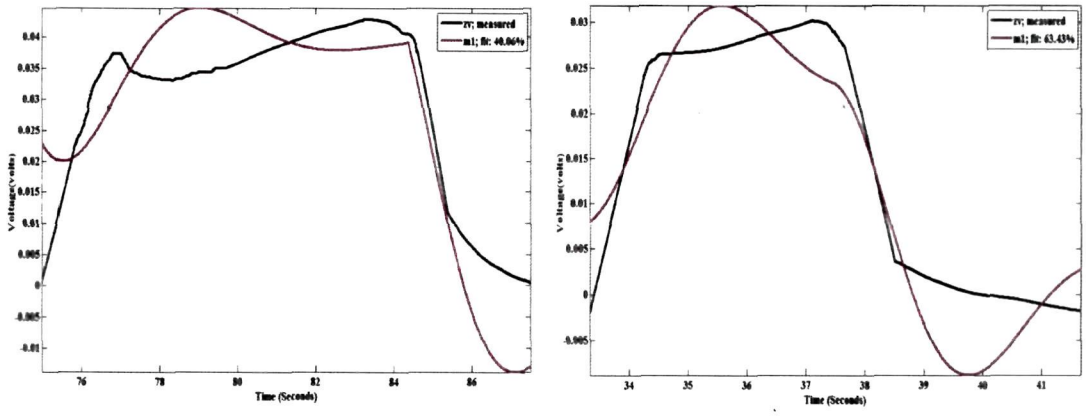

(g) (h)

Fig. 4.15. Sensor responses measured and simulated for TGS-842 at (a) 10mHz and 50% duty cycle, (b) 40mHz and 50% duty cycle, (c) 80mHz and 50% duty cycle, (d) 120mHz and 50% duty cycle, (e) 10mHz and 75% duty cycle, (f) 40mHz and 75% duty cycle, (g) 80mHz and 75% duty cycle, and (h) 120mHz and 75% duty cycle.

The simulated and the measured results for sensor TGS-2611 and TGS-842 are shown in Fig.4.14 (a)-(h) and Fig.4.15 (a)-(h) respectively. The percentage of fit from the simulated results is tabulated in Table 4.7 and the best fit is computed for both the sensors. Fig. 4.14(f) and Fig. 4.15(h) shows the best fit results which are shown in bold in Table 4.7.

Table 4.7: Table showing the percentage of best fit for upper range of frequency:

Sensors	Frequency (mHz)	Duty Cycle (%)	Percentage of best fit (%)	Best transfer function
TGS-2611	10	50	29.51	$\bar{H}(z)_{40mHz} = \frac{(1.7\times10^{-7})}{(z-0.996)}$
	40		57.25	
	80		59.75	
	120		23.8	
	10	75	28.79	
	40		**67.24**	
	80		55.5	
	120		39.71	

TGS-842	10	50	1.01	$H(z)_{120mHz} = \frac{(4.248\times10^{-7})(z-0.963}{(z-0.9995)(z-0.9992}$
	40		4.4	
	80		7.926	
	120		55.76	
	10	75	1.04	
	40		46	
	80		40.06	
	120		**63.43**	

It is seen that the frequencies and duty cycles at which the transfer function was most stable for TGS-2611 and TGS-842 is obtained at **40mHz** and **75%** and at **120mHz** and **75%** respectively. The fit percentage for MOS gas sensor TGS-2611 is also observed to be best at **40mHz** frequency and **75%** duty cycle which is **67.24%**. Similarly, for MOS gas sensor TGS-842, the fit percentage is highest at **120mHz** and **75%** duty cycle which is **63.43%**. The results of the preceding sections (*4.4* and *4.5*) corresponds to stability analysis of the MOS gas sensors during its signal inactive period i.e. without applying any gas, however the adsorption kinetics takes place with atmospheric oxygen. The chemisorption of O_2 at the sensor surface results in the removal of electrons from the conduction band. The model will behave in a similar manner with reference to stability for reducing and oxidizing gases. Therefore, the classification percentage has been analyzed for ten gas vapors using the most stable transfer function operated at the specified pulse frequency and duty cycle.

The experiment was followed by the gas classification and on the achieving of better classification percentage of the sample gases with the most suitable temperature modulation for both ranges of frequencies. The time constant of sensor response has been used as a feature of ANN classifier as discussed in *Section 2.6* of **Chapter 2**. The results of the experiment before and after the selection were compared.

4.6 Improvement of Classification

In this part of experiment the dynamic analysis was conducted for different pulse modulating temperature with the application of ten different gas samples namely acetone, acetonitrile, chloroform, ethanol, ethyl acetate, isopropylalcohol, kerosene,

methanol, n-hexane and petroleumether. The frequency and duty cycle of the sensors were controlled by a PC through the DAQ card and LabVIEW as discussed in **Chapter 2**, *Section 2.2.1.4*, Fig.2.8.

In this section, the classification enhancement by selecting the suitable frequency of heater pulse voltage and using time-constant as a feature has been discussed. At first, the sensor temperature was pulsed arbitrarily at a frequency of 10mHz and duty cycle of 50% to generate the sensor responses in the presence of the gas. The sensor signals were acquired at a sampling frequency of 1 kHz. The time constants were determined for each cycle which was used as the sample vectors for the gas classification. Next, the sensor temperature was pulsed at the selected frequencies and duty cycles to generate the sensor responses.

The sizes of the data matrices used for ANN classification are:

Lower Frequency Range:

Arbitrary frequency (5mHz & 50% duty cycle):

m×**n**×**N** = 2×10×200

Best frequency (2mHz & 50% duty cycle for TGS-2611):

m×**n**×**N** = 1×10×100

Best frequency (1mHz & 50% duty cycle for TGS-822):

m×**n**×**N** = 1×10×100

Upper Frequency Range:

Arbitrary frequency (10mHz & 50% duty cycle):

m×**n**×**N** = 2×10×200

Best frequency (40mHz & 75% duty cycle for TGS-2611):

m×**n**×**N** = 1×10×100

Best frequency (120mHz & 75% duty cycle for TGS-842):

m×**n**×**N** = 1×10×100

where, **m** = No. of sensors; **n**= No. of gases; **N**= no. of data cycles.

Once the most stable transfer functions and their corresponding best values of pulse frequency and duty cycle are obtained, the PCA was worked out with two pairs of

sensors: TGS-822/TGS-2611 and TGS-842/TGS-2611 for ten different gas samples.

4.6.1 Classification Enhancement (Lower Frequency Range):

Before Selection- The data obtained from the two sensors for the 10 sample gases were analyzed by PCA and ANN using MATLAB. The results of the PCA before the selection of modulation are shown in Fig. 4.16. The first three principal components were considered for analysis because they accounted for 92.1749% of the variance in the data set. The variance and load values for each of 3 principal components (Fig. 4.16) are shown in Table 4.8.

Table 4.8. The results of PCA for the time constants before selection of frequency and duty cycle.

PC	% Variance	Eigen Values	Principal Components		
			$Sensor_1$	$Sensor_2$	$Sensor_3$
PC_1	92.1749	0.2156	0.9245	0.2722	-0.2311
PC_2	5.3328	0.1821	-0.1367	0.7631	-0.3182
PC_3	2.1323	0.0823	-0.0572	-0.1893	0.6322

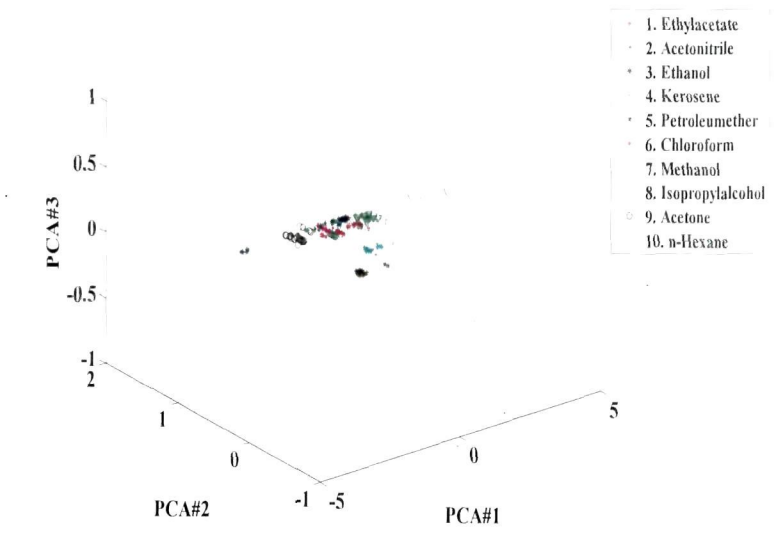

Fig. 4.16. PCA with frequency 5mHz and 50% duty cycle for TGS-2611 and TGS-822.

After Selection- The first three principal components were considered for analysis after selection of frequency and duty cycle because they accounted for 95.4216% of the variance in the data set. The variance and load values for each of 3 principal components (Fig. 4.17) are shown in Table 4.9.

Table 4.9. The results of PCA for the time constants after selection of frequency and duty cycle.

PC	% Variance	Eigen Values	Principal Components		
			$Sensor_1$	$Sensor_2$	$Sensor_3$
PC_1	95.4216	0.1856	-0.1036	-0.5213	-0.1334
PC_2	2.1084	0.0637	0.0112	-0.3212	0.2765
PC_3	1.7644	0.0188	-0.7650	0.1254	-0.0178

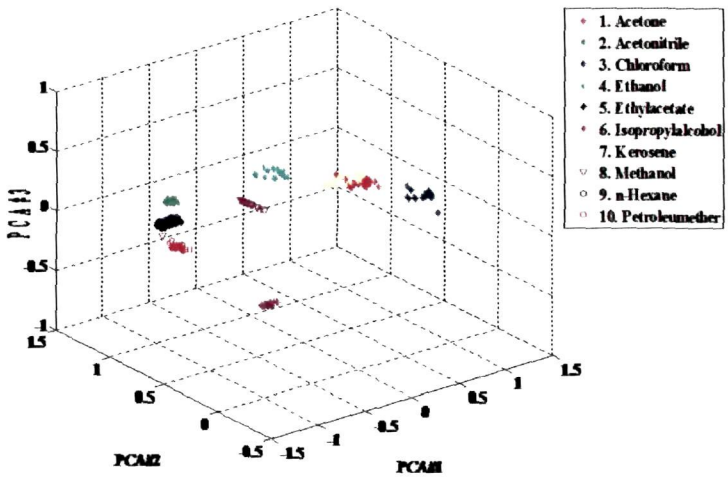

Fig. 4.17. PCA with frequency 2mHz & 50% duty cycle for TGS-2611 and 1mHz & 50% duty cycle for TGS-822.

The classification of data performed using MLP and RBF were used for the classification purpose. Training of the neural networks was performed with 50% of the whole data set and the rest 50% of the data sets were used for testing the neural network paradigms. A total of 30 data sets of dimensions (1×100) for each of the sensors were formed, thus 15 data sets were used for training and remaining 15 data sets were used to test the performance of the ANN paradigm. The architecture of the two ANNs used in this experiment is tabulated in Table 4.10.

Table 4.10 Architecture of the two ANN paradigms (MLP and RBF):

Neural Networks	Architecture
Multi-layer Perceptron (MLP)	2 input neurons, 6 hidden neurons, 10 output neurons, 0.5 adaptive learning rate with momentum 0.42 (one for each sample type).
Radial Basis Function(RBF)	2 input neurons, 10 neurons in the output layer, spread constant 0.8.

a) Multi Layer Perceptron (MLP):

An MLP network was programmed in MATLAB environment with 2 input neurons, from the two sensors, 6 hidden neurons and 10 output neurons chosen for the ten sample gases. The activation function for the neurons in the hidden layers employed is the '*logsig*' function and for the input and output neurons the activation function is also the '*logsig*' function. The weights were trained with the back propagation algorithm. The network was able to reach a classification rate of 74.6% before the selection of frequency and duty cycle i.e. at 5mHz and 50% duty cycle. The system identification determined the most stable transfer function based on the best fit, the overshoot percentage and the pole-zero plot of the transfer function. After the selection of frequency and duty cycle i.e. at 2mHz & 50% duty cycle for TGS-2611 and 1mHz & 50% duty cycle for TGS-822, the network achieved the classification percentage of 91.5%.

b) Radial Basis Function (RBF):

RBF adopts the supervised learning method with architecture of 2 input neurons, 10 neurons in the output layer and spread constant 0.8 as given in Table 4.10. The neurons are added to the network until the sum-squared error (SSE) reduced to a specified error goal which was set as 10×10^{-5}. The network was able to reach a classification rate of 87% before the selection of frequency and duty cycle. After the selection of frequency and duty cycle the network performed the classification of 94.1% was obtained. The training was completed in 130 epochs with a training time of approximately 32 minutes,

hence showing better performance and less training time than MLP. The training performances of MLP and RBF used in the experiments are shown in Table 4.11.

Table 4.11 Training performance of Artificial Neural Network paradigms:

Neural Networks	Training time
Multi-layer Perceptron (MLP)	118mins
Radial Basis Function(RBF)	32 minutes

The comparison of the classification percentage before and after the best modulation frequency determination is tabulated in Table 4.15. Similar classification was also performed and tested for the upper range of frequencies and duty cycles.

4.6.2 Classification Enhancement (Upper Frequency Range):

Before Selection- The data was analyzed in a similar way as described in the earlier section. The results of the PCA before the selection of modulation are shown in Fig. 4.18. The first three principal components were considered for analysis because they accounted for 93.7735% of the variance in the data set. The variance and load values for each of 3 principal components (Fig. 4.18) are shown in Table 4.12.

Table 4.12. The results of PCA for the time constants before selection of frequency and duty cycle.

PC	% Variance	Eigen Values	Principal Components		
			$Sensor_1$	$Sensor_2$	$Sensor_3$
PC_1	93.7735	0.3271	0.8266	0.2163	0.0121
PC_2	3.8586	0.1152	-0.0865	-0.7373	-0.5328
PC_3	2.1679	0.0528	-0.0943	-0.1104	0.6552

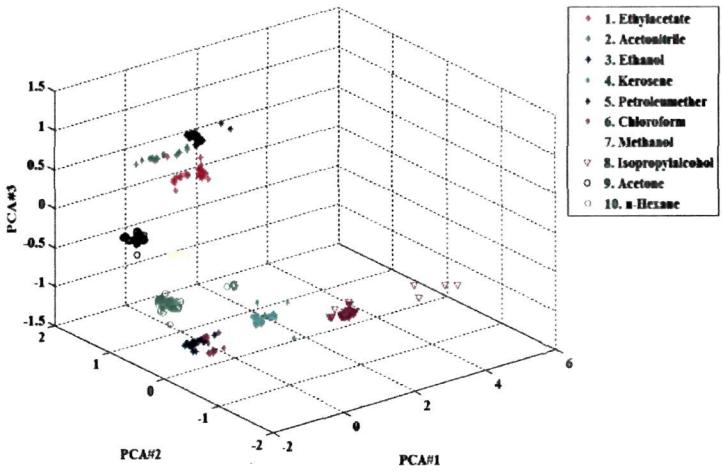

Fig. 4.18. PCA with frequency 10mHz and 50% duty cycle for TGS-2611 and TGS-842.

After Selection- The first three principal components were considered for analysis after selection of frequency and duty cycle because they accounted for 96.8477% of the variance in the data set. The variance and load values for each of 3 principal components (Fig. 4.19) are shown in Table 4.13.

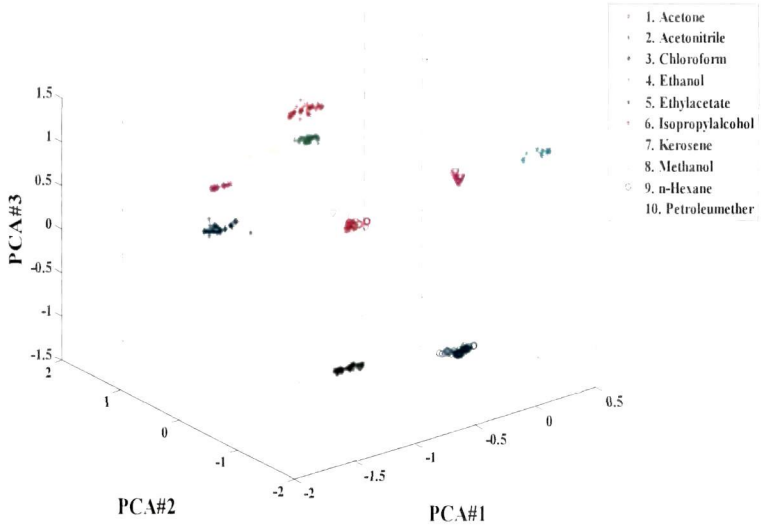

Fig. 4.19. PCA with frequency 40mHz & 75% duty cycle for TGS-2611 and 120mHz & 75% duty cycle for TGS-842.

Table 4.13. The results of PCA for the time constants after selection of frequency and duty cycle.

PC	% Variance	Eigen Values	Principal Components		
			$Sensor_1$	$Sensor_2$	$Sensor_3$
PC_1	96.8477	0.3422	-0.0988	-0.7551	-0.2512
PC_2	2.2525	0.1477	0.2312	-0.5122	0.1983
PC_3	0.0668	0.0821	-0.8631	0.0952	-0.1523

The architecture of the two ANNs (MLP and RBF) used in this experiment is tabulated in Table 4.11.

a) Multi Layer Perceptron (MLP):

The network was able to reach a classification rate of 76.2% before the selection of frequency and duty cycle i.e. at 10mHz and 50% duty cycle. The system identification determined the most stable transfer function based on the best fit, the overshoot percentage and the pole-zero plot of the transfer function. After the selection of frequency and duty cycle i.e. at 40mHz & 75% duty cycle for TGS-2611 and 120mHz & 75% duty cycle for TGS-842, the network achieved the classification percentage of 86.7% was obtained.

b) Radial Basis Function (RBF):

The network was able to reach a classification rate of 88.5% before the selection of frequency and duty cycle. After the selection of frequency and duty cycle the network performed the classification of 93.4% was obtained. The training was completed in 142 epochs with a training time of approximately 38 minutes, hence showing better performance and less training time than MLP. The training performances of MLP and RBF used in the experiments are shown in Table 4.14.

Table 4.15 shows the PCA results and the classification percentage for both (lower frequency and upper frequency) range.

Table 4.14 Training performance of Artificial Neural Network paradigms:

Neural Networks	Training time (min)
Multi-layer Perceptron (MLP)	139
Radial Basis Function(RBF)	38

Table 4.15. PCA results and comparison of the classification percentage for both (lower frequency and upper frequency) range:

Operating conditions		PCA results (%)	ANN Classifier	
			MLP	RBF
Arbitrary frequency (Lower Range)	5mHz, 50% duty cycle (for TGS-2611 and TGS 822)	92.1749	74.6%	87%
Selected Frequency (Lower Range)	2mHz, 50% duty cycle (for TGS-2611) 1mHz and 50% duty cycle (for TGS-822)	95.4216	91.5%	94.1%
Arbitrary frequency (Upper Range)	10mHz, 50% duty cycle (for TGS-2611 and TGS 842)	93.7735	76.2%	88.5%
Selected Frequency (Upper Range)	40mHz, 75% duty cycle (for TGS-2611) 120mHz and 75% duty cycle (for TGS-842)	96.8477	86.7%	93.4%

Thus we find that the classification performed using the best set of frequencies and duty cycle gives better classification results in both the cases. It is seen that the system identification technique could effectively find the best modulation frequencies to obtain good results in the identification of the gases studied. The selection ensured the classification enhancement by a maximum of 91.5% for MLP and 94.1% for RBF.

4.7 Conclusions

In this work a study aimed at the selection of most suitable frequencies and duty cycles based on system identification technique is presented. The method is applied to study

the stability of MOS gas sensors and the transfer function determination based on the pole-zero plots and the overshoot percentage. The sensor temperature was pulsed at two ranges of frequencies: *lower frequency* range of 1mHz, 2mHz, 3mHz, 4mHz and 5mHz and duty cycles of 50% and 75% and *upper frequency* range of 10mHz, 40mHz, 80mHz and 120mHz and duty cycles of 50% and 75%, to generate the sensor responses. The transfer functions obtained thus are proposed to work best with the specified frequency and duty cycle. The classification was done for comparison with the arbitrarily chosen frequency and duty cycle operated transfer functions. The classification has been performed by using time constant of response curve of the dynamic classification.

Once the most stable transfer functions and their corresponding best values of pulse frequency and duty cycle are obtained, the PCA was worked out with two pairs of sensors: TGS-822/TGS-2611 and TGS-842/TGS-2611 for ten different gas samples. The PCA accounted for higher percentage when sensors are operated by the best heater pulse frequency compared to arbitrary chosen frequency and duty cycle. Further, using these best suited frequencies and duty cycle for both the ranges of frequencies, the classification of different gases is performed using two ANN classifiers – MLP and RBF. The ANN classifier also better classification efficiency when the best frequency is used.

The objectives for developing a technique for selection of heater pulse frequency and duty cycle based on stability criterion and system identification is achieved in this research. As stated earlier for **Chapter 2** we have found that the best pulse frequency and duty cycle for the three sensors are 10mHz, 75% duty cycle, which is based on noise analysis however, the stability analysis shows that this value is 40mHz, 75% duty cycle (TGS-2611) and 120mHz, 75% duty cycle (TGS-842) for upper frequency range and for lower frequency range the stability was found at 1mHz, 50% duty cycle (TGS-822) and 2mHz, 50% duty cycle (TGS-2611). Therefore selection of best operating frequency of heater pulse voltage is a trade-off between requirement of noise behavior and stability of the MOS gas sensor responses.

The system identification technique could therefore effectively find the modulation frequencies to obtain good results in the identification of the gases studied.

4.8 Publications on this chapter

1. Dutta, N., & Bhuyan, M. Optimal Temperature Modulation of MOS Gas Sensors by System Identification, *Journal of Signal Processing, Image Processing and Pattern Recognition* **5** (2), 17-27, 2012.
2. Dutta, N., Dewan, S.K., & Bhuyan, M. System Identification of MOS Gas Sensors and Stability Analysis, *Sensors and Transducers* **143** (8), 127--135, 2012.
3. Dutta, N., & Bhuyan, M. System Identification of MOS Gas Sensors and Classification Enhancement through Optimal Temperature Modulation, in International Multi-conference on Intelligent Systems, Sustainable, New and Renewable Energy Technology and Nanotechnology'2012, Klawad, Haryana, India, 149-153.
4. Dutta, N., & Bhuyan, M. Classification Enhancement of MOS Gas Sensors by Optimized Temperature Modulation Using System Identification, *Association for the Advancement of Modelling and Simulation Techniques in Enterprises*. (In Press)

CHAPTER 5

Chapter 5

MODELING OF MOS GAS SENSORS

5.0 Introduction:

Metal oxide films are highly sensitive and are being used in solid-state gas sensors and electronic noses[205]. The adsorption of gas molecules on gas sensitive MOS films leads to a large change in its electrical resistivity. Different parametric models developed based on the transient responses help in the design of new devices and interpretation of new data[132, 206]. Moreover the dynamic responses have shown to provide information which shows the improvement of gas recognition[101, 132]. A mathematical model of the gas sensor system can be constructed either from the observed input-output data or from the physical model. To build mathematical models of dynamical systems from measured data, system identification techniques can be employed which includes the optimal design of experiments for generating efficiently informative data for fitting such models. The system identification approach helps to observe the gas sensor as a dynamic system and employ suitable methods to model its behavior under different conditions. MOS gas sensors change their electrical resistances upon oxidative reactions, or with adsorption of reducing gases. Several attempts were usually made to overcome selectivity of MOS gas sensors such as- by using chromatographic columns to separate components, by operating at different temperatures, by choosing different burning-in procedures, dopants, surface chemical modification etc[207-209]. Among the different approaches to overcome these drawbacks, modulating the temperature of gas sensors have been remarkably successful in many applications[120, 121,210, 211].

Research has been carried out on the modeling of the gas sensor response characteristics using a number of variables in an attempt to classify gases and to detect gas concentration[212-214]. SPICE models for the static and transient response of resistive gas

sensors have also been reported[215, 216]. Work has also been carried out on the modeling of gas sensor for detecting individual components of gas mixtures and for measuring the concentrations of the component gases, presenting a systematic study for the enhancement of all the parameters of a neural network, including the pre-processing techniques[217]. But the modeling of the gas sensor using measured input-output data has not been attended so far. The aim of this study is to simulate the sensor dynamics when the operating temperature of the sensors is modulated using by temperature pulses.

5.1 MOS gas Sensor Modeling: Necessity and benefits:

The model of a system describes the essential behavior of the system. Sensor modeling and simulation is required to support the development and verification of sensor system. A thick film MOS gas sensor operates on the principle of change in conductance due to the chemisorption of gas molecules on the sensor surface. Several experimental and theoretical analysis have been proposed earlier for understanding the sensing mechanisms of tin-oxide sensor[218, 219]. In another work, an empirical relationship between the sensitivity and concentration of gas was proposed[220]. A non-linear diffusion reaction model was proposed in[206, 221] for analyzing the change in conductivity. A microscopic model based on the electron theory of chemisorption of thin-film gas sensors was proposed in[222, 223]. In a recent work[224], a model of adsorption–desorption noise in MOS gas sensors was proposed. This model was based on the simplest adsorption isotherm which is derived from Langmuir's theory. This model was intended to be a first step towards an overall modeling of noise in metal oxide gas sensors. The development of a simple dynamic model for sensors helps in designing experiments, and also in deeply understanding the behavior of such sensors. In recent years, many studies have been carried out with the aim of understanding the surface reactions of MOS gas sensors, considering simple cases such as interaction with mixtures of oxygen (O_2), carbon monoxide (CO) and water vapor[199, 225-233]. Many works have discussed about about the development of some simplified models by different researchers[199, 229, 234]. It is therefore seen that the modeling of MOS gas sensors was successful in predicting the behavior of such sensors when the characteristics of the sensor electrodes are varied. The modeling of such sensors helps to describe its dynamic behavior in the presence of various gases. The modeling treats the entire system including the surface

reactions, adsorption-desorption processes occurring at the sensor surface presenting a complete description about the physical and chemical process of the sensor system.

In this work, modeling of the sensor dynamics is carried out based on the system measured input output data obtained by modulating the heater temperature. The response of the gas sensors to modulating temperature primarily depends on the analytical model which is based on the physical and chemical properties of the sensor material and the heater. Several numerical models describing the electric responses of the resistive metal-oxide gas sensors to temperature changes have been proposed[235-238]. How stable a gas response we get from a MOS gas sensor primarily depends on the temperature profile over the sensor surface that depends on the thermal conductivity model of the heater to the sensor surface. This model primarily concerns with the sensor under ambient air condition without application of any gas, which can be termed as a baseline model of the sensor. The baseline model is dominated by the heater construction and the heater to sensor surface thermal conductivity. Identifying a baseline model of the sensor can help simulating the sensor dynamics for different arbitrary temperature functions and frequencies. Choosing the best function and the best frequency to achieve a stable dynamics that follow the concentration of the analyte is an important optimization strategy of the gas sensor. In most of the works where modulating temperature has been adopted, the frequency of modulation is selected on trial and error method[19, 21-23, 27, 28, 115, 119-121, 193-195, 239-241]. We have chosen a set of best frequencies for the first time in MOS gas sensors based on system identification based sensor baseline modeling.

5.2 Model Dynamics of MOS gas sensor:

The MOS gas sensor model can be broadly divided into two stages, the heater model and the sensor model. The sensor model comprises of the chemical and physical law of adsorption and the conductance model. The sensing mechanism is divided into two parts: the chemical system, which changes due to its interaction with the sample gas, and the electrical system, which transduces the change in the chemical system into an electrical signal. In principle, these systems can be easily determined by fitting the model to a few simple experiments. The interaction of gas molecules with solid-state sensors takes place by absorption, adsorption or chemical reactions with thin or thick

films of the sensor material. The sensor device detects the physical and/or chemical changes incurred by these processes.

5.2.1 Heater temperature dynamics:

Metal oxides work on the principle that a change in some property of the material occurring due to the interaction with odour leads to a change in the resistance of the sensor. The mechanisms that lead to these resistance changes are different for each material type however, the structure and layout of conductivity sensors prepared using these materials are essentially the same. Figure 5.1 shows a schematic of a typical micro-hotplate type MOS gas sensor design.

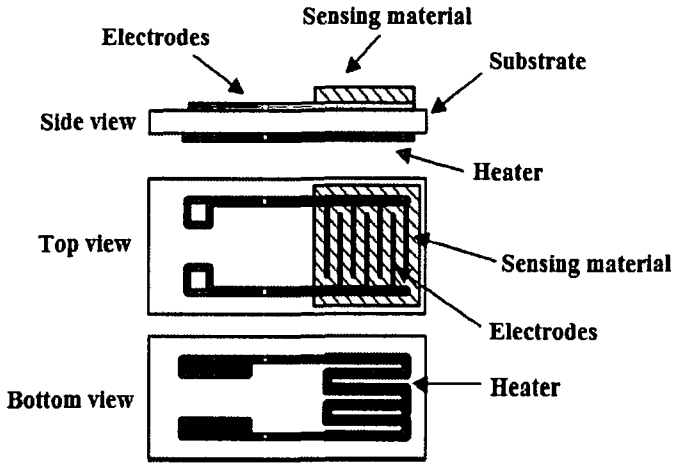

Figure 5.1: Typical schematic of a micro-hotplate type metal-oxide sensor.

A sensor element normally comprises the following parts:

a) *Sensitive layer*

b) *Substrate*

c) *Electrodes* and

d) *Heater*

The sensing layer is deposited over the substrate that is provided over the electrodes for the measurement of the electrical characteristics. The device is heated by its own heater which is separated from the sensing layer and the electrodes by an electrical insulating layer. The performance of the sensor depends on the measurement parameters, such as

sensitive layer polarization or temperature, which are controlled by using different electronic circuits. The elementary reaction steps of gas sensing will be transduced into electrical signals measured by suitable electrode structures. The sensing itself can take place at different sites of the structure depending on the morphology. As described earlier, the changes in composition of the ambient atmosphere will determine the changes in the resistance of the sensing layers. In general, the relationship between sensor resistance and concentration of the target gas usually follows a power law given by:

$$R \cong K.C^{\pm n} \tag{5.1}$$

where C is the concentration of the target gas, K is a measurement constant, and n has values between 0.3 and 0.8. The positive sign is used for oxidizing gases and the negative sign for reducing gases.

The metal-oxide film is kept at an elevated temperature (300 – 400 °C) in order to enhance reactions with gases. This temperature prerequisite is the basis of surface chemical reactions induced gas sensitivity and also the main reason for the consumption of power. The characteristic feature of the current state-of-art MOS gas sensors is that they are based on the micro hot plates fabricated using advanced silicon technology[230]. On the other hand, the conventional Taguchi gas sensor is always based on ceramic fabrication processes. Apparently, micro hot plate platform has several advantages over the conventional ceramic MOS gas sensors. They provide faster start-up, faster response, lower power consumption, and more accurate temperature control and thus provide more accurate detection and identification characteristics. However, one of the crucial issues that determine sensitivity and selectivity to gases in both sensor types is the sensor material.

The operating principle of the gas sensors is based on the change in the electrical conductivity of heated metal oxide layers as a function of the composition of the gases applied. The most common sensing layer is a porous thick film of polycrystalline SnO_2. In normal ambient air, oxygen and water vapor-related species are adsorbed at the surface of the SnO_2 layer. There are two types of MOS gas sensors; *n*-type (zinc oxide, tin dioxide, titanium dioxide or iron (III) oxide) which respond to reducing gases and *p*-

type (nickel oxide, cobalt oxide) which respond to oxidizing gases[231]. Under normal atmospheric conditions and typical working temperatures of 300–600°C *n*-type MOS gas sensors develop an electron-depleted surface layer. This electron depletion layer is caused by atmospheric oxygen that at high temperature adsorbs on the surface and grabs electrons from the MOS film surface to form reactive O^{-2} or O^{-} species. The gas reaction mechanism causes energetic bands in the grain boundaries which influence the conduction property of sensitive layers. The interaction of the sensing material with gas molecules causes change in the conduction property of sensitive layers. Reducing gases like CO and H_2 react with the highly sensitive MOS surface and remove some of the chemisorbed oxygen while infusing electrons back into the MOS, which causes a reduction in the thickness of the depletion layer thereby increasing the conductivity.

The *p*-type sensors respond to oxidizing gases like O_2, NO_2, and Cl_2 as these gases remove electrons and produce holes (charge carriers). The reaction that takes place with the pre-adsorbed oxygen and water vapor-related species decreases the resistance of the sensor. The magnitude of the changes depends on certain aspects such as: the microstructure and composition/doping of the base material, on the morphology and geometrical characteristics of the sensing layer and substrate, as well as on the temperature at which the sensing takes place. Any change in these parameters allow for the alteration of the sensitivity towards different gases or classes of gases as shown in Fig.5.2. The equations (5.2) and (5.3) describe the surface reactions:

$$\frac{1}{2}O_2 + e^{-} \rightarrow O^{-}(s) \tag{5.2}$$

$$R(g) + O^{-}(s) \rightarrow RO(g) + e \tag{5.3}$$

In our experiment of modeling of the MOS gas sensor, the sensor temperature is modulated during the dynamic measurement and the complicated response transients are considered to be related to different reaction kinetics of the gas molecules. The temperature modulation does not cause any equilibrium among the surface oxygen species and hence reactions between reducing and oxidizing gases are drastically influenced. Recently different dynamic models have been formulated where the gas molecules diffuse into the sensing film and adsorbed at fixed sites throughout the metal

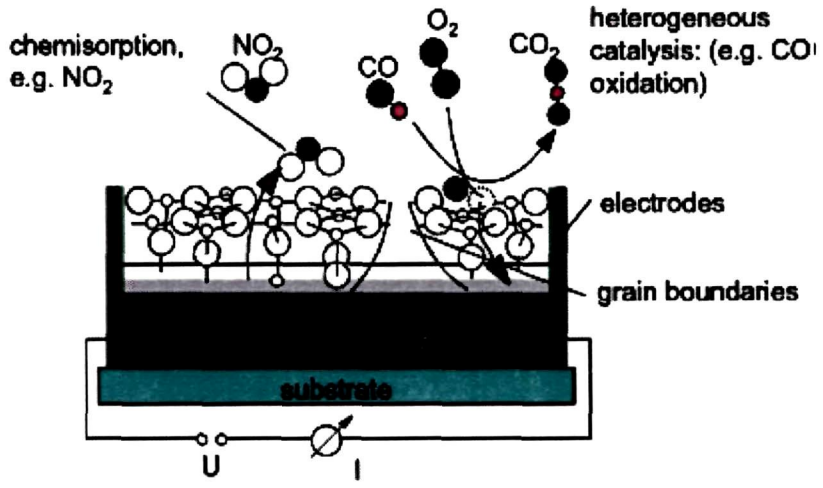

Fig.5.2: Schematic of a MOS gas sensor illustrating the resistance change of the sensing layer when molecules react on the surface. (Courtesy: Thesis on An Artificial Neural Network Based Electronic-Nose System: Tea and Spice Flavour Discrimination and Drift Parameter Determination by K.R.Kashwan, Tezpur University, India)

oxide film simultaneously[132, 206]. The transient behavior of gas sensors in response to abrupt changes in the gaseous concentration have been studied and modeled in previous works[132-135]. The dynamic response of the sensors is influenced by the operating temperature especially when the temperature is modulated. The sensor temperature modulations help in gas reactions in different regions of heating. In most of our experiments it is seen that the sensor response to heater pulse is characteristic of a first or second order system like in[202].

On application of a heater pulse, without applying any stimulant gas the sensor produces a transient response (step like) which was observed in our experiments. Therefore, it can be perceived that the sensor adsorption to conductance variation model is also a lower order (first order or second-order) one. This gives us a total model order of two for the MOS gas sensor. Fig. 5.3 (a) and (b) shows a typical transient response for the sensor TGS-2611 and TGS-842 in the presence of dry air.

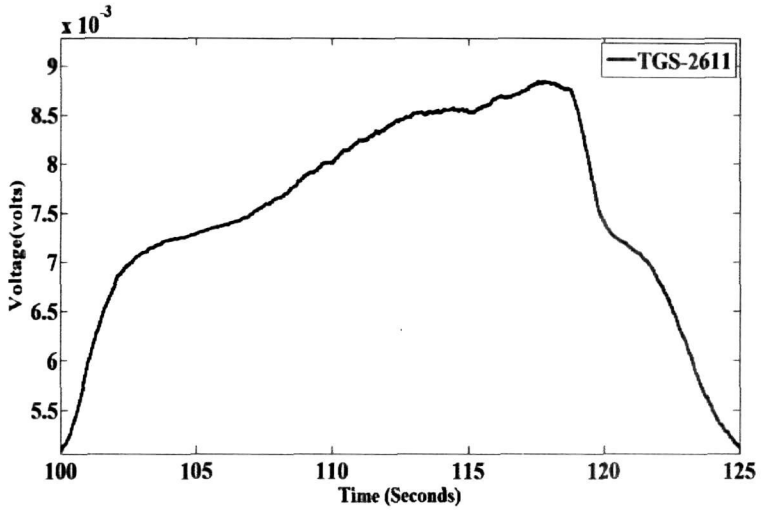

(a)

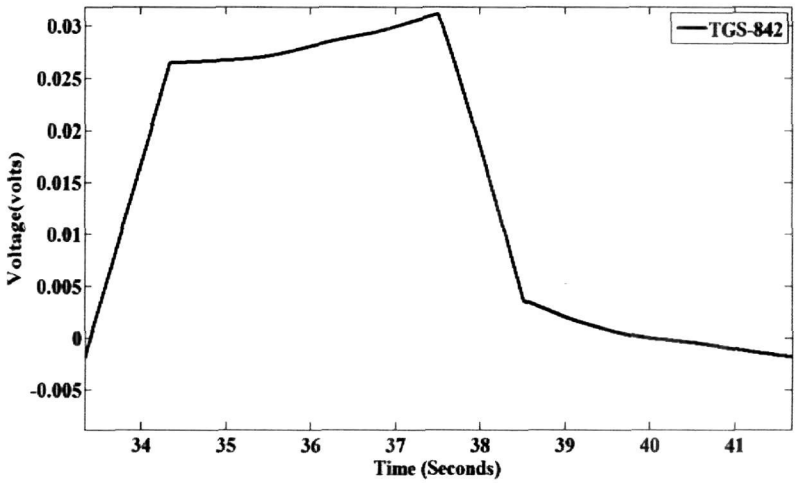

(b)

Fig.5.3. Typical transient responses of sensor (a) TGS-2611 at 40mHz and 75% duty cycle and (b) TGS-842 at 120mHz and 75% duty cycle.

5.3 Theoritical Modeling:

Research on the behavior of analytical models has suggested that the static responses i.e. conductance G_s of the sensor devices follow a simple, reversible, binding Freundlich isotherm[132, 242, 243] in the presence of gases given by-

$$G_s = G_0 + kC^r \tag{5.4}$$

where C is the maximum concentration of the gas pulses, G_0 is the baseline conductance, k is the sensitivity coefficient and r is the power law exponent for oxides. The dependence of G_0, k and r in eqn. (5.4) on the temperature [244, 245] is given by-

$$G_s = G_{0T} e^{-E_{A0}/KT} + (k_{1T} e^{-E_A/KT}) \times C^{nKT} \tag{5.5}$$

where, G_{0T} = pre-exponential factor (represents the bulk intra-grain conductance) (Ω^{-1}),

k = Sensitivity coefficient,

K= Boltzmann constant (electron-volt/Kelvin),

T= Temperature of the sensor (Kelvin),

E_{Ao}=Activation energy of the baseline conductance (eV),

E_A=Activation energy of the change in conductance caused by gas (eV).

C=Maximum concentration of the gas pulses (mol/m^3).

n=Pre-factor of the power law exponent for oxides.

Eqn. (5.5) is applicable to static temperature profile, however for dynamic temperature condition, the temperature has to be expressed in dynamic model. The heater pulse to baseline response of the sensor can be described by a first order model[202] where the response is exponential. We have experimentally verified that the heater temperature of the MOS gas sensors show an exponential response given by a first order model. The temperature of the heater was indirectly determined using the heater as a temperature sensor. The heater current was measured using the circuit shown in Fig. 5.4. From the current and the applied voltage the heater resistance R_h was calculated from which the change in heater temperature ΔT was determined given by eqn.-

$$\Delta T = \left(\frac{1}{\alpha}\right)\left(\left(\frac{R_h}{R_{h0}}\right) - 1\right) \tag{5.14}$$

where α is the positive resistance temperature co-efficient (PTC) of the platinum heater ($3500 \times 10^{-6} / {}^0C$); R_h is the heater resistance, R_{ho} is the heater resistance at room temperature i.e. at 30^0C (in our case). At the same time we have measured the sensor resistance (R_s) on application of heater voltage. At first the heater voltage was varied gradually to a maximum of 5V and the heater currents were measured. The measured

and calculated values are tabulated in Table 5.1 and Table 5.2 for TGS-2611 and TGS-842 respectively.

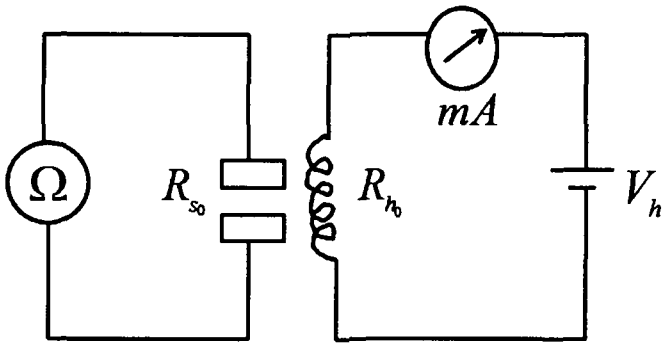

Fig. 5.4: Circuit for measuring heater current and sensor resistance

We have found the initial resistances of heater and sensor as-

For TGS-2611, R_{h0} = 59Ω and for TGS-842, R_{h0} = 30.0 ± 3.0Ω.

(5.15)

For TGS-2611, R_{S0} = 350kΩ; and for TGS-842, R_{S0} = 995kΩ;

R_{S0} is the sensor resistance at room temperature.

Table 5.1: Values of heater current, heater resistance, sensor resistance, change in temperature, and temperature w.r.t varying heater voltage for TGS-2611:

Heater Voltage(V_h) (volts)	Heater Current (I_h) (mA)	Heater Resistance for TGS-2611 (R_h) (Ω)	Sensor Resistance for TGS-2611 (R_s) (kΩ)	Change in temperature ΔT (°C)	Temperature (T) (Kelvin)
1.3	21.7	59.90	220	13.6400	316.6400
1.4	23	60.86	216	18.1553	321.1553
1.5	24.6	61.97	214	23.3761	326.3761
1.6	25.7	62.25	212	24.6931	327.6931
1.7	26.8	63.43	211	30.2432	333.2432
1.8	28.3	64.6	209	35.7462	338.7462
2.1	31.7	66.24	195	43.4599	346.4599
2.2	32.3	67.11	187	47.5519	350.5519
2.4	35	68.57	178	54.4189	357.4189
2.5	36.3	68.87	175	55.8299	358.8299
2.6	37.2	69.89	170	60.6274	363.6274
2.7	38.4	70.31	161	62.6029	365.6029

2.8	39.3	71.24	156	66.9771	369.9771
2.9	40.4	71.78	150	69.5170	372.5170
3.0	41.6	72.11	145	71.0691	374.0691
3.1	42.7	72.59	138	73.3267	376.3267
3.2	43.6	73.39	132	77.0895	380.0895
3.3	44.7	74.82	122	83.8154	386.8154
4.3	52.1	82.53	71	120.0790	423.0790
4.5	53.6	83.95	69	126.7579	429.7579
4.6	54.4	84.55	64	129.5800	432.5800
4.7	55.2	85.14	61	132.3550	435.3550
4.8	56	85.71	58	135.0360	438.0360
4.9	56.8	86.26	44	137.6229	440.6229
5.0	57.3	87.26	35	142.3263	445.3263

Table 5.2: Values of heater current, heater resistance, sensor resistance, change in temperature, and temperature w.r.t varying heater voltage for TGS-842:

Heater Voltage(V_h) (volts)	**Heater Current (I_h) (mA)**	**Heater Resistance for TGS-2611 (R_h) (Ω)**	**Sensor Resistance for TGS-842 (R_s) (kΩ)**	**Change in temperature ΔT (°C)**	**Temperature (T) (Kelvin)**
1.5	0.0497	30.1642	495	1.4674	304.4674
1.8	0.0567	31.7720	423	15.8356	318.8356
2.0	0.0609	32.8278	401	24.6931	328.2708
2.4	0.0708	33.9100	303	34.9419	337.9419
2.5	0.0716	34.9400	220	44.1466	347.1466
2.8	0.0783	35.7700	140	51.5639	354.5639
2.9	0.0784	36.9900	98	62.4665	365.4665
3.1	0.0837	37.0500	87	63.0027	366.0027
4.0	0.1050	38.1000	51	72.3861	375.3861
4.5	0.1113	40.4208	48	93.1260	396.1260
4.6	0.1109	41.4800	35	102.5916	405.5916
5.0	0.1163	42.9800	26	115.9964	418.9964

The heater voltage (V_h) to heater temperature (T) transfer function was determined which can be modeled by a first order transfer function given by-

$$\frac{T}{V_h} = \frac{K}{(1+s\tau)} \tag{5.16}$$

Where K is the static sensitivity and τ is the time constant. To determine the static sensitivity (K), the slope of the plot between V_h and T characteristic as shown in Fig. 5.5 was determined given by-

For TGS-2611, $K_{1,TGS-2611} = (316.6-445.3)/(1.3-5)$

$= 34.783$ Kelvin/Volt

For TGS-842, $K_{1,TGS-842} = (304.5-419)/(1.5-5)$

$= 32.57$ Kelvin/Volt

Further we have observed the step response of the heater current dynamics by applying a 5V heater pulse as shown in Fig. 5.6.

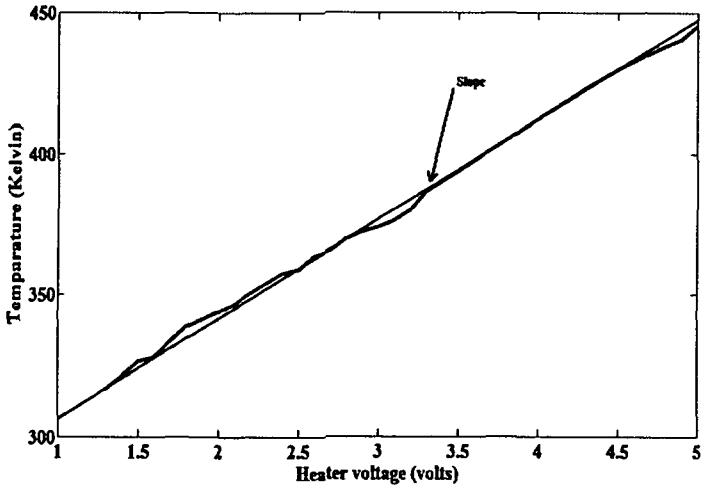

(a)

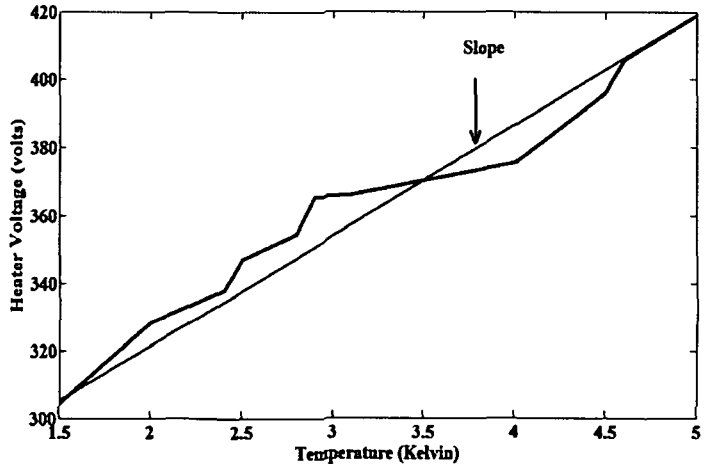

(b)

Fig.5.5: Variation of temperature with heater voltage (a) for TGS-2611 and (b) for TGS-842.

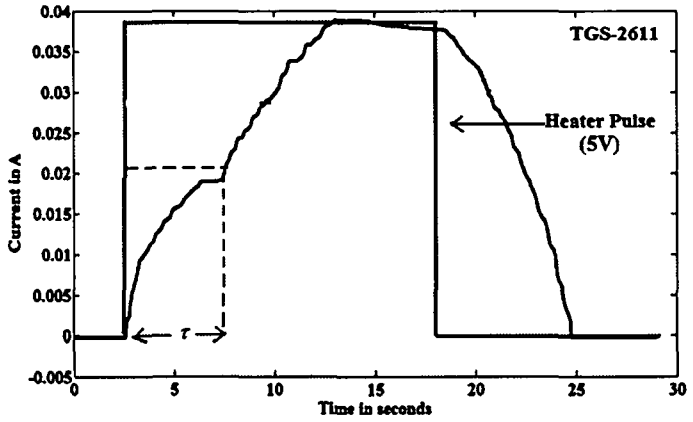

(a)

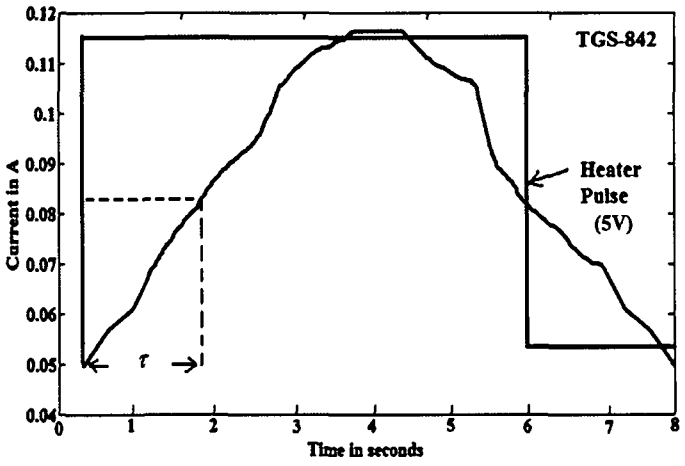

(b)

Fig.5.6: Variation of heater current with time (a) for sensor TGS-2611 and (b) for sensor TGS-842.

From these responses the value of τ is found to be approximately 6 s for TGS-2611 and 1.3 s for TGS-842.

The heater temperature profile can thus be expressed as the first order response for T_{ON} and T_{OFF}, given by,

$$T_{ON} = T_{\max}(1 - e^{-t/\lambda}) \tag{5.17}$$

$$T_{OFF} = T_{\max}(e^{-t/\lambda}) \tag{5.18}$$

where $T_{\max}$ is the maximum heater temperature and λ is the heater time constant. Substituting (5.17) and (5.18) in (5.5) and writing a voltage equation we get,

$$V_0 = [V_{b\max} e^{-E_{A0}/KT_{\max}(1-e^{-t/\lambda})} + V_{s\max} e^{-E_{As}/KT_{\max}(1-e^{-t/\lambda})} \times C^{nKT_{\max}}] +$$

$$[V_{b\max} e^{-E_{A0}/KT_{\max}(e^{-t/\lambda})} + V_{s\max} e^{-E_{As}/KT_{\max}(e^{-t/\lambda})} \times C^{nKT_{\max}}] \quad (5.19)$$

Rearranging eqn. (5.19) we get,

$$V_0 = V_{b\max}[e^{-E_{A0}/KT_{\max}(1-e^{-t/\lambda})} + e^{-E_{A0}/KT_{\max}(e^{-t/\lambda})}] +$$

$$V_{s\max}[e^{-E_{As}/KT_{\max}(1-e^{-t/\lambda})} + e^{-E_{As}/KT_{\max}(e^{-t/\lambda})}] \times C^{nKT_{\max}} \quad (5.20a)$$

$$= V_b + V_s' \quad (5.20b)$$

Since the sensor surface is not stimulated by any gas, the baseline model can be written by putting the term $C^{nKT_{max}}$ =0 and writing $V_0 = V_b$ the equation for baseline voltage reduces to-

$$V_b = V_{b\max}[e^{-E_{A0}/KT_{\max}(1-e^{-t/\lambda})} + e^{-E_{A0}/KT_{\max}(e^{-t/\lambda})}] \quad (5.21)$$

where V_{bmax} is the highest baseline voltage level.

Eqn. (5.21) therefore describes the surface reaction of the sensor in the presence of dry air without the interaction of any gases. Fig.5.7 shows the block diagram of the sensor-heater and response model for metal oxide gas sensors. The input to the baseline model block is only the device operating temperature which is set by the heater model. In our case, the experiments were performed in the absence of gases and only the sensor baseline model is taken into account. The heater model block elevates the temperature of the sensor and sets the operating temperature. The baseline model block emulates the sensor baseline conductance which is given by Eqn. (5.21). In this work the modeling of the sensor baseline has been done without the affect of any gases on the sensor surface.

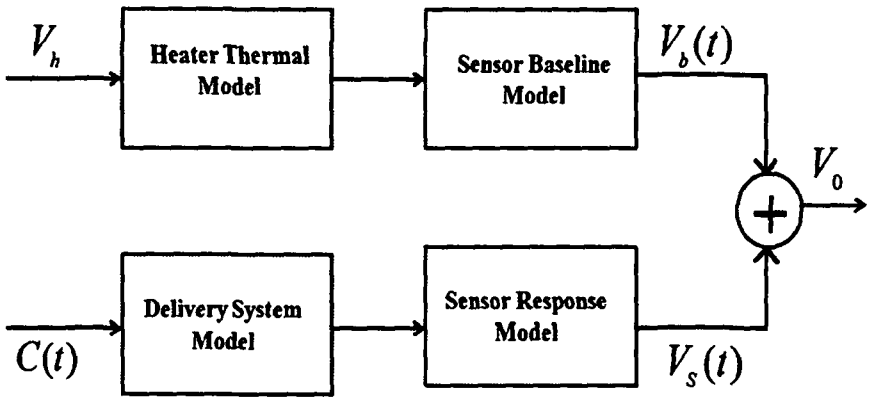

Fig. 5.7 Sensor-Heater and response model.

5.4 Sensor Activation Energy:

The activation energy is the minimum extra amount of energy absorbed by the reactant molecules so that their energy becomes equal to threshold value. At room temperature, most of the reactant molecules have less energy than the threshold value. However, if the energy is supplied in the form of heat, this energy is absorbed by the reactant molecules and becomes equal to or greater than threshold value. The activation energy is usually expressed in kilojoules per mole.

As the temperature increases, the velocity of gas molecules' (or kinetic energy) also increases. This means that as temperature increases, more molecules will have higher kinetic energy, and hence the fraction of molecules that have high enough energy to exceed the minimum energy needed for a reaction also increase. The fraction of molecules that has energy equal to or greater than E_{Ao} is given by the exponential term in the Arrhenius equation:

$$k = Ae^{\frac{-E_{A0}}{KT}} \tag{5.22}$$

where k is the rate constant

K= Boltzmann constant = 86×10^{-6} eV/K ,

E_{Ao} = Activation energy of the baseline conductance (eV),

T = Heater temperature (Kelvin)

A is the Arrhenius factor.

Taking the natural log of both sides in eqn. (5.22),

$$\ln k = \ln A - \frac{E_{A0}}{KT} \tag{5.23}$$

Eqn (5.23) has the form of a straight line, $y = mx + b$. Plotting $\ln k$ vs 1/T, the equation represents a straight line with a slope of $m = -\frac{E_{A0}}{K}$ and a y-intercept of $\ln A$ as shown in Fig.5.8.

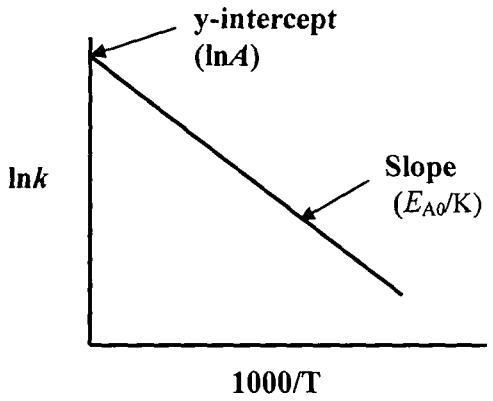

Fig. 5.8 Arrhenius Plot for Eqn.(5.23).

The heater voltage was modulated while performing the experiments with a maximum heater voltage of 5V. To determine the activation energy for TGS-2611 and TGS-842 the relative values of the sensor resistance drift (dR_s/R_s) of the sensor material at each individual temperature 'T' obtained from Table 5.1 and Table 5.2 were plotted as a function of $1/T$.

The Arrhenius plot for determining the activation energy of sensor TGS-2611 and TGS-842 used in our experiment is shown in Fig. 5.9 (a) and (b) respectively.

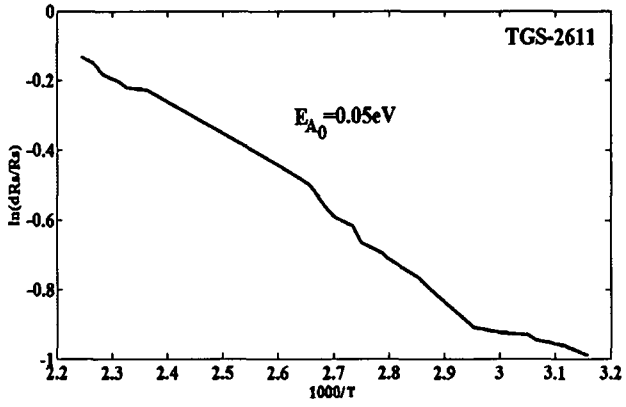

(a)

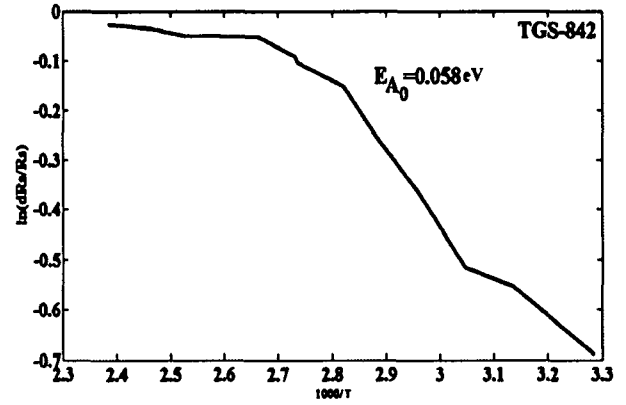

(b)

Fig. 5.9. Activation energy for MOS gas sensor, (a) TGS-2611 and (b)TGS-842.

For TGS-2611, the activation energy is given from the slope of Fig. 5.8 (a) as-

$$E_{Ao,\ TGS\text{-}2611} = K \times m \times 1000 \tag{5.24}$$

where K is the Boltzmann constant and m is found as,

$$m = (-0.34+1)/(3.2-2.2)$$
$$= 0.66$$

Hence, using eqn. (5.24)-

$$E_{Ao,\ TGS\text{-}2611} = 86\times10^{-6} \times 0.66 \times 1000$$
$$= 0.05\text{eV}$$

For TGS-842, the activation energy is given from the slope of Fig. 5.8 (b) as-

$$E_{Ao,\ TGS\text{-}842} = K \times m \times 1000 \tag{5.25}$$

where K is the Boltzmann constant and m is found as,

$$m = (-0.02+0.7)/ (3.3-2.3)$$
$$= 0.68$$

Hence, using eqn. (5.25)-

$$E_{Ao,\ TGS\text{-}842} = 86\times10^{-6} \times 0.68 \times 1000$$
$$= 0.058\text{eV}$$

The experimentally determined sensor parameters as shown below were used to simulate the sensor response for a time duration of heater pulse voltage t_{ON} and t_{OFF} using eqn.(5.21).

For TGS-2611,	For TGS-842,
E_{Ao}= 0.05eV	E_{Ao}= 0.058eV
T_{max} = 445K	T_{max} = 420K
V_{bmax} = 0.0088V	V_{bmax} =0.04V
τ = 6s	τ = 1.3s
t_{ON}= 18.75 s	t_{ON}= 6 s
t_{OFF} = 6.25 s	t_{OFF} = 2 s

The simulated results of sensor responses are shown in Fig. 5.10 (a) and (b) for TGS-2611 and TGS-842 respectively.

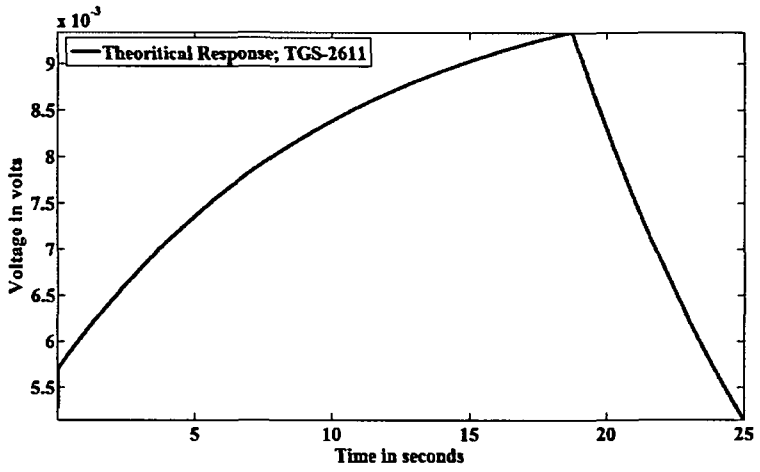

(a)

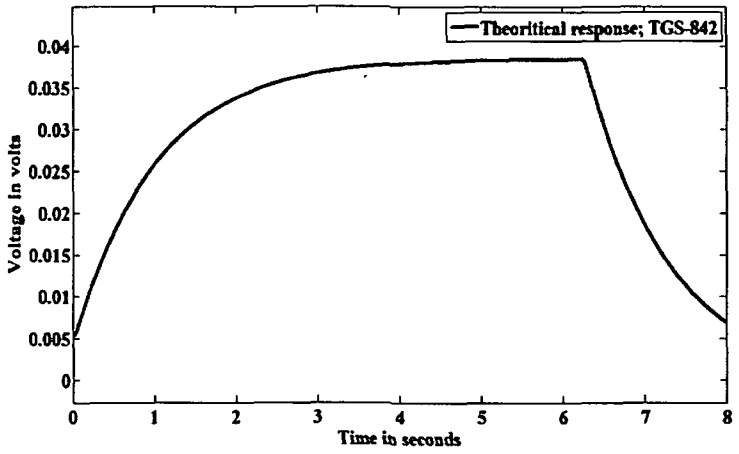

(b)

Figure 5.10: Response of sensor obtained from theoretical results for (a) TGS-2611 at 40mHz and 75% duty cycle and (b) TGS-842 at 120mHz and 75% duty cycle.

From Fig. 5.10 (a) and (b) it is seen that the simulated response is an ideal MOS gas sensor baseline response. The baseline model simulates the behaviour of the sensor when operating at pulsed frequency. It is observed that the sensors behaves as a first order system with a first-order transfer function for sensor TGS-2611 and as a second-order transfer function for sensor TGS-842 since behavior of both the systems are different with different system parameters.

5.5 Transfer Function Validation from System Identification:

The measured input-output data of the MOS gas sensor is used to build the sensor model which is chosen with the best dynamic performance based on the stability analysis hence determining the corresponding best frequency and duty cycle. We compare here the simulated results of the theoretical models of the MOS gas sensors discussed in *Section 5.3* with the model obtained from system identification.

In our work the transfer function of the sensor TGS-2611 determined by the system identification technique was found to be most stable and generated the best fit percentage. The determination of the most stable transfer function was done based on the pole zero plot and overshoot percentage as described in **Chapter 4** (*Section 4.4*). The transfer function that was most stable was then simulated for the best fit percentage

(*Section 4.5*). The most stable transfer function for TGS-2611 was determined at 40mHz and 75% duty cycle given as:

$$H(z)_{40mHz,75\%} = \frac{(1.7\times10^{-7})}{(z-0.996)} \tag{5.25}$$

In Laplace form:

$$H(s)_{40mHz,75\%} = \frac{0.00016999}{(s+0.08627)} \tag{5.26}$$

For TGS-842, the stable transfer function was determined at 120mHz and 75% duty cycle which is given as:

$$\hat{H}(z)_{120mHz,75\%} = \frac{(4.248\times10^{-7})(z-0.9639)}{(z-0.9995)(z-0.9992)} \tag{5.27}$$

In Laplace form:

$$\hat{H}(s)_{120mHz,75\%} = \frac{(4.248\times10^{-4})(s+0.9639)}{(s+0.9995)(s+0.9992)} \tag{5.28}$$

The models can be simulated to observe the behaviour of the sensor when the operating temperature is modulated by applying pulse signal to the heating element. Fig.5.11 shows the simulated responses of the sensor TGS-2611 when subjected to pulsed temperature modulation obtained from system identification compared with that obtained from the theoritical analysis. From Fig.5.11 (a) it is seen that the system identification returns a model of first order at 40mHz frequency and 75% duty cycle for TGS-2611, given by Eqn.(5.25) and (5.26). From Fig.5.11 (b) it is seen that the system identification returns a model of second order at 120mHz frequency and 75% duty cycle for TGS-842, given by Eqn.(5.27) and (5.28).

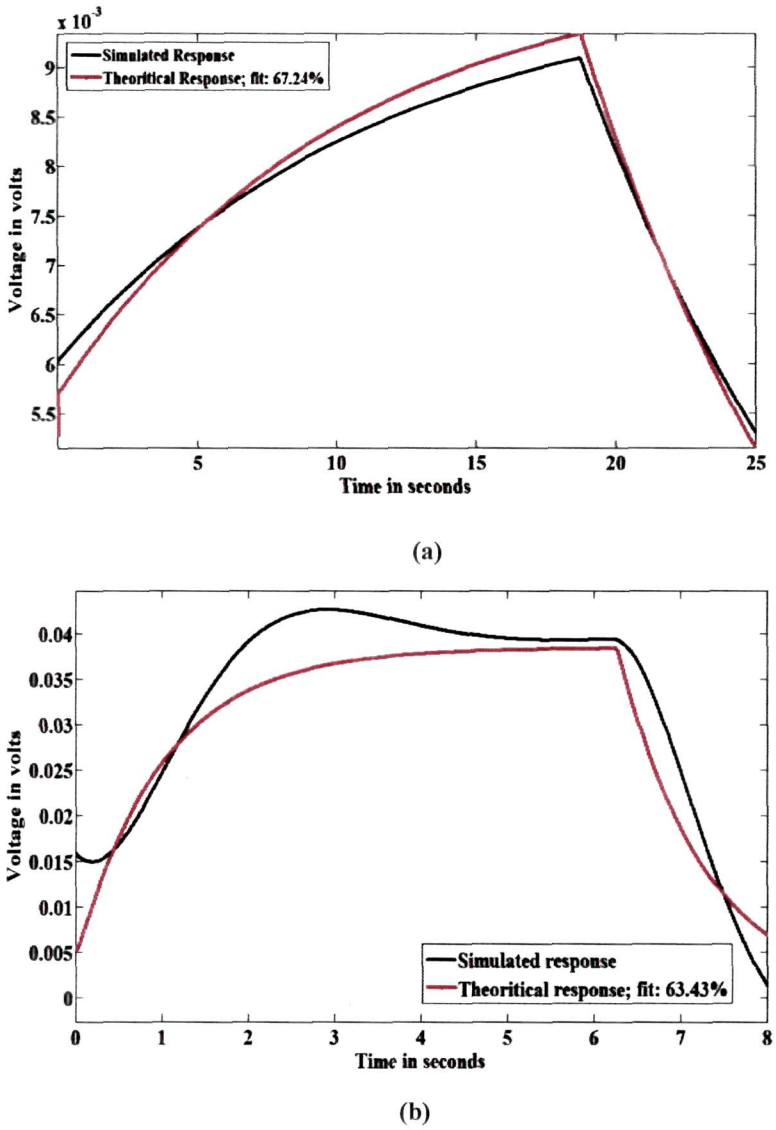

Fig 5.11. Response of (a) sensor TGS-2611 and (b) sensor TGS-842 by simulation of the transfer function obtained from system identification and that obtained from theoritical analysis.

From Fig.5.11 (a) it is seen that the sensor responses are first order responses with a time constant of approximately 6s and from Fig.5.11 (b) it is seen that the sensor responses have a time constant of approximately 1.3s. The best fit percentage for TGS-2611 at 40mHz and 75% and for TGS-842 at 120mHz and 75% duty cycle is found to be 67.24% and 63.43% respectively. The responses and model parameters are similar with the actual sensor responses given in Fig. 5.3 (a) and (b).

5.6 Conclusions:

Though MOS gas sensors are widely used, yet their sensing mechanisms are not completely understood. In this chapter we present a baseline model of the MOS gas sensor TGS-2611 and TGS-842 which accurately depicts the dynamic responses of the sensor. The model equation was derived from the Freundlich isotherm equation by finding the unknown sensor parameters- activation energy. In our experiment, the sensor was excited by the heater voltage to develop the temperature which was measured indirectly by using the heater filament as the temperature sensor i.e. the heater current was used to determine the temperature and heater resistance. The heater model was found to be a first order one and the time-constant and sensitivity was determined. Further, Arrhenius plot was made for the sensor to determine the activation energy of the sensor material. With this derivation, we concluded the theoritical model equation of the MOS gas sensors (TGS-2611 and TGS-842). The theoritical model derived was compared with the model obtained by system identification and it was found that the fit percentage were 67.24% and 63.43% for TGS-2611 and TGS-842 respectively. The model presented in this work can be extended to other resistive sensors based on conducting polymers.

5.7 Publication on this chapter

1. Dutta, N., & Bhuyan, M. Modeling of MOS Gas Sensor Based Electronic Nose Using System Identification, *International Journal of Engineering Systems Modelling and Simulation.* (Under Communication)

CHAPTER 6

CHAPTER 6

CONCLUSION AND FUTURE SCOPE

This thesis presents a descriptive and analytical report on the noise feature analysis, compensation and modeling of MOS gas sensors under pulsed temperature modulation. The dynamic analysis of the sensor responses and classification of different gases is also performed using a novel technique of Artificial Neural Network based Electronic Nose (E-nose).

This research can be divided into six boarder areas in the field of noise feature analysis, its reduction and modeling. These areas are as follows:

1. Review of literature of the recent works carried out in the field of noise analysis, noise reduction and modeling of MOS gas sensors based E-nose;
2. Development of the MOS gas sensor set-up;
3. The statistical and frequency analysis of noise under pulsed modulated heater for selection of best pulse frequency and discrimination of different gases using best frequency and duty cycle ;
4. Reduction noise using Amplitude Demodulation (AD) technique and Wavelet analysis;
5. Sensor system identification and stability analysis under pulsed temperature modulation for selection of best pulse frequency and classification of gases using best frequencies and duty cycles; and
6. Sensor modeling based on theoritical analysis of MOS sensors and system identification on.

Chapter 1 gives the introduction to an inclusive literature as basic knowledge for the research work. The different types of gas sensors with a detailed description of MOS gas sensors are described in parallel. To address the improvement of selectivity of MOS gas sensors, the temperature modulation is described. The chapter throws light upon different types of noise in MOS based gas sensors along with different statistical parameters of noise such as Probability Distribution Function (PDF), histogram and Signal-to Noise ratio (SNR). A new noise feature- NSF and NPF were introduced at four different frequencies namely 10mHz, 40mhz, 80mHz and 120mHz and at two different duty cycles namely 50% and 75%. Modeling of the noise process has been discussed in the light of Fast Fourier Transform (FFT) for frequency analysis. A detailed review of the different noise filtering techniques followed by the advantage of the proposed Amplitude Demodulation (AD) technique and its comparison with wavelet filter has been presented. The dynamic behaviour of the MOS gas sensors followed by sensor modeling using system identification is also described. A systematic method to determine the best suitable temperature modulation frequencies to solve a given gas analysis problem using stable transfer functions was developed. The E-nose is described in details and concluded that it is an operated with suitable pulse frequency of the heater voltage. It is able to fit its pulse frequency for the most stable dynamics. The odour classification and discrimination performed by MOS sensors is achieved by using Artificial Neural Network (ANN). Multi-layered perceptron (MLP) and Radial Basis Function (RBF) were used for ANN classification.

Chapter 2 presents the experimental set-up of the MOS gas sensor based E-nose of the entire work and the noise analysis (statistical and frequency based) of the sensor response. The techniques of temperature modulation, data acquisition, feature extraction, feature selection, and classification are described. Three MOS based gas sensors, TGS-2611, TGS-822 and TGS-842 of FIGARO INC, Japan were used which are sensitive to odours such as alcohol, volatile organic compounds (VOCs) etc. A computer controlled switching and diaphragm pumps were designed. The data acquisition and online logging of the data was performed by using Data Acquisition (DAQ) card (PCI6024E, National Instruments) and data acquisition software-LabVIEW. The chapter presents a complete analysis-both statistical and frequency analysis of the noise in MOS gas sensors based E-nose by pulsed heater modulation

under different frequencies and duty cycles. The study determined the best frequency and duty cycle at which the noise was minimum. This is followed by the dynamic analysis of the sensor data and the discrimination using ANN of ten different sample gases performed using two sets of frequency and duty cycle.

The experiment has two parts- one the noise analysis i.e. for baseline noise without the application of gas and the other the dynamic analysis in presence of gas. The frequency and duty cycle of the heater pulse at which the noise was minimum was determined based on the noise behaviour. Classification of ten different gases using this best frequency and duty cycle was performed using ANN (MLP and RBF) to verify the selection of best frequency and duty cycle obtained from noise analysis. The PCA identified successfully ten gas sample clusters and shows better classification when best selected pulse frequency is used. It was found that the RBF network provided better classification accuracy with lesser training time than the MLP network. ANN based E-nose system provided better classification rate for the ten sample gases when the sensors were pulsed using best frequency and duty cycle.

Since noise in MOS gas sensors and the measuring circuit is a pertinent problem of E-nose systems we have attempted to suggest possible measure to suppress and filter the noise. Chapter 3 describes the techniques of noise reduction in the MOS gas sensors using different filtering methods. The AD technique was analyzed and used in this research to extract the original signal from the responses of noise modulated low sensitivity sensor signal. A low sensitivity sensor (TGS-2611) produced responses which were mostly dominated and buried with noise and hence it was used to perform the AD process. The signal was added with white noise and a low frequency sine signal and then the filtering was carried on. The feasibility of the AD technique was observed by using another filter named wavelet filter. Further the wavelet based filter was also used to denoise the sensor responses and it was found that this technique has less denoising capability compared to AD technique. The spectral analysis of signal components obtained from both the methods was performed using FFT and the bandwidth was determined. Hence it was concluded that the AD technique can be suggested for removal of noise from MOS gas sensor responses.

Chapter 4 presents the method of system identification in the area of gas sensors. The method consists of studying the sensor baseline response when their operating temperature is modulated. A detailed procedure of the determination of the most stable transfer functions and the best fit transfer function using system identification is described. Validation of the best frequency and duty cycle obtained from the system identification is examined.

In the first experiments, the system identification was performed for a lower range of frequencies 1mHz, 2mHz, 3mHz, 4mHz and 5mHz with duty cycles of 50% and 75%. The transfer functions were determined and the most stable transfer function was chosen based on the pole-zero plots and the overshoot percentage which was found to be 2mHz and 50% duty cycle for TGS-2611 and 1mHz and 50% duty cycle for TGS-822. In the experiments that followed the first ones, the stable transfer functions for a higher set of frequencies i.e. 10mHz, 40mHz, 80mHz and 120mHz with duty cycles of 50% and 75% were determined with the stability chosen under the same conditions of shorter distance of the poles in the pole-zero plot and lesser overshoot percentage. It is seen that the frequencies and duty cycles at which the transfer function was most stable for TGS-2611 and TGS-842 was obtained at 40mHz and 75% and at 120mHz and 75% respectively. A slow change in sensor heater voltage helps to attain a quasi-isothermal state leading to the preservation of sensor dynamics and hence the experiment was performed for two ranges of frequencies. Once the most stable transfer functions and their corresponding best values of pulse frequency and duty cycle are obtained, the PCA was worked out with two pairs of sensors: TGS-822/TGS-2611 and TGS-842/TGS-2611 for ten different gas samples. It was observed that the most stable transfer function also showed the best fit percentage. The enhancement of the suitable results for both the ranges of frequencies was proved by the discrimination of ten different sample gases using ANN. The results of classification using the selected set of frequencies and duty cycles were encouraging. The classification was done with the help of MLP and RBF. From the results, it was evident that MOS gas sensor based E-nose was capable of discriminating the ten sample gases by the ANN techniques. A classification percentage of 94.1% was reached in case of RBF for lower frequency range than in case of MLP (91.5%). Similarly, for higher range of frequency, the RBF performed better yielding a

classification percentage of 93.4% compared to MLP (86.7%). We observed that RBF was much faster compared to MLP network.

As stated earlier for chapter 2 we have found that the best pulse frequency and duty cycle for the three sensors are 10mHz, 75% duty cycle, which is based on noise analysis however, the stability analysis shows that this value is 40mHz, 75% duty cycle (TGS-2611) and 120mHz, 75% duty cycle (TGS-842) for upper frequency range and for lower frequency range the stability was found at 1mHz, 50% duty cycle (TGS-822) and 2mHz, 50% duty cycle (TGS-2611). Therefore selection of best operating frequency of heater pulse voltage is a trade-off between requirement of noise behavior and stability of the MOS gas sensor responses.

Chapter 5 gives an analysis on the modeling of the sensor dynamics based on the measured input output data obtained. The thesis presents a theoritical analysis on the system kinetics of the MOS gas sensor. Based on a mathematical model obtained from MOS gas sensor theory as well as from system identification theory, the simulation was performed. This research work gives a layout of the dynamic behavior of the MOS gas sensor without the application of any stimulant gas and determines the baseline model. The baseline model proposed can simulate the behavior of the sensors (TGS-2611 and TGS-842) when the operating temperature is modulated by applying an arbitrary function (pulse sequence in our case) to the heating element.

In the conclusion a novel intelligent E-nose has been developed with the capability of the classification of different sample gases using best frequency and duty cycle obtained from noise feature analysis as well as from system identification technique under pulsed temperature modulation.

6.1 Future Scope:

During this research, a quite accurate and capable E-nose is developed, despite of the fact that further work is necessary to assess the long term reliability of the MOS gas sensor based E-nose system. The use of the E-nose in the selection of frequencies and duty cycles can be suitable for commercial applications for continuous monitoring of different sample gases. When the sensors were temperature modulated by a signal with

a frequency content that corresponded to the best values, the gases could be perfectly discriminated. The selected thermal modulation of the working temperature of the MOS gas sensor based E-nose can significantly increase the selectivity of metal oxide sensors. Therefore, the systematic process to employ the selection of modulating frequencies, permits to ensure a remarkable increase in performance for metal oxide based multisensor systems. The simplicity of the methods implemented can ultimately lead to the development of intelligent e-noses. The method can be used in any gas analysis problem or extended to other types of sensors also.

The E-nose technology will play a crucial role in the field of medical sciences enabling a low cost substitute to the more costly diagnosis method for most of the diseases at present. The combination of E-noses with other electronic medical instruments will facilitate the development and availability of improved real-time information of patient conditions, leading to even more effective decisions and treatments by physicians. Now, the E-nose industry is at the stage where the designing and manufacturing have been explored and the path forward has shifted to designing e-noses that are smaller, less expensive, more application-specific, easier to be handled, and produce results that are easily interpreted by the user due to limited data outputs.
To conclude, E-nose has enormous potential area for further exploration in research and study. It is undoubtedly a high challenging field to be investigated.

The scientific contributions of this thesis are collected in four journal papers, four international conference proceedings and one book chapter.

****

REFERENCES

REFERENCES

1. Wang, X., Carey, W.P., & Yee, S.S. Monolithic thin film metal oxide gas sensor arrays with application to monitoring of organic vapors , *Sensors and Actuators B: Chemical* **28** (1), 63–70, 1995.
2. Mitsubayashi, K., Matsunaga, H., Nishio, G., Ogawa, M., & Saito, H. Biochemical gas sensor (Bio-sniffer) for breath analysis after drinking , in SICE Annual Conference'2004, Sapporo, 97-100.
3. Williams, D.E. Semiconducting oxides as gas-sensitive resistors, *Sensors and Actuators B: Chemical* **57** (1-3), 1–16, 1999.
4. Barsan, N., Berberich, M.S., & Gopel, W. Fundamental and practical aspects in the design of nanoscaled SnO_2 gas sensors: a status report, *Fresenius J Anal. Chem.* **365** (4), 287–304, 1999.
5. Korotcenkov, G. Gas response control through structural and chemical modifications of metal oxide films: state of the art and approaches, *Sensors and Actuators B:Chemical* **107** (1), 209–232,2005.
6. Ihokura, K. & Watson, J. *The Stannic Oxide Gas Sensor: Principles and Applications*, CRC Press Inc., 1994.
7. Heiland, G. Zum Einfluss von Wasserstoff auf die elektrische Leitf'ahigkeit von ZnO Kristallen, *Zeit. Physik* **138** ,459–464,1954.
8. Bielanski, A., Deren, J., & Haber, J. Electric conductivity and catalytic activity of semiconducting oxide catalysts, *Nature* **179** (4561), 668–669, 1957.
9. Seiyama, T., et al. A new detector for gaseous components using semiconductive thin films, *Analytical Chemistry* **34** (11), 1502-1503, 1962.
10. Taguchi, N. *Gas detecting device,* **US Patent No. 3631436**, December 28, 1971.
11. Moseley, P. & Tofield, B. *Solid state gas sensors*, Adam Hilger, Bristol, U.K., 1987.
12. Marco, S., et al. Gas identification with tin oxide sensor array and self organizing maps, *IEEE Transactions on Instrumentation and Measurement* **47** (1), 316- 321,1997.
13. Heilig, A., et al. Gas identification by modulating temperatures of SnO_2 based thick film sensors, *Sensors and Actuators B* **43** (1-3), 45-51, 1997.

14. Ortega, A., et al. An intelligent detector based on temperature modulation of a gas sensor with a digital signal processor, *Sensors and Actuators B: Chemical* **78 (1)**, 32-39, 2001.
15. Göpel, W. New materials and transducers for chemical sensors, *Sensors and Actuators B: Chemical* **18 (1-3)**, 1-21, 1994.
16. Demarne, V. & Sanjines, R. *Gas sensors: Principles, Operation and Development*, Kulwer Academic Publishers, Netherlands, 89-116, 1992.
17. Kohl, D. The role of noble metals in the chemistry of solid-state gas sensors, *Sensors and Actuators B: Chemical* **1**(1-6), 158-165, 1990.
18. Le Vine, H. D. *Method and apparatus for operating a gas sensor*, **US Patent No. 3906473**, September 16, 1975.
19. Eicker, H. *Method and apparatus for determining the concentration of one gaseous component in a mixture of gases*, **US Patent No. 4012692**, March 15, 1977.
20. Owen, L. J. *Gas monitors*, **US Patent No. 4185491**, January 29, 1980.
21. Advani, G. N., Beard, R. and Nanis, L. *Gas measurement method*, **US Patent No. 4399684**, August 23, 1983.
22. Lantto, V., & Romppainen, P. Response of some SnO_2 gas sensors to H_2S after quick cooling, *J. Electrochem. Society* **135** (10), 2550-2556, 1988.
23. Bulkowiecki, S., Pfister, G., Reis, A., Troup, A. P., and Ulli, H. P. *Gas or vapor alarm system including scanning gas sensors*, **US Patent No. 4567475**, January 28, 1986.
24. Sears, W.M., Colbow, K., & Consadori, F. General characteristics of thermally cycled tin oxide gas sensors, *Semiconductor Science and Technology* **4** (5) , 351– 359,1989.
25. Sears, W.M., Colbow, K., & Consadori, F. Algorithms to improve the selectivity of thermally cycled in oxide gas sensors, *Sensors and Actuators* **19** (4), 333-349, 1989.
26. Suehle, J.S., et al. Tin oxide gas sensor fabricated using CMOS micro-hotplates and in situ processing, *IEEE Electron Device Letters* **14** (3), 118-120, 1993.
27. Cavicchi, R.E., et al. Fast temperature programmed sensing for micro-hotplate gas sensors, *IEEE Electron Device Letters* **16** (6), 286-288, 1995.

28. Cavicchi, R.E., et al. Optimized temperature-pulse sequences for the enhancement of chemically specific response patterns from micro-hotplate gas sensors, *Sensors and Actuators B: Chemical* **33** (1-3), 142-146, 1996.
29. Heilig, A., et al. Gas identification by modulating temperatures of SnO_2-based thick-film sensors, *Sensors and Actuators B: Chemical* **43** (1-3), 45-51, 1997.
30. Capone, S., et al. Metal oxide gas sensor array for the detection of diesel fuel in engine oil, *Sensors and Actuators B: Chemical* **131** (1) , 125–133, 2008.
31. Alfeeli, B., et al. A. Sub-Nanoliter Spectroscopic Gas Sensor, *Sensors* **6** (10), 1308-1320, 2006.
32. Morante, M.A., et al. New micro-optic cell for optical fibre gas sensors with interferometric noise reduction, Electronics *letters* **33** (16), 1407-1409, 1997.
33. Bosco, A., et al. Noise Reduction for CFA Image Sensors Exploiting HVS Behaviour, *Sensors* **9** (3), 1692-1713, 2009.
34. Tian, F., et al. Circuit and Noise Analysis of Odourant Gas Sensors in an E-Nose, *Sensors* **5** (1), 85-96, 2005.
35. Philipps, H. Development of a statistical model for powerline communication channels, in International Symposium on Powerline Communications (ISPLC'2000), Limerick, Ireland.
36. Kundur, D., & Hatzinakos, D. Blind image deconvolution, *IEEE Signal Processing Magazine.* **13**(3), 43-64, 1996.
37. Mazouzi, S., et al. A multi-agent segmentation of depth image based polyhedral objects. A new approach to image segmentation, *Journal of Science and Technology Information* **28** (3), 365-393, 2009.
38. Chehdi, K., & Sabri, M. A new approach to identify the nature of the noise affecting an image, in IEEE International Conference on Acoustics, Speech, and Signal Processing (ICASSP'92), San Francisco, CA, 285-288.
39. Alexander, S. T. Adaptive Signal Processing, Springer Verlag, NewYork, 1986.
40. Bellanger, M. *Adaptive Digital Filters*, 2nd ed., Marcel Dekker, Inc., NewYork, 2001.
41. Strobach, P. *Linear Prediction Theory*, Springer Verlag, NewYork,1990.
42. Widrow, B. & Stearns, S. D. *Adaptive Signal Processing*, Prentice Hall, Englewood Cliffs, NJ, 1985.
43. Treichler, J. R., Johnson, C. R. & Larimore, M. G. *Theory and Design of Adaptive Filters*, JohnWiley & Sons, NewYork, NY, 1987.

44. Farhang-Boroujeny, B. *Adaptive Filters: Theory and Applications*, John Wiley & Sons, New York, NY, 1998.

45. Haykin, S. *Adaptive Filter Theory*, 4th ed., Prentice Hall, Englewood Cliffs, NJ, 2002.

46. Jaffari, N.; Vleugels, K.; Wooley, B.A. Zero-pole modulation and demodulation for noise reduction in charge amplifiers, in Custom Integrated Circuits Conference (CICC'2011), San Jose, CA, 1 – 4.

47. Perin, G., et al. Amplitude demodulation-based EM analysis of different RSA implementations, in Design, Automation & Test in Europe Conference & Exhibition (DATE'2012), Dresden, 1167 – 1172.

48. Hornero, G., Casas, O., & Pallàs-Areny, R. Signal to noise ratio improvement by power supply voltage switching, in 16th IMEKO TC4 Symposium Exploring New Frontiers of Instrumentation and Methods for Electrical and Electronic Measurements'2008, Florence, Italy.

49. Chou, W. C., Hsu, Y. C., & Liao, L. P. Modulation/ Demodulation System for Capacitive Sensors, in IEEE International conference on Microsystems, Packaging, Assembly Conference Taiwan (IMPACT'2006), Taipei, Taiwan, 1 – 4.

50. Figaro USA Inc. <http://www.figarosensor.com>.

51. Simon, I., et al. Micromachined metal oxide gas sensors: opportunities to improve sensor performance, *Sensors and Actuators B: Chemical* **73**(1), 1–26, 2001.

52. Benesty, J., Gansler, T., Morgan, D. R., Sondhi, M. M. & Gay, S. L. *Advances in Network and Acoustic Echo Cancellation*, Springer, New York, 2001.

53. Hansler, E. & Schmidt, G. *Acoustic Echo and Noise Control: A Practical Approach*, Wiley, New Jersey, 2004.

54. Cohen, I. Relative transfer function identification using speech signals, *IEEE Transactions on Speech and Audio Processing* **12** (5), 451–459, 2004.

55. Huang, Y., Benesty, J., & Chen, J. A blind channel identification-based two stage approach to separation and dereverberation of speech signals in a reverberant environment, *IEEE Transactions on Speech and Audio Processing* **13** (5), 882– 895,2005.

56. Wu, M., & Wang, D. A two-stage algorithm for one-microphone reverberant speech enhancement, *IEEE Transactions on Audio, Speech and Language Processing* **14** (3), 774–784, 2006.

57. Araki, S., et al. The fundamental limitation of frequency domain blind source separation for convolutive mixtures of speech, *IEEE Transactions on Speech and Audio Processing* **11** (2), 109-116, 2003.

58. Talantzis, F., Ward, D. B., & Naylor, P. A. Performance analysis of dynamic acoustic source separation in reverberant rooms, *IEEE Trans. Audio, Speech and Language Processing* **14** (4), 1378–1390, 2006.

59. Gannot, S., Burshtein, D., & Weinstein, E. Signal enhancement using beam forming and non-stationarity with applications to speech, *IEEE Transactions on Signal Processing* **49**(8), 1614–1626, 2001.

60. Gannot, S., & Cohen, I. Speech enhancement based on the general transfer function GSC and post filtering, *IEEE Transactions on Speech and Audio Processing* **12**(6), 561–571, 2004.

61. Juricek, B.C., Seborg, D.E., & Larimore, W.E. Process control applications of subspace and regression-based identification and monitoring methods, in IEEE American Control Conference'2005, Portland.

62. Ogata, K. *Modern Control Engineering*, Prentice Hall, India. 1982.

63. Roberts, M. J. *Fundamentals of Signals and Systems*, Tata McGraw Hill, India, 2007.

64. Dorf, R. C. & Bishop, R. H. *Modern Control Systems*, 9th ed., Prentice Hall, Upper Saddle River, NJ, 2001.

65. Nise, N. S. *Control Systems Engineering*, 4th ed., Wiley, Hoboken, NJ, 2004.

66. Hua, Z., Ying, C., & Zhi, X. An identification method for sensors' dynamic modeling, *Journal of Transducer Technology*, 2004.

67. Rong, Z., et al. Several simulation methods comparison of signal reconstruction for acceleration sensor, *Foreign Electronic Measurement Technology*, 2010.

68. Hai, Bi., et al. A Least Square Method Based on Walsh Function for Dynamic Modeling and Its Application, *Acta Metrologica Sinica*, 1998.

69. Dei-hui, W.U., & Xiao-hong, W. Dynamic Model Identification Method Based on SVM for Sensors, *Chinese Journal of Sensors and Actuators*, 2006.

70. Xiao-hong, W., & Dei-hui, W.U. Identification for Hammerstein Model of Transducer Based on Support Vector Regression, *Chinese Journal of Sensors and Actuators*, 2007.

71. Dong, SUN. Application of orthonormal nonlinear model in dynamic compensation of sensors, *Journal of Transducer Technology*, 2003.

72. **Lee,** C.S., Kim, K.Y., Bae, J., & Hong, D. System identification of the pressure transducer and the force sensor on intelligent excavator, in ICCAS-SICE'2009, Fukuoka, 2200-2205.

73. Pardo, A., Marco, S., & Samitier, J. Dynamic measurements with chemical sensor arrays based on inverse modeling, in Instrumentation and Measurement Technology Conference (IMTC'96), Brussels, 570- 574.

74. Boulet, B., et al., System Identification and Modelling of a High Performance Hydraulic Actuator, *Lecture Notes in Control and Information Sciences* **190**, 503-520, 1993.

75. Chang, H., & Tzenog, P.K. Analysis of the dynamic characteristics of pressure sensors using ARX system identification, *Sensors and Actuators A: Physical* **141**(2), 367–375, 2008.

76. Soderstrom, T. & Stoica, P. *System Identification*, Prentice Hall International, Paperback Edition, Hemel Hempstead, 1994

77. Ljung, L. & Soderstrom, T. *Theory and Practice of Recursive Identification*, MIT Press, Cambridge, MA, 1983.

78. Kartalopoulous, S.V. *Understanding Neural Networks and Fuzzy Logic: Basic Concepts and Applications*, IEEE Press, PHI, 2000.

79. Nagle, H.T., Gutierrez-Osuna, R., & Schiffman, S.S. The how and why of electronic noses, *IEEE Spectrum* **35**(9), 22–31, 1998.

80. Schild, D. *Chemosensory information processing* (*NATO ASI series H: Cell Biology*), Springer, Berlin, 1990.

81. Meredith, M. Neural circuit computation: complex patterns in the olfactory bulb, *Brain Research Bulletin* **29**(1), 111-117, 1992.

82. Trincavelli, M., Coradeschi, S., & Loutfi, A. Odour classification system for continuous monitoring applications, *Sensors and Actuators B: Chemical* **139**(2). 265–273, 2009.

83. Olafsoon, R., et al. Monitoring of fish freshness using tin oxide sensors, *Sensory systems for an electronic nose*, 257 272, 1992.

84. Winquist, F., et al. Performance of an electronic nose for quality estimation of ground meat, *Measurement Science and Technology* **4**(12), 1493–1500, 1993.

85. Kleperis, J., Lusis, A., Zubkans, J., & Veidemanis, M. Two years experience with Nordic e-nose, Int. Symposium on Olfaction & Electronic Nose (ISOEN'1999), Tubingen, 11–14.

86. Hermle, T., Weimar, U., Rosenstiel, W., & Gopel, W. Performance of selected evaluation methods for a hybrid sensor system, 6th Int. Symposium on Olfaction & Electronic Nose (ISOEN'1999), Tubingen.

87. Fiorillo, A.S., et al. Ppy thin layers grown onto copper salt replica for sesor array fabrication, *Sensors and Actuators B: Chemical* 7(1-3), 399–403, 1992.

88. Grate, J.W., Martin, S.J., & White, R.M. Acoustic wave micro-sensors, Part I. *Analytical Chemistry* **65** (21), 940–948, 1993.

89. Lundstrom, I., et al. Electronic nose based on field effect structures, *Sensors and sensory systems for an electronic nose* **212**, 303–319, 1992.

90. Moseley, P., Morris, J. & Williams, D. *Techniques and mechanism in gas sensing*, Adam Hilger Series, Bristol, 1991.

91. Seitz, W.R. Chemical sensors based on fiber optics. *Analytical Chemistry* **56** (1), 16–34, 1984.

92. Russell. R. *Odour Detection by Mobile Robots*, World Scientific Publishing Co, London, UK, 1999.

93. Dutta, R., et al. Bacteria classification using cyranose 320 electronic nose. *Biomedical Engineering Online* **1** (4), 2002.

94. Blum, A., & Langley, P. Selection of relevant features and examples in machine learning, *Artificial Intelligence* **97** (1-2), 245-271, 1997.

95. Dash, M., & Liu, H. Feature selection for classifications, *Intelligent Data Analysis* **1** (1-4), 131-156, 1997.

96. Kohavi, R., & John, G. Wrappers for feature subset selection, *Artificial Intelligence* **97** (1-2), 273-324, 1997.

97. Das, S. Filters, wrappers and a boosting-based hybrid for feature selection, in Eighteenth International Conference on Machine Learning (ICML'2001), San Francisco, CA, USA, 74-81.

98. Langley, P. Selection of relevant features in machine learning, in Proceedings of the AAAI Fall Symposium on Relevance, AAAI Press, 1994.

99. Han, J. & Kamber, M. *Data Mining: Concepts and Techniques*, Morgan Kauffmann Publishers, San Francisco, 2001.

100. Sarry, F., & Lumbreras, M. Gas discrimination in an airconditioned system, *IEEE Transactions on Instrumentation and Measurement* **49**(4), 809–812, 2000.

101. Llobet, E., Brezmes, J., Vilanova, X., Fondevila, L., & Correig, X. Quantitative Vapor Analysis Using the Transient Response of Non-Selective Thick-Film Tin Oxide Gas Sensors, in International Conference on Solid State Sensors and Actuators (Transducers '97), Chicago, 971-974.

102. Nanto, H., et al. Identification of aromas from alcohols using a Japanese-lacquer-film-coated quartz resonator gas sensor in conjunction with pattern recognition analysis, *Sensors and Actuators B: Chemical* **35** (1–3), 183-186, 1996.

103. Corcoran, P., et al. Best configuration of a thermally cycled gas sensor array with neural network pattern recognition, *Sensors and Actuators B: Chemical* **48** (1–3), 448-455, 1998.

104. Zhang, S., et al. An entire feature extraction method of metal oxide gas sensors, *Sensors and Actuators B* **132**, 81-89, 2008.

105. Zhang, S., et al. A method of feature extraction from desorption part of MOX's response curves to gases, *IEEE Sensors Journal* **8** (11) , 2008.

106. Zhang, S., et al. A method of feature extraction on recovery curves for fast recognition application with metal oxide gas sensor array, *IEEE Sensors Journal*, **9** (12), 2009.

107. Qinlan, J. R. *Introduction of decision trees. Machine Learning*, Kluwer Academic Publishers, Boston, 1986.

108. Freund, Y. Boosting a weak learning algorithm by majority, *Information and Computation* **121**(2), 256-285, 1995.

109. Lu, H., Setiono, R., & Liu, H. Effective data mining using neural networks, *IEEE Transactions on knowledge and data engineering* **8**(6), 957-961, 1996.

110. Boser,B. E., Guyon, I. M., & Vapnik, V. N. A training algorithm for best margin classifiers, in 5th Annual ACM Workshop on Computational Learning Theory'1992, New York, NY, 144-152.

111. Vapnik,V. N. *The Nature of Statistical Learning Theory*, Springer, Verlag, 1995.

112. Qu, J., Chai, Y., & Yang, S.X. A Real-Time De-Noising Algorithm for E-Noses in a Wireless Sensor Network, *Sensors* **9**, 895-908, 2009.

113. Pawlak, Z. *Rough Sets: Theoretical Aspects of Reasoning About Data*, Springer, 1991.

114. Lee, P.A., & Reedy, B.J. Temperature modulation in semiconductor gas sensing, *Sensors and Actuators B* **60** (1) 35--42, 1999.

115. Heiling, A., et al. Gas Identification by Modulating Temperatures of SnO_2-Based Thick Film Sensors, *Sensors and Actuators B* **43** (1-3) 45--51, 1997.

116. Huang, X., et al. Gas sensing behaviour of a single tin dioxide sensor under dynamic temperature modulation, *Sensors and Actuators B* **99** (2-3) 444–450, 2004.

117. Vergara, A., Llobet, E., Brezmes, J., Vilanova, X., M., Stankova, I., Cané, C., & Correig, X. Optimized multi-frequency temperature modulation of micro-hotplate gas sensors, in IEEE Sensors Conference'2004, Vienna ,1392-1395.

118. Vine, H. D. Le. *Method and apparatus for operating a gas sensor*, **U.S. Patent No. 3906473**, September 16, 1975.

119. Owen, L.J. *Gas monitors*, **U.S. Patent No. 4185491**, January 29, 1980.

120. Sears, W.M., et al. General characteristics of thermally cycled tin oxide gas sensors, *Semicond. Sci. Technol.* **4**, 351--359, 1989.

121. Sears, W.M., et al. Algorithms to improve the selectivity of thermally cycled in oxide gas sensors, *Sens. Actuators B* **19** (4), 333--349, 1989.

122. Horak, G., Bilas, V., & Vasic, D. Noise Analysis of the Pulse-Width Modulator for Quasi-Digital Sensors, in IEEE International Instrumentation and Measurement Technology Conference (IMTC'2008), Victoria, Vancouver Island, Canada, 12-15.

123. Ugryumov, R. B., et al. Spectral and Static Noise Characteristics of Semiconductor Gas Sensors in Equiresistance Conditions, *Technical Physics* **49** (7), 941--943, 2004.

124. Mielle, P., & Marquis, F. Gas Sensors Arrays ('Electronic Noses'): a study about the speed/accuracy ratio, *Sens. Actuators B* **68** (1-3), 9--16, 2000.

125. Gomri, S., Seguin, J. L., & Aguir, K. Gas Sensor Selectivity Enhancement by Noise Spectroscopy: A Model of Adsorption-Desorption Noise, in IEEE, Research in Microelectronics and Electronics (PRIME'2005), Lausanne, Switzerland, 151- 154.

126. Contaret, T., Gomri, S., Seguin, J.L., & Aguir, K. Noise Spectroscopy Measurements in Metallic Oxide Gas Microsensors, in IEEE Sensors Conference' 2008, Lecce, Italy, 200-203.

127. Tian, F., Yang, S.X., & Dong, K. Circuit and Noise Analysis of Odourant Gas Sensors in an E-Nose, *Sensors* **5** (1), 85--96, 2005.

128. Vergara, A., et al. Feature extraction of metal oxide gas sensors using dynamic moments, *Sensors and Actuators B* **122** (1), 219–226, 2007.

129. Gutierrez, F.J., et al. Use of complex impedance spectroscopy in chemical sensor characterisation, *Sensors and Actuators B* **4** (3-4), 359-363, 1991.

130. Gutierrez, F.J., et al. Properties of polycrystalline gas sensors based on d.c. and a.c. measurements, *Sensors and Actuators B* **8** (3), 231-235, 1992.

131. Amrani, H., et al. Multi-frequency measurements of organic conducting polymers for sensing of gases and vapours, *Sensors and Actuators B* **33** (1-3), 137-141, 1996.

132. Vilanova, X., et al. Analysis of the conductance transient in thick-film tin oxide gas sensors, *Sensors and Actuators B* **31** (3), 175-180, 1996.

133. Llobet, E., et al. Conductance transient analysis of thick-film tin oxide gas sensors under successive gas injection steps, *Meas. Sci. Technol.* **8** (10), 1133-1138, 1997.

134. Llobet, E., et al. Transient response of thick-film tin oxide gas sensors to multicomponent gas mixtures, *Sensors and Actuators B* **47** (1-3), 104-112, 1998.

135. Llobet, E., et al. Model for the steady-state and transient behaviour of thick-film tin oxide gas sensors in the presence of gas mixtures, *Journal of the Electrochemical Society* **145** (5), 1772-1779, 1998.

136. Llobet, E., et al. Qualitative and quantitative analysis of volatile organic compounds using transient and steady-state responses of a thick-film tin oxide gas sensor array, *Sensors and Actuators B* **41** (1-3), 13-22, 1997.

137. Llobet, E. "Selectivity enhancement of metal oxide semiconductor chemical sensors through the study of their transient response to a step-change in gas concentration", Ph. D. Thesis, Universitat Politècnica de Catalunya, Barcelona, 1997.Print.

138. Duran, C., Brezmes, J., Llobet, E., Vilanova, X., & Correig, X. Enhancing sensor selectivity through flow modulation, in IEEE Sensors Conference' 2005, Irvine, California, 428-431.

139.Zhang, Q., et al. Sensory analysis of Chinese vinegars using an electronic nose, *Sens. Actuators B* **128** (2), 586-593, 2008.

140.Zhang, Q., et al. Characterization of Chinese vinegars by electronics nose, *Sens. Actuators B* **119** (2), 538-546, 2006.

141.Zhang, Q., et al. Identification and pattern recognition analysis of Chinese liquors by doped nano ZnO gas sensor array, *Sens. Actuators B* **110** (2), 370-376, 2005.

142.Corcoran, P., et al. Optimal configuration of a thermally cycled gas sensor array with neural network pattern recognition, *Sens. and Actuators B* **48** (1–3), 448-455, 1998.

143.Gardener, J.W. Detection of vapors and odours from a multisensory array using pattern recognition Part1. Principal components and cluster analysis, *Sens. and Actuators B* **4** (1-2), 109-115, 1991.

144.Gardener, J.W., et al. Detection of vapors and odours from a multi sensor array using pattern-recognition techniques Part 2. Artificial neural networks, *Sens. and Actuators B* **9** (1), 9-15, 1992.

145.Bermak, A., Belhouari, S., Shi, B.M., and Martinez, D. "Pattern Recognition Techniques for Odour Discrimination in Gas Sensor Array" *Encyclopedia of Sensors*.Ed.American Scientific Publishers, 1–17, 2006. Print.

146.Rumelhart, D.E., et al. Learning representations by back propagating errors, *Nature* **323**, 533–536, 1986.

147.Goodner, K. L., et al. The dangers of creating false classifications due to noise in e-nose and similar multivariate analyses, *Sens. and Actuators B* **80** (3), 261-266, 2001.

148.Qu, J., et al. A Real-Time De-Noising Algorithm for E-Noses in a Wireless Sensor Network, *Sensors* **9** (2), 895-908, 2009.

149.Hosur, S., & Tewfik, A. H. Wavelet transform domain adaptive FIR filtering, *IEEE Trans. Signal Processing* **45** (3), 617–630, 1997.

150.Erdol, N., & Basbug, F. Wavelet transform based adaptive filters: analysis and new results, *IEEE Trans. Signal Processing* **44** (9), 2163–2171, 1996.

151.Donoho, D. L., & Johnstone, I. M. Adaptating to unknown smoothness via wavelet shrinkage, *J. Amer. Statist. Assoc.* **90** (432), 1200–1224, 1995.

152.Donoho, D. L., Johnstone, I. M., Kerkyacharian, G., & Picard, D. Wavelet shrinkage: Asymptopia?, *J. Roy. Statist. Soc. B.* **57** (2), 301–337, 1995.

153.Donoho, D. L. De-noising by soft-thresholding, *IEEE Trans. Inform. Theory* **41** (3), 613–627, 1995.

154.Nason, G. P. Wavelet shrinkage by cross-validation, *J. Roy. Statist. Soc. B* **58**, 463–479, 1996.

155.Bruce, A., & Gao, H.Y. UnderstandingWaveShrink: Variance and bias estimation," *Biometrika* **83** (4), 727-745, 1996.

156.Lang, M., et al. Noise reduction using an undecimated discrete wavelet transform, *IEEE Signal Processing Lett.* **3** (1), 10–12, 1996.

157.Johnstone, I. M., & Silverman, B.W. Wavelet threshold estimators for data with correlated noise, *J. Roy. Statist. Soc. B* **59** (2), 319–351, 1997.

158.Abramovich, F., Sapatinas, T., & Silverman, B. W. Wavelet thresholding via a Bayesian approach, *J. Roy. Statist. Soc. B* **60** (4), 725-749, 1998.

159.De Cheveigné, A., & Simon, J. Z. Sensor noise suppression, *J Neurosci Methods* **168** (1), 195–202, 2008

160.Hu, X., et al. Removal of baseline wander from ECG signal based on a statistical weighted moving average filter, *Journal of Zhejiang University - Science C* **12** (5), 397-403, 2011.

161.Boucheham, B., et al. Piecewise linear correction of ECG baseline wander: a curve simplification approach, *Comput. Methods Programs Biomed* **78** (1), 1-10 2005.

162.Burattini, L., Zareba, W., & Burattini, R. The effect of baseline wandering in automatic T-wave alternans detection from holter recordings, in Computers in Cardiology'2006, Valencia, Spain, 257- 260.

163.Leski, J.M., & Henzel, N. ECG baseline wander and powerline interference reduction using nonlinear filter bank, *Signal Processing* **85** (4), 781-793, 2005.

164.Xu, L.S., et al. Baseline wander correction in pulse waveforms using wavelet-based cascaded adaptive filter, Computers in Biology and Medicine **37** (5), 716-731, 2007.

165.Clifford, G.D, Azuaje, F. & McSharry, P.E. *Advanced Methods and Tools for ECG Data Analysis*, Artech House Publishers, 2006.

166.Platt, R. S., Hajduk, E. A., Hulliger, M., & Easton, P. A. A modified Bessel filter for amplitude demodulation of respiratory electromyograms, *J Appl Physiol* **84** (1), 378-388, 1998.

167.Qiu, H., et al. Wavelet filter-based weak signature detection method and its application on rolling element bearing prognosis, *J. Sound Vib.* **289** (4-5), 1066–1090, 2006.

168.Qiu, H., et al. Robust performance degradation assessment methods for enhanced rolling element bearing prognostics, *Adv. Eng. Inform.* **17** (3-4), 127–40, 2003.

169.Lin, J., & Zuo, M.J. Gearbox fault diagnosis using adaptive wavelet filter, *Mech. Syst. Signal Process.* **17** (6), 1259–1269, 2003.

170.Bozchalooi, I. S., & Liang, M. A smoothness index-guided approach to wavelet parameter selection in signal de-noising and fault detection, *J. Sound Vib.* **308** (1-2), 246–67, 2007.

171.Bozchalooi, I. S., & Liang, M. A joint resonance frequency estimation and in-band noise reduction method for enhancing the detectability of bearing fault signals, *Mech. Syst. Signal Process.* **22** (4), 915–33, 2008.

172.Badzey, R. L., & Mohanty, P. Coherent Signal Amplification in Bistable Nanomechanical Oscillators by Stochastic Resonance, *Nature* **437**, 995-998, 2005.

173.Heslop, D., & Dekkers, M.J. Spectral analysis of unevenly spaced climatic time series using CLEAN: signal recovery and derivation of significance levels using a Monte Carlo simulation, Physics of the Earth and Planetary Interiors, **130**, 103–116, 2002.

174.Chou, W.C., Hsu, Y.C., & Liao, L. P. Modulation/ Demodulation System for Capacitive Sensors, in IEEE International conference on Microsystems, Packaging, Assembly Conference Taiwan (IMPACT'2006), Taipei, Taiwan, 1 – 4.

175.Lita, I., Sofron, E., Serban, G., & Visan, D. A Method of Noise Reduction in Data Acquisition Systems from Sensors, in 24th International Spring Seminar on Electronics Technology: Concurrent Engineering in Electronic Packaging' 2001, Calimanesti-Caciulata, Romania, 253 – 257.

176.Boymans, M., & Dreschler, W.A. Field trials using a digital hearing and with active noise reduction and dualmicrophone directionality, *Audiology* **39** (5), 260–268, 2000.

177.Walden, B., et al. Comparison of benefits provided by different hearing aid technologies, *Journal American Academy of Audiology* **11** (10), 540–560, 2000.

178.Chung, K., et al. Effects of directional microphone and adaptive multi-channel noise reduction algorithm on cochlear implant performance, *Journal of Acoustical Society of America* **120** (4), 2216–2227, 2006.

179.A low-noise high-sensitivity readout circuit for MEMS capacitive sensors, in Circuits and Systems (ISCAS), Proceedings of 2010 IEEE International Symposium on, Paris, 3280- 3283.

180.Benedetto, J.J., & Teolis, A. A wavelet auditory model and data compression, *Appl. Comput. Harmon. Anal.* **1** (1), 3–28, 1993.

181.Moshou, D., et al. Dynamic muscle fatigue detection using self-organizing maps, *Appl. Soft Comput.* **5** (4), 391–398, 2005.

182.Wickerhauser, M.V. *Acoustic Wavelets: A Tutorial in Theory and Applications*, Academic Press Professional, Inc. San Diego, CA, USA, 1992.

183.Graps, A. An introduction to wavelets, *IEEE Comput. Sci. Eng.* **2** (2), 50–61, 1995.

184.Daubechies, I. Orthonormal bases of compactly supported wavelets, *Commun. Pur. Appl. Math.* **41**, 909–996, 1988.

185.Mallat, S.G. A theory for multiresolution signal decomposition: the wavelet representation, *IEEE Trans. Pattern Anal. Mach. Intell.* **11** (7), 674–693, 1989.

186.Eykhoff, P. *System Identification: Parameter and State Estimation*, Wiley-Interscience, University of Michigan, 1974.

187.Goodwin, C. G. and Payne, R. L. *Dynamic System Identification: Experiment Design and Data Analysis*, Academic Press, 1977.

188.Ljung, L. *System Identification: Theory for the User*. 2nd ed. Prentice Hall, Englewood Cliffs, New Jersey, 1999.

189.Nelles, O. *Nonlinear System Identification: from Classical Approaches to Neural Networks and Fuzzy Models*, Springer, 2001.

190.Ljung L. *System Identification.* Prentice-Hall, Englewood Cliffs, New Jersey,1987.

191.Cavicchi, R.E., et al. Fast temperature programmed sensing for micro-hotplate gas sensors, *IEEE Electron Device Lett.* **16** (6), 286–288, 1995.

192.Cavicchi, R.E., et al. Optimized temperature-pulse sequences for the enhancement of chemically specific response patterns from micro-hotplates gas sensors, *Sensors and Actuators B* **33,** 142–146, 1996.

193.-Khalifa, S., Gardner, J.W., & Craine, J.F. Characterization of a thermal wave microsensor for intelligent analysis of atmospheric gases, in Sensors and their Applications' 97, Glasgow, 89–94.

194. Al-Khalifa, S., Gardner, J.W., & Maldonado-Bascon, S. Rapid multicomponent analysis using thermally modulated resistive gas microsensors and a discrete wavelet transform, in Sensors and their Applications'2001, London, 103–108.

195.Llobet, E., et al. Multicomponent gas mixture analysis using a single tin oxide sensor and dynamic pattern recognition, *J. IEEE Sensors* **1**, 207–213, 2001.

196.Llobet, E., et al. Wavelet transform fuzzy ARTMAP based pattern recognition for fast gas identification using a microhotplate gas sensor, *Sensors and Actuators B* **83** 238–244, 2002.

197.Al-Khalifa, S., Maldonado-Bascon, S., & Gardner, J.W. Identification of CO and NO_2 using a thermally resistive microsensor and support vector machine, *IEE Sci., Meas. Technol.* **150**, 11– 14, 2003.

198.Ionescu, R. et al. Response model for thermally modulated tin oxide-based micro-hotplate gas sensors, *Sensors and Actuators B* **95**, 203–211, 2003.

199.Vergara, A., et al. Optimised temperature modulation of metal oxide micro-hotplate gas sensors through multilevel pseudo random sequences, *Sensors and Actuators B* **111–112** (11), 271–280, 2005.

200.Vergara, A., et al. Optimized Temperature Modulation of Micro-Hotplate Gas Sensors Through Pseudorandom Binary Sequences, *IEEE Sensors Journal* **5** (6), 1369 -1378, 2005.

201.Dutta, N., & Bhuyan, M. Optimal Temperature Modulation of MOS Gas Sensors by System Identification, *International Journal of Signal Processing, Image Processing and Pattern Recognition* **5** (2), 17-27, 2012.

202.Dutta, N., Dewan, S. K., & Bhuyan, M. System Identification of MOS Gas Sensors and Stability Analysis, *Sensors & Transducers Journal* **143** (8), 127-135,2012.

203.Gutierrez, O. R., Korah, S., & Perera, A. Multi-frequency temperature modulation for metal-oxide gas sensors, in 8th Intl. Symp. On Olfaction and Electronic Nose'2001, Washington DC, 1-7.

204.Derbel, F. Modeling fire detector signals by means of system identification techniques, *IEEE Transactions on Instrumentation and Measurement* **50** (6), 1815- 1821, 2001.

205. Gardner, J. W. *Microsensors: Principles and Application*, 2nd ed., Wiley, the University of Michigan, 1994.

206. Gardner, J. W. A non-linear diffusion-reaction model of electrical conduction in semiconductor gas sensors, *Sensors and Actuators B* **1** (1-6), 166-170, 1990.

207. Barsan, N., et al. Calibration curve for SnO2-based gas sensors, *Sensors and Actuators B* **19** (1-3), 466–469, 1994.

208. Weimar, U., & Gopel, W. AC measurements on tin oxide sensors to improve selectivities, *Sensors and Actuators B* **26** (1-3), 13-18, 1995.

209. Wada, K., & Egashira, M. Improvement of gas-sensing properties of SnO_2 by surface chemical modification with diethoxydimethylsilane, *Sensors and Actuators B* **53** (3), 147–154, 1998.

210. Nakata, S. et al. Detection and quantification of CO gas based on the dynamic response of a ceramic sensor, *Chem. Lett.*, 1505–1508, 1991.

211. Nakata, S. et al. New strategy for the development of a gas sensor based on the dynamic characteristics: principle and preliminary experiment, *Sensors and Actuators B* **8** (2), 187–189, 1992.

212. Nambo, H., Hirobayashi, S., Kimura, H., & Oyabu, T. Detection of Gaseous Indoor-air Pollutants Using Multi Gas Sensor System and a Production System, in 7th International Meeting on Chemical Sensors, Technical Digest' 1998, Beijing International Convention Center, Beijing, China, 181-183.

213. Oyabu, T., Kimura, H., & Ishizaka, S. Indoor Air-pollution Detector using Tin Oxide Gas Sensor, *Sensors and Materials* **7** (6), 431-436, 1995.

214. Oyabu, T., Hirobayashi, S., & Kimura, H. Detection of gaseous indoor-air pollution using multisensor system, *Sensors and Materials* **9** (3), 177-186, 1997.

215. Gardner, J. W., Llobet, E., & Hines, E.L. PSpice model for resistive gas and odour sensors, *Circuits, Devices and Systems* **146** (3), 101-104, 1999.

216. Llobet, E., et al. Electrical equivalent models of semiconductor gas sensors using PSpice, *Sensors and Actuators B* **77**, 275–280, 2001.

217. Martin, M.A., et al. Application of artificial neural networks to calculate the partial gas concentration in a mixture, *Sensors and Actuators B: Chemical* **77** (1-2), 468–471, 2001.

218. Clifford, P. K. Homogenous semiconducting gas sensors: A comprehensive model, in Int. Meet. Chemical Sensors'1983, Fukuoka, Japan, Kodansha, Tokyo/Elsevier, Amsterdam, 135-146.

219.Morrison, S. R. Semiconductor Gas Sensors, *Sensors and Actuators* **2**, 329-341, 1982.

220.Morrison, S. R. Mechanism of semiconducting gas sensor operation, *Sensors and Actuators* **11** (3), 283-287, 1987.

221.Gardner, J.W. Electrical conduction in solid state gas sensors, *Sensors and Actuators* **18** (3-4), 373-387, 1989.

222.Geinstlinger, H. Electron theory of thin film gas sensors, *Sensors and Actuators B* **17** (1), 47-60, 1993.

223.Geinstlinger, H. Device modeling of semiconductor gas sensors, *Sensors and Actuators B* **13**, 685-686, 1993.

224.Gomri, S., et al. Modelling on oxygen chemisorption induced noise in metallic oxide gas sensors, *Sensors and Actuators B* **107** (2), 722–729, 2005.

225.Barsan, N., & Weimar, U. Conduction model of metal oxide gas sensors, *J. Electroceramics.* 7 (3), 143–167, 2001.

226.McAleer, J.F., et al. Tin dioxide gas sensors. Part 2.—The role of surface additives, *J. Chem. Soc., Faraday Trans. 1* **84** (2), 441-457, 1987.

227.Barsan, N., & Weimar, U. Understanding the fundamental principles of metal oxide based gas sensors; the example of CO sensing with SnO_2 sensors in presence of humidity, *J. Phys.: Condens. Matter* **15** (20), 813–839, 2003.

228.Brynzary, V., et al. Simulation of thin film gas sensors kinetics, *Sensors and Actuators B Chem.* **61** (1-3), 143–153, 1999.

229.Ding, J., et al. Surface state trapping models for SnO_2-based micro-hotplate sensors, *Sensors and Actuators B Chem.* 77 (3), 597–613, 2001.

230.Rantala, T.S., et al. Rate equation simulation of the height of Schottky barriers at the surface of oxidic semiconductor, *Sensors and Actuators B Chem.* **13** (1-3), 234–237, 1993.

231.Pulkkinen, U., et al. Kinetic Monte Carlo simulation of oxygen exchange of SnO_2 surface, *J. Mol. Catal. A Chem.* **166** (1), 15–21, 2001.

232.Hahn, S.H., et al. CO sensing with SnO_2 thick film sensors: role of oxygen and water vapour, *Thin Solid Films* **436** (1), 17–24, 2003.

233.Schmid, W., et al. Sensing of hydrocarbons and CO in low oxygen conditions with tin dioxide sensors: possible conversion paths, *Sensors and Actuators B Chem.* **103** (1-2), 362–368, 2004.

234.Brynzary, V., et al. Simulation of thin film gas sensors kinetics, *Sensors and Actuators B Chem.* **61** (1-3), 143–153, 1999.

235.Fort, A., et al. CO sensing with SnO_2-based thick film sensors: surface state model for conductance responses during thermal-modulation, *Sensors and Actuators B Chem.* **116**(1-2), 43–48, 2006.

236.Fort, A., et al. Simplified models for SnO2 sensors during chemical and thermal transients in mixtures of inert, oxidizing and reducing gases, *Sensors and Actuators B Chem.* **124** (1), 245–259, 2007.

237.Fort, A., et al. Surface state model for conductance responses during thermal-modulation of SnO2-based thick film sensors: Part I—Model derivation, *IEEE Trans. Instrum. Meas.* **55** (6), 2102–2106, 2006.

238.Fort, A., et al. Surface state model for conductance responses during thermal-modulation of SnO2-based thick film sensors: Part II—Experimental verification, *IEEE Trans. Instrum. Meas.* **55** (6), 2107–2117, 2006.

239.Le Vine, H.D. *Method and apparatus for operating a gas sensor*, **U.S. Patent No. 3906473**, September 16, 1975.

240.Llobet, E., et al. Wavelet transform fuzzy ARTMAP based pattern recognition for fast gas identification using a micro-hotplate gas sensor, *Sensors and Actuators B* **83** (1-3), 238–244, 2002.

241.Al-Khalifa, S., et al. Identification of CO and NO_2 using a thermally resistive microsensor and support vector machine, *IEE Proc. Sci. Meas. Technol.* **150** (1), 11–14, 2003.

242.Moseley, P.T. & Tofield, B.C. *Solid State Gas Sensors*, Adam Hilger Series on Sensors, Bristol, 1987.

243.Clifford, P.K., & Tuma, D.T. Characteristics of semiconductor gas sensors, I. Steady state gas response , *Sensors and Actuators* **3,** 233-254, 1983.

244.Clifford, P.K., & Tuma, D.T. Characteristics of semiconductor gas sensors, II. Transient response to temperature change, *Sensors and Actuators* **3,** 255-281, 1983.

245.Vilanova, X., et al. Influence of moisture and working temperature on the steady-state and transient response of thick-film tin oxide gas sensors, Internal report GSM 98/01, Universitat Rovira i Virgili, 1998.

APPENDICES

Table A2.1: Time constants for various gases used in the experiment at 10mHz frequency and 75% duty cycle.

Sensors	Time constants of Gases at 10mHz frequency and 75% duty cycle (shown for 10 cycles)									
	Ethylacetate (sec)	Acetonitrile (sec)	Ethanol (sec)	Kerosene (sec)	Petroleumether (sec)	Chloroform (sec)	Methanol (sec)	Isopropyl-alcohol (sec)	Acetone (sec)	N-Hexane (sec)
TGS-2611	18	14	12.5	11.7	14.4	11.4	12.9	9	10	13
	12	12.3	16.3	13.2	13.1	13.5	16.4	12.4	13.3	11
	10	14.5	11.7	19	13.9	12.9	19.3	11	13.9	10.8
	12	13.3	13	11.9	15.1	13.9	15	11.4	12.8	12.1
	18	16.3	17.6	15.8	18.4	19.3	14	16.6	11.8	9.9
	14.5	12.1	12.7	13.2	14	15	14	11.2	14.7	11.9
	15	15.5	14.6	15.9	15.8	16.7	15.5	13.5	15.2	12.8
	18.2	17	13.1	18.3	12.9	18.2	18	14	12.9	18
	14.6	15.2	15	14	14.5	13.2	14.6	14.2	12.9	12.8
	15	15.1	12.3	15.5	15.3	18.1	15.8	12.5	13.1	13.9
TGS-822	12.3	13	11	13.6	14.4	11	10.3	11.2	12.5	11.9
	14	15	13	18	11.3	13.5	11.3	13.1	13.01	15.8
	13.9	11.9	14.8	15	14.1	10	12.1	10.3	11.2	13.2
	11.6	12	12.8	12.2	12.5	12	12.1	12.8	15.4	15.9
	11.9	13.6	12	14.6	13.01	13.4	13	11.9	13.4	18.3
	12	18	11.2	13	11.2	11	11.4	19	10.3	14
	13.6	15	16	13	15.4	12.3	14.1	13.8	11.4	15.5
	18	12.2	13	12	13.4	15.1	13.1	14.7	15	11.5
	13	14.6	11	11.1	10.3	11.3	11.3	15.7	16	12.9
	12	13	17.1	10.4	11.4	13.4	13	13	15.1	13
TGS-842	14.8	14.1	15	11	13.4	13	10.3	11.6	13.1	11.2
	12.8	12.5	14	11.2	14	17.6	11.9	11.9	12.1	13.1
	12	13.01	14	10.8	15.8	12.7	10.7	12	9.8	9.8
	11.2	11.2	15.5	9.4	12.9	14.6	11.9	13.6	10.4	11.3
	16	15.4	18	12.4	14.5	13.1	11	18	12.7	11.9
	13	13.4	14.6	11	15.3	15	10.5	13	13.2	13.9
	11	10.3	15.8	11.4	10.2	12.3	13.9	12	13.6	13.2
	17.1	11.4	15	16.6	11.7	12.2	12.9	11.1	17	12.8
	12.6	12.9	11.8	11.2	11.5	11.6	13.1	10 2	12.6	14.1
	15	10.3	11	13.5	13	14.4	11.1	13.1	14.5	12.9

Table A4.1: Table showing the step input-output of sensor TGS-822 at 1mHz and 50% duty cycle.

Step Input (For 1mHz TGS-822 at 1mHz and 50% duty cycle)				Sensor Output (For 1mHz TGS-822 at 1mHz and 50% duty cycle)			
Time (secs)	Voltage (volts)	Time (secs)	Voltage (volts)	Time (secs)	Voltage (volts)	Time (secs)	Voltage (volts)
0 000000	5 000000	0 640000	5 000000	0 000000	0 0012	0 640000	0 009012
0 010000	5 000000	0 650000	5 000000	0 010000	0 0013	0 650000	0 009013
0 020000	5 000000	0 660000	5 000000	0 020000	0 0014	0 660000	0 009117
0 030000	5 000000	0 670000	5 000000	0 030000	0 0015	0 670000	0 009213
0 040000	5 000000	0 680000	5 000000	0 040000	0 0016	0 680000	0 009215
0 050000	5 000000	0 690000	5 000000	0 050000	0 0017	0 690000	0 009337
0 060000	5 000000	0 700000	5 000000	0 060000	0 0019	0 700000	0 009345
0 070000	5 000000	0 710000	5 000000	0 070000	0 0020	0 710000	0 009213
0 080000	5 000000	0 720000	5 000000	0 080000	0 0021	0 720000	0 009188
0 090000	5 000000	0 730000	5 000000	0 090000	0 0023	0 730000	0 009934
0 100000	5 000000	0 740000	5 000000	0 100000	0 0024	0 740000	0 009529
0 110000	5 000000	0 750000	5 000000	0 110000	0 0025	0 750000	0 009532
0 120000	5 000000	0 760000	5 000000	0 120000	0 0026	0 760000	0 009621
0 130000	5 000000	0 770000	5 000000	0 130000	0 0027	0 770000	0 009623
0 140000	5 000000	0 780000	5 000000	0 140000	0 0028	0 780000	0 009712
0 150000	5 000000	0 790000	5 000000	0 150000	0 0029	0 790000	0 009715
0 160000	5 000000	0 800000	5 000000	0 160000	0 0030	0 800000	0 009878
0 170000	5 000000	0 810000	5 000000	0 170000	0 0031	0 810000	0 009912
0 180000	5 000000	0 820000	5 000000	0 180000	0 0032	0 820000	0 009986
0 190000	5 000000	0 830000	5 000000	0 190000	0 0033	0 830000	0 009993
0 200000	5 000000	0 840000	5 000000	0 200000	0 0034	0 840000	0 0111
0 210000	5 000000	0 850000	5 000000	0 210000	0 0035	0 850000	0 0112
0 220000	5 000000	0 860000	5 000000	0 220000	0 0036	0 860000	0 0113
0 230000	5 000000	0 870000	5 000000	0 230000	0 0037	0 870000	0 0114
0 240000	5 000000	0 880000	5 000000	0 240000	0 0038	0 880000	0 0115
0 250000	5 000000	0 890000	5 000000	0 250000	0 0040	0 890000	0 0116
0 260000	5 000000	0 900000	5 000000	0 260000	0 0041	0 900000	0 0117
0 270000	5 000000	0 910000	5 000000	0 270000	0 0042	0 910000	0 0118
0 280000	5 000000	0 920000	5 000000	0 280000	0 0043	0 920000	0 0119
0 290000	5 000000	0 930000	5 000000	0 290000	0 0045	0 930000	0 0120
0 300000	5 000000	0 940000	5 000000	0 300000	0 0046	0 940000	0 0122
0 310000	5 000000	0 950000	5 000000	0 310000	0 0047	0 950000	0 0123
0 320000	5 000000	0 960000	5 000000	0 320000	0 0048	0 960000	0 0124
0 330000	5 000000	0 970000	5 000000	0 330000	0 0049	0 970000	0 0125
0 340000	5 000000	0 980000	5 000000	0 340000	0 0050	0 980000	0 0126
0 350000	5 000000	0 990000	5 000000	0 350000	0 0051	0 990000	0 0127
0 360000	5 000000	1 000000	5 000000	0 360000	0 0052	1 000000	0 0128
0 370000	5 000000	1 010000	5 000000	0 370000	0 0053	1 010000	0 0129
0 380000	5 000000	1 020000	5 000000	0 380000	0 0056	1 020000	0 0130
0 390000	5 000000	1 030000	5 000000	0 390000	0 0058	1 030000	0 0132
0 400000	5 000000	1 040000	5 000000	0 400000	0 0059	1 040000	0 0133
0 410000	5 000000	1 050000	5 000000	0 410000	0 0060	1 050000	0 0135
0 420000	5 000000	1 060000	5 000000	0 420000	0 0061	1 060000	0 0137
0 430000	5 000000	1 070000	5 000000	0 430000	0 0062	1 070000	0 0138
0 440000	5 000000	1 080000	5 000000	0 440000	0 0063	1 080000	0 0140
0 450000	5 000000	1 090000	5 000000	0 450000	0 0065	1 090000	0 0142
0 460000	5 000000	1 100000	5 000000	0 460000	0 0066	1 100000	0 0143
0 470000	5 000000	1 110000	5 000000	0 470000	0 0067	1 110000	0 0145
0 480000	5 000000	1 120000	5 000000	0 480000	0 0068	1 120000	0 0146
0 490000	5 000000	1 130000	5 000000	0 490000	0 0069	1 130000	0 0147
0 500000	5 000000	1 140000	5 000000	0 500000	0 0070	1 140000	0 0148
0 510000	5 000000	1 150000	5 000000	0 510000	0 0071	1 150000	0 0150
0 520000	5 000000	1 160000	5 000000	0 520000	0 0072	1 160000	0 0151
0 530000	5 000000	1 170000	5 000000	0 530000	0 0073	1 170000	0 0153
0 540000	5 000000	1 180000	5 000000	0 540000	0 0076	1 180000	0 0154
0 550000	5 000000	1 190000	5 000000	0 550000	0 0078	1 190000	0 0155
0 560000	5 000000	1 200000	5 000000	0 560000	0 0079	1 200000	0 0157
0 570000	5 000000	1 210000	5 000000	0 570000	0 0080	1 210000	0 0160
0 580000	5 000000	1 220000	5 000000	0 580000	0 0083	1 220000	0 0167
0 590000	5 000000	1 230000	5 000000	0 590000	0 0086	1 230000	0 0166
0 600000	5 000000	1 240000	5 000000	0 600000	0 0088	1 240000	0 0168
0 610000	5 000000	1 250000	5 000000	0 610000	0 0089	1 250000	0 0169
0 620000	5 000000	1 260000	5 000000	0 620000	0 0090	1 260000	0 0170

Table A4.2: Table showing the step input-output of sensor TGS-842 at 80mHz and 50% duty cycle.

Step Input (For 80mHz TGS-842 at 1mHz and 50% duty cycle)				Sensor Output (For 80mHz TGS-842 at 1mHz and 50% duty cycle)			
Time (secs)	Voltage (volts)	Time (secs)	Voltage (volts)	Time (secs)	Voltage (volts)	Time (secs)	Voltage (volts)
0 000000	5 000000	0 640000	5 000000	0 000000	0 0033	0 640000	0 0124
0 010000	5 000000	0 650000	5 000000	0 010000	0 0035	0 650000	0 0125
0 020000	5 000000	0 660000	5 000000	0 020000	0 0034	0 660000	0 0127
0 030000	5 000000	0 670000	5 000000	0 030000	0 0037	0 670000	0 0128
0 040000	5 000000	0 680000	5 000000	0 040000	0 0040	0 680000	0 0129
0 050000	5 000000	0 690000	5 000000	0 050000	0 0045	0 690000	0 0130
0 060000	5 000000	0 700000	5 000000	0 060000	0 0047	0 700000	0 0132
0 070000	5 000000	0 710000	5 000000	0 070000	0 0048	0 710000	0 0134
0 080000	5 000000	0 720000	5 000000	0 080000	0 0049	0 720000	0 0136
0 090000	5 000000	0 730000	5 000000	0 090000	0 0050	0 730000	0 0138
0 100000	5 000000	0 740000	5 000000	0 100000	0 0052	0 740000	0 0140
0 110000	5 000000	0 750000	5 000000	0 110000	0 0054	0 750000	0 0141
0 120000	5 000000	0 760000	5 000000	0 120000	0 0056	0 760000	0 0142,
0 130000	5 000000	0 770000	5 000000	0 130000	0 0057	0 770000	0 0145
0 140000	5 000000	0 780000	5 000000	0 140000	0 0059	0 780000	0 0147
0 150000	5 000000	0 790000	5 000000	0 150000	0 0060	0 790000	0 0148
0 160000	5 000000	0 800000	5 000000	0 160000	0 0061	0 800000	0 0149
0 170000	5 000000	0 810000	5 000000	0 170000	0 0062	0 810000	0 0150
0 180000	5 000000	0 820000	5 000000	0 180000	0 0063	0 820000	0 0151
0 190000	5 000000	0 830000	5 000000	0 190000	0 0064	0 830000	0 0152
0 200000	5 000000	0 840000	5 000000	0 200000	0 0067	0 840000	0 0154
0 210000	5 000000	0 850000	5 000000	0 210000	0 0068	0 850000	0 0155
0 220000	5 000000	0 860000	5 000000	0 220000	0 0069	0 860000	0 0157
0 230000	5 000000	0 870000	5 000000	0 230000	0 0070	0 870000	0 0159
0 240000	5 000000	0 880000	5 000000	0 240000	0 0071	0 880000	0 0162
0 250000	5 000000	0 890000	5 000000	0 250000	0 0072	0 890000	0 0163
0 260000	5 000000	0 900000	5 000000	0 260000	0 0073	0 900000	0 0164
0 270000	5 000000	0 910000	5 000000	0 270000	0 0074	0 910000	0 0165
0 280000	5 000000	0 920000	5 000000	0 280000	0 0075	0 920000	0 0167
0 290000	5 000000	0 930000	5 000000	0 290000	0 0076	0 930000	0 0170
0 300000	5 000000	0 940000	5 000000	0 300000	0 0079	0 940000	0 0173
0 310000	5 000000	0 950000	5 000000	0 310000	0 0080	0 950000	0 0178
0 320000	5 000000	0 960000	5 000000	0 320000	0 0081	0 960000	0 0180
0 330000	5 000000	0 970000	5 000000	0 330000	0 0082	0 970000	0 0182
0 340000	5 000000	0 980000	5 000000	0 340000	0 0084	0 980000	0 0183
0 350000	5 000000	0 990000	5 000000	0 350000	0 0085	0 990000	0 0185
0 360000	5 000000	1 000000	5 000000	0 360000	0 0086	1 000000	0 0186
0 370000	5 000000	1 010000	5 000000	0 370000	0 0088	1 010000	0 0187
0 380000	5 000000	1 020000	5 000000	0 380000	0 0090	1 020000	0 0188
0 390000	5 000000	1 030000	5 000000	0 390000	0 0091	1 030000	0 0189
0 400000	5 000000	1 040000	5 000000	0 400000	0 0092	1 040000	0 0193
0 410000	5 000000	1 050000	5 000000	0 410000	0 0096	1 050000	0 0194
0 420000	5 000000	1 060000	5 000000	0 420000	0 0098	1 060000	0 0195
0 430000	5 000000	1 070000	5 000000	0 430000	0 0101	1 070000	0 0197
0 440000	5 000000	1 080000	5 000000	0 440000	0 0102	1 080000	0 0201
0 450000	5 000000	1 090000	5 000000	0 450000	0 0103	1 090000	0 0203
0 460000	5 000000	1 100000	5 000000	0 460000	0 0104	1 100000	0 0208
0 470000	5 000000	1 110000	5 000000	0 470000	0 0105	1 110000	0 0209
0 480000	5 000000	1 120000	5 000000	0 480000	0 0105	1 120000	0 0211
0 490000	5 000000	1 130000	5 000000	0 490000	0 0106	1 130000	0 0213
0 500000	5 000000	1 140000	5 000000	0 500000	0 0109	1 140000	0 0216
0 510000	5 000000	1 150000	5 000000	0 510000	0 0110	1 150000	0 0220
0 520000	5 000000	1 160000	5 000000	0 520000	0 0111	1 160000	0 0223
0 530000	5 000000	1 170000	5 000000	0 530000	0 0112	1 170000	0 0228
0 540000	5 000000	1 180000	5 000000	0 540000	0 0113	1 180000	0 0230
0 550000	5 000000	1 190000	5 000000	0 550000	0 0114	1 190000	0 0232
0 560000	5 000000	1 200000	5 000000	0 560000	0 0115	1 200000	0 0234
0 570000	5 000000	1 210000	5 000000	0 570000	0 0116	1 210000	0 0235
0 580000	5 000000	1 220000	5 000000	0 580000	0 0118	1 220000	0 0238
0 590000	5 000000	1 230000	5 000000	0 590000	0 0119	1 230000	0 0243
0 600000	5 000000	1 240000	5 000000	0 600000	0 0120	1 240000	0 0246
0 610000	5 000000	1 250000	5 000000	0 610000	0 0121	1 250000	0 0249
0 620000	5 000000	1 260000	5 000000	0 620000	0 0122	1 260000	0 0258

PUBLICATIONS

LIST OF PUBLICATIONS

1. Dutta, N., & Bhuyan,M. *Odour Impact Assessment Handbook* , Chapter 3, Wiley Publisher. Print.
2. Dutta, N., & Bhuyan, M. Noise Feature Analysis in Pulse Temperature Modulated MOS Gas Sensors, *Sensors and Transducers* **120** (9), 107--118, 2010.
3. Dutta, N., & Bhuyan, M. Statistical Analysis of Noise in MOS Gas Sensor Based Electronic Nose with Pulsed Temperature Modulation, in Computational Vision and Robotics (ICCVR'2010), Bhubaneswar, India, 23-27.
4. Dutta, N., & Bhuyan, M. Amplitude Demodulation and Spectrum Analysis of Noise in MOS Gas Sensor Based Electronic Nose, in Advances in Communication, Network, and Computing (CNC'2010), Calicut. Kerala, India, 160-162.
5. Dutta, N., & Bhuyan, M. Dynamic Response Based Odour Classification Using MOS Gas Sensors, in Emerging Applications of Information Technology (EAIT'2011), Kolkata, India, 231-234.
6. Dutta, N., & Bhuyan, M. Optimal Temperature Modulation of MOS Gas Sensors by System Identification, *Journal of Signal Processing, Image Processing and Pattern Recognition* **5** (2), 17-27, 2012.
7. Dutta, N., Dewan, S.K., & Bhuyan, M. System Identification of MOS Gas Sensors and Stability Analysis, *Sensors and Transducers* **143** (8), 127--135, 2012.
8. Dutta, N., & Bhuyan, M. System Identification of MOS Gas Sensors and Classification Enhancement through Optimal Temperature Modulation, in International Multi-conference on Intelligent Systems, Sustainable, New and Renewable Energy Technology and Nanotechnology'2012, Klawad, Haryana, India, 149-153.
9. Dutta, N., & Bhuyan, M. Classification Enhancement of MOS Gas Sensors by Optimized Temperature Modulation Using System Identification, *Journal of Signal Processing and Pattern Recognition,* Association for the Advancement of Modelling and Simulation Techniques in Enterprises. (In Press)

10. Dutta, N., & Bhuyan, M. Modeling of MOS Gas Sensor Based Electronic Nose Using System Identification, *International Journal of Engineering Systems Modelling and Simulation*. (Under Communication)